UNIVERSIDAD DE CANTABRIA

ESCUELA DE DOCTORADO DE LA UNIVERSIDAD DE CANTABRIA

DOCTORADO EN INGENIERÍA DE COSTAS, HIDROBIOLOGÍA Y GESTIÓN DE SISTEMAS ACUÁTICOS (IH2O)

TESIS DOCTORAL

MODELO DE EVOLUCIÓN DE PLAYAS CONSIDERANDO PLANTA Y PERFIL, EN ESCALAS DE MEDIO A LARGO PLAZO

PhD THESIS

BEACH EVOLUTION MODEL CONSIDERING PLANFORM AND PROFILE IN THE MEDIUM TO LONG TERM SCALES

Presentada por: **CAMILO JARAMILLO CARDONA**

Dirigida por: **Prof. ERNESTO MAURICIO GONZÁLEZ RODRÍGUEZ**

Prof. RAÚL MEDINA SANTAMARÍA

Santander, junio de 2020

UNIVERSITY OF CANTABRIA

DOCTORAL SCHOOL OF THE UNIVERSITY OF CANTABRIA

DOCTORATE IN COASTAL ENGINEERING, HYDROBIOLOGY AND MANAGEMENT OF ACUATIC SYSTEMS (IH2O)

PhD THESIS

BEACH EVOLUTION MODEL CONSIDERING PLANFORM AND PROFILE IN THE MEDIUM TO LONG TERM SCALES

Presented by: **CAMILO JARAMILLO CARDONA**

Supervised by: **Prof. ERNESTO MAURICIO GONZÁLEZ RODRÍGUEZ**

Prof. RAÚL MEDINA SANTAMARÍA

Santander, june of 2020

A mi familia

The sea complains upon a thousand shores.

Alexander Smith

AGRADECIMIENTOS / ACKNOWLEDGEMENTS

Transcurridos años de aprendizaje continuo, esfuerzo, dedicación y entrega, culmina una etapa fundamental en mi vida. El desarrollo de la presente tesis no habría sido posible sin el acompañamiento personal y profesional de muchas personas.

En primera instancia quisiera agradecer muy especialmente a mis directores Raúl Medina y Mauricio González, no sólo por encauzar el desarrollo de esta investigación, sino por transmitirme sus conocimientos, por brindarme incontables consejos y por permitirme ser partícipe de sus enseñanzas magistrales. Gracias a ambos por haber depositado su confianza en mí y por abrirme las puertas en vuestro equipo de trabajo.

Además de mis directores, agradezco a todos aquellos que han colaborado de forma más activa en esta investigación. A Jara Martinez por su orientación y esencialmente por ser quien me encaminó en la interesante temática abordada. A Elena Sánchez, Imen Turki y Marissa Yates por ser personas clave en la discusión y puesta en marcha de distintas metas enmarcadas en este trabajo. Mil gracias por brindarme su ayuda y transmitirme vuestros conocimientos.

Gracias Vero, Omar, Nacho, María M., Erica, Íñigo, Juan, Cris, Roland y todos aquellos miembros que hicieron y/o hacen parte del grupo de Ingeniería y Gestión de la Costa de IHCantabria en el transcurso de este tiempo. Ha sido un placer trabajar y compartir experiencias conjuntamente. Igualmente, a todos los compañeros del IHCantabria con los que he tenido la fortuna de afrontar los retos de tantos proyectos.

Asimismo, mil gracias a todos aquellos quienes más que amigos se convirtieron en mi familia en el exterior: Michele + Chiara, Alfonso, Felipe, Tommaso, Camino, Cavi + Nati, Helios + Nuria, El Okar, June, Paulinha, Laura, Germán, Coco, Dieguín, Alicia, María S., Rogacheski… Valoro enormemente haberlos encontrado en este camino y ojalá la vida nos permita múltiples oportunidades para reencontrarnos. Espero en un futuro acompañarlos en vuestras visitas al país del realismo mágico del cual les he hablado tanto; ¡mi natal Colombia!

Agradezco infinitamente a esas tres personas que son mi motor, que aun estando lejos físicamente las siento a mi lado en todo momento. GRACIAS FAMILIA por sus sabios consejos y por su apoyo incondicional en todo momento.

Por último, gracias a la Fundación Instituto de Hidráulica Ambiental de la Universidad de Cantabria por la financiación recibida para la realización de esta tesis doctoral.

List of Contents

List of Tables

List of Figures

List of Symbols

$\overline{\boldsymbol{\alpha_s(t)}}$: arithmetic mean of the shoreline orientation dataset

$\overline{\boldsymbol{S(t)}}$**:** arithmetic mean of the shoreline position dataset

∅: memory decay

∅': dimensionless shape function

a: constant

A: scale parameter

a_1: empirical coefficient

A_1: the maximum distance from the spiral pole to the coast considered by Berenguer and Enríquez (1989)

B: berm height

b: constant

B': empirical coefficient

b': linear rate of net shoreline progradation or retreat

b_1: empirical coefficient

c: calibration parameter

C^-: proportionality constant of erosion

C^+: proportionality constant of accretion

C_0, C_1, C_2: coefficients of the PBSE

$C_{\alpha s}$: free coefficient

D*: energy dissipation per unit volume

D: sediment size

D': total window width of the weighted average of ShoreFor model

D_{50}: median sediment grain size

E: wave energy

E_{eq}: equilibrium wave energy

E_y: alongshore component of the wave energy

F: forcing term

F^-: forcing term for erosion process

F^+: forcing term for accretion process

g: acceleration due to gravity

h*: closure depth

h: water depth

H_{0s}: significant wave height at undefined depths

H_b: breaking wave height

h_d: diffraction point

H_o: deepwater wave height

Hs: significant wave height

Hs_{12}: significant wave height exceeded 12 hours per year

K: constant

k: empirical coefficient

K': rapidly-varying forcing

k_1: damping coefficient

L^-: proportionality constant for counterclockwise shoreline rotation

L: wave length

L': half-length of the shoreline

L^+: proportionality constant for clockwise shoreline rotation

m: free dimensionless parameter

m': slope of the beachfront

m_1: empirical coefficient

n: number of elements in a set

n': constant

n_1: free dimensionless parameter

P: wave power

P_0: down-coast control point

R*: response rate parameter

r: erosion ratio

R: radius length

R': shoreline response

R'_{eq}: equilibrium shoreline response

R_0: control line length joining the updrift diffraction point to the down-coast control point

R_1, R_2: two consecutive radii measured from the center of a logarithmic spiral curve

S*: separation between the headlands that shelter the beach

S: shoreline position

S_0: initial shoreline position

S_{bb}: non-erodible back beach cross-shore location

$S_{data,i}$: shoreline position measured

S_{eq}: equilibrium shoreline position

S_{model}: shoreline position modeled

std(S(t)): standard deviation of the shoreline position dataset

std(α_s(t)): standard deviation of the shoreline orientation dataset

t: time

Tp: peak wave period

Ts: characteristic response time

Ts_{12}: mean wave period associated with Hs_{12}

v_{lt}: linear trend term

Vs: sediment volume in active beach profile

W*: width of the active surf zone defined out to the breakpoint

w_f: sediment fall velocity

x: distance from the coastline

X: longshore distance from the tip of the headland breakwater

X': beach parameter

x': distance along the coast

X'_{eq}: equilibrium condition of the beach parameter, X'

x_t: horizontal position to the steady toe

y': perpendicular distance to the coast

z: elevation contour

z': vertical displacement of the beach

α: characteristic constant angle between the tangent to the curve and radius at any point along the spiral (Krumbein, 1944)

α_{min}: angle that determines the location of the point P_o, (González and Medina 2001)

α_s: shoreline orientation

α_{s0}: initial shoreline orientation

α_{seq}: equilibrium shoreline orientation

α_{st}: coefficient of the PBSE

α_y: standard deviation of the shoreline

$\alpha_{\Delta\Omega}$: standard deviation of ΔΩ

β: wave obliquity

β_r: distance parameter

γ: constant of proportionality between wave height and breaking depth

ΔE: energy disequilibrium

ΔS_{eq}: equilibrium shoreline change

Δt: time step

$\Delta X'$: beach parameter disequilibrium

$\Delta \alpha_s$: shoreline orientation disequilibrium

$\Delta \Omega$: dimensionless fall velocity disequilibrium

θ: angle between wave crest and R (Hsu and Evans 1989)

θ': variable angle between R1 and R2 (Krumbein, 1944)

θ_{FE}: mean energy flux direction

θ_m: mean wave direction

θ_w: wave direction

ρ: seawater density

σ: wave radian frequency

ω: beach change rate

Ω: dimensionless fall velocity

Ω_{eq}: dimensionless fall velocity at equilibrium

List of Acronyms

1-D: One Dimension

2-D: Two Dimensions

AWAC: Acoustic Waves and Currents

BOI: Beach Orientation Index

CCA: Canonical Correlation Analysis

CCP: Cross-shore Control Profile

CNES: Centre National d'Etudes Spatiales

CP: Control Point

DGPS: Differential Global Positioning System

DLT10: model proposed by Davidson et al. (2010)

DOW: Downscaled Ocean Waves

DST13: model proposed by Davidson et al. (2013)

DT09: model proposed by Davidson and Turner (2009)

EEF: Equilibrium Energy Function

ENSO: El Niño–Southern Oscillation

ESA: European Space Agency

EWDF: Equilibrium Wave Direction Function

GOW: Global Ocean Waves

HBB: Headland Bay Beach

IH-MOOSE: MOdel Of Shoreline Evolution

JA15: model proposed by Jara et al. (2015)

LANDSAT: Land Remote-Sensing Satellite (System)

LP12: model proposed by Long and Plant, (2012)

MDA: Maximum Dissimilarity Algorithm

MHHL: Mean Higher High Water Level

MHWL: Mean High Water Level

MLLW: Mean Lower Low Water

MSL: Mean Sea Level

NAO: North Atlantic Oscillation

NCAR: National Center for Atmospheric Research

NCEP: National Center for Environmental Prediction

NIWA: National Institute of Water and Atmospheric Research

NSW: New South Wales

OPPE: Organismo Público de Puertos del Estado

PBSE: Parabolic Bay Shape Equation

PCA: Principal Component Analysis

R.I.P.S.A.: Repsol Investigaciones Petrolíferas S.A.

RBF: Radial Basis Functions

RMSE: Root Mean Square Error

RTK-GPS: Real Time Kinematic - Global Positioning System

SEBP: Static Equilibrium Beach Profile

SEP: Static Equilibrium Planform

SHOREX: SHOReline EXtraction

SMC: Coastal Modeling System

SPI: Shoreline Position Index

SPOT: Satellite Pour l'Observation de la Terre

UC: University of Cantabria

USA: United States of America

USACE: United States Army Corps of Engineers

USGS: United States Geological Survey

WEPA: West Europe Pressure Anomaly

YA09: model proposed by Yates et al., (2009)

Resumen en Castellano[1]

I. Introducción

En la actualidad, más del 66% de la población mundial vive a menos de 100 km de la costa (Biausque et al., 2016), estando el 10% en zonas costeras bajas, es decir, a menos de 10 m por encima del nivel medio del mar actual (McGranahan et al., 2007). En el futuro, se espera que la densidad poblacional aumente aún más en estas zonas debido a las altas tasas de crecimiento demográfico y de urbanización (Neumann et al., 2015), por lo que los asentamientos urbanos en las zonas bajas son especialmente vulnerables a los riesgos derivados de los cambios que sufre el litoral.

Las zonas costeras son entornos dinámicos, condicionadas por agentes tan diversos como el oleaje, los vientos, las corrientes, el nivel del mar, las modificaciones de origen antrópico, así como otros factores oceanográficos y de suministro de sedimentos a diferentes escalas espacio-temporales. Los depósitos sedimentarios costeros, como las playas, son sistemas intrínsecamente adaptables, a menudo en un estado de cuasi-equilibrio, las cuales reaccionan constantemente a las diferentes condiciones de forzamiento.

Las playas constituyen depósitos naturales de sedimentos en movimiento dinámico, donde los oleajes incidentes altamente energéticos provocan una consiguiente erosión costera, mientras que

[1]Este resumen en castellano es una versión reducida del contenido total de la tesis. Si bien contiene los fundamentos, resultados y conclusiones principales, se remite al lector a la versión en inglés para una información más detallada.

largos períodos de calma permiten la recuperación de la playa. Recientemente, Luijendijk et al., (2018) y Mentaschi et al., (2018) presentaron observaciones globales de erosión y acumulación costera a largo plazo. Según Luijendijk et al., (2018), el 24% de las playas arenosas del mundo se están erosionando a un ritmo superior a los 0,5 m/año, lo cual es motivo de gran preocupación. Además, el calentamiento de la parte superior del océano, una consecuencia del calentamiento global, está provocando un cambio en el clima del oleaje, lo que hace que las olas sean más energéticas (Reguero et al., 2019). Cabe señalar que las tormentas costeras extremas, como los huracanes y los ciclones extratropicales, pueden movilizar y redistribuir rápidamente grandes cantidades de sedimentos (Harley et al., 2017).

A partir de lo anterior, se deduce que las playas están en continuo movimiento, sufriendo acumulación y erosión en respuesta a los diversos factores. Sin embargo, cabe señalar que las playas abiertas sujetas a la deriva del transporte de sedimentos son generalmente mucho más sensibles a las condiciones cambiantes del oleaje; mientras que las playas encajadas, que están limitadas por contornos laterales son sistemas de circulación de sedimentos predominantemente cerrados (Sedrati and Anthony, 2007). Esta tesis se centra particularmente en la morfodinámica de las playas encajadas.

Las playas encajadas se caracterizan por ser sistemas cerrados en donde se da lugar a una interacción entre la hidrodinámica (oleaje, corrientes, etc.) y el transporte de sedimentos, definiendo una forma en planta y un perfil de playa. Como consecuencia, todos los procesos hidrodinámicos y sedimentarios que tienen lugar en una playa son procesos tridimensionales. Estos procesos son difíciles de analizar debido a nuestra capacidad de entenderlos y a las limitaciones de las herramientas o formulaciones existentes.

En términos generales, la morfodinámica de las playas encajadas se considera un fenómeno complejo (Biausque et al., 2016); por lo que científicos e ingenieros han asumido que la variabilidad de la línea de costa es un indicador fiable para describir el cambio global de la playa a diferentes escalas espacio-temporales (Smith and Bryan, 2007). Las observaciones de variabilidad de línea de costa resultan esenciales para cuantificar tendencias de retroceso a largo plazo, regular el desarrollo en zonas costeras y diseñar obras de protección. Por lo tanto, los gestores encargados de entornos litorales deben evaluar la posición de la línea de costa, dónde ha estado en el pasado y dónde estará en el futuro.

La posición de la línea de costa es sumamente útil para cuantificar tasas de erosión histórica (p. ej. Anders y Byrnes, 1991; Crowell et al., 1991; Moore, 2000; Mentaschi et al., 2018) y el ancho y/o volumen de la playa (p. ej. Douglas et al., 1998; Short y Trembanis, 2004; Farris y List, 2007),

principalmente con el fin de monitorizar continuamente las playas, para preservar sus funcionalidades de protección, recreación y valor natural (Jiménez et al., 2007).

Tradicionalmente, las posibles fuentes de datos para obtener posiciones de líneas de costa se limitaban a levantamientos de campo, fotografías históricas, fotografías aéreas, cartas náuticas, sistemas de radar y cámaras de vídeo. **Las posiciones de línea de costa obtenidas a partir de imágenes de satélite han sido descartadas debido a que la resolución disponible para el público es muy grosera (10 - 30 m o más), lo cual imposibilita la identificación de movimientos a pequeña escala en las costas.**

Los conjuntos de datos de posición de línea de costa son el *input* principal para calibrar, validar o predecir la evolución de la costa. Son la piedra angular de múltiples modelos de evolución, como son los modelos de una línea o "*one-line"* (p. ej. Pelnard-Considere, 1956; Hanson y Kraus, 1991; Dabees y Kamphuis, 1998), modelos de N líneas o *"multi-line"* (p. ej. Bakker, 1970; Perlin y Dean, 1979; 1983; Hanson y Larson, 2000), modelos de evolución de línea de costa tendentes al equilibrio (p. ej. Kriebel y Dean, 1993; Miller y Dean, 2004; Yates et al., 2009; Long y Plant, 2012; Davidson y Turner, 2009; Davidson et al., 2010, 2013; Castelle et al., 2014; Splinter et al., 2014; Jara et al., 2015; Doria et al., 2016), y modelos combinados (p. ej. Robinet et al., 2017; Vitousek et al., 2017). Estos modelos pueden separarse en diversas clasificaciones de acuerdo con los criterios elegidos; por naturaleza, precisión, escalas de aplicación, dirección principal de los procesos involucrados, entre otros.

Por ejemplo, dependiendo de la escala temporal de aplicación, hay modelos de corto plazo (horas-días), medio plazo (días-año) y largo plazo (años-décadas). Mientras que, dependiendo de la escala espacial, se pueden distinguir modelos de pequeña escala (decenas de metros), mediana escala (cientos de metros) y gran escala (kilómetros).

De acuerdo con Hanson et al., (2003) todavía no existe un modelo universal que permita analizar y predecir la evolución de la costa y sus procesos en las diferentes escalas espacio-temporales. En cambio, dependiendo de la naturaleza y los objetivos del proyecto objeto de estudio, existe una amplia gama de modelos disponibles, cada uno de los cuales se centra en un problema complejo desde un punto de vista específico.

La presente tesis se enfoca en el desarrollo de modelos de evolución de posición de línea de costa tendentes al equilibrio. Estos modelos resultan ser los más simples, pues requieren el menor número de parámetros de calibración, son computacionalmente eficientes y pueden ser aplicados para investigar cambios morfológicos de medio y largo plazo (Davidson and Turner, 2009).

Conceptualmente, estos modelos se basan en el equilibrio entre fuerzas destructivas y constructivas que actúan sobre una playa. En términos generales, se establecen sobre la siguiente ecuación cinética de primer orden:

$$\frac{dX'(t)}{dt} = \mathrm{K}' \cdot \Delta X' \tag{1}$$

donde el parámetro morfológico X' varía a lo largo del tiempo, $\frac{dX'(t)}{dt}$, dependiendo del producto entre un forzamiento que varía rápidamente, K', y el desequilibrio existente del parámetro X' a lo largo del tiempo, $\Delta X'$. Este desequilibrio es la diferencia entre las condiciones actuales y un equilibrio teórico (por ejemplo, $\Delta X' = X' - X'_{eq}$). Tal como establecen Madsen y Plant, (2001) un conjunto particular de condiciones del oleaje incidente está asociado a un correspondiente estado de equilibrio estable de la playa. Esto es, si las condiciones del oleaje son estables, la playa se aproximará asintóticamente a un estado independiente del estado inicial.

El parámetro, K', es función tanto de las condiciones del oleaje predominantes (p. ej. la energía, E, o la potencia del oleaje, P) como de las características morfológicas de la playa, tales como el tamaño medio de sedimento, D_{50}, la longitud de la playa, l, la profundidad de cierre, h*, entre otros.

Cabe señalar que el uso de estos modelos ha aumentado en los últimos años, gracias a su fácil y eficaz aplicación. Hasta la fecha, a partir de la hipótesis de ortogonalidad de los procesos que tienen lugar en las playas, estos modelos se han separado en función a la dirección del transporte de sedimentos, en sentido transversal o longitudinal, respondiendo únicamente a los movimientos del perfil de la playa o a la variabilidad de la forma en planta de la playa.

Tal como se presenta más adelante en la sección 2.5, existen múltiples propuestas de modelos empíricos de evolución de línea de costa tendentes al equilibrio que contemplan únicamente procesos de transporte transversal o "*cross-shore"*; sin embargo, **en la literatura hay pocas propuestas de este tipo de modelos que consideren los procesos de transporte longitudinal o "*longshore"*, que dan lugar a rotación de la playa.**

Hasta ahora, los modelos de evolución de línea de costa tendentes al equilibrio para transporte *cross-shore* han sido empleados en múltiples estudios, asumiendo que la variación de la costa ocurre de diferentes maneras (p. ej., la posición de la costa como un punto o un tramo lineal que avanza/retrocede); sin embargo, **ningún autor ha evaluado dicha variación por medio de un modelo de evolución tendente al equilibrio, que considere la playa en toda su extensión con una forma en planta curva. Por lo tanto, con el objetivo de reproducir la evolución de la**

costa de playas encajadas, es esencial combinar los procesos de transporte transversal y longitudinal en un único modelo de complejidad reducida.

Además, cabe señalar que la mayoría de las playas alrededor del mundo tienen una tendencia de avance o retroceso progresivo durante años o incluso décadas, y este patrón es producto de múltiples factores, que pueden ser de origen natural o antrópico. **Por lo tanto, para predecir la variabilidad de la costa en tales casos, los modelos numéricos de evolución morfológica deben contemplar una tasa de cambio para ganancia o pérdida neta de sedimentos.**

Por todo lo anterior, es de gran interés centrarse en evaluar la variabilidad de las playas encajadas y analizar cómo se adaptarán estas playas a las condiciones cambiantes del oleaje. Más específicamente, es de sumo interés continuar desarrollando mejoras e integraciones de procesos (cross-shore y longshore) considerando los modelos de evolución de la línea de costa tendentes al equilibrio.

a. Preguntas de investigación

A continuación, se presentan las preguntas de investigación (PI) propuestas:

- **PI1**: ¿Es posible calibrar y validar los modelos de evolución de la línea de costa tendentes al equilibrio empleando imágenes satelitales de resolución media?
- **PI2**: ¿Cómo podría incluirse la variabilidad del volumen del perfil de la playa en los modelos de evolución de posición de línea de costa tendentes al equilibrio?
- **PI3**: ¿Es posible modelar la variabilidad de la costa de playas encajadas en el medio-largo plazo?
- **PI4**: ¿Cómo modelar la rotación de la línea de costa en planta a medio y largo plazo?

A lo largo del desarrollo de esta tesis se irá respondiendo a las preguntas de investigación citadas.

b. Objetivos de la tesis

A partir de la motivación expuesta anteriormente, y las preguntas de investigación presentadas en la sección anterior, el objetivo principal de esta tesis es desarrollar un nuevo modelo de evolución de línea de costa tendente al equilibrio considerando planta y perfil de playa, en escalas de medio a largo plazo.

Este objetivo principal se logra mediante la consecución de objetivos específicos, que se corresponden en este caso con los temas de cada uno de los capítulos principales de esta tesis:

- Evaluar la aplicabilidad de las imágenes satelitales de resolución media para la calibración y validación de modelos de evolución de línea de costa tendentes al equilibrio (respondiendo a la PI1).

- Desarrollar un modelo de evolución de la línea de costa tendente al equilibrio considerando la variabilidad del volumen del perfil de playa (respondiendo a la PI2).
- Desarrollar un nuevo modelo basado en formulaciones de planta y perfil de equilibrio aplicable a playas encajadas (respondiendo a la PI3).
- Desarrollar un nuevo modelo de evolución de rotación de línea de costa tendente al equilibrio (respondiendo a la PI4).

c. Estructura de la tesis

La tesis consta de ocho capítulos y se estructura de la siguiente forma:

El capítulo 1 incluye una introducción general, presenta la motivación de la tesis y establece el objetivo general de estudio junto con los objetivos específicos.

En el capítulo 2 se presentan los antecedentes generales y el estado del arte en relación a las playas encajadas, las condiciones de equilibrio (planta y perfil) de las playas, la definición de la línea de costa y, por último, una descripción detallada de los desarrollos previos relacionados con modelos de evolución de línea de costa.

En el capítulo 3 se presenta un análisis comparativo entre conjuntos de datos de posición de línea de costa obtenidos a partir de sistemas de videocámara y de imágenes de satélite, con el fin de explorar la aplicabilidad de las imágenes de satélite de resolución media con un algoritmo de resolución sub-pixel para la calibración y validación de modelos de evolución de línea de costa tendentes al equilibrio. (Como resultado de este capítulo se ha publicado un artículo en *Journal of Coastal Research* (Jaramillo et al., 2020d)).

El capítulo 4 presenta un modelo de evolución de posición de línea de costa tendente al equilibrio que incluye una componente de tasa de cambio para considerar ganancias o pérdidas de sedimento. Esta componente a su vez modifica la relación de equilibrio entre posición de línea de costa y energía incidente del oleaje, como una función que avanza o retrocede con el tiempo. (Como resultado de este capítulo se ha publicado un artículo en *Coastal Engineering* (Jaramillo et al., 2020b)).

El capítulo 5 presenta un nuevo modelo de evolución de línea de costa tendente al equilibrio basado en la integración de planta y perfil de playa. Este modelo es aplicable exclusivamente a playas encajadas y está influenciado principalmente por el desplazamiento cross-shore. (Como resultado de este capítulo, se ha elaborado un artículo que se encuentra en revisión en *Coastal Engineering*).

El capítulo 6 presenta un nuevo modelo de rotación de la línea costera tendente al equilibrio, asumiendo que el movimiento de rotación de la playa es inducido por la potencia y dirección del

oleaje incidente. (Como resultado de este capítulo, se ha elaborado un artículo que se encuentra en revisión en *Coastal Engineering*).

Finalmente, en el capítulo 7 se resumen los principales resultados y conclusiones de la tesis. Además, en este capítulo se presentan futuras líneas de investigación.

II. Antecedentes y conceptos básicos

A continuación, se presenta un breve resumen de antecedentes y conceptos básicos, siendo este una base fundamental previa al desarrollo de los modelos de evolución de posición de línea de costa propuestos en esta tesis. Esta revisión bibliográfica permite, por un lado, identificar carencias en el estado del arte, contextualizar las nuevas aportaciones realizadas y, por otro, exponer las herramientas existentes.

En las secciones III a VI se resumen los aportes de esta tesis, resaltando las carencias que se identificaron en el estado del arte y que motivaron el desarrollo del presente estudio.

a) Playas encajadas

Las playas encajadas se encuentran a lo largo de la mayoría de los márgenes continentales e insulares del mundo, representando aproximadamente el 50% de la costa mundial (Inman and Nordstrom, 1971). Se trata de unidades fisiográficas en las que tanto el perfil como la forma en planta de la playa están confinados lateralmente por contornos impermeables naturales o artificiales, y el fondo está cubierto en su mayor parte por arena. Los promontorios laterales afectan la hidrodinámica y las condiciones del oleaje, lo que resulta en un equilibrio entre la circulación del flujo y la respuesta de la línea de costa. Esta interacción se traduce en formas características de las playas encajadas (Daly et al., 2014), generalmente conocidas en inglés como "*curved*", "*crenulated*", "*embayed*", "*hooked*", "*pocket*" o "*headland-bay beaches*".

b) Condición de equilibrio estático en playas

Según González et al., (2010), la hipótesis de equilibrio determina: si la acción de las dinámicas actuantes se mantiene indefinidamente, la forma de la playa alcanzará una posición final constante, que puede denominarse "playa de equilibrio". La playa alcanza su estado de equilibrio desde el momento en que no se presentan cambios en su forma en planta o en su perfil. Se dice que está en equilibrio estático cuando el transporte neto de arena es nulo.

La existencia de una playa encajada en perfecto estado de equilibrio estático sólo puede obtenerse en un laboratorio, donde es posible controlar el oleaje incidente. En la naturaleza las olas y el nivel del mar están cambiando constantemente; sin embargo, esas variaciones hidrodinámicas están acotadas, lo cual se traduce en que las variaciones de las playas también están limitadas. Por

lo anterior, en la naturaleza, se puede admitir la existencia de una playa en equilibrio estático que sufre variaciones en función al clima marítimo existente.

A partir de lo anterior, varios autores han despertado su interés por proponer múltiples formulaciones empíricas, que intentan reproducir las condiciones de equilibrio estático tanto del perfil de la playa como de la forma en planta de la playa:

- *Perfil de equilibrio estático:* en la literatura se encuentran múltiples propuestas considerando el perfil de playa en un tramo (p. ej. Bruun 1954; Wright et al., 1982; Boon y Green 1988; Bowen 1980; Dean 1991; Kriebel et al., 1991; Vellinga 1983; Komar y Mcdougal 1994), dos tramos (p. ej. Inman et al., 1993; Bernabeu 1999; Larson et al., 1999) o incluso tres tramos (p. ej. Requejo et al., 2008). Entre los perfiles citados el más ampliamente utilizado es el perfil propuesto por Dean, (1991).
- *Forma en planta de equilibrio estático:* en la literatura se tienen numerosas propuestas considerando la forma en planta de la playa ajustada a expresiones como espiral logarítmica (p. ej. Krumbein 1944; Silvester 1960; Yasso 1965; Berenguer y Enríquez 1989), parabólica (p. ej. Hsu y Evans 1989; Tan y Chiew 1994; González y Medina 2001) o tangente hiperbólica (p. ej. Moreno y Kraus 1999). Entre las formulaciones citadas, la más conocida y empleada en el campo de ingeniería costera es la expresión parabólica propuesta por Hsu y Evans (1989).

c) Definición de línea de costa

Debido a la dinámica espacio-temporal del oleaje tanto longitudinal como transversalmente y a la influencia de la dinámica del nivel del mar, la interfaz de separación entre tierra y agua no es un concepto idealizado evidente que defina una única "posición de línea de costa" para una zona costera específica. Sin embargo, este criterio es fundamental para definir la línea de costa instantánea como la posición de la interfaz agua-tierra en un momento dado.

En la literatura, la definición de línea de costa ha sido ampliamente investigada en base a consideraciones geográficas, morfológicas o hidrológicas (p. ej. Fenster et al., 1993; Camfield y Morang 1996; Douglas et al., 1998; Moore, 2000; Boak and Turner 2005; Toure et al., 2019).

Con el fin de obtener la posición de la línea de costa, existen diversas fuentes de datos, tales como levantamientos de campo, fotografías históricas, imágenes de video-cámaras, imágenes satelitales, entre otros.

d) Movimientos de la línea de costa

Varios autores han analizado el comportamiento de las playas con el fin de identificar los modos dominantes del movimiento de la línea de costa (p. ej. Miller y Dean 2007; Turki et al., 2013b;

Ratliff y Murray 2014; Blossier et al., 2017). De acuerdo a la mayoría de los estudios existentes, la variabilidad de la costa en playas encajadas se puede descomponer en tres movimientos principales: 1) movimiento de traslación relacionado con intercambios de sedimentos entre la costa y el mar (p. ej. Davidson et al., 2013; Palalane et al., 2016), 2) movimiento de rotación, el cual está asociado a la oblicuidad del oleaje incidente y a la consiguiente transferencia de sedimentos desde un extremo de la playa hacia el otro (p. ej. Klein et al., 2002; Thomas et al., 2010; Turki et al., 2013) y 3) movimiento de respiración o pulsación de la playa, que está asociado a gradientes de energía a lo largo de la playa (p. ej. Ratliff y Murray, 2014). La Fig. 1 presenta de forma esquemática estos 3 movimientos.

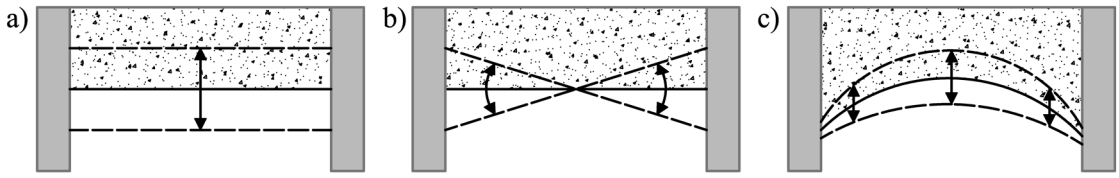

Fig. 1. Movimientos de la línea de costa: a) traslación, b) rotación y c) pulsación.

e) Modelos de evolución de línea de costa tendentes al equilibrio

La presente tesis se centra en el desarrollo de modelos de evolución de línea de costa tendentes al equilibrio. Estos modelos se basan conceptualmente en el equilibrio entre las fuerzas destructivas y constructivas que actúan sobre una playa, permitiéndonos obtener la posición de la línea de costa en un momento dado, bien sea debido a la acción de tormentas, cambios estacionales y/o cambios provocados por efectos interanuales.

El enfoque de estos modelos puede descomponerse de acuerdo con la dirección del transporte de sedimentos; transporte longitudinal o "*longshore*", que se da lugar a lo largo de la playa y transporte transversal o "*cross-shore*" que se da lugar perpendicularmente a la costa.

En la literatura se tienen múltiples propuestas de modelos de evolución de posición de línea de costa tendentes al equilibrio que consideran únicamente el desplazamiento transversal de la costa (p. ej. Wright y Short 1984; Kriebel y Dean 1993; Miller y Dean 2004; Yates et al., 2009; Long y Plant 2012; Davidson y Turner 2009; Davidson et al., 2010; 2013; Castelle et al., 2014; Splinter et al., 2014; Jara et al., 2015; Doria et al., 2016). Por otro lado, existen pocas propuestas de este tipo de modelos considerando el transporte longitudinal de sedimentos (p. ej. Turki et al., 2013a; Blossier et al., 2015; 2017). Hasta la fecha, no existe ningún modelo de evolución de costa tendente al equilibrio que integre los movimientos transversal y longitudinal.

En los siguientes apartados se presentan los principales resultados de esta tesis y la justificación de los mismos. La Fig. 2 recoge la localización de las zonas de estudio seleccionadas.

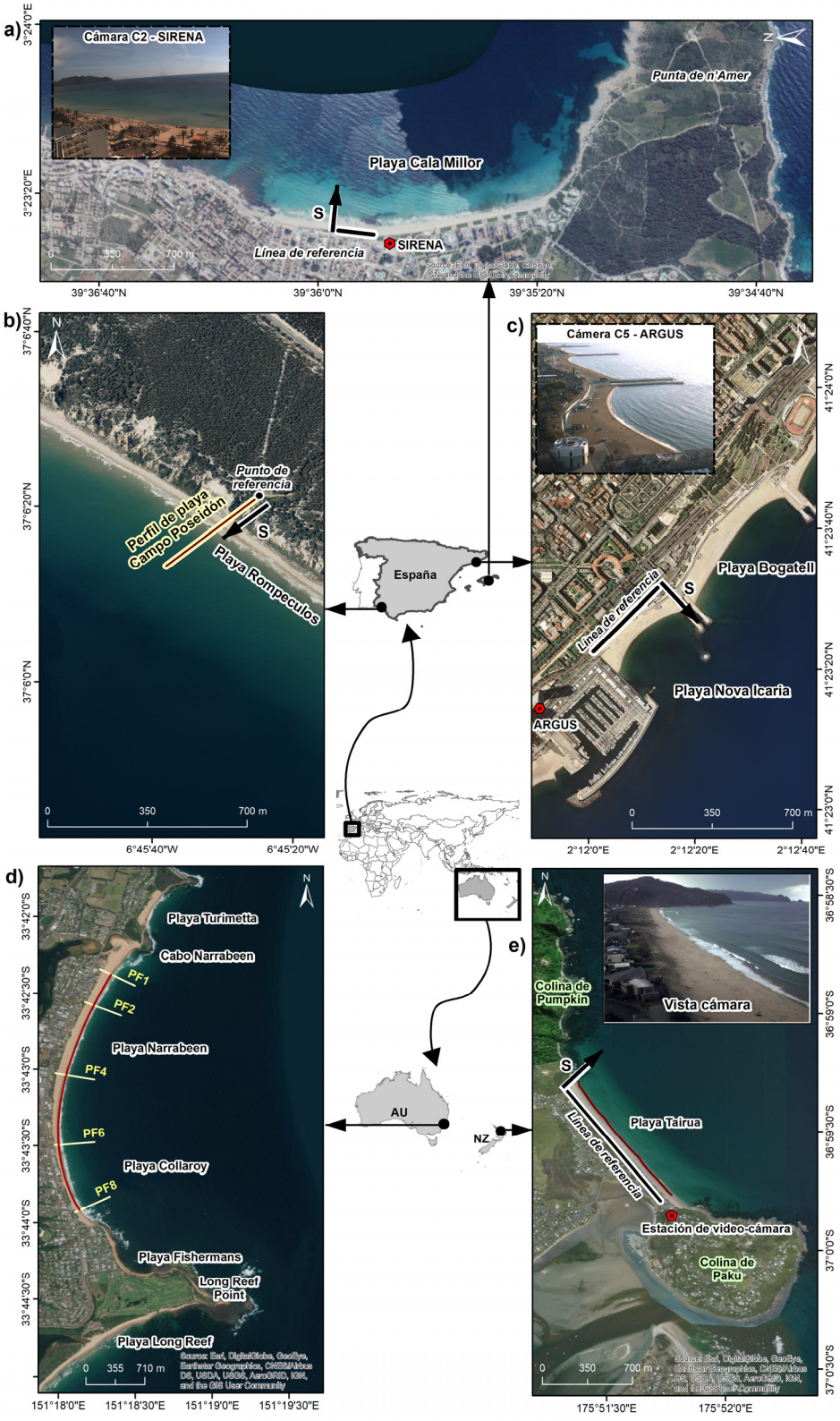

Fig. 2. Localización de zonas de estudio seleccionadas: a) playa de Cala Millor, b) perfil de playa Campo Poseidón, c) playa de Nova Icaria, d) playa de Narrabeen y e) playa de Tairua. En los distintos mapas se incluye la ubicación de las fuentes de información, bien sean levantamiento de perfiles o imágenes a partir de sistemas de videocámara. Además, se indica la referencia a partir de la cual se mide la posición de la costa, S.

III. Líneas de costa derivadas de imágenes de satélite para su uso en modelos de evolución de línea de costa tendentes al equilibrio

Tal como se mencionó anteriormente, los datos de posición de línea de costa han sido considerados la piedra angular de los modelos morfodinámicos, entre ellos, los modelos de evolución de línea de costa tendentes al equilibrio, que son el enfoque de la presente tesis.

Hasta hace tan solo unos años, los registros históricos de datos de líneas de costas se obtenían a partir de exhaustivas campañas de campo. Este tipo de compilación de datos tiene algunas limitaciones fundamentales, como, por ejemplo, que son relativamente costosas y tan solo permiten obtener datos en puntos específicos. Sin embargo, en la actualidad existen diversas fuentes alternativas, como fotografía aérea, radar, sistemas de videocámara e imágenes satelitales.

En la gran mayoría de las zonas costeras, los datos históricos son limitados o inexistentes; por lo tanto, la elección de qué datos usar en un sitio específico generalmente está determinada por la disponibilidad de datos (Boak y Turner, 2005). De esta manera, las imágenes satelitales son la única fuente de datos que tiene la gran ventaja de cubrir grandes áreas a lo largo del mundo e incluyen cobertura regular de la mayoría de las costas durante todos los climas y estaciones.

La principal limitación de los datos satelitales para los estudios costeros es su resolución. La mayoría de los datos satelitales disponibles para el público tiene una resolución de 10 a 30 m o más, lo cual imposibilita identificar la variabilidad espacial de pequeña escala. Por este motivo, el propósito de este estudio es evaluar la aplicabilidad de líneas de costa obtenidas a partir de imágenes satelitales procesadas con un algoritmo de mejora de resolución, para su uso en la calibración y validación de modelos de evolución.

Entre los diversos modelos de evolución de línea de costa existentes en la literatura (véase Sección II-e)), se seleccionaron en este estudio, los propuestos por Yates et al. (2009) (en adelante "YA09") y Jara et al. (2015) (en adelante "JA15"). El primero es probablemente el modelo más empleado de este tipo en los últimos años; mientras el segundo es un novedoso modelo que requiere el menor número de parámetros de calibración entre todos los modelos de la misma tipología. Ambos se basan en una ecuación cinética de primer orden, donde la variación de la posición de línea de costa a lo largo del tiempo, $\frac{\partial S(t)}{\partial t}$, es función de unas constantes de calibración ($C^{\pm}$, siendo C^{+} una constante de proporcionalidad de acreción y C^{-} una constante de erosión), la energía incidente, E, y la energía de equilibrio, E_{eq}:

$$\frac{\partial S(t)}{\partial t} = f(C^{\pm}, E, E_{eq}) \tag{2}$$

El algoritmo empleado para extraer líneas de costa con precisión sub-píxel a partir de imágenes de satélite de resolución media es conocido como SHOREX (*SHOReline EXtraction system)* (Pardo-Pascual et al. 2018; Palomar-Vázquez et al. 2018). Este algoritmo ha sido probado en estudios previos (Pardo-Pascual et al. 2018; Almonacid-Caballer et al. 2016; Sánchez-García et al. 2015), en los cuales los resultados han alcanzado una precisión aproximada de 5 m en la determinación de la posición de la costa.

A partir de lo anterior, en este capítulo se presenta un análisis comparativo mediante la calibración y validación de los modelos de evolución seleccionados (YA09 y JA15), empleando conjuntos de datos de líneas de costa derivados de sistemas de vídeo-cámara e imágenes de satélite procesadas con el algoritmo SHOREX.

Los modelos de evolución se aplicaron en dos playas situadas en el litoral mediterráneo de España, expuestas a régimen micromareal (ver Fig. 2a y Fig. 2c). Por un lado, se analizaron alrededor de 4 meses en la playa de Nova Icaria, Barcelona, en donde las líneas de costa a partir de imágenes derivadas del sistema de video-cámara ARGUS se utilizaron como referencia. Por otro lado, se evaluó la evolución de la costa durante un año y medio en la playa de Cala Millor, Mallorca (ver ejemplo de resultado en Fig. 3). En este caso las líneas de costa obtenidas a partir del sistema de video-cámara SIRENA se utilizaron como referencia.

Cabe señalar que en este estudio se eligió el indicador *instantaneous water line* (ver Sección 2.4) para definir la posición de línea de costa tanto a partir de los sistemas de video-cámaras (ARGUS y SIRENA) como de las imágenes de satélite (SHOREX).

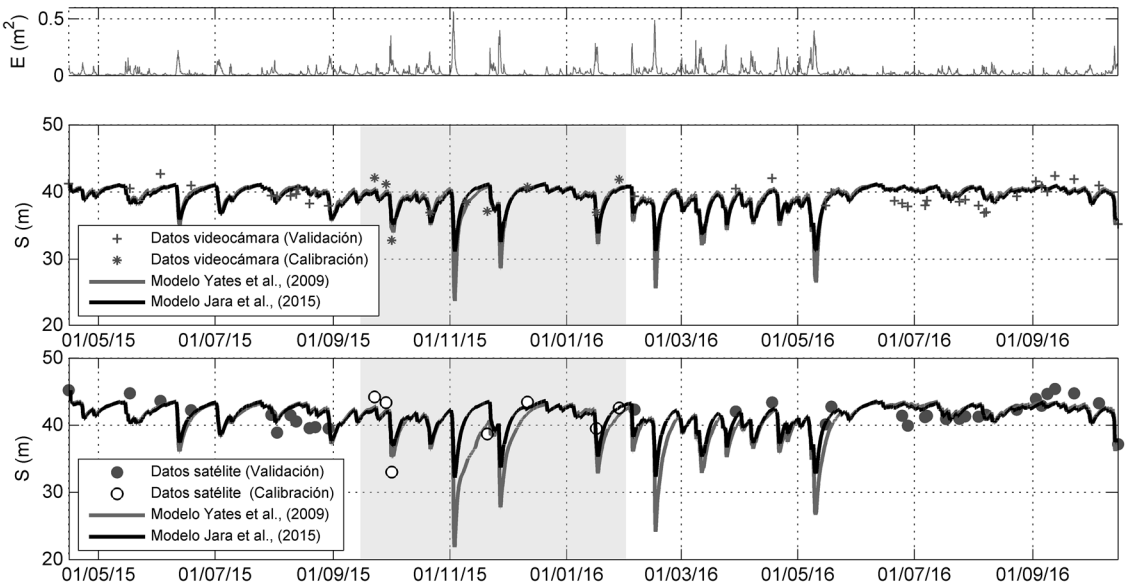

Fig. 3. Resultados en la playa de Cala Millor. Series temporales de energía del oleaje incidente (panel superior), validación de los modelos de evolución seleccionados empleando costas derivadas de videocámara (panel central), y validación de los modelos de evolución seleccionados empleando costas derivadas de satélites procesadas con el algoritmo SHOREX (panel inferior). El área sombreada es el período de estudio seleccionado para calibración.

Los resultados obtenidos en ambas playas revelaron que los modelos de evolución seleccionados (YA09 y JA15) representan adecuadamente la tendencia general de erosión-acreción de la costa tanto con mediciones obtenidas a partir de videocámara como de satélite. A partir de lo anterior, se concluyó que el procesamiento subpixel de imágenes satelitales es una técnica prometedora que es extremadamente útil para monitorizar y predecir cambios en las playas y resulta de suma utilidad como fuente de información para emplear los modelos de evolución de línea de costa tendentes al equilibrio en cualquier lugar del mundo.

IV. Modelo de evolución de línea de costa que considera la variabilidad del volumen en el perfil de playa

La mayoría de las playas arenosas de todo el mundo sufren una tendencia progresiva de avance o retroceso de la línea de costa durante años o incluso décadas (Mentaschi et al., 2018), y este patrón es producto de múltiples factores, que pueden ser de origen natural o antrópico, como la deriva de sedimentos a lo largo de la costa, la descarga de sedimentos por los ríos, las obras de regeneración costera, la erosión de los sistemas dunares, el retroceso de los acantilados, el transporte eólico de sedimentos, entre otros. **Por lo tanto, para predecir en el medio-largo plazo la variabilidad de la costa en estos casos, los modelos de evolución deben contemplar una tasa de cambio debido a ganancia o pérdida neta de sedimentos, no existiendo en la**

actualidad modelos de evolución de línea de costa basados en una relación de equilibrio que tengan en cuenta esta variabilidad de volumen.

Jara et al. (2015) concluyeron que en los modelos de evolución de línea de costa basados en una relación de equilibrio, relación biunívoca entre posición de costa y energía del oleaje conocida como *Equilibrium Energy Function, EEF*, esa relación está implícitamente influenciada por las características morfológicas de la playa, como lo es el volumen de arena contenido en la unidad fisiográfica. Así entonces una EEF constante es aplicable a sitios en donde se conserva el volumen de arena, pero no lo es para zonas en las que se presenta un déficit o superávit de volumen neto de sedimentos. **Con base en lo anterior, el objetivo de este capítulo es presentar un nuevo modelo de evolución de posición de línea de costa tendente al equilibrio considerando una tasa de variabilidad de volumen del perfil de playa.**

El modelo propuesto se basa en la formulación presentada por Yates et al., (2009):

$$\frac{dS(t)}{dt} = C^{\pm} E^{1/2} \cdot \left(E - E_{eq}\right) \tag{3}$$

donde S(t) y E son la posición de costa y la energía del oleaje incidente, respectivamente en el tiempo "t", $E^{1/2}$ es la raíz cuadrada de la energía considerada como un factor de ponderación del modelo, $C^{\pm}$ son constantes de proporcionalidad: de acreción, C^{+}, cuando $\Delta E < 0$, o erosión, C^{-}, cuando $\Delta E > 0$. El valor de E_{eq} es determinado en el modelo YA09 mediante una función lineal que sigue la expresión:

$$E_{eq}(S) = aS + b \tag{4}$$

donde a y "b" son parámetros de calibración.

A continuación, Yates et al. (2009) definieron la posición de costa de equilibrio, S_{eq}, para una determinada energía del oleaje, tal como sigue:

$$S_{eq} = \frac{E - b}{a} \tag{5}$$

La correlación analítica de la Ec. (5) es la EEF definida previamente (Jara et al., 2015). Básicamente, esta correlación es la piedra angular de los modelos de evolución de línea de costa basados en una condición de equilibrio.

Sabiendo que una EEF constante es válida únicamente para sitios de estudio que preservan el volumen de sedimento a lo largo del tiempo, en este estudio se propone una extensión al modelo YA09 incluyendo un término de tendencia lineal, v_{lt}, que modifica el comportamiento de la EEF,

para considerar los efectos de ganancia o pérdida de sedimentos a lo largo de la playa. Así entonces, la Ec. (5) debe evolucionar en el tiempo de tal forma que la relación sea una función creciente o decreciente, dependiendo de la tasa de ganancia/pérdida de sedimentos que actúe sobre la unidad fisiográfica. En este estudio, el EEF adopta la siguiente forma:

$$S_{eq} = \frac{E - b}{a} + v_{lt} \cdot t \tag{6}$$

La Fig. 9 presenta un ejemplo de la EEF en el modelo propuesto, basado en el sitio de estudio de la playa de Nova Icaria. El panel superior de la Fig. 9 muestra solo un mes de la serie temporal de energía de oleaje incidente, y el panel inferior ilustra la correspondiente aproximación empírica de la EEF (línea negra). Los puntos son medidas consecutivas que están coloreados de acuerdo con la tasa de cambio de la línea de costa.

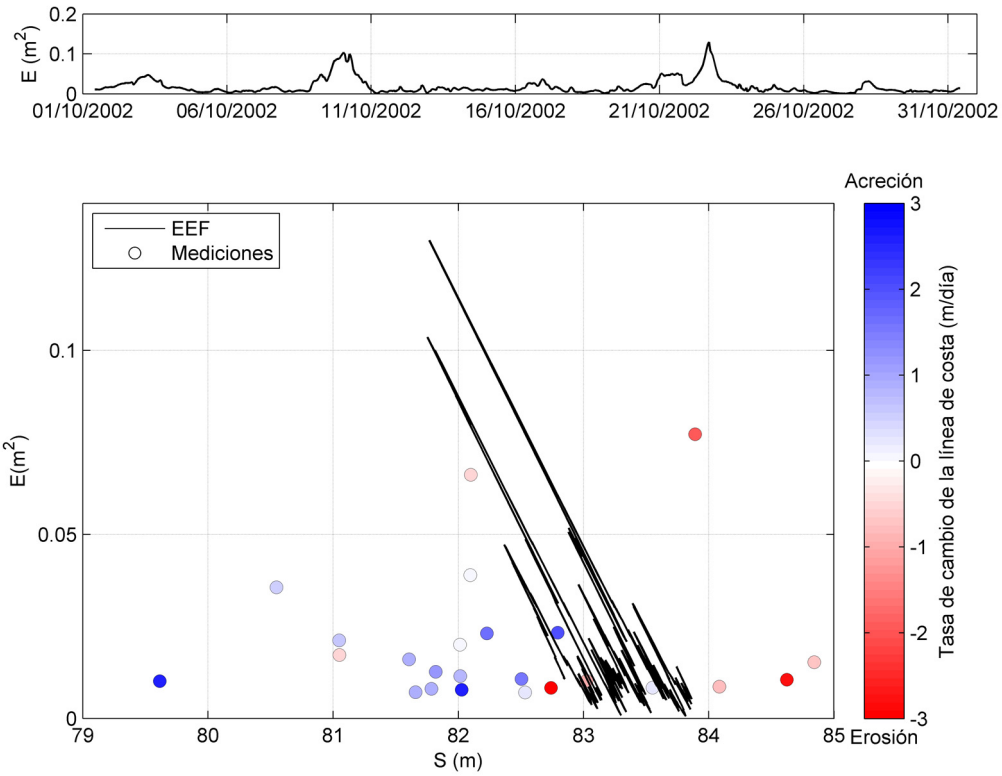

Fig. 4. Un mes de la serie temporal de energía del oleaje incidente en la playa de Nova Icaria (panel superior) como forzamiento de la EEF (línea negra en el panel inferior). Los puntos son medidas consecutivas que están coloreadas de acuerdo con la tasa de cambio de la línea de costa.

Cabe señalar que el término de tendencia v_{lt}, puede obtenerse a partir de registros históricos de evolución de línea de costa (tan extensos como sea posible) o evaluando, por ejemplo, la tasa de transporte media anual de sedimentos calculada a partir de oleaje histórico propagado a costa.

El modelo propuesto se aplicó en dos sitios de estudio de la costa española (ver Fig. 2b y Fig. 2c). Por un lado, un año y medio de datos de posición de línea de costa obtenidos a partir del sistema de videocámara ARGUS en la playa de Nova Icaria, Cataluña, se utilizaron para evaluar la evolución de la costa durante un periodo de aportación de sedimentos, que se atribuye a un proceso de *bypass* de arena procedente de la playa de Bogatell (ver resultados en Fig. 5). Por otro lado, se utilizaron 16 años de datos de posición de línea de costa obtenidos a partir de levantamientos de perfil de playa en Campo Poseidón, Huelva, para reproducir la evolución de la costa, teniendo en cuenta la tendencia de pérdida de sedimentos debida a la deriva de sedimentos a lo largo de la playa.

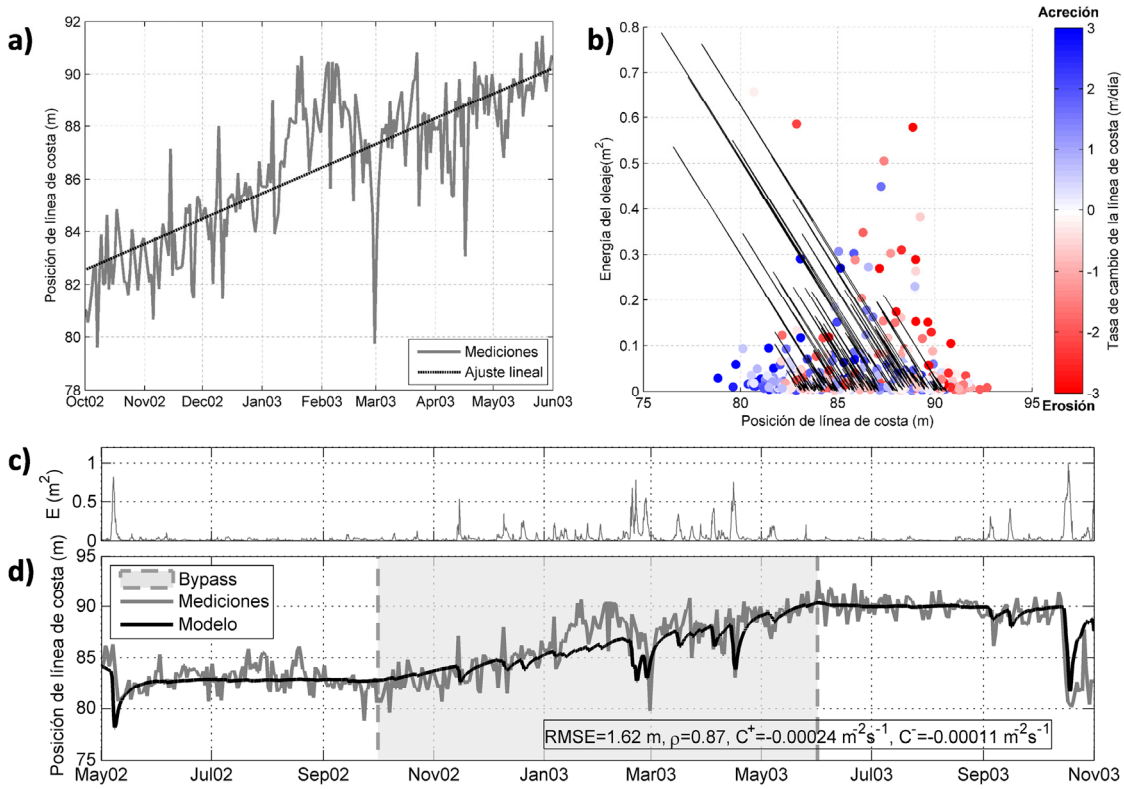

Fig. 5. Resultados para la playa de Nova Icaria. a) Ajuste lineal a la evolución de la línea de costa durante el periodo de bypass. b) EEF (línea negra) considerando el periodo de estudio completo. c) Serie temporal de energía incidente del oleaje en el punto de rotura. d) Validación del modelo de evolución de línea de costa propuesto.

Los resultados obtenidos en ambos sitios de estudio utilizando el modelo propuesto mostraron un desempeño general satisfactorio. El modelo representó con éxito las oscilaciones generales de erosión-acreción y la tendencia progresiva de ganancias o pérdidas de sedimentos a través de la relación evolutiva entre la posición de equilibrio de la línea de costa y la energía incidente del oleaje.

V. Modelo de evolución de línea de costa en playas encajadas, basado en formulaciones cross-shore y de forma en planta de equilibrio

Los modelos de evolución de línea de costa tendentes al equilibrio para movimiento cross-shore se han utilizado en múltiples estudios asumiendo la variación de la posición de la línea de costa de diferentes maneras: 1. posición de costa como un punto que avanza/retrocede a lo largo de un perfil de playa (ver Fig. 6a), 2. posición de costa como la distancia promedio a lo largo de un tramo de playa (ver Fig. 6b) o 3. posición de costa como la distancia promedio a lo largo de toda la playa asumida como un ajuste lineal (ver Fig. 6c). **Hasta la fecha, ningún autor ha considerado la variación cross-shore de la línea de costa en playas encajadas (forma en planta curva), mediante un modelo de evolución tendente al equilibrio (ver Fig. 6d).**

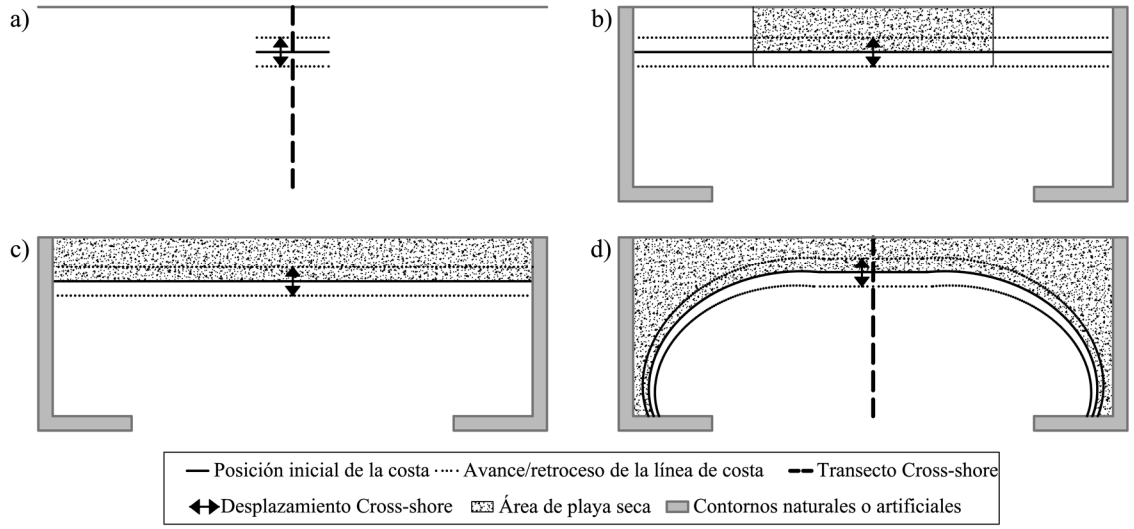

Fig. 6. Esquema de variabilidad costera en sentido "cross-shore", considerando a) punto a lo largo de un perfil de playa, b) tramo de costa monitorizado, c) playa como un ajuste lineal y d) playa encajada con forma curva.

Cabe señalar que la evolución de la playa en forma curva es posible obtenerse mediante los modelos de evolución existentes; sin embargo, se requeriría la discretización de la playa en transectos o tramos, y a continuación, el modelo se debería aplicar a cada uno de ellos, lo cual implica múltiples calibraciones y un alto coste computacional.

A partir de lo anterior, **el propósito de este capítulo es presentar un nuevo modelo de evolución de línea de costa y/o área de playa seca para playas encajadas, denominado IH-MOOSE (*MOdel Of Shoreline Evolution*)**, mediante la integración de un modelo de evolución cross-shore (se ha seleccionado el modelo propuesto por Yates et al., 2009) y una expresión de forma en

planta de equilibrio (se ha seleccionado la formulación propuesta por Hsu y Evans 1989), aplicable a escalas de tiempo que pueden abarcar días, meses o varios años.

El modelo propuesto se basa en dos hipótesis fundamentales: 1) el perfil y la forma en planta de la playa tienden a una forma de equilibrio, y 2) el perfil y la forma en planta de la playa están vinculados, de tal forma que cualquier variación en la posición de la línea de costa debido al proceso cross-shore afectará la forma en planta de la playa y viceversa.

El modelo IH-MOOSE considera únicamente la traslación o movimiento cross-shore de la línea de costa, no incluyendo los movimientos de rotación o pulsación de la playa. El modelo asume que todos los contornos batimétricos siguen una forma parabólica, con lo cual el avance/retroceso de la línea de costa corresponde a un movimiento homotético entre parábolas (ver esquema general en Fig. 7).

En general, el modelo IH-MOOSE pasa de considerar la variabilidad de la costa en una única sección a evaluar toda la evolución de la costa en playas encajadas.

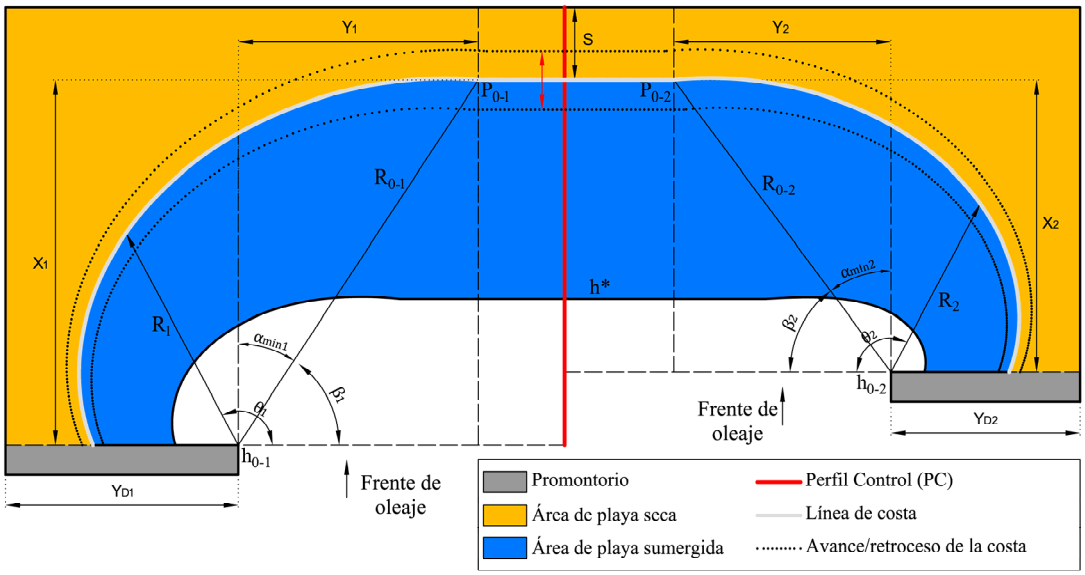

Fig. 7. Esquema del modelo IH-MOOSE considerando una playa totalmente encajada con dos promontorios que gobiernan la difracción del oleaje en los extremos. La línea roja corresponde al perfil de control (PC), mientras que la línea gris es la línea de costa en forma parabólica. Las variables con el subíndice 1 están relacionadas con la parábola izquierda, mientras que el subíndice 2 se refiere a la parábola derecha.

La Fig. 8 presenta de forma resumida en un diagrama de flujo el procedimiento de cálculo propuesto para el modelo IH-MOOSE. La descripción detallada de cada uno de los pasos se presenta en la versión inglesa de esta tesis en la Sección 5.2.3.

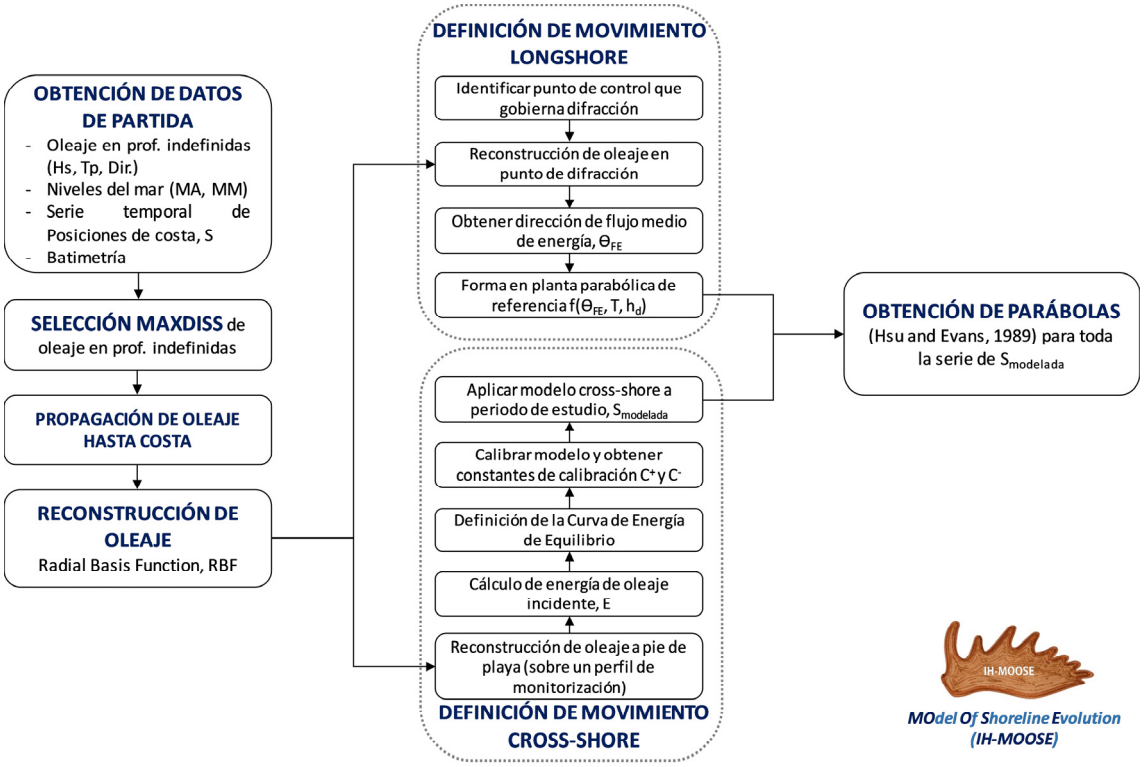

Fig. 8. Diagrama de flujo del modelo IH-MOOSE.

El modelo propuesto ha sido aplicado en la bahía de Collaroy-Narrabeen, Australia (ver Fig. 2d) en donde se ha obtenido un buen desempeño general, logrando reproducir con éxito la tendencia general de acreción/ erosión de toda la costa. Por un lado, se contrastaron las posiciones de línea de costa modeladas con respecto a la serie temporal de costas medidas en cada uno de los 5 perfiles monitorizados a lo largo de la playa. Por otro lado, como producto derivado del modelo, se contrastó la evolución de área de playa seca modelada versus medida (ver Fig. 9). Para calcular el área de playa seca se siguió el procedimiento descrito en el Apéndice 4.

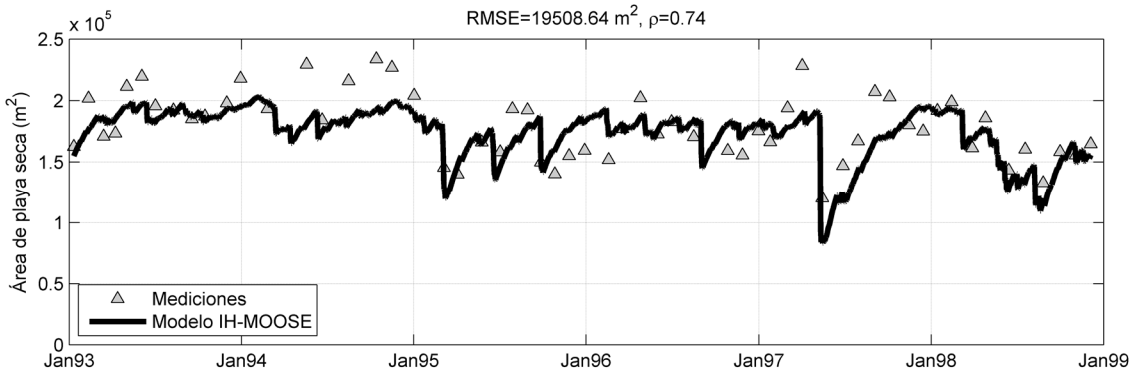

Fig. 9. Simulación de evolución de área de playa seca obtenida con el modelo IH-MOOSE durante 6 años en la playa de Narrabeen.

VI. Un modelo de rotación de línea de costa tendente al equilibrio

La rotación de la línea de costa ocurre cuando un extremo de la playa avanza, mientras el extremo opuesto retrocede. Este fenómeno se atribuye a cambios periódicos o a fenómenos de largo plazo en el clima marino. **Con el fin de simular de forma sencilla y eficaz la variabilidad de la orientación de la línea de costa, el objetivo de este capítulo es presentar un nuevo modelo heurístico de rotación de línea de costa tendente al equilibrio. Este modelo se basa en la suposición de que el movimiento de rotación de la playa es inducido por la potencia y la dirección del oleaje.**

De forma similar a Turki et al., (2013b) y Harley et al., (2013), la orientación de la línea de costa, α_s, se define en este estudio mediante el siguiente proceso: 1) el promedio de la serie temporal de ancho de playa seca se resta a todos los datos medidos de posición de costa; 2) a continuación, se realiza un ajuste lineal a la costa filtrada en el paso anterior; y finalmente, 3) la orientación de la costa se considera como el ángulo entre la línea perpendicular al ajuste lineal y el norte geográfico (como se presenta en la Fig. 10a). El panel izquierdo de la Fig. 10 presenta un esquema general de las principales variables utilizadas en el modelo; mientras el panel derecho ilustra un ejemplo de cómo se calcula la rotación de la línea de costa.

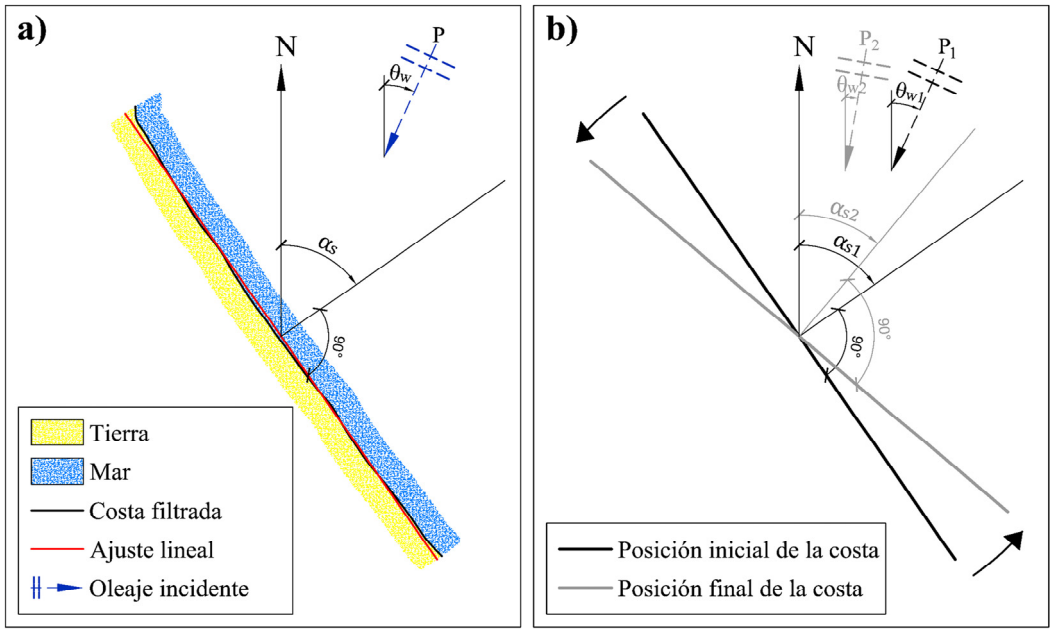

Fig. 10. a) Esquema general con las principales variables del modelo; orientación de costa, α_s, considerada como el ángulo entre la línea perpendicular al ajuste lineal de la costa filtrada y el norte geográfico, la potencia del oleaje, P, y la dirección del oleaje incidente, θ_w. b) Esquema de rotación de playa; en este caso, la posición inicial de la costa (línea negra) está asociada con la potencia de oleaje incidente, P1, y la dirección incidente, θ_{w_1}; la cual rota en sentido antihorario en función a la potencia, P2 y la dirección, θ_{w_2}. Como resultado, la playa rota desde una orientación inicial, α_{s1} a una nueva orientación, α_{s2}.

La ecuación cinética propuesta en este estudio, para simular la variación de orientación de línea de costa resulta de la siguiente forma:

$$\frac{d\alpha_s(t)}{dt} = L^{\pm}\mathrm{P}\left(\alpha_s - \alpha_{s_{eq}}\right) \tag{7}$$

donde $\alpha_s(t)$ es la orientación de la costa en el tiempo "t", P es la potencia del oleaje incidente considerada como un factor de ponderación del modelo, la cual resulta del producto entre la altura de ola significante al cuadrado, Hs^2, y el periodo de pico del oleaje, Tp, $P = Hs^2 \cdot Tp$. $L^{\pm}$ son constantes de proporcionalidad; L^+ cuando la rotación de la costa es en sentido horario y L^- cuando es antihorario. $\alpha_{s_{eq}}$ es la orientación de costa en el equilibrio, la cual se obtiene a partir de la siguiente relación lineal definida como "*Equilibrium Wave Direction Function"*, EWDF:

$$\alpha_{s_{eq}} = \frac{\theta_w - b}{a} \tag{8}$$

donde a y b son parámetros de calibración y θ_w es la dirección del oleaje incidente.

El modelo propuesto se ha aplicado en dos playas encajadas que se sitúan en el Océano Pacífico Sur (ver Fig. 2d y Fig. 2e). Por un lado, se utilizaron cerca de quince años de posiciones de línea de costa extraídas de imágenes de videocámara en la playa de Tairua, Nueva Zelanda, y por otro lado, treinta y siete años de datos de posición de línea de costa obtenidos a partir de levantamientos de perfiles en la playa de Narrabeen, Australia. A modo de ejemplo, la Fig. 11 presenta los resultados obtenidos en la playa de Narrabeen.

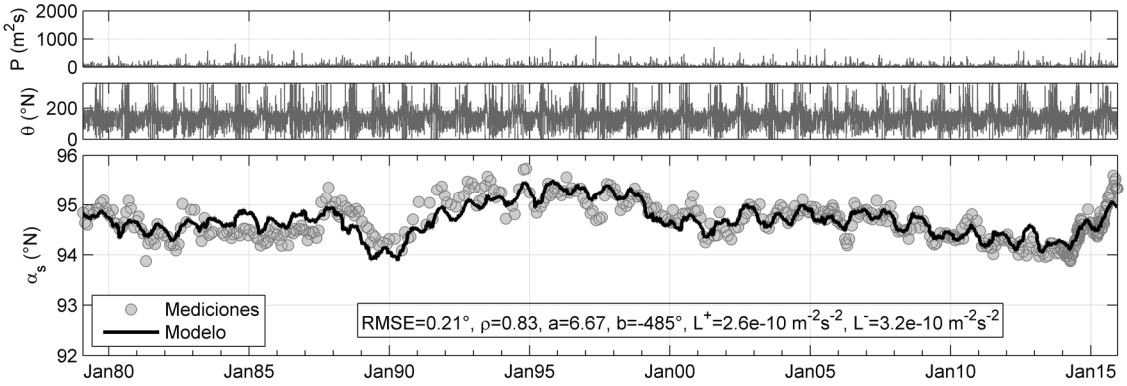

Fig. 11. Serie temporal de energía del oleaje incidente (panel superior), dirección del oleaje (panel central) y validación del modelo de evolución de orientación de la costa propuesto (panel inferior).

Los resultados fueron estadísticamente robustos considerando que el coeficiente de correlación entre la orientación de la línea de costa observada y la modelada excedió 0.75 en ambos sitios de

estudio. En general, las rotaciones de la costa en sentido horario y antihorario han sido satisfactoriamente representadas, tanto cualitativa como cuantitativamente.

VII.Futuras líneas de investigación

En esta tesis se desarrollaron una serie de mejoras y nuevos modelos, los cuales permiten dar un paso adelante en nuestra capacidad de modelar y evaluar la variabilidad de la costa en playas encajadas. Sin embargo, aún existen muchos temas en este campo sobre los que se debe profundizar en futuros trabajos de investigación. De entre ellos, los temas principales directamente relacionados con los asuntos abordados en esta tesis son:

- Integrar en un único modelo de evolución de línea de costa tendente al equilibrio: el desplazamiento *cross-shore* (añadiendo el término de tendencia), la forma en planta de la playa y el concepto de rotación.
- Con el fin de validar ampliamente la predicción aportada por los modelos propuestos en esta tesis, se hace necesario aplicar los mismos en múltiples playas sometidas a condiciones climáticas diversas y características morfológicas variables.
- A partir de lo anterior, con miras a poder emplear los modelos propuestos en distintos casos de estudio, resulta de gran interés evaluar herramientas o algoritmos que permitan la detección automática de la posición de línea de costa en cualquier parte del mundo, como podría ser la herramienta CoastSat propuesta por Vos et al., (2019), la cual permite adquirir líneas de costa derivadas de imágenes de satélite empleando Google Engine.
- Explorar el desempeño del modelo IH-MOOSE considerando la integración de diversas combinaciones entre modelos cross-shore (p. ej. Davidson et al., 2013; Castelle et al., 2014; Splinter et al., 2014; Jara et al., 2015) y formas en planta de equilibrio (p. ej. Yasso 1965; Tan y Chiew 1994; Moreno y Kraus 1999). En caso de evaluar sitios de estudio con formas en planta irregulares debido a presencia de islas y/o fondos rocosos, sería necesario recurrir a modelos de forma en planta basados en procesos, como el propuesto por Gainza et al., (2018).
- Con el fin de evaluar la evolución de posición de línea de costa en el muy largo plazo, sería necesario incorporar en los modelos de evolución propuestos, un término adicional que permita simular el retroceso de la costa a causa del ascenso del nivel medio del mar derivado de los efectos del cambio climático.
- Para que los parámetros de calibración de los modelos propuestos sean variables en el tiempo, se propone incluir un algoritmo de asimilación de datos, como el Filtro de Kalman. Este algoritmo permite ajustar automáticamente los parámetros de calibración a medida que se tienen mediciones para asimilar; sin embargo, una vez asimilada la última

medición disponible, los parámetros permanecerán constantes durante todo el período de previsión.

1 INTRODUCTION AND SCOPE

1.1 Introduction and Motivation

Currently, more than 66% of the global population lives within 100 km of coastlines (Biausque et al., 2016) with 10% living in low-lying coastal areas, i.e., less than 10 m above the current mean sea level (MSL) (McGranahan et al., 2007). In the future, the population density is expected to increase even more in these areas due to high rates of population growth and urbanization (Neumann et al., 2015), so urban settlements in coastal lowlands are especially vulnerable to risks of the littoral area.

Coastal zones are dynamic environments; all around the world, coastlines are shaped by forcing agents as diverse as waves, winds, nearshore currents, sea levels, storm surges, human modifications and other oceanographic and sediment supply factors on different spatio-temporal scales. Coastal sedimentary deposits, such as beaches, are inherently adaptable systems, often in a state of quasi-equilibrium, constantly reacting to the varying forcing conditions.

Beaches are dynamic natural sediment stores, where the arrival of storms leads to consequent coastal erosion, while long calm periods allow sediment to return to the coast. Recently, Luijendijk et al., (2018) and Mentaschi et al., (2018) each reported global long-term observations of coastal erosion and accretion. According to Luijendijk et al., (2018), 24% of the world's sandy

beaches are eroding at rates exceeding 0.5 m/yr, raising cause for serious concern. In addition, upper-ocean warming, a consequence of anthropogenic global warming, is changing the global wave climate, making waves stronger (Reguero et al., 2019). It should be noted that extreme coastal storms such as hurricanes and extratropical cyclones can rapidly mobilize and redistribute vast quantities of sediment (Harley et al., 2017).

As explained above, beaches are continuously changing, undergoing accretion and erosion in response to various factors. However, open-coast beaches subject to longshore drift are generally much more sensitive to these changing conditions than embayed beaches which are generally bounded by cell boundaries and are dominantly closed sediment circulation systems (Sedrati and Anthony, 2007). This thesis focuses particularly on the morphodynamics of embayed beaches, at the scale of the embayment.

Embayed beaches are characterized by being closed systems where there is an interaction between hydrodynamics (waves, currents, etc.) and the sediment transport, defining a beach planform and beach profile. Consequently, all the hydrodynamic and sedimentary processes that take place on a beach are three-dimensional processes. These processes are difficult to analyze due to our inability to understand them fully and the limitations of the existing tools or formulations.

In general terms, the morphodynamics of embayed beaches is considered a complex phenomenon (Biausque et al., 2016); thus, scientists and engineers have assumed that shoreline variability is a reliable proxy to describe the overall beach change (Smith and Bryan, 2007) for different spatio-temporal scales. Observations of shoreline variability are essential to quantify long-term recession trends, regulate coastal development and design coastal protection works. Therefore, coastal managers must evaluate the current shoreline position, where it has been in the past, and where it will be in the future.

The shoreline position is extremely useful to quantify historical erosion rates (e.g., Anders and Byrnes, 1991; Crowell et al., 1991; Moore, 2000; Mentaschi et al., 2018) and beach width and volume (e.g., Douglas et al. 1998; Short and Trembanis, 2004; Farris and List, 2007), mainly for the purpose of continuous beach monitoring, to preserve its functionalities of protection, recreation and natural values (Jiménez et al., 2007).

Traditionally, potential data sources for shoreline positions were limited to field surveys, historical photographs, coastal maps and charts, aerial photography, radar and video-camera systems. **Shoreline positions derived from satellite images have been neglected because the resolution available to the public is too coarse (10 – 30 m or more), which prevents the identification of small-scale coastline movements.**

Shoreline-position datasets are required as the main input to calibrate, validate or predict shoreline evolution. They are the cornerstone of several shoreline evolution models, such as one-line shoreline models (e.g., Pelnard-Considere, 1956; Hanson and Kraus, 1991; Dabees and Kamphuis, 1998), multi-line shoreline models (e.g., Bakker, 1970; Perlin and Dean, 1979; 1983; Hanson and Larson, 2000), conceptual or equilibrium shoreline evolution models (e.g., Kriebel and Dean, 1993; Miller and Dean, 2004; Yates et al., 2009; Long and Plant, 2012; Davidson and Turner, 2009; Davidson et al., 2010, 2013; Castelle et al., 2014; Splinter et al., 2014; Jara et al., 2015; Doria et al., 2016), and combined models (e.g., Robinet et al., 2017; Vitousek et al., 2017). These models can be separated or classified into numerous classifications according to the criteria chosen; by nature, accuracy, application scales, the main direction of the processes involved, among others.

For example, depending on the time scale of the model application, there are short-term (hours-days), medium-term (days-year) and long-term (years-decades) models. Whereas, depending on the spatial scale, small-scale (tens of meters), medium-scale (hundreds of meters) and large-scale (kilometers) models can be distinguished.

According to Hanson et al., (2003) there is still no universal model for analyzing and predicting coastal evolution and its governing processes on the different time scales. Instead, depending on the nature of the problem and project objectives, there is a wide range of models available, each focusing on the problem complex from a specific standpoint.

The present thesis deals with the development of equilibrium shoreline evolution models. These models turn out to be the simplest because they require fewer calibration parameters, are computationally efficient and can be applied to investigate mid to long term morphological changes (Davidson and Turner, 2009).

Conceptually, these models are based on the balance between destructive and constructive forces that act upon a beach. In general terms, they are established on the following governing differential equation:

$$\frac{dX'(t)}{dt} = \mathrm{K}' \cdot \Delta X' \tag{9}$$

where the beach parameter X' varies over time, $\frac{dX\prime(t)}{dt}$, depending on the product between a rapidly varying forcing, K', and the evolving disequilibrium through time, $\Delta X'$. This disequilibrium is the difference between the current conditions and a theoretical equilibrium (i.e., $\Delta X' = X' - X'_{eq}$). As stated by Madsen and Plant, (2001) a particular set of incident wave conditions is associated

with a corresponding stable equilibrium state of the beach. That is, if wave conditions are steady, a beach will asymptotically approach a single state independent of the initial state.

The rate parameter, K', is a function of both the prevailing wave conditions (e.g., the wave energy, E, or wave power, P) and the beach morphological characteristics, such as the mean grain size, D_{50}, beach length, l, closure depth, h*, among others.

It should be noted that the use of these models has increased in recent years, thanks to their easy and effective application. To date, based on the orthogonality hypothesis of the processes that take place on beaches, they have been separated according to the direction of sediment transport, cross-shore or longshore, responding only to beach profile movements or beach planform variability.

As presented later in Section 2.5, there are multiple proposals for empirical equilibrium shoreline evolution models that contemplate only cross-shore migration processes; however, **in the literature, there are very few proposals of these type models considering longshore processes.**

So far, the equilibrium shoreline evolution models for cross-shore migration have been used in multiple studies, and they assume the shoreline variation in different ways (e.g. shoreline position as a point or linear stretch that advances/retreats); however, **no author has evaluated the shoreline position variation by means of an equilibrium cross-shore evolution model, which considers the entire beach as an embayed planform.** Therefore, with the aim of reproducing the entire embayed shoreline beach evolution, **it is essential to combine cross-shore and longshore processes into a single reduced-complexity shoreline model** that accounts for the complexity of offshore and nearshore wave transformation (Robinet et al., 2018).

In addition, it is important to note that most sandy beaches worldwide have a tendency of progressive shoreline advances or retreats for years or even decades, and this pattern is a product of multiple factors, which may be of natural or anthropic origin. **Therefore, to predict the shoreline variability in such cases, the numerical models of morphological evolution must contemplate a rate of change of shoreline position for sediment gain or loss.**

From all of the above, it is of great interest to focus on embayed beaches variability and how they will potentially adapt to changing wave conditions. More specifically, it is necessary to continue developing improvements and processes integrations (cross-shore and longshore) considering the equilibrium shoreline evolution models.

1.2 Research Questions

According to the motivation of this thesis, there is a need to continue studying and developing equilibrium shoreline evolution models. Based on the existing gaps, several research questions can be posted:

- **RQ1:** Is it possible to calibrate and validate equilibrium shoreline evolution models using mid-resolution satellite images datasets?
- **RQ2:** How could the variability of the beach profile volume (net erosion/accretion) be included in the equilibrium-based shoreline evolution models?
- **RQ3:** Is it possible to model the cross-shore variability of embayed beaches in the medium-long term?
- **RQ4:** How to model the shoreline rotation in the medium to long term?

Throughout the development of this thesis, we will be able to answer the proposed research questions.

1.3 Objectives of the thesis

Following the motivation exposed above, and the research questions presented in the previous section, the primary objective of this thesis is to develop a new equilibrium-based shoreline evolution model integrating planform and profile in the medium to long term scales.

This main goal is achieved by the consecution of sequence-specific objectives, which ultimately are the topics of each of the main chapters of this thesis:

- Assess the applicability of mid-resolution satellite-image data for the calibration and validation of equilibrium shoreline evolution models in the context of cross-shore motion (Answering RQ1).
- Develop an equilibrium-based shoreline evolution model considering the variability of the beach profile volume (Answering RQ2).
- Develop a new model for embayed beaches based on cross-shore and planform equilibrium models applicable for cross-shore migration (Answering RQ3).
- Develop a new equilibrium-based shoreline rotation model (Answering RQ4).

1.4 Thesis outline

The thesis comprises eight chapters and it is structured as follows:

Chapter 1, in which this introduction is included, presents the motivation of the thesis and establishes its main objectives.

Chapter 2 presents a general background and state of the art related to embayed beaches, the equilibrium beach conditions, shoreline definition and finally special description on the previous investigations throughout the literature related to shoreline evolution models.

Chapter 3 presents a comparative analysis between shoreline-position datasets obtained from video-camera systems and satellite imagery with the aim to explore the applicability of mid-resolution satellite imagery with a sub-pixel acquisition method for the calibration and validation of equilibrium shoreline evolution models. This chapter targets RQ1.

Chapter 4 presents an extension of an existing equilibrium shoreline evolution model adding a rate of change component, which in turn modifies the relationship between the equilibrium shoreline position and the incident wave energy, as a function that advances or retreats over time. This chapter targets RQ2.

Chapter 5 presents a new equilibrium shoreline evolution model based on the integration of cross-shore and planform equilibrium models. It is exclusively applicable to embayed beaches and is mainly influenced by cross-shore displacement. This chapter targets RQ3.

Chapter 6 presents a new equilibrium-based shoreline rotation model derived from a shoreline migration formulation, assuming that beach rotation movement is induced by the incoming wave power and direction. This chapter targets RQ4.

Finally, **Chapter 7** summarizes the main results and conclusions of the thesis. In addition, in this chapter future research lines in this field are drawn.

2 BACKGROUND AND LITERATURE REVIEW

2.1 Introduction

This chapter summarizes the bibliographic review carried out as work prior to the development of the shoreline evolution models proposed in this thesis. This literature review allows, on the one hand, to contextualize the new contributions made and, on the other hand, to expose the already existing tools.

This chapter is split into four subsections. The first one deals with the definition of embayed beaches, which are the main focus of this thesis. The second subsection is a general understanding of the equilibrium beach conditions. A compilation of the main existing empirical formulations is presented for both, equilibrium beach profile and equilibrium beach planform. The third subsection presents the various indicators that could define the shoreline position and then, the movements in which shoreline variability can be decomposed. Finally, a summary of most up-to-date literature related to the different shoreline evolution models is presented; with special emphasis on equilibrium-based shoreline evolution models due to cross-shore and longshore sediment transport.

2.2 Embayed beaches

As aforementioned in Chapter 1, the present study is mainly focused on embayed beaches or Headland Bay Beaches (HBBs).

Embayed beaches lie along the majority world's continental and island margins, representing approximately 50% of the world's coastline (Inman and Nordstrom, 1971). These are physiographic units in which both the beach profile and the planform are laterally confined by natural or artificial impermeable contours, and the bottom is covered mostly by sand. The contour headlands affect the hydrodynamics and wave conditions, resulting in an equilibrium between flow circulation and shoreline response. This interaction is translated into the characteristic shapes of embayed beaches (Daly et al., 2014), usually recognized as curved, crenulated, embayed, hooked, pocket or headland-bay beaches.

Many detailed studies of these beaches have been conducted in recent years (e.g., Bowman et al., 2009; Van de Lageweg et al., 2013; Daly et al., 2015; Blossier et al., 2016; Elshinnawy et al., 2017; Gainza et al., 2018). Fig. 2-1 shows some examples of embayed beaches in natural coastal settings, in which the contours are rocky headlands; and urban embayed beaches bounded by artificial headlands as man-made coastal structures related to shore protection and harbour development, namely groynes and breakwaters.

Fig. 2-1. Embayed beaches bounded by a) natural and b) artificial contours. Images taken from Google Earth.

The distinctive curvature of embayed beaches attributed to both wave diffraction and variations in the incoming wave climate has inspired coastal researchers to propose different empirical planform geometry approaches. The most well-known scientific contributions in the literature are the logarithmic spiral model (Silvester and Ho, 1972; Silvester et al., 1980 and Yasso, 1965), the parabolic model (Hsu and Evans, 1989), and more recently, the hyperbolic-tangent model (Moreno and Kraus, 1999). These beach planforms approximations are presented in detail in section 2.3.2.

2.3 Static equilibrium beach conditions

All hydrodynamic and sedimentary processes that occur on a beach are three-dimensional. These processes become difficult to analyze due to our ability to understand them and the various limitations of the available tools or formulations. For this reason, the scientific community has assumed the orthogonality hypothesis, in which, any beach movement can be analyzed by studying independently the beach profile (cross-shore movements) and the beach planform (longshore movements).

Coastal researchers have evaluated the term “equilibrium beach” for both, the beach profile and beach planform. According to González et al., (2010), the equilibrium hypothesis postulates that if the action of the acting dynamics is maintained indefinitely, the beach shape will reach a constant final position, which can be denominated “equilibrium beach”. The beach achieves its equilibrium state from the moment it does not present changes in its shape in planform or in its profile.

The existence of an embayed beach in perfect equilibrium state can only be obtained in a laboratory, where the incoming waves are controlled. In nature the waves and sea levels are constantly changing; however, those hydrodynamic variations are limited, which translates, the beach variations are also limited. Therefore, in nature, it can be admitted the existence of an equilibrium beach that suffers variations depending on the existing marine climate.

Based on the above, several authors have aroused their interest in proposing multiple empirical formulations, which try to reproduce the equilibrium conditions of both the beach profile and the beach planform.

2.3.1 Static equilibrium beach profile models

Various authors have extensively analyzed the static equilibrium beach profile, SEBP. Some of the most representative SEBPs found in the literature are summarized below, in chronological order (see Table 2-1).

Table 2-1. Static equilibrium beach profile models.

Authors	Beach profile	Formulation
Bruun (1954)	1 section	$h(x) = Ax^{2/3}$ (10)
Dean (1977)	1 section	$h(x) = Ax^{n'}\ ;\ n' = \frac{2}{3}$ (11)
Bowen (1980)	1 section	$h = \mathrm{g}\left(\frac{5.7w_f}{\sigma^2}\right)^{2/5}$ (12)
Vellinga (1983)	1 section	$h(x) = Ax^{0.78}$ (13)
Bodge (1992)	1 section	$h(x) = B'\left(1 - e^{-k_1 x}\right)$ (14)
Komar and Mcdougal (1994)	1 section	$h(x) = \frac{m'}{k}\left(1 - e^{-k_1 x}\right)$ (15)
Inman et al. (1993)	2 sections	$h(x) = Ax^{n'}\ ;\ n'\ varies\ for\ each\ section$ $A\ varies\ for\ each\ section$ (16)
Bernabeu, (1999)	2 sections	$x = \left(\frac{h}{A}\right)^{3/2} + \frac{B}{A^{3/2}}h^3\ ;\ Surf\ profile$ $x = x_0 + \left(\frac{h}{C}\right)^{3/2} + \frac{D}{C^{3/2}}h^3\ ;\ Shoaling\ profile$ (17)
Larson et al. (1999)	2 sections	$h(x) = Ax^{n'}\ ;\ n' = \frac{2}{3}\ ;\ Surf\ profile$ $h(x) = Ax^{n'}\ ;\ n' = 0.25\ ;\ Shoaling\ profile$ $A\ varies\ for\ each\ section$ (18)

Appendix 1 describes in detail the above-mentioned SEBPs together with the definition of the respective variables. Additionally, the proposed formulations for determining the scale parameter,

A, are included. It should be noted that in addition to the profiles cited in Table 2-1, there are other SEBP models proposed in the literature.

2.3.2 Static equilibrium beach planform models

Numerous researchers have recognized the existence of a pattern in the planform shape of beaches located sheltered from a cape or headland. This section compiles the main empirical equations found in the literature to obtain and fit the Static Equilibrium Planform (SEP) of embayed beaches (see Table 2-2).

Table 2-2. Static equilibrium beach planform models, SEP.

Authors	Beach planform	Formulation
Krumbein (1944)	Log-spiral	$R_2 = R_1 e^{\theta' cot\alpha}$ (19)
Silvester and Ho (1972)	Log-spiral	$\frac{R_2}{R_1} = e^{\theta' cot\alpha}$; α *correlated to the incident wave angle* (20)
Hsu and Evans (1989)	Parabolic	$R = R_0 \cdot \left(C_0 + C_1 \frac{\beta}{\theta} + C_2 \left(\frac{\beta}{\theta}\right)^2 \right)$ (21)
Tan and Chiew (1994)	Parabolic	$\frac{R}{R_0} = [1 - \beta \cot(\beta) + \alpha_{st}] + [\beta \cot(\beta) - 2\alpha_{st}] \left(\frac{\beta}{\theta}\right) + \alpha_{st} \left(\frac{\beta}{\theta}\right)^2$ (22)
Moreno and Kraus (1999)	Hyperbolic-tangent	$y' = \pm a_1 tanh^{m_1}(b_1 x')$ (23)

Appendix 2 describes in detail the above-mentioned SEPs together with the definition of the respective variables. Other remarkable proposals related to the exposed planforms are also included or cited in Appendix 2. In addition to the static equilibrium beach planform models presented in Table 2-2, there are various others proposed in the literature.

2.4 Shoreline definition

In the literature, the shoreline definition has been broadly investigated based on geographical, morphological or hydrological considerations (e.g. Fenster et al., 1993; Camfield and Morang, 1996; Douglas et al., 1998; Moore, 2000; Toure et al., 2019).

Boak and Turner (2005) listed 45 coastline indicators used around the world for coastal monitoring studies. The detailed study presented by Boak and Turner (2005) separates shoreline

proxies into visually discernible coastal features (see upper panel of Fig. 2-2) and specific tidal datum (see bottom panel of Fig. 2-2). Concerning the last one, the shoreline position is defined as the intersection of the beach profile with a specific vertical elevation.

According to Boak and Turner (2005), the identification of a "shoreline" involves two stages. The first requires the selection and definition of a shoreline indicator that will act as a proxy for the land-water interface. The second stage is related to the detection of the chosen shoreline indicator within the available data source.

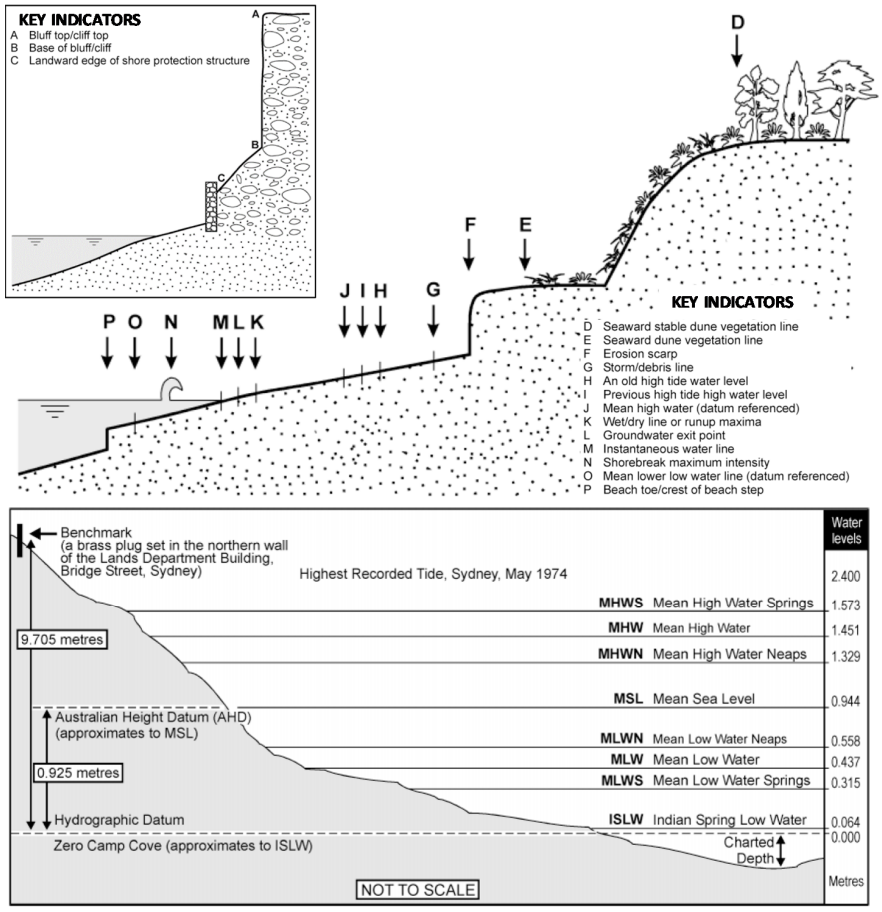

Fig. 2-2. Shoreline indicators based on visually discernible coastal features (upper panel) and specific tidal datum – a case example of datums used along the New South Wales coastline, Australia (bottom panel). Adapted from Boak and Turner (2005).

In order to obtain the shoreline position, there are diverse data sources, such as field surveys, historical photographs, coastal maps and charts, aerial photography, radar, video-camera systems, satellite images, among others.

In this thesis, data sources such as field surveys, video-camera images and satellite images were used. To define the shoreline position, the *instantaneous water line* indicator was selected in the images from video-camera systems and satellite. On the other hand, when the source of information was from beach profile surveys, different contours or elevations were selected.

2.4.1 Shoreline movements

According to most of the existing studies, the shoreline variability of embayed beaches can be broken down into three main movements: 1) breach migration, 2) beach rotation and 3) beach breathing, which are detailed below and presented schematically in Fig. 2-3.

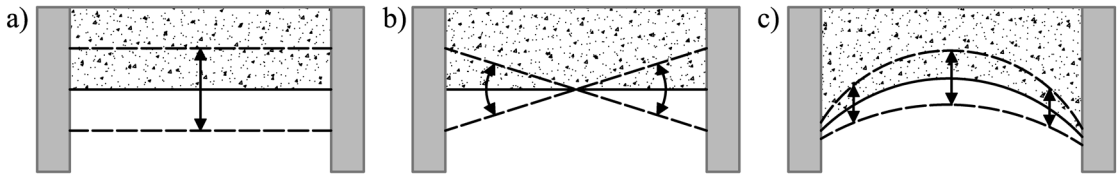

Fig. 2-3. Shoreline movements: a) beach migration, b) beach rotation and c) beach breathing.

- *Beach migration:*

The first mode corresponds to beach migration or cross-shore movement. It is related to sediment exchanges between the shore and the offshore (e.g., Davidson et al., 2013; Palalane et al., 2016). The alternating occurrence of storms and calm periods cause significant profile changes that vary from severe erosion to post-storm slower recovery. The impact of storms on beaches is complex simply due to the non-linear response of the morphology to the forcing (Angnuureng et al., 2015).

For example, if a beach is in a 'summer state', its erosion by a storm will be much larger; conversely, during winter, the state of the beach is more adapted to repeated storms and the net erosion due to each storm is lower than in summer.

- *Beach rotation:*

The beach rotation is associated with the obliquity of incident waves and a consequent longshore transfer of sediments from one extremity of the beach towards the other (e.g., Klein et al., 2002; Thomas et al., 2010; Turki et al., 2013). Basically, the rotation process occurs when an extremity of the beach accretes while the other erodes and vice versa. This phenomenon has been extensively investigated by numerous authors, who have found a strong relationship between the shoreline orientation and the incoming wave climate. Most of the studies proposed to date correspond to embayed beaches where sediment volume is preserved (e.g., Klein et al., 2002; Thomas et al., 2010; Bryan et al., 2013; Short et al., 2014; Blossier et al., 2017; Wiggins et al., 2019); nonetheless, authors such as Thomas et al., (2016) have also identified the subaerial beach rotation at open coasts. Moreover, the rotation has been recognized in sandy or gravel beaches (e.g. Dolphin et al., 2011; Harley et al., 2014) subjected to different tidal ranges; microtidal (e.g. Turki et al., 2013a), mesotidal (e.g. Velegrakis and Schimmels, 2013) and macrotidal environments (e.g. Thomas et al., 2015).

Klein et al., (2002) identified the shoreline rotation as a periodical shape change through shifts in the alongshore sediment transport, resulting in the opposite ends being out of phase with each other. In terms of temporal scale, rotation has been commonly associated with seasonal changes in the wave climate; however, it could also occur on the daily to weekly scale related to storm events (Ojeda and Guillén, 2008), or during the long-term linked to different phases of climatic oscillations, including El Niño/La Niña Southern Oscillation (ENSO) (e.g. Short et al., 2000; Anderson et al., 2018), North Atlantic Oscillation (NAO) (e.g. Thomas et al., 2011) or West Europe Pressure Anomaly (WEPA) (e.g. Burvingt et al., 2018).

- *Beach breathing:*

Finally, the third mode corresponds to the so-called "beach breathing" which was initially identified by Ratliff and Murray, (2014). The breathing mode characterizes changes in shoreline curvature, as sand moves from the middle of the pocket beach to the edges and back. This movement has been little studied since it is commonly considered as a residual movement; however, its importance has been recognized by some other authors (e.g. Blossier et al., 2017; Lazarus et al., 2019; Antolínez et al., 2019).

All three movements play an important role in shoreline evolution; depending on the spatio-temporal scale, one movement tends to be dominant; for example, a small pocket beach subjected to multi-directional incoming waves would experience a strong beach rotation movement. However, as highlighted by authors, such as Dai et al., (2010), Daly et al., (2011) and Blossier et al., (2017), cross-shore migration usually dominates over the others.

2.5 Equilibrium-based shoreline evolution models

The present thesis deals with the development of equilibrium shoreline evolution models, applicable to embayed beaches. They are conceptually based on the balance between the destructive and constructive forces that act upon a beach; thus, they allow us to obtain the shoreline position at a certain time. These models aim to evaluate changes that occur in the shoreline position due to storm response, seasonal and yearly changes.

The equilibrium models approach can be further separated in agreement with the sediment transport direction; longshore transport, which is performed along the coastline and transverse or cross-shore transport, which takes place perpendicular to it. In the following, the equilibrium-based models according to the sediment transport direction are detailed.

2.5.1 Equilibrium-based shoreline evolution models for cross-shore movement

Several equilibrium models to predict the shoreline evolution related to cross-shore sediment are available in the literature. These models require very few calibration parameters, which makes them simplified models with great potential to predict the shoreline position; in fact, the use of these models has increased in recent years.

Table 2-3 presents some of the most representative proposals of equilibrium-based shoreline evolution models for cross-shore movement available in the literature. Appendix 3 describes in detail the mentioned models together with the definition of the respective variables.

It should be highlighted that the model proposed by Yates et al., (2009) has been one of the main references in this thesis.

Table 2-3. Equilibrium-based shoreline evolution models for cross-shore movement. See Appendix 3 for a detailed explanation of the different parameters.

Authors	Formulation
Wright and Short, (1984)	$\frac{dR'(t)}{dt} = k \cdot \Omega^2(\Omega - \Omega_{eq})$ (24)
Kriebel and Dean (1993)	$\frac{dR'(t)}{dt} = \frac{1}{Ts} \cdot \left(R'_{eq} - R'(t)\right)$ (25)
Miller and Dean (2004)	$\frac{dS(t)}{dt} = k\left(S_{eq}(t) - S(t)\right)$ (26)
Yates et al., (2009)	$\frac{\partial S(t)}{\partial t} = C^{\pm} \cdot E^{1/2}(E - E_{eq})$ (27)
Long and Plant, (2012)	$\frac{dS(t)}{dt} = \nu_{lt} + C^{\pm}E^{1/2} \cdot \Delta E(S)$ (28)
Davidson and Turner (2009)	$\frac{dz'(x,t)}{dt} = R^* \left\lvert \Omega_{eq} - \Omega(t) \right\rvert \Omega^n(t) \emptyset'(\mathrm{x,t})$ (29)
Davidson et al. (2010)	$\frac{dS(t)}{dt} = \mathrm{b}' + \mathrm{c}\left(\Omega_{eq} - \Omega(t)\right)\Omega^{\mathrm{k}}(t)$ (30)
Davidson et al. (2013)	$\frac{dS(t)}{dt} = \mathrm{b}' + C^{\pm}P^{1/2}\left(\Omega_{eq}(t) - \Omega(t)\right)$ (31)

Splinter et al. (2014)	$\frac{dS(t)}{dt} = \mathrm{c}(F^{+} + rF^{-}) + \mathrm{b}'$ (32)
Jara et al. (2015)	$\frac{\partial S(t)}{\partial t} = C^{\pm} \cdot \left(E - E_{eq}\right)$ (33)
Doria et al., (2016)	$\frac{dS(t)}{dt} = \begin{cases} C^{\pm} E^{1/2} \cdot \Delta E(S) & \text{for } S > S_{bb} \\ 0 \text{ for } S \leq S_{bb} \end{cases}$ (34)

As presented by Jara et al., (2018), the existing equilibrium-based shoreline evolution models can be divided into two approaches: 1. models based on an equilibrium condition correlated with the shoreline position (e.g., Yates et al., 2009; Jara et al., 2015) and 2. models based on an equilibrium condition as a weighted average of antecedent conditions (e.g., Davidson et al., 2013; Splinter et al., 2014).

2.5.2 Equilibrium-based shoreline evolution models for longshore movement

As presented in the previous section, there are multiple proposals for empirical equilibrium shoreline evolution models that contemplate only cross-shore migration processes; however, in the literature, there are very few proposals for equilibrium shoreline evolution models considering longshore processes.

It should be noted that the longshore sediment transport depends on the angle between the breaking waves and the shoreline, and reaches zero when waves are normal to the beach. The longshore transport is translated into a varying morphological development of the beach profile along the embayment, and the result on the shoreline (mainly on embayed beaches) is a rotational movement. Table 2-4 compiles the existing equilibrium shoreline evolution models that consider longshore processes. The cited models are also described in detail in Appendix 3.

Table 2-4. Equilibrium-based shoreline evolution models for longshore movement. See Appendix 3 for a detailed explanation of the different parameters.

Authors	Formulation
Turki et al., (2013a)	$\frac{\partial R'(t)}{\partial t} = \omega \cdot \left(R'_{\mathrm{eq}} - R'(t)\right)$ (35)
Blossier et al. (2015)	$\frac{\partial \alpha_s}{\partial t} = K \cdot \left(m \cdot E_y + n_1\right)$ (36)

Blossier et al., (2017)	$\frac{d\alpha_s(t)}{dt} = C_{\alpha_s}\mathrm{E}[sen(\theta_w)\cdot\cos(\theta_w) - \alpha_s\cos(2\theta_w)]$ (37)

2.6 Conclusions

As it was advanced in the Introduction (Chapter 1) and presented in this chapter, the use of equilibrium-based shoreline evolution models has increased in recent years, thanks to their easy and effective application. According to the detailed review of the available literature, the following conclusions reveal the main existing limitations or gaps:

- All the equilibrium-based shoreline evolution models applications in the literature correspond to target study sites where high-resolution data were available (video-camera systems or topo-bathymetric surveys). However, no studies had applied yet shoreline-position datasets from satellite imagery for not being accurate enough.
- Based on the orthogonality hypothesis of the processes that take place on beaches, the equilibrium-based shoreline evolution models have been separated according to the direction of sediment transport, cross-shore or longshore, responding only to beach profile movements or beach planform variability. Based on the above, these models have managed to simulate the migration or rotation shoreline movements separately.
- In order to predict the shoreline variability in beaches subject to a tendency of progressive shoreline advances or retreats, there is no equilibrium shoreline evolution model based on a time-varying equilibrium condition correlated with the shoreline position considering a trend rate of sediment gain or loss.
- There are multiple proposals considering cross-shore migration processes; however, there are very few proposals for equilibrium shoreline evolution models considering longshore processes.

Considering the objectives proposed in this thesis (see Section 1.3) and the background related to the equilibrium-based shoreline evolution models explained in this chapter, the following chapters provide answers to different identified gaps. Relevant solutions are obtained and explained to cover each of them.

3 SUB-PIXEL SATELLITE DERIVED SHORELINES AS VALUABLE DATA FOR EQUILIBRIUM SHORELINE EVOLUTION MODELS †

† This Chapter is based on Jaramillo et al., (2020d): Jaramillo, C., E. Sánchez-García, M. S. Jara, M. González, and J. M. Palomar-Vázquez. 2020. Sub-pixel satellite derived shorelines as valuable data for equilibrium shoreline evolution models. Journal of Coastal Research - *In press*.

3.1 Introduction

For coastal engineers, shoreline-position datasets have been considered the cornerstone of multiple coastal morphodynamic models, such as the equilibrium shoreline evolution models which are the focus of this thesis. These models have been proposed to describe shoreline migration on beaches as a function of the incident wave energy. Long temporal series of shoreline position are required as the main input to calibrate, validate or predict shoreline evolution.

Until only a few years ago, historical shoreline dataset records had to be compiled from exhaustive field surveys. This type of data collection has some fundamental limitations; for example, such field campaigns are relatively expensive and only a limited number of instruments are available at specific points. This case is true for well-known multi-decadal monitoring programmes at specific study sites (e.g., Rhode Island-USA, Lacey and Peck, 1998; Dutch central coast-Netherlands, Wijnberg and Terwindt, 1995; Moruya-Australia, McLean and Shen, 2006; Narrabeen-Australia, Turner et al., 2016; Duck-USA, Lippmann and Holman, 1990; Ludiatowo-Poland, Rózyński et al., 2001; Hasaki-Japan Kuriyama, 2002). However, multiple alternative data sources can currently be used to identify the shoreline position and obtain different types of morphological variables along coastal zones (e.g., Gorman et al., 1998; Mason et al., 2000; Boak and Turner, 2005), such as aerial photography, radar, video-camera systems (e.g., ARGUS system by Holman and Stanley, 2007; CoastView by Medina et al. 2007; CoastalCOMS by Lane et al., 2009; SIRENA by Nieto et al., 2010; HORUS by Osorio et al., 2007; COSMOS by Taborda and Silva, 2012; Beachkeeper plus by Brignone et al., 2012; ORASIS by Vousdoukas, 2013; C-Pro by Sánchez-García et al. 2017; CoViMoS by Widyantara et al., 2017), and satellite imagery.

At the great majority of coastal sites, historical data is limited or non-existent; thus, the choice of what data to use at a specific site is generally determined by the availability of data (Boak and Turner, 2005). In this manner, satellite imagery is the only data source that has the great advantage of covering large areas of the world and including regular coverage of most coasts during all climates and seasons. The coverage of a single image covers medium (25 km²) to large scales (> 10.000 km²), and historical repositories often have successive captures that are taken by the satellite over the same area, with periodicity between daily and monthly. Additionally, these images have the advantage of providing information regarding areas of restricted or difficult access by both land and navigation.

The main limitation of satellite data to coastal studies is the pixel resolution. The resolution of most satellite data that are available to the public is 10 - 30 m or greater. Among the many missions and space programs for the observation of the Earth, the following stand out for their

applications to coastal morphodynamics: Landsat, which has been operated by the United States Geological Survey (USGS) and the National Aeronautics and Space Administration (NASA), USA, since 1972; the SPOT program, which was developed by the French Centre National d'Etudes Spatiales (CNES) in collaboration with Belgium and Sweden in 1986; and Sentinel, which was developed by the European Space Agency (ESA) within the framework of the Copernicus Program in 2014. These data have been adequate to recognize the evolutionary trends of large-scale coastal areas over the medium to long term in many locations, such as the evolution of the Nile delta in Egypt (White and El Asmar, 1999), the Maritsa River delta in Turkey (Ekercin, 2007), and others. In such cases, the accuracy of the information that is extracted from the image is assumed to be worse than the resolution of the original images (10-30 m).

Most efforts by researchers have focused on defining an optimal method to locate the shoreline position with satellite images, identifying each pixel of the image as sea or land, such as supervised classification techniques (e.g., Hoeke et al., 2001; Espinosa and Rodríguez, 2009; Hannv et al., 2013; Yousefi et al., 2015), unsupervised classification techniques (e.g., Ekercin, 2007; Guariglia et al., 2006) and thresholding techniques (e.g., Bayram et al., 2008; Kuleli et al., 2011; Liu and Jezek, 2004; Maiti and Bhattacharya, 2009).

The typical spatial resolution of satellite images that are available to the public (approximately 10-30 m) is too coarse to provide information on most coastal morphodynamic changes, so new remote-sensing techniques have been developed recently, such as sub-pixel methods, which can improve satellite-image resolution by assigning portions as sea and land within the same pixel (e.g., Pardo-Pascual et al. 2012; Almonacid-Caballer et al. 2016; Pardo-Pascual et al. 2018). These methods are based on the use of fuzzy logic (Foody et al., 2005) or improved solutions based on super-resolution mapping methods (Muslim et al., 2007). These methods have been recently used in many different applications (e.g., Hagenaars et al., 2018; Luijendijk et al., 2018; Vos et al., 2019).

The purpose of this study is to assess the applicability of satellite-image data, which are available worldwide with a historical record of more than 40 years, to provide satellite-derived long shoreline datasets for the calibration and validation of equilibrium shoreline evolution models in the context of cross-shore motion. To demonstrate the above, the evolution of Nova Icaria Beach in Barcelona and Cala Millor Beach in Mallorca (Spain) are evaluated.

This chapter is organized as follows. The shoreline evolution models and the sub-pixel shoreline acquisition method (SHOREX algorithm) are presented in Section 3.2. Section 3.3 describes all the data that are related to the study sites, including the wave climate, sea levels, and shoreline positions derived from both video-camera systems and satellite images. The results, which prove

the solvency of the techniques for coastal-evolution studies, are shown in Section 3.4. Finally, a discussion and the main conclusions are summarized in Section 3.5 and Section 3.6, respectively.

3.2 Methods

As previously mentioned, the aim of this analysis is to assess the applicability of sub-pixel satellite-derived shorelines in the use of equilibrium shoreline evolution models, which require accurate data series of shoreline positions to calibrate, validate and predict the future behaviour of coasts. This section describes the shoreline evolution models, including the required data for their application, and the sub-pixel shoreline extraction method (SHOREX algorithm) to process mid-resolution satellite images. In the first sub-section, two specific models are presented by describing their calculation formulations, inputs, calibration parameters and outputs.

3.2.1 Shoreline evolution models

The equilibrium shoreline evolution models are conceptually based on the balance between destructive and constructive forces that act upon a beach, enabling us to obtain the shoreline position, S, at a time "t". These models aim to evaluate changes in shoreline position that occur because of storm responses and seasonal changes.

Among the several shoreline evolution models that are related to cross-shore sediment transport in the literature (see Section 2.5.1), the models developed by Yates et al. (2009) (hereafter referred to as "YA09") and Jara et al. (2015) (hereafter referred to as "JA15") were selected for use in this present study. The former is probably the most widely used model of this type in recent years, and the second is a novel model that requires the lowest number of calibration parameters of all the models of the same type.

Both models are based on a differential equation, where the shoreline position's variation along time, $\frac{\partial S(t)}{\partial t}$, is a function of calibration constants ($C^{\pm}$, with C^{+} being a proportionality constant of accretion and C^{-} being a constant of erosion), the incident energy, E, and the equilibrium energy, E_{eq}:

$$\frac{\partial S(t)}{\partial t} = f(C^{\pm}, E, E_{eq}) \tag{38}$$

In summary, Table 3-1 consolidates the inputs for the model and calibration process, the calibration parameters and the outputs of the two selected models. Further details of both models can be found in Appendix 3 and Jara et al. (2015) and Yates et al. (2009).

Table 3-1. Inputs and calibration parameters of the selected equilibrium shoreline evolution models.

Model	Model Inputs	Calibration parameters
YA09	E	a, b, C^+, C^-
JA15	E, D_{50}, B, Vs, γ, x_t, h*	C^+, C^-

Both equilibrium shoreline evolution models require shoreline-position measurements as input for their calibration. In Section 3.2.2, the selected sub-pixel shoreline-acquisition method is described.

3.2.2 Sub-pixel technique for satellite images

The acquisition technique that is used to obtain sub-pixel shorelines from satellite images is named SHOREX (SHOReline EXtraction system). This is an algorithm that can extract the shoreline position from mid-resolution satellite images with sub-pixel accuracy (Pardo-Pascual et al. 2018; Palomar-Vázquez et al. 2018). The algorithm integrates all the necessary phases to achieve the solution: image downloading, pre-processing (storing, format conversions, pixel-value transformation, clipping, cloud masking and image georreferencing), and the final processing based on the shoreline extraction itself. This methodology has been tested in previous studies (Pardo-Pascual et al. 2018; Almonacid-Caballer et al. 2016; Sánchez-García et al. 2015), showing results at approximately 5 m of accuracy in shoreline determination, which suggests its usefulness for coastal-evolution studies and especially for the applicability of equilibrium shoreline evolution models.

Regarding the extraction process, which is the central core of SHOREX, the algorithm initially takes an approximate pixel-level shoreline throughout a chosen threshold by following the bimodal nature of the histogram of an infrared band when water and land are both present. If possible, a unique digitized or available pixel-level shoreline for the whole set of temporal images of an area could also be used instead. Then, every candidate pixel is analysed according to its neighbourhood to determine the shoreline position at the sub-pixel level (Pardo-Pascual et al. 2012). After resampling this initial neighbourhood, a complete fifth-degree polynomial surface fits the data using the least-squares method and its inflection contour lines are found. Then, the sub-pixel shoreline is found where the Laplacian of this fitted polynomial is null. Having in each analysis window different candidate curves as a potential solution, the result with the largest gradient module will define finally the sub-pixel shoreline position, such as in Fig. 3-1.

Moreover, in a preliminary process, SHOREX deals with the potential error that the satellite imagery has in its inner georreferencing, thereby making this error negligible –below the 0.1

pixels. This is done by computing the Fourier cross-correlation through a PNOA orthophoto of the study site as shown in Almonacid-Caballer et al. (2017).

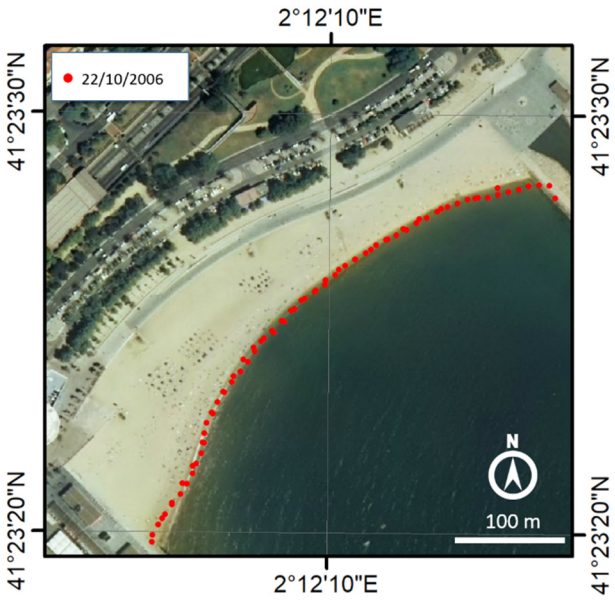

Fig. 3-1. Sub-pixel shoreline solution in Nova Icaria Beach with the SHOREX algorithm. Sensor: Landsat 5. Band 5.

3.3 Study sites

This section presents the selected study sites, the derived shoreline position datasets from video-camera systems and satellite images, and wave characterization of the study areas as the main driving force of the equilibrium shoreline evolution models.

The selected study sites correspond to the microtidal Spanish beaches of Nova Icaria and Cala Millor at the Western Mediterranean (see Fig. 3-2). Both study sites were selected because they have a continuously monitoring video-camera system, which enables us to contrast the processed satellite-derived shorelines.

Regarding the shoreline position datasets, according to Section 2.4, in this study, the *instantaneous water line* was chosen to recognize the shoreline position from both video-camera systems (ARGUS and SIRENA) and satellite images (SHOREX).

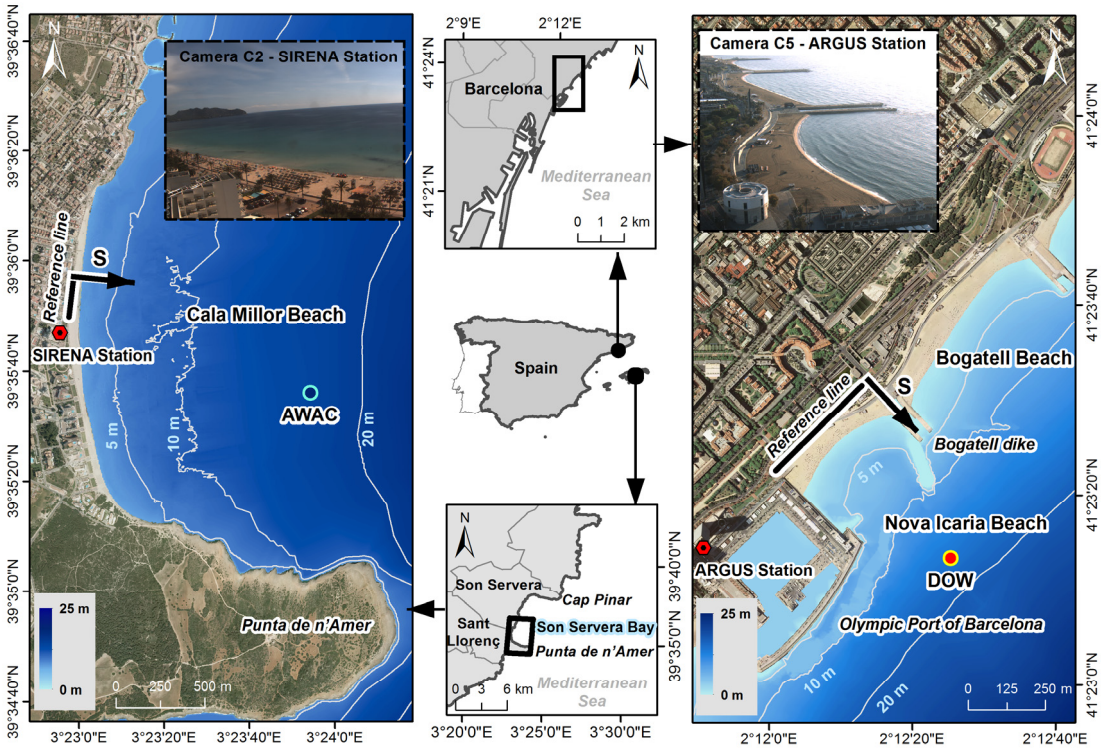

Fig. 3-2. Location of the selected study sites. Cala Millor Beach (lower and left panel) including the directional Acoustic Waves and Currents (AWAC) sensor position, SIRENA station with the corresponding Camera C2 view and the reference line to estimate the shoreline position, S. Nova Icaria Beach (upper and right panel) including "Downscaled Ocean Waves" (DOW) position, ARGUS station with the corresponding Camera C5 view and the reference line.

3.3.1 Nova Icaria Beach

3.3.1.1 Study site

Nova Icaria Beach is located in Barcelona (Catalonia), north-eastern Spain (see Fig. 3-2). This beach was a component of the Barcelona sea-front recovery project (Peña and Covarsl, 1994), which was conducted for the Olympic Games in 1992.

Nova Icaria is a 400 m-long non-barred sandy beach that is embedded between the Olympic Port in Barcelona to the south and the Bogatell dike to the north. This beach is also protected by a semi-submerged curved breakwater, which is an extension of the Bogatell dike (Z = 0 m with respect to the MSL), and a small breakwater that protects the boat-access ramp in the north-eastern section of the Olympic Port (see Fig. 3-2). The average orientation of the beach is 135° with respect to the north.

It is important to note that this beach was analysed by Jara et al. (2015), who successfully calibrated and validated the "JA15 model" for the period from January 2005 to December 2006.

Regarding the morphological parameters at Nova Icaria Beach, the median sediment grain size is D_{50}=0.75 mm (Turki et al. 2013; Jara et al. 2015). The average annual closure depth (Hallermeier, 1981) is close to 6.5 m and the corresponding horizontal position from the reference line in the backshore, x_t, is 255 m according to the local bathymetry from the means of a DGPS by Iberport Consulting in March 2008 (see Fig. 3-2). In addition, the available bathymetry permits the determination of a beach berm height, B, of 1.53 m.

3.3.1.2 Wave climate

The wave climate close to Nova Icaria Beach was acquired from the "Downscaled Ocean Waves" (DOW) reanalysis database (Camus et al., 2013) by means of a hybrid methodology based on both dynamical and statistical downscaling. The DOW database is a historical reconstruction of coastal waves for a period of 68 years from 1948 to 2015 along the Spanish coast, providing hourly sea states with different wave parameters (e.g., significant wave height Hs, peak period Tp, mean wave direction θm, etc.). Specifically, DOW is a downscaled wave re-analysis of coastal zones from a Global Ocean Waves (GOW) database (Reguero et al., 2012), which is generated with the WAVEWATCH III model (Tolman, 1992) and forced by the (NCEP/NCAR) wind field re-analysis (Kalnay et al., 1996). Detailed descriptions of the GOW database can be found in Reguero et al. (2012) and Perez et al. (2017).

The DOW point that was selected near Nova Icaria Beach is located at 41.387° latitude, 2.207° longitude, and 13.3-m depth. The scatter diagram that correlates the significant wave height, Hs, with the peak period, Tp, and the directional rose of Hs are plotted in Fig. 3-3. The dominant or more frequent waves and the most energetic waves originated from the ESE (23.82% of the time), followed by waves from the E (21.9%) and SE (21.7%). Hs and Tp were 0.01–5 m and 1–13.4 s, respectively. The wave height that exceeds 50% of the time is 0.41 m and the significant wave height exceeded 12 hours per year (Hs_{12}) is around 3 m.

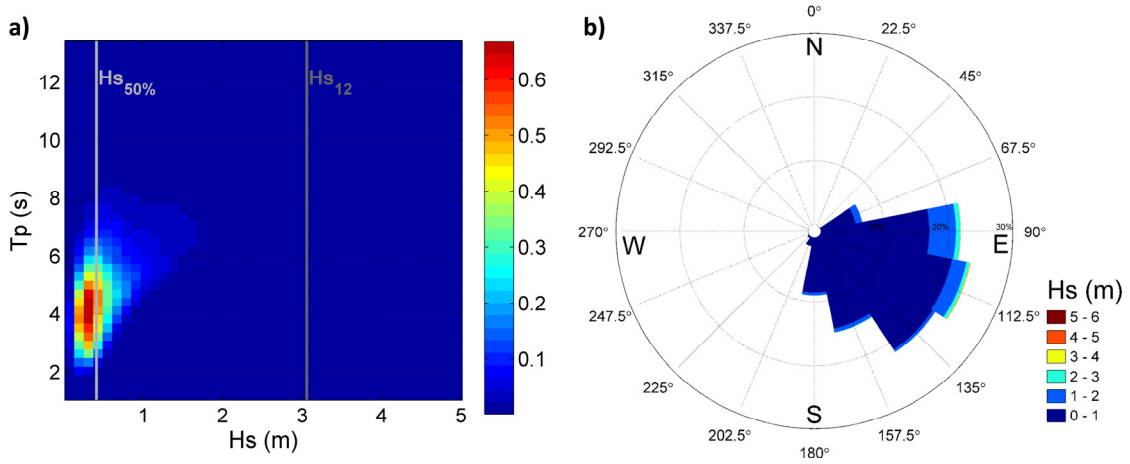

Fig. 3-3. Wave characteristics at the DOW point: a) Scatter diagram Hs-Tp. b) Directional rose of Hs.

3.3.1.3 Shoreline data

3.3.1.3.1 Video-derived shorelines

The ARGUS video system, which is located on top of the Mapfre Building by the Olympic Marina at approximately 142 m above the mean sea level (MSL), was used to obtain high-resolution shoreline positions at Nova Icaria Beach (see Fig. 3-2). This ARGUS system, which is called the "Barcelona Littoral Station", consists of five video cameras that are operated by the Mediterranean Center for Marine and Environmental Research (CMIMA), which covers a 180° view of the coast.

Daily shoreline records during 2005-2007 were obtained from snap images that were taken by camera C5. The shoreline was manually plotted and digitized in an oblique picture and then rectified by means of a Direct Linear Transformation technique, with a maximal expected error of 1 m at the northern tip of the beach (Jara et al. 2015).

3.3.1.3.2 Satellite-derived shorelines

The sub-pixel satellite-derived shorelines at Nova Icaria Beach were obtained with SHOREX from all the useful images that were available (cloud-free) from the Landsat 5 and Landsat 7 satellites between January 2005 and March 2007. The time of passage of the satellite in these scenes always oscillated between 10:20 h and 10:30 h GMT.

Fig. 3-4 shows the temporal distribution of the data used for the assessment, both from video-camera and from satellite captures, including a data record table. Until mid-2006, only a few measurements had been obtained from Landsat 7. The largest number of measurements was obtained from the Landsat 5 satellite for the period from October 2006 to March 2007.

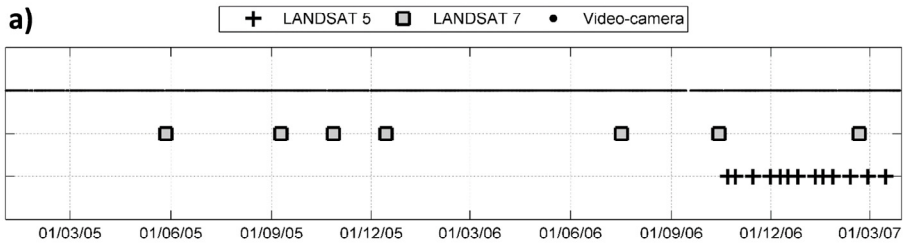

b)

Source	# Data
LANDSAT 5	13
LANDSAT 7	7
Video-camera	804

Fig. 3-4. a) Temporal distribution of video-camera and satellite data used for the assessment at Nova Icaria Beach, and b) data record table.

Fig. 3-5c shows a comparison example of the shoreline position derived from a video camera system (a) and from a satellite image using the SHOREX system (b).

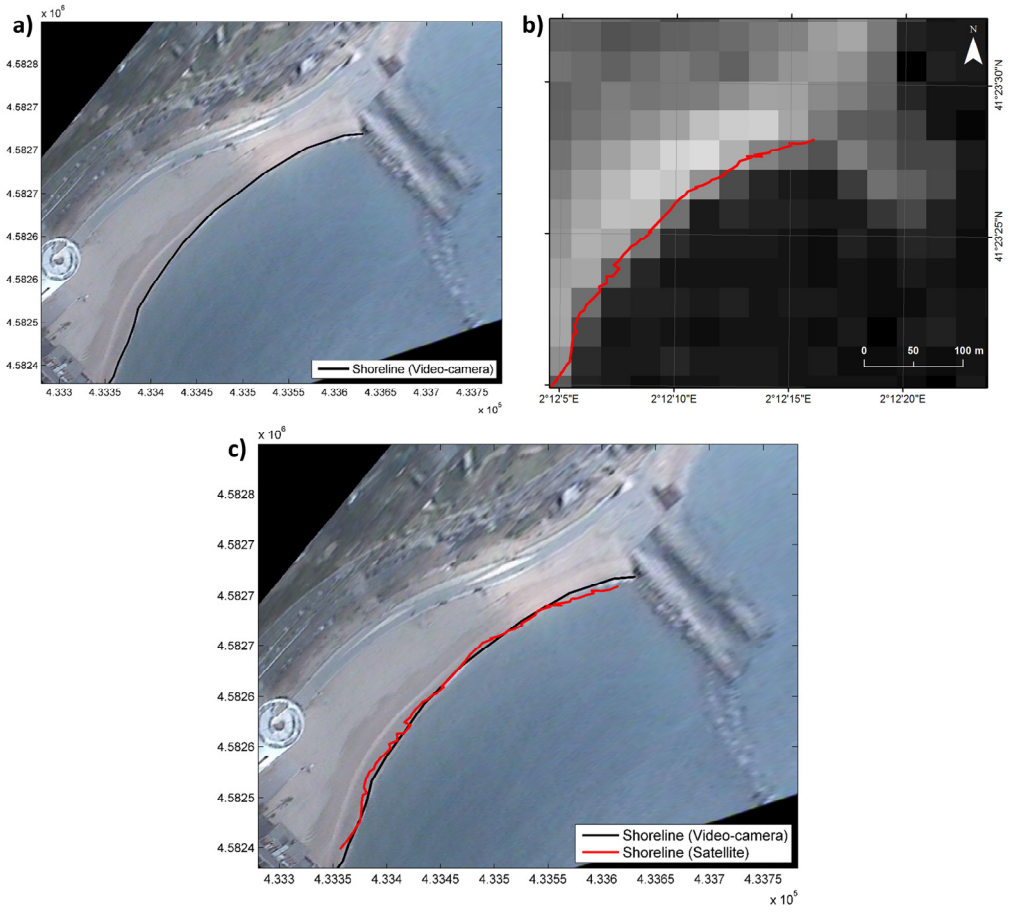

Fig. 3-5. Shoreline obtained from a) a video-camera image and b) a satellite image with SHOREX at Nova Icaria Beach, 09/09/2005. c) Comparison between both data sources (video camera and satellite).

3.3.2 Cala Millor Beach

3.3.2.1 Study site

The second study site corresponds to Cala Millor Beach (see Fig. 3-2). It is located on the eastern coast of Mallorca, between Sant Llorenç des Cardassar and Son Servera municipalities (Balearic Islands), Spain. Cala Millor is a 1700 m-long microtidal sandy beach with a configuration of transverse and crescentic bars, bounded by two rocky headlands, Punta de n'Amer southwards and Cap Pinar northwards. The beach has a concave shape backed by a boulevard, hotels and residential houses (Tintoré et al., 2009). The average orientation of the beach is around 90° with respect to the north.

The seabed from 6 to 35 m water depths is covered by a seagrass meadow of Posidonia oceanica, which acts as a cover to sediment exchange and as a friction obstacle to waves (Infantes et al., 2009).

Regarding the morphological parameters at Cala Millor Beach, the beach consists of medium to fine carbonate bioclastic sands, being the median sediment size (D_{50}) on the beach around 0.34 mm (Tintoré et al., 2009) and 0.36 mm on the selected study beach stretch. The average annual closure depth is close to 5 m and the corresponding horizontal position from the reference line in the backshore, x_t, is 230 m according to the local bathymetry of June 2016 contributed by the Balearic Islands Coastal Ocean Observing and Forecasting System, SOCIB (see Fig. 3-2). The beach berm height, B, is close to 1 m.

3.3.2.2 Wave climate

The wave climate close to Cala Millor Beach was acquired from a directional Acoustic Waves and Currents (AWAC) sensor located at 39.592° latitude, 3.399° longitude, and 17-m depth. This instrument provides the incident wave height, period, and direction. The temporary wave series has been recorded between 2011 and 2017.

Fig. 3-3a shows the scatter diagram that correlates the significant wave height, Hs, with the peak period, Tp, and Fig. 3-3b the directional rose of Hs. The dominant or more frequent waves and the most energetic waves originated from the ESE (30.9% of the time), followed by waves from the E (29.8%) and ENE (22.6%). Hs and Tp were 0.01–4.7 m and 2-25 s, respectively. The annual mean significant wave height, $Hs_{50\%}$, is around 0.37 m and Hs_{12} of 3.01 m.

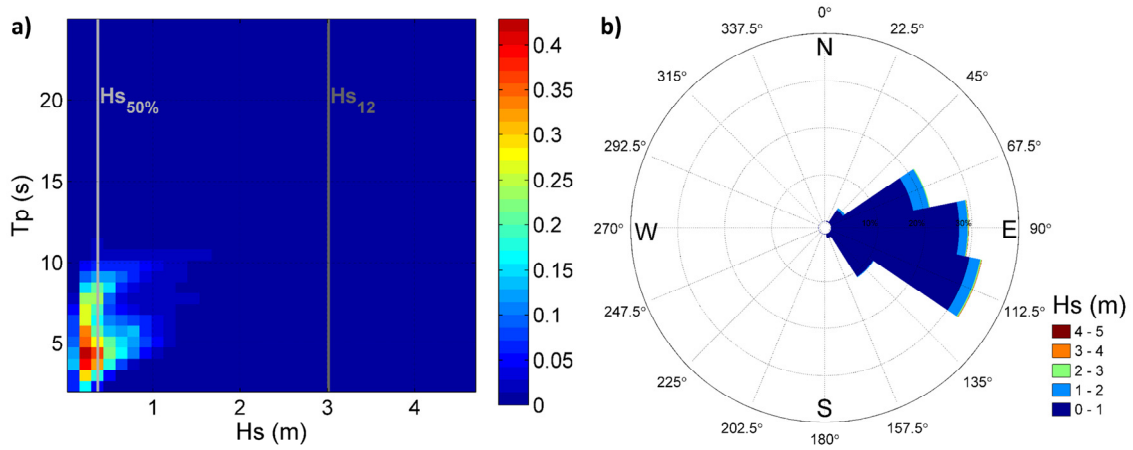

Fig. 3-6. Wave characteristics at the DOW point: a) Scatter diagram Hs-Tp. b) Directional rose of Hs.

3.3.2.3 Shoreline data

3.3.2.3.1 Video-derived shorelines

The SIRENA station video-monitoring system (Nieto et al., 2010) was developed by SOCIB and the Mediterranean Institute of Advanced Studies, IMEDEA. It consists of five video cameras located at an elevation of 46.5 m, covering and monitoring continuously the whole view of the beach site in Cala Millor (see Fig. 3-2). The system acquires snapshot images, variance image and time exposure images (widely known as Timex images) resulting from averaging 4500 images taken within 10 min each hour (Gómez-Pujol et al., 2013).

In this case, the Timex images taken by camera C2 were selected at the closest time to the satellite passage (see Section 3.3.2.3.2), for almost one and a half years (April 2015- November 2016). Before georeferencing the images, and to ensure accurate video-derived shorelines, other image pre-processing tasks were required such as distortion corrections and registering due to obvious camera displacements over time. The distortion correction inherent of the camera device was overcome by using the Camera Calibration Toolbox (Bouguet, 2015); and the displacement correction between images was solved through a cross-correlation search process to derive the affine transformation parameters. Once the registration process was done, the georectification for the whole set of images –above each corresponding sea level value– was carried out using the C-Pro tool getting a root mean square error (RMSE) of 1.54 m (Sánchez-García et al., 2017). Finally, shorelines were carefully digitized following the land-water edge between both interfaces obtaining this way the high-resolution shoreline positions for Cala Millor Beach.

3.3.2.3.2 Satellite-derived shorelines

The sub-pixel satellite-derived shorelines at Cala Millor Beach were obtained with SHOREX from all the useful images that were available from Landsat 8 and Sentinel satellites between

April 2015 and November 2016. Fig. 3-7 shows the temporal distribution of the data used for the assessment, both from video-camera and from satellite captures, including a data record table.

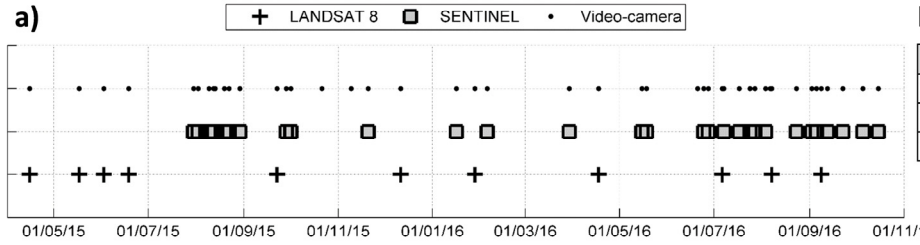

Source	# Data
LANDSAT 8	11
SENTINEL	29
Video-camera	45

Fig. 3-7. a) Temporal distribution of video-camera and satellite data used for the assessment at Cala Millor Beach, and b) data record table.

3.4 Results

This section presents the performance of the equilibrium shoreline evolution models (YA09 and JA15 models) using the selected remote-sensing data (video-camera and satellite) on the two study sites (Nova Icaria and Cala Millor Beach). In both cases, the time waves series have been propagated to the breaking point, using linear wave theory, and Thornton and Guza (1983) linear breaking criterion. The wave breaking conditions have been used to obtain the incident wave energy, the main model's driver.

Regarding the shoreline position, it has been computed as the mean position in relation to a constant reference line in the backshore (see Fig. 3-2).

In order to use the equilibrium shoreline evolution models as predictive tools, we must first identify a representative study period where the adjustment parameters of each model should be calibrated. Derived calibration parameters are then used on the unseen portion of the data to produce a blind hindcast (Splinter et al. 2013). Generally, the accuracy degree of the calibration process mainly depends on the availability of high-quality and adequate-duration input datasets.

The calibration procedure of the equilibrium shoreline evolution models was described in detail in Jara et al. (2015) and Yates et al. (2009). Basically, this calibration consists of finding the best model fit with an error-minimizing technique to solve the calibration parameters.

In this study, an iteration algorithm was used to find the proportionality constants of accretion, C^+, and erosion, C^-, which produced the lowest RMSE (Eq. (39)) between the modeled and measured shoreline positions.

$$RMSE = \sqrt{\frac{\sum_{i=1}^{n}\left(S_{data,i} - S_{model,i}\right)^2}{n}} \tag{39}$$

where i and n represent each data and the total size of the sample, respectively.

The model performance is investigated using the root-mean-square error, the correlation coefficient, ρ, and the Skill index, s, or index of agreement (Willmott, 1981).

The Skill index (Eq. (40)) is a standardized measure of the degree of model prediction error, which varies between 0 and 1; an s value equal to 1 is indicative of a perfect agreement between the two series, while a value of 0 is associated with a complete disagreement.

$$s = 1 - \frac{\sum|x - x_m|^2}{\sum(|x - \overline{x_m}| + |x_m - \overline{x_m}|)^2} \tag{40}$$

3.4.1 Results from Nova Icaria Beach

As mentioned above, the satellite-derived shorelines obtained with the SHOREX algorithm have a final accuracy of around 5 m (see Section 3.2.2), while the ARGUS video-derived shorelines have an accuracy close to 1 m (see Section 3.3.1.3.1). For Nova Icaria Beach, the equilibrium evolution models must be calibrated for a study period in which the shoreline displacement is representative (greater than 5 m). However, it should be noted that the model simulation has a resolution of the order of centimeters according to the magnitude of the incident wave energy.

The upper panel of Fig. 3-8 shows the result of the JA15 model when using the calibration parameters ($C^+ = C^- = -9 \cdot 10^{-5}$ $m^{-2}s^{-1}$) and beach-profile invariants from Jara et al. (2015) during the period from January 2005 to March 2007. According to the results of the JA15 simulation, one storm of greater intensity that would cause the greatest displacement of the coast was identified on 24/12/2006. The grey shaded box represents the selected study period for the calibration, while the dashed lines delimit the complete study period where the models will be validated. The lower panel in Fig. 3-8 shows a zoom of the selected calibration period, including the video-derived and satellite-derived shoreline data.

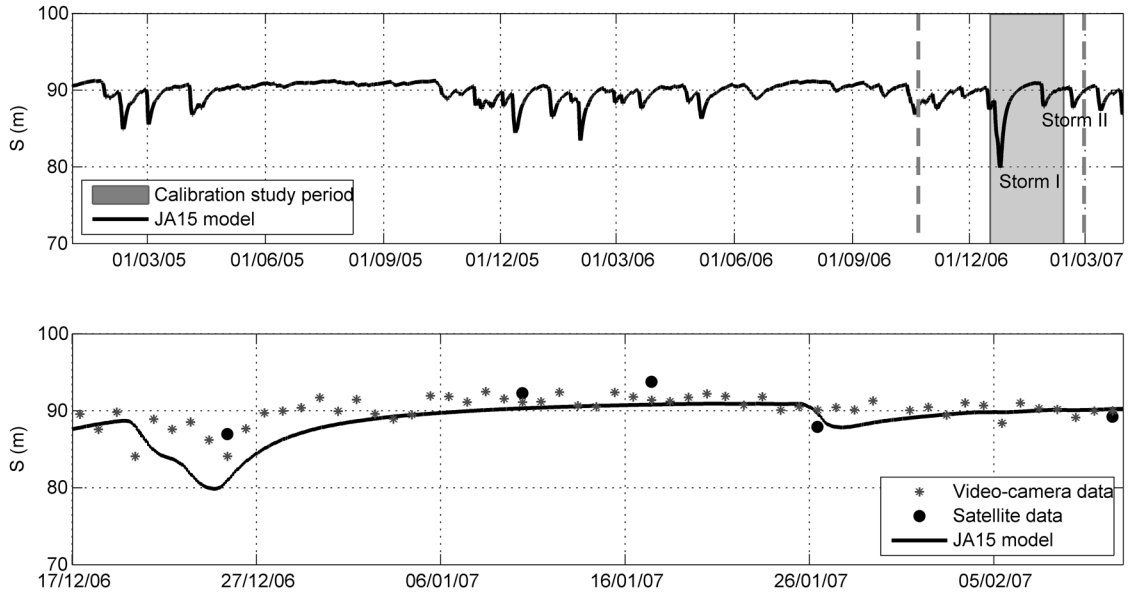

Fig. 3-8. Selection of the calibration study period. a) Shoreline position that was obtained with the JA15 model when using the parameters from Jara et al. (2015). The shaded area represents the selected study period for the calibration, considering the presence of the strongest storm during this record. The dashed lines delimit the complete study period. b) Zoom of the selected calibration study period that shows the shoreline-position data from a video camera and satellite images that were processed with the SHOREX algorithm.

As shown in Fig. 3-8a, the selected study period spanned from 22/10/2006 to 28/02/2007, with around one month for model calibration and four months for model validation. This period is relatively short, with several available satellite images.

The calibration period lasted from 17/12/2006 to 12/02/2007 met two minimum requirements to perform model calibration: at least two storm events with different magnitude and two processes, namely, accretion and erosion. The starting point of the calibration period coincided with beach recovery after Storm I, which caused the greatest erosion in the record. The fourth measurement of satellite data corresponded to erosion that was caused by Storm II.

Fig. 3-9 shows the models' performance when using video-camera and satellite data during the four-month period between 22/10/2006 and 28/02/2007 for model validation. According to the results, general shoreline advances and retreats were adequately represented by the selected models for both data sources. The observed and modeled shoreline positions showed fast erosion after major storms and relatively fast accretion during post-storm recovery for both models.

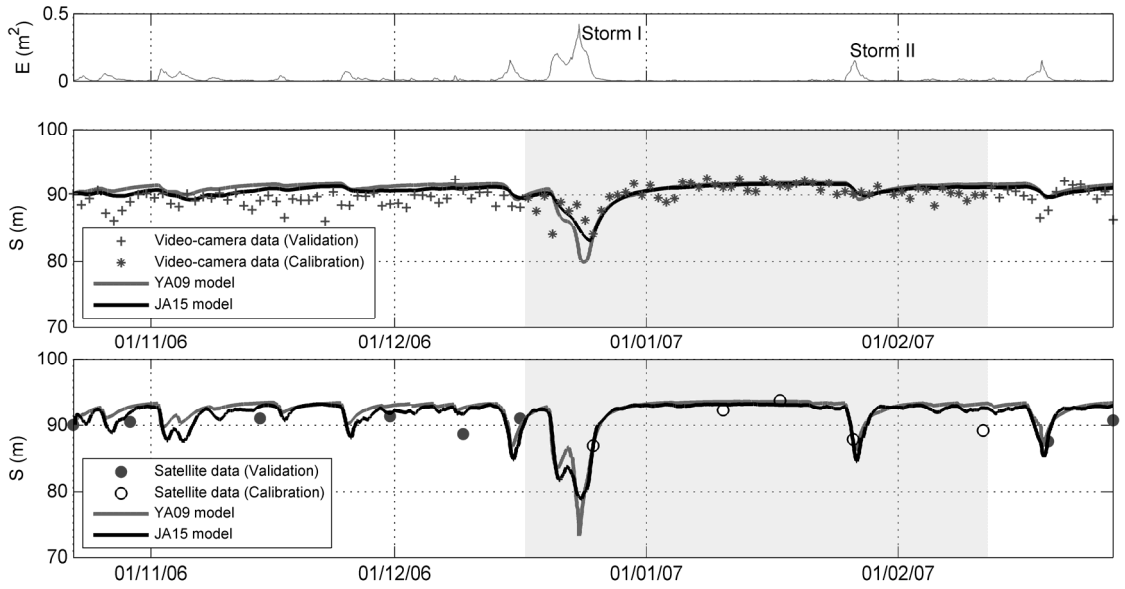

Fig. 3-9. Results from Nova Icaria Beach. Time series of the wave energy (upper panel), validation of the shoreline evolution models with video-derived shorelines (middle panel), and validation of the shoreline evolution models with satellite-derived shorelines processed with the SHOREX algorithm (lower panel). The shaded area represents the selected study period for the calibration.

Table 3-2 lists the best fits for all the calibration parameters, the RMSE, the correlation coefficient, ρ, and the Skill index, s, for the validation period considering the application of both selected equilibrium shoreline evolution models with each data source.

Table 3-2. Calibration parameters, root mean square error (RMSE), correlation coefficient and Skill index between the observed and modelled shoreline positions at Nova Icaria Beach.

Model	**Using video-derived shorelines**				**Using satellite-derived shorelines**			
	Calibration	**Validation**			**Calibration**	**Validation**		
	Calibration parameters	**RMSE (m)**	**ρ**	**s**	**Calibration parameters**	**RMSE (m)**	**ρ**	**s**
YA09	C^+= -2.4·10^{-3} m^{-2}s^{-1} C^-= -8.05·10^{-5} m^{-2}s^{-1} a= -0.0187 m b= 1.7250 m^2	1.99	0.45	0.63	C^+= -3.8·10^{-3} m^{-2}s^{-1} C^-= -1.68·10^{-2} m^{-2}s^{-1} a= -0.0194 m b= 1.8175 m^2	2.18	0.73	0.77
JA15	C^+= -2.5·10^{-4} m^{-1}s^{-1} C^-=-4.2·10^{-5} m^{-1}s^{-1}	1.58	0.55	0.69	C^+= -2.9·10^{-3} m^{-1}s^{-1} C^-=-4.5·10^{-4} m^{-1}s^{-1}	1.72	0.72	0.82

Generally, the calibration parameters from the video-camera data were lower than the calibration parameters from the satellite data. This result is reflected in the smoother behaviour of the model when using video-camera data and faster erosion and accretion when using satellite data. This

result can be explained by the fewer satellite-derived shorelines and the models attempting to adjust to positions with large displacements.

3.4.2 Results from Cala Millor Beach

In the case of Cala Millor Beach, almost five months (September 2015 to February 2016) of shoreline measurements were considered for calibration purposes of the equilibrium shoreline evolution models. Then, the models using video-camera and satellite data were validated for more than one and a half years (from April 2015 until November 2016), as shown in Fig. 3-10. The iteration technique mentioned at the beginning of Section 3.4 was used to find the best set of free parameters that minimize the RMSE between the modeled and observed shorelines.

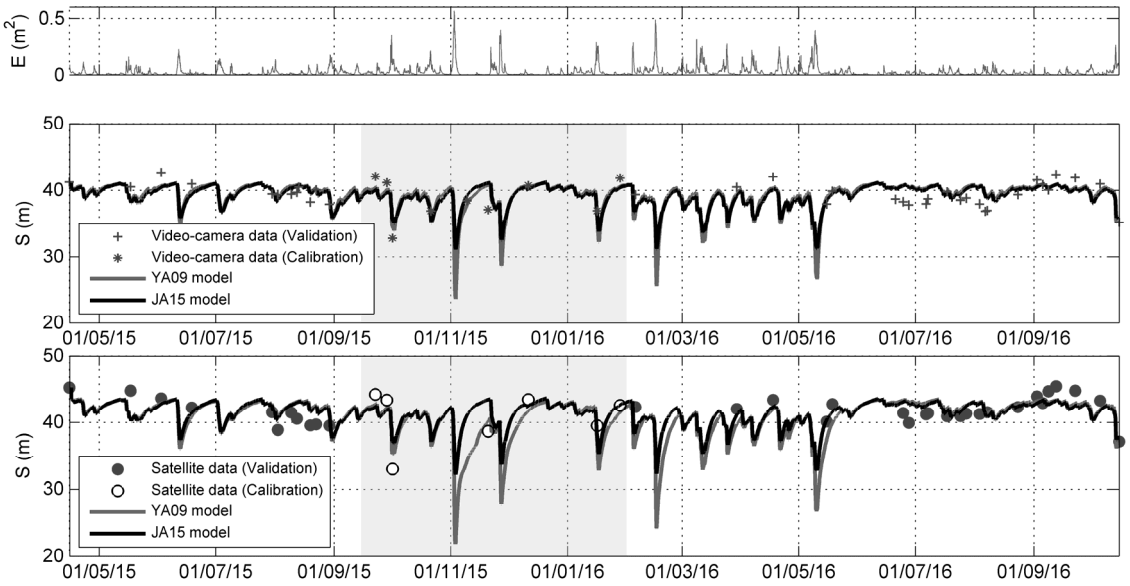

Fig. 3-10. Results from Cala Millor Beach. Time series of the wave energy (upper panel), validation of the shoreline evolution models with video-derived shorelines (middle panel), and validation of the shoreline evolution models with satellite-derived shorelines processed with the SHOREX algorithm (lower panel). The shaded area represents the selected study period for the calibration.

Fig. 3-10 shows a seasonal variation of the incident wave energy, with strong storms during winter periods and low energy waves during the summers. The results reveal that the selected models for both data sources, again, have achieved good performance, successfully reproducing the general advance/retreat shoreline trend.

The best fits for all the calibration parameters, RMSE, ρ and s for the validation period considering the application of both selected models with each data source are listed in Table 3-3.

Table 3-3. Calibration parameters, root mean square error (RMSE), correlation coefficient and Skill index between the observed and modelled shoreline positions at Cala Millor Beach.

Model	Using video-derived shorelines				Using satellite-derived shorelines			
	Calibration	Validation			Calibration	Validation		
	Calibration parameters	RMSE (m)	ρ	s	Calibration parameters	RMSE (m)	ρ	s
YA09	C^+= -3.1·10^{-3} m^{-2}s^{-1} C^-= -1.1·10^{-3} m^{-2}s^{-1} a= -0.0133 m b= 0.5533 m^2	1.56	0.61	0.76	C^+= -1.3·10^{-3} m^{-2}s^{-1} C^-= -1.8·10^{-3} m^{-2}s^{-1} a= -0.0133 m b= 0.5933 m^2	2.02	0.60	0.77
JA15	C^+= -2.5·10^{-4} m^{-1}s^{-1} C^-=-3.4·10^{-4} m^{-1}s^{-1}	1.58	0.62	0.72	C^+= -2.1·10^{-4} m^{-1}s^{-1} C^-=-4.6·10^{-4} m^{-1}s^{-1}	1.90	0.60	0.75

In both cases (Nova Icaria Beach and Cala Millor Beach), the resulting RMSE between the observed and modeled shoreline positions with both models was around 1.5 - 2 m. The correlation coefficient between the observed and modeled shoreline positions were satisfactory values.

3.5 Discussion

The empirical nature of shoreline evolution models requires high-quality observational datasets to calibrate model parameters. All the cross-shore evolution model applications in the literature correspond to target study sites where high-resolution data were available (video-camera systems or topo-bathymetric surveys). However, no studies had applied yet shoreline-position datasets from satellite imagery for not being accurate enough – contrary to the just several meters of definition that SHOREX is able to reach. Thus, this study is a pioneering study with a promising future.

A comparative analysis between video-derived and satellite-derived shorelines was conducted to explore the applicability of these sub-pixel processed satellite-image data in equilibrium shoreline evolution models. The applications of these shoreline evolution models at Nova Icaria Beach and Cala Millor Beach show overall good performance. Fig. 3-11 shows six panels, where the first two present scatter plots that relate the coincident data between video-camera images and satellite images used for model calibration and validation in both study sites. The following panels present scatter plots that relate the modeled shorelines (YA09 and JA15 models) with the measured shorelines (from video-camera and satellite images). It should be noted that the RMSE of the coincident positions between video-derived and satellite-derived shorelines was only 2.49 m in the case of Nova Icaria Beach and 2.46 m at Cala Millor Beach.

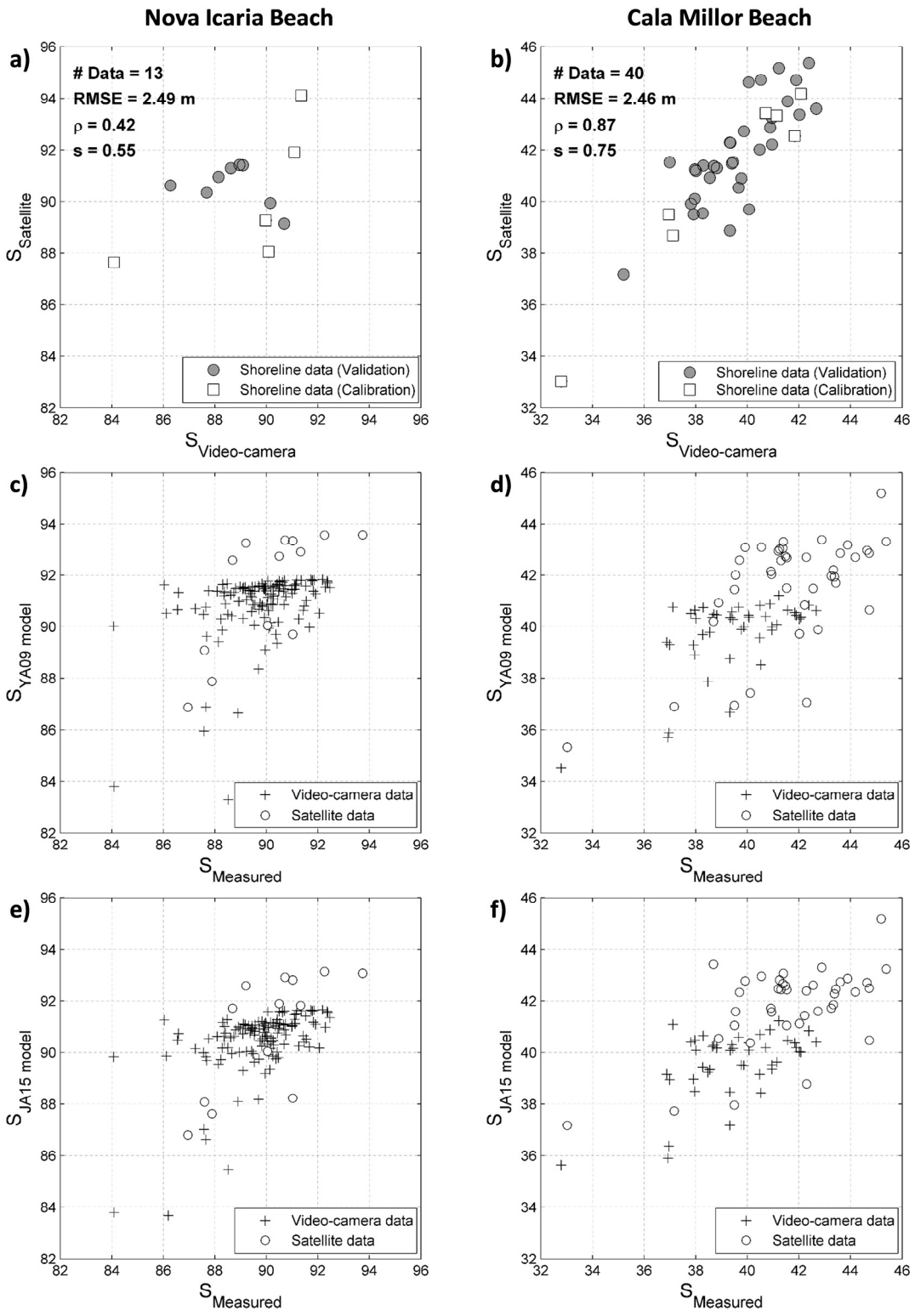

Fig. 3-11. Scatter plots for Nova Icaria Beach (left panels) and Cala Millor Beach (right panels) considering: coincident shoreline positions from video-camera and satellite data (a and b), measured shoreline positions with YA09 model results (c and d) and measured shoreline positions with JA15 model results (e and f).

The development of this study enabled us to evaluate the advantages and limitations of mid-resolution satellite images as an alternative data source to obtain temporal series of shoreline positions in short- to medium-term model analysis.

On the one hand, earth-observation satellites have the great advantage of providing information anywhere in the world and at any time of the year, regardless of the season. Currently, a wide variety of satellites have specific temporal and spatial resolutions depending on their purpose. However, the turning point has been the disclosure of what can be accomplished with mid-resolution satellite images. The USGS and the ESA have released their archives of Landsat and Sentinel-2 scenes free of charge. The historical record can reach 40 years of data around the world, covering large geographical scales. Currently, mid-resolution satellite images have the best balance between resolution and revisiting time (Li and Roy, 2017). The synergy between Landsat and Sentinel-2 builds a monitoring system with a global median average revisit interval of 2.9 days.

On the other hand, satellite images have certain limitations, such as the temporal frequency of satellite observations. Additionally, image visualization can be compromised by the presence of clouds or other agents (distortion, failures, etc.). Moreover, coarse spatial resolutions limit usage; the solution to this problem is to develop algorithms that work accurately at the sub-pixel level. These limitations could become very relevant if they prevent us from visualizing the movements of an entire coast or if the lack of captures simply does not allow us to evaluate the effect of strong waves on shoreline retreat. Therefore, the combination of satellite data with accurate sub-pixel acquisition techniques (SHOREX algorithm) is a promising tool for coastal studies.

In this study, Nova Icaria and Cala Millor beaches were intentionally selected because both are located in a microtidal zone, guaranteeing that neither the video-camera nor satellite images would experience difficulty when identifying the water-land interface. Currently, remote-sensing techniques (video-cameras and satellites) still have trouble automatically detecting the shoreline position in macrotidal environments and along beaches with the presence of bars, shoals or rhythmic shapes.

Finally, the shoreline position in the two selected beaches is controlled by both natural and anthropogenic factors, the latter of which inhibit the analysis of natural shoreline evolution on the order of many years or decades.

3.6 Conclusions

Coastal engineers, scientists and managers require historical records of shoreline positions to monitor shoreline erosion-accretion trends and general beach variability. Experts usually use evolution models to predict future shoreline positions. In this case, equilibrium shoreline evolution models require high-quality shoreline-position series for calibration and validation.

- Sub-pixel processed satellite-image data represent an opportunity to improve the comprehension of morphodynamics in coastal zones, such as analysing beach-trend evolution, coastal erosion from storms, beach recovery, nourishment monitoring, climate-change effects or developing and testing predictive models for coastal variability. These valuable data should be applicable for equilibrium shoreline evolution models (cross-shore and longshore) and different types of empirical models, such as bar-line position variation (e.g., Plant et al., 1999; Blossier et al. 2016) or other distinguishable morphological parameters on satellite images.
- This work explored the applicability of accurately obtained satellite-derived shorelines as input data for the calibration of shoreline evolution models. A comparative analysis on model calibration and validation that used shoreline datasets derived from a video-camera system and satellite imagery was conducted for Nova Icaria Beach and Cala Millor Beach. In both cases, the general erosion-accretion trend was adequately represented by equilibrium shoreline evolution models compared to shoreline measurements at a qualitative and quantitative level.
- It should be noted that the selected study sites are located in micro-tidal environments. Considering meso or macrotidal zones, the shoreline definition could be compromised in areas with very low slopes and high tidal ranges, where the intertidal space may be hundreds of meters wide. Nonetheless, authors such as Sánchez-García, (2019) and Sánchez-García et al., (2019) have proposed solutions to continue providing methodological robustness regardless of beach typology and tidal conditions.
- Finally, the synergy between evolution models and satellite data with a robust sub-pixel acquisition method is expected to facilitate influential coastal evolutionary studies and improve both retrospective and future predictions. The limitation of temporary image data would be solved with the model, and any spatial limitations would be solved by the worldwide availability of images.

4 A MODEL CONSIDERING THE VARIABILITY OF THE BEACH PROFILE VOLUME‡

4.1 Introduction

Most sandy beaches worldwide have a tendency of progressive shoreline advances or retreats for years or even decades, and this pattern is a product of multiple factors, which may be of natural or anthropic origin. In addition, the beaches usually suffer from specific alterations at a shorter

‡ This Chapter is based on Jaramillo et al., (2020): Jaramillo, C., Jara, M.S., González, M., Medina, R., 2020. A shoreline evolution model considering the temporal variability of the beach profile sediment volume (sediment gain / loss). Coast. Eng. 156, 103612. https://doi.org/10.1016/j.coastaleng.2019.103612

time scale, which are reflected by a representative sediment deficit or surplus (Mentaschi et al., 2018). Therefore, to predict the shoreline variability in such cases, the numerical models of morphological evolution must contemplate a rate of change of shoreline position for sediment gain or loss.

As presented in Section 2.5, in the literature, there is an extensive list of different types of models that simulate shoreline evolution. The computational cost of the process-based morphodynamic models (van Rijn et al., 2003) prevents their application to multi-annual or even inter-annual morphological changes. In contrast, equilibrium shoreline evolution models are computationally efficient and can be applied to investigate long-term morphological changes (Davidson and Turner, 2009).

The equilibrium shoreline evolution models try to reproduce the shoreline evolution based on a kinetic equation in which the change rate is proportional to the difference between a theoretical equilibrium condition and the current conditions. Recently, Jara et al., (2018) presented a summary of most up-to-date literature related to this type of model, and the summary was divided into two approaches: 1. models based on an equilibrium condition correlated with the shoreline position (e.g., Yates et al., 2009; Jara et al., 2015; Doria et al., 2016) and 2. models based on an equilibrium condition as a weighted average of antecedent conditions (e.g., Davidson et al., 2013; Splinter et al., 2014). The model proposed in this chapter is framed into the first group.

Most likely, the most widely used model based on an equilibrium condition correlated with the shoreline position corresponds to the proposal of Yates et al., 2009 (hereafter defined as the YA09 model). The YA09 model has been successfully applied to various beaches governed by strong seasonal and interannual variability due to cross-shore sediment transport (e.g., Yates et al., 2011; Castelle et al., 2014; Lemos *et al.*, 2018); however, these study cases did not experience a marked trend of sediment gains or losses in the medium-long term.

To extend the application of the empirical equilibrium models and to account for unexplained shoreline motions, such as long-term trends that are uncorrelated with wave climate changes at small time scales (days or weeks), some authors have added a constant to the model equation. In this way, Long and Plant, (2012) proposed a shoreline change model incorporating short- and long-term evolution integrated into a data assimilation framework. They considered a linear trend term for longshore approximation; nevertheless, they followed the YA09 bases, assuming a constant relationship between the equilibrium shoreline position and the incident wave energy (this relation is known as the “equilibrium energy function”, EEF; Jara et al., 2015) for forecasting purposes. Long and Plant, (2012) tested their model in a synthetic case of 2 years of monthly sampled data, but not in any cases of real beaches.

Jara et al. (2015) concluded that the relationship between the equilibrium shoreline position and the incident wave energy is implicitly related to the morphological beach characteristics; more specifically, a constant linear relationship would be associated with a constant sediment volume delimited in the active beach profile. The above relation is translated into the following consequence: if an empirical equilibrium model uses a constant EEF for a study site with a net sediment volume deficit or surplus, then the evolution model would amplify or overestimate the accretion-erosion oscillations in an unrealistic way. Therefore, a constant EEF is not appropriate for study sites subjected to significant sediment gains or losses.

Based on the above, **the aim of this study is to present a new extension of the YA09 model; this extension considers the variation in the EEF by means of a trend rate of sediment gain or loss, v_{lt}.** This rate is a source or sink of sediments related to unresolved processes, as defined by Vitousek et al., (2017). There are multiple natural or anthropic origins that may cause this trend rate on sandy beaches, such as littoral sediment drift alongshore (e.g., Komar and Inman, 1970; Miller, 1999), sediment discharge by the rivers (e.g., Baban, 1995; Boateng et al., 2012), nourishments (e.g., Hanson et al., 2002; Ludka et al., 2018; Tonnon et al., 2018), dune erosion (e.g., Castelle et al., 2017; Splinter et al., 2018), cliff retreat (e.g., Limber et al., 2018; Young, 2018), aeolian sediment transport (e.g., Davidson-Arnott and Bauer, 2009; Cohn et al., 2018) and others.

This chapter is organized as follows: first, the theoretical development of the proposed model is explained in Section 4.2. Two study sites were selected to test the model: first, we used one and a half years of shoreline position data obtained from a video camera system at Nova Icaria Beach, Catalonia; and second, we used approximately 20 years of shoreline position data acquired from beach profile surveys at Campo Poseidón, Huelva. The study sites, marine conditions and shoreline acquisition methods are detailed in Section 4.3. The model results for both study sites are shown in Section 4.4, and further discussions are provided in Section 4.5. Finally, the main conclusions are summarized in Section 4.6.

4.2 Model development

As stated previously, several shoreline evolution models based on an equilibrium condition correlated with the shoreline position have been developed to simulate the shoreline position variability due to storm response and seasonal changes. These models relate the rate of cross-shore shoreline displacement, dS/dt, to the incident wave energy and the wave energy

disequilibrium between the wave energy and the equilibrium wave energy that would cause no change to the present shoreline location (Castelle et al., 2014).

The model proposed in the present study is based on the kinetic equation defined by Yates et al. (2009). According to the YA09 model, the governing equation that describes the rate of shoreline change is of the form (Eq. (41)):

$$\frac{dS(t)}{dt} = C^{\pm} E^{1/2} \cdot \Delta E(S) \tag{41}$$

$$\Delta E = \left(E - E_{eq}\right) \tag{42}$$

where S(t) and E are the shoreline position (m) and the incident wave energy (m^2), respectively, at time "t", $E^{1/2}$ is the square root of the incident wave energy as an energy weighting factor that prevents nonphysical changes in the shoreline position (Yates et al., 2009), ΔE (see Eq. (42)) is the wave energy disequilibrium, $C^{\pm}$ is the proportionality constant of accretion ($m^{-2}s^{-1}$), C^{+}, when $\Delta E < 0$, or erosion, C^{-}, when $\Delta E > 0$, and E_{eq} is the equilibrium wave energy.

The shoreline position, S, is computed as the average position of the shoreline in relation to a constant reference point or line in the backshore (see Fig. 4-2). Following Jara et al., (2018), the incident wave energy, E can be expressed as the zero-order moment of the wave height at breaking, H_b, according to Thornton and Guza, (1983).

$$E = \left(\frac{H_b}{4.004}\right)^2 \tag{43}$$

In both formulations (Eq. (41) and (42)), it remains to be defined how the equilibrium wave energy, E_{eq}, is estimated. The value of Eeq is determined in the YA09 model using a linear function of the shoreline position following the next expression:

$$E_{eq}(S) = aS + b \tag{44}$$

where "a" and "b" are the slope (m^2/m) and the ordinate axis intercept (m^2), respectively.

Yates et al. (2009) defined the equilibrium shoreline position, S_{eq}, for a given wave energy as follows:

$$S_{eq} = \frac{E - b}{a} \tag{45}$$

The analytical correlation of Eq. (45) is the previously defined EEF (Jara et al., 2015). Basically, this correlation is the cornerstone of shoreline evolution models based on an equilibrium condition correlated with the shoreline position. As Jara et al. (2015) concluded, the EEF implicitly considers the sediment volume available in the physiographic unit; therefore, a constant EEF is useful for beaches that preserve their sediment volume over time. However, a constant EEF is not useful for study sites subjected to significant sediment gains or losses.

Based on the aforementioned aspects, we propose an extension of the YA09 model including a linear trend term, v_{lt}, for the longshore approximation (m/s) and this term should be considered in the EEF behavior while the beach under study is subjected to net sediment gains or losses. In this sense, Eq. (45) must evolve over time in such a way that the relationship is an increasing or decreasing function, depending on the rate of sediment gain/loss acting on the physiographic unit. In this study, the EEF takes the following form:

$$S_{eq} = \frac{E - b}{a} + v_{lt} \cdot t \tag{46}$$

It is important to note that Long and Plant, (2012) (hereafter referred to as the LP12 model), included the linear trend term, v_{lt}, to the YA09 model, but in the Eq. (41) adding also the Kalman filter. This data assimilation method automatically adjusts the model parameters (a, b, C± and v_{lt}) during runtime to best fit any available observed shoreline data at the concurrent time step (Vitousek et al. 2017). In other words, as concluded by Vitousek et al. (2017), the Kalman filter is used as a largescale calibration tool, and after the last available shoreline observation is assimilated, the model parameters remain constant for the entire forecasting period. From the above, it is inferred that the LP12 model, including the Kalman filter, uses an EEF that evolves during the calibration period, but then, it remains constant for the forecasting period.

Fig. 4-1 shows an EEF example of the proposed model based on the study site of Nova Icaria Beach, which is evaluated in detail in Section 4.4.1. The upper panel of Fig. 4-1 shows only one month of time series of incident wave energy, and the bottom panel shows the corresponding empirical approximation of the EEF (black line). The points are consecutive measurements that are colored according to the shoreline change rate.

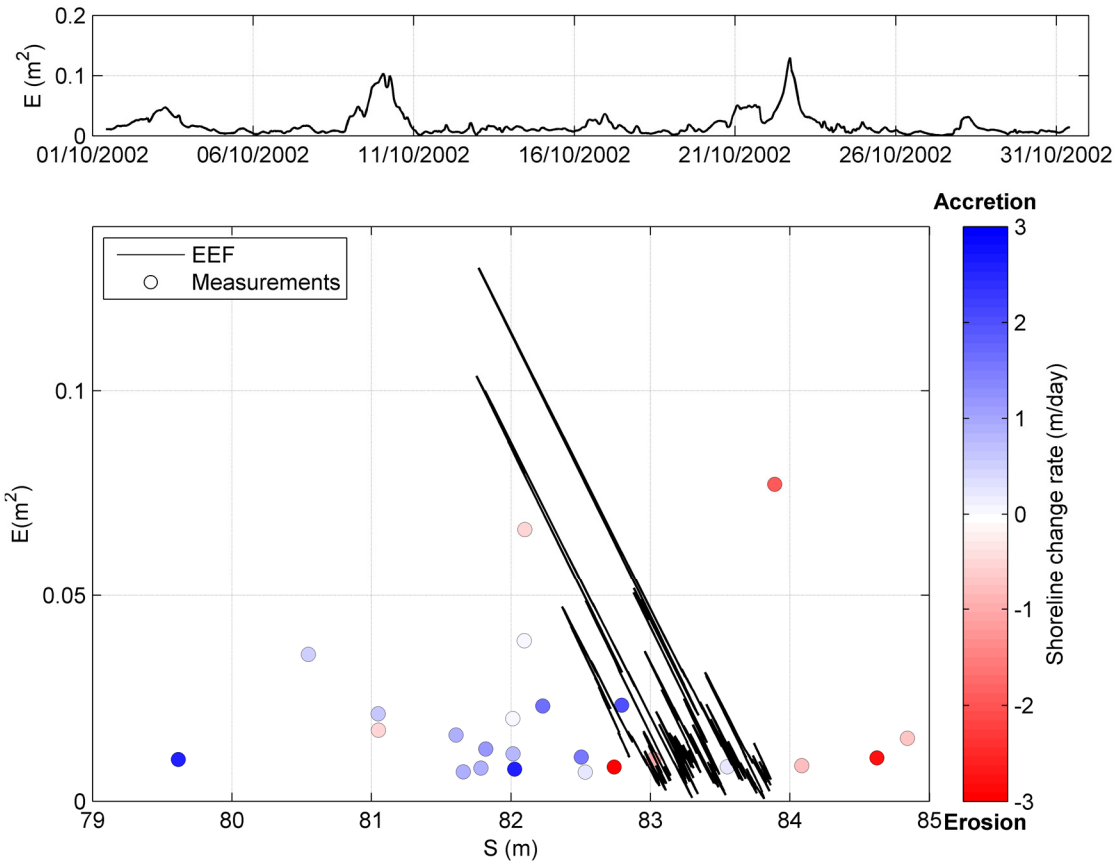

Fig. 4-1. One month of incident wave energy at Nova Icaria Beach (upper panel) as driver of an EEF (black line in bottom panel). The points are consecutive measurements that are colored according to the shoreline change rate.

4.2.1 Model hypotheses and assumptions

The proposed model in this study assumes the same bases as the YA09 model, in terms that shoreline changes mainly respond to wave energy and it is insensitive to wave direction, and as such, it is best suited for locations where waves are the primary driver of shoreline response. Also, the model does not account for short-scale processes such as beach cusp formation, alongshore variable bar welding, or rip current embayments (Splinter et al., 2014).

By neglecting the wave directionality of each sea state, the model is not able to capture the short-term variability of the longshore sediment transport. However, the long-term shoreline change due to gradients in longshore transport and/or onshore/offshore feeding/loss of sand may be captured by the linear trend term, v_{lt}. This linear term has been included to consider the overall longshore processes, considering that where these processes cannot be captured by the linear term (or the wave-driven model component), the model does not accurately resolve the shoreline response.

Following the conclusions found by Yates et al., (2009); (2011) the sediment grain size affect the magnitude of the equilibrium slope "a" and the rate change coefficients $C^{\pm}$, both of which affect the rate of beach change. From the above, variations of free parameter values between sites are implicitly associated with the beach's physical characteristics. In this study, it is considered that the calibration parameters (C^{-} and C^{+}) associated to erosion and accumulation processes remain constant during the entire model simulation.

With respect to the tidal range, the model does not explicitly include any additional parameters. Nonetheless, as suggested by Castelle et al., (2014) the equilibrium shoreline evolution models can be applied to a range of elevation contours in the intertidal zone to evaluate the effect of wave energy at different altitudes along the intertidal beach profile, with satisfactory efficiency. Castelle et al., (2014) concluded that the best shoreline proxy in their mesotidal study site was related to the mean high water level, where the inner-bar and berm dynamics have little influence on the shoreline cross-shore displacement. This conclusion was supported by Lemos et al., (2018) who analyzed a macrotidal environment and found that the equilibrium models show a good predictive ability in the upper intertidal zone where the sediment dynamics depend mainly on the waves energy.

As suggested by Splinter et al., (2014), the exclusion of water level precludes the impacts of changes in mean water level due to climatological impacts, such as storm surge, El Niño - Southern Oscillation (ENSO), and sea level rise.

4.2.2 Model implementation

From the governing equations described above, this section presents a brief methodology to apply the proposed model.

The first step is to identify whether the beach under study is subjected to a net gain or loss of sediments. For this, the slope of the trend term, v_{lt}, relies on the regression of historical data as long as possible. This term can be obtained by historical records of shoreline surveys or, for example, by evaluating the average rate of alongshore sediment transport by means of historical wave data propagated to the coast.

The next step is to determine the remaining calibration parameters (a, b and $C^{\pm}$). For this, it is necessary to define a calibration time period in which a constant EEF is evaluated by means of Eqs. (41), (42) and (46), considering that $v_{lt} = 0$. This initial relationship is the best fit line to the observed average wave energy causing no change in the shoreline position. The calibration parameters $C^{\pm}$ must be obtained through an iterative algorithm.

The calibration period can be considered as follows:

- A period of time in which there is no significant trend of a gain or loss of sediments.
- A period of time with a significant trend of a gain or loss of sediments. In this case, the trend term, v_{lt}, must be filtered.

Once all the calibration parameters (a, b, $C^{\pm}$ and v_{lt}) have been defined, the model is validated using Eqs. (41), (42) and (46), considering that $v_{lt} \neq 0$. In summary, the EEF starts from an initial linear relationship from which it evolves according to the rate of sediment gain/loss acting on the beach.

4.3 Study sites

In this section, the selected study sites are presented. The right panel of Fig. 4-2 corresponds to Nova Icaria Beach, as this represents a study site where the beach accretion process was experienced in a limited time period (Ojeda and Guillén, 2006); on the left panel of Fig. 4-2, there is a monitored beach profile of Rompeculos Beach (referred to as the Campo Poseidón beach profile), where a continuous sediment loss process has been recorded (Fernández et al., 1990).

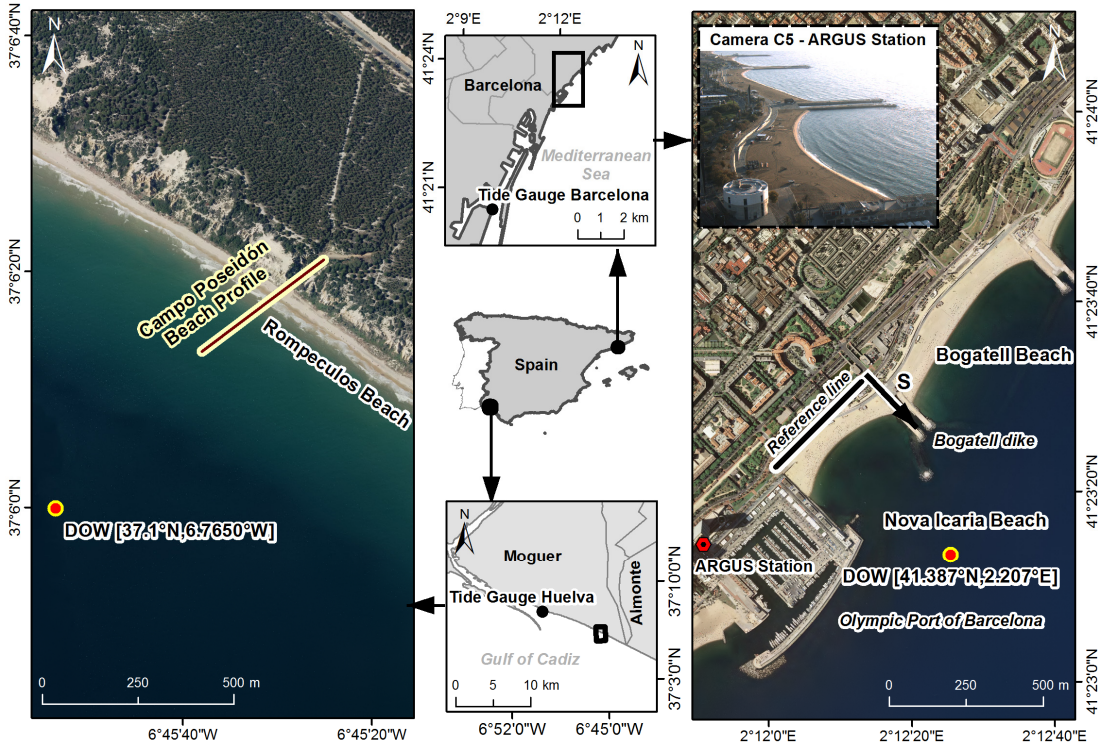

Fig. 4-2. Location of the selected study sites. Campo Poseidón (lower and left panel), including the "Downscaled Ocean Waves" (DOW) position, Tide Gauge Huelva and monitoring beach profile. Nova Icaria Beach (upper and right panel), including the DOW position, Tide Gauge Barcelona and the ARGUS station with the corresponding Camera C5. In both cases, the reference point or line to estimate the shoreline position, S, is indicated.

The marine conditions acting in the vicinity of both study sites (see Sections 4.3.1.2and 4.3.2.2) are characterized by the incoming waves acquired from the "Downscaled Ocean Waves" (DOW) (Camus et al., 2013) and the sea levels recorded by the closest tide gauges.

The DOW database is a historical reconstruction of coastal waves by means of a hybrid methodology based on both dynamical and statistical downscaling for a period of 68 years (1948 to 2015) along the Spanish coast; this database provides hourly sea states with different wave parameters (e.g., significant wave height, Hs, peak period, Tp, mean wave direction, θ_m). Specifically, the DOW is a downscaled wave reanalysis of coastal zones from a Global Ocean Waves (GOW) database (Reguero et al., 2012), which considers a correction of open sea significant wave height through a directional calibration (Mínguez et al., 2011) and has been validated with records from the closest buoys.

Regarding sea levels, the Spanish Grid of Gauges (REDMAR) provides data for astronomical tide levels and surge tide levels. The selected tide gauges correspond to the Port of Barcelona and the Port of Huelva for Nova Icaria Beach and Campo Poseidón, respectively.

4.3.1 Nova Icaria Beach

4.3.1.1 Study site

Nova Icaria Beach is a 400 m-long non-barred sandy beach located at Barcelona (Catalonia), northeastern Spain (see Fig. 4-2). The beach is embedded between the Olympic Port of Barcelona to the south and the Bogatell dike to the north. The beach is also protected by a semi-submerged curved breakwater, which is an extension of the Bogatell dike (Z = 0 m with respect to the MSL), and a small breakwater that protects the boat-access ramp in the northeastern section of the Olympic Port. The average direction normal to the beach orientation is close to 135° with respect to north, and the beach sediment is characterized by an average median grain size (D50) of approximately 0.43 mm (Ojeda and Guillén, 2008).

Nova Icaria Beach is one of the most intensively studied coastal sites in Catalonia (e.g., Ojeda and Guillén, 2006; Guillén et al., 2008; Ribas et al., 2010; Ojeda et al., 2011; Turki et al., 2012; 2013; Jara et al., 2015), and its historical morphodynamic variability has been reported in detail. In this study, it is worth highlighting the shoreline monitoring analysis of Barcelona's beaches developed by Ojeda and Guillén (2006) and Guillén et al. (2008), who identified a process of sediment bypass from Bogatell Beach to Nova Icaria Beach. This event occurred months after nourishment works at Bogatell Beach were carried out between 13th June and 5th July 2002, with a sediment contribution of approximately 70,000 m^3.

It is important to highlight that headland bypassing due to moving sand around the Bogatell dike (see Fig. 4-2) was initially reported by Peña and Covarsl (1994), who used drift monitoring analysis using transects. This sediment drift was controlled in 2010 when the construction of a submerged barrier was implemented to delimit the sand contained in the physiographic unit of Bogatell Beach.

4.3.1.2 Marine conditions

The Catalan coast (Western Mediterranean) is a microtidal region where the astronomical tide is characterized by a semi-diurnal regime (mean range of 0.23 m), and storm surges can reach values up to 0.5 m greater than the astronomically predicted tide level. In this region, the effect of tides on the morphology of the beaches is significantly less than waves.

The selected DOW point near Nova Icaria Beach is located at latitude 41.387° and longitude 2.207°, with a water depth of 13.3 m (see Fig. 4-2). This point has been validated with measurements of an OPPE (*Organismo Público de Puertos del Estado*) buoy at Barcelona. Fig. 4-3a shows the scatter diagram that correlates the significant wave height, Hs, with the peak period, Tp, and Fig. 4-3b depicts the directional rose of the Hs.

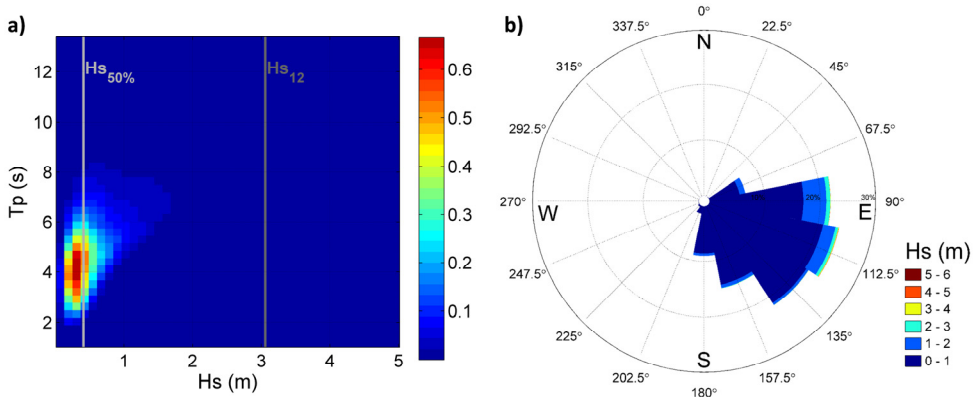

Fig. 4-3. Wave characteristics of DOW point at Nova Icaria Beach. a) Scatter diagram Hs-Tp. b) Directional rose of Hs.

A statistical analysis of the wave conditions from 1948 to 2015 shows that the dominant or more frequent waves and the most energetic waves come from the ESE (24% of the time), followed by waves coming from the E (21.9%) and SE (21.7%). The Hs and Tp have ranges of 0.01–5 m and 1–13.4 s, respectively. The wave height exceeded 50% of the time is 0.41 m, and the Hs_{12} is approximately 3 m. The significant wave height time series presents a cyclical behavior, with storm periods (October - April) separated by periods of low storm activity (May - October).

4.3.1.3 Shoreline data

Daily shoreline records during the time period, which spanned from May 2002 to October 2003, were obtained from snap images taken by the Argus video system "Barcelona Littoral Station" located on top of the Mapfre Building by the Olympic Marina approximately 142 m above mean sea level (MSL). This Argus system consists of five video cameras operated by the Mediterranean Center for Marine and Environmental Research (CMIMA), and these cameras have a 180° view of the coast.

The shorelines were manually plotted and digitized over oblique pictures taken by camera C5 and then rectified by means of a direct linear transformation technique, with a maximal expected error of 1 m at the northern tip of the beach (Jara et al. 2015).

Fig. 4-4a shows an example of a rectified snap picture including two shorelines associated with the summers before and after the bypass period (approximately from October 2002 to June 2003) from Bogatell Beach to Nova Icaria Beach. Fig. 4-4b shows the time-series evolution of the mean cross-shore position.

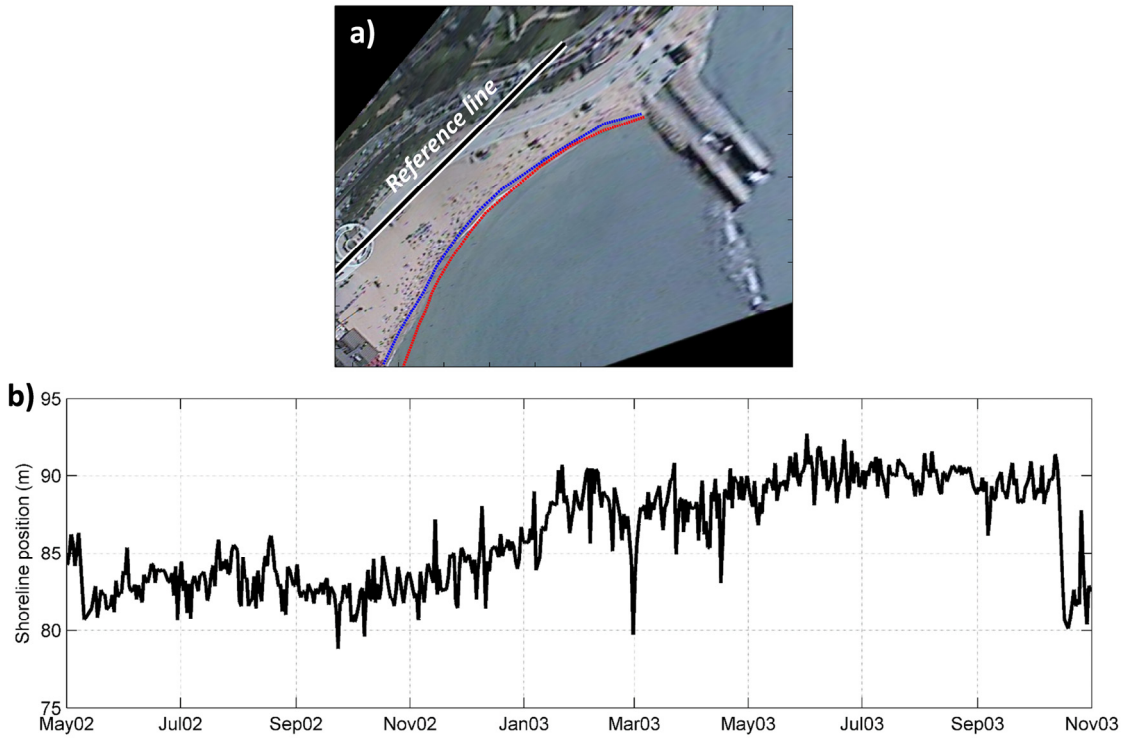

Fig. 4-4. Shoreline position at Nova Icaria Beach. a) Example of rectified snap picture showing two surveys: the blue line is the shoreline associated with the day 1507//2002 (before bypass), and the red line is the shoreline associated with 15/07/2003 (after bypass). b) Time-series of shoreline positions.

The shoreline position, S, for the entire beach has been computed as the mean position in relation to the constant reference line in the backshore (see Fig. 4-4a). The shoreline reference level

corresponds to the local MSL. To minimize the possible overestimation of shoreline changes due to storm surges and wave set-up, the shoreline positions extracted from rectified pictures have been corrected with the MSL position at the moment the picture was captured, considering the astronomical tide, storm surge and wave set-up.

4.3.2 Campo Poseidón

4.3.2.1 Study site

The second study site corresponded to the Campo Poseidón beach profile (see Fig. 4-2). This monitoring section is located at Rompeculos Beach in Moguer municipality (Huelva), on the southwest coast of Spain. It is a coastline stretching 3000 m-long and encompasses a long sandy beach (more than 50 km) bounded by the Port of Mazagón and the delta of the Guadalquivir River.

The average direction normal to the Rompeculos Beach orientation is close to 210° with respect to the north, and the beach sediment is characterized by D_{50}=0.3 mm (Fernández et al., 1992).

The east coast of Huelva has a long history of monitoring programs, which have shown how highly recessive this area is. Fernández et al. (1990) quantified the coastline retreat at a rate of 1.5 m/yr over 30 years (since the 1960s). This value is consistent with the estimated trend from data measured over more than 16 years (December 1998 to July 2015) at the Campo Poseidón beach profile (see Section 4.4.2). As Medina *et al.* (1992) concluded, the coastal retreat of this region has been caused by two different reasons: first, the littoral drift from west to east, and second, the reduction in the volume of sand transported by the rivers to the coast mainly caused by human actions (e.g., construction of dams, littoral barriers).

4.3.2.2 Marine conditions

The Gulf of Cadiz faces the Atlantic Ocean and is characterized by a mesotidal regime with a medium neap to spring variation (1.20–3.30 m) (Muñoz-Perez et al., 2001). According to datum references of the Tide Gauge of Port of Huelva, the mean lower low water (MLLW) level is 0.47 m, the MSL is 2.03 m and the mean higher high water level (MHHL) is 3.63 m, all of which are above the reference level or zero of the port. The storm surges can reach values up to 0.6 m greater than the astronomically predicted tide level.

The selected DOW point near Campo Poseidón is located at latitude 37.1° and longitude 6.765°, with a water depth of 6.3 m (see Fig. 4-2). This point has been validated with measurements of OPPE-Sevilla. Fig. 4-5a shows the scatter diagram Hs-Tp, and Fig. 4-5b shows the directional rose of the Hs.

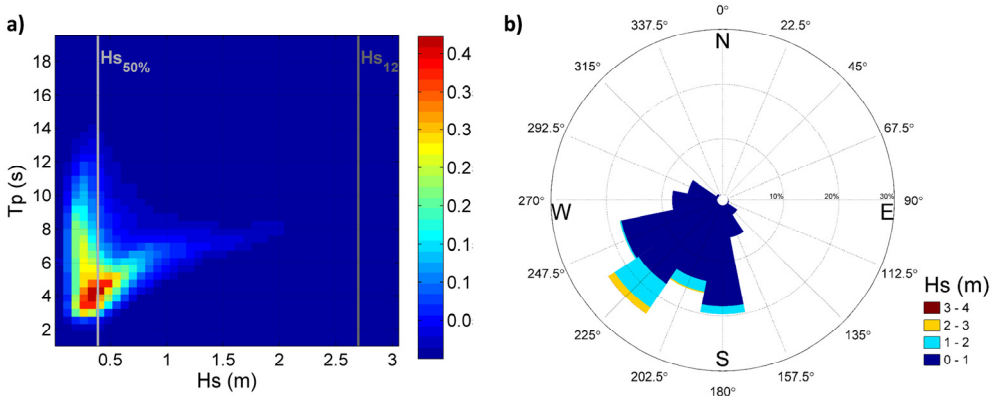

Fig. 4-5. Wave characteristics of DOW point at Campo Poseidón. a) Scatter diagram of Hs-Tp. b) Directional rose of Hs.

The statistical analysis of wave conditions from 1948 to 2015 shows that the most frequent and most energetic waves come from the SW (24% of the time), followed by waves from the S (19%) and WSW (18%). The Hs and Tp have ranges of 0.01–4 m and 1–19 s, respectively. The wave climate is strongly seasonally modulated, with an annual mean significant wave height, Hs, of 0.39 m and an Hs_{12} of approximately 2.7 m. The winter is the most energetic period (i.e., December-January).

4.3.2.3 Shoreline data

Repsol Investigaciones Petrolíferas S.A. (R.I.P.S.A.) has monitored the Campo Poseidón beach profile since December 1998. From the beginning until 2013, 10 campaigns per year of intertidal beach profile surveys were carried out, and these sampling were monthly except in the months of July and August. From 2013 onwards, the program was extended to 12 measurements per year, including profiles for July and August.

Following the research developed by Castelle et al., (2014) and Lemos et al., (2018), the intersection of the coastal profile with the vertical elevation MHHL was selected as a shoreline proxy. According to these authors, the shoreline cross-shore displacement related to the MHHL contour is slightly influenced by the inner-bar and berm dynamics. Based on the above information, Fig. 4-6 shows the time-series evolution of the mean cross-shore position associated with the MHHL contour.

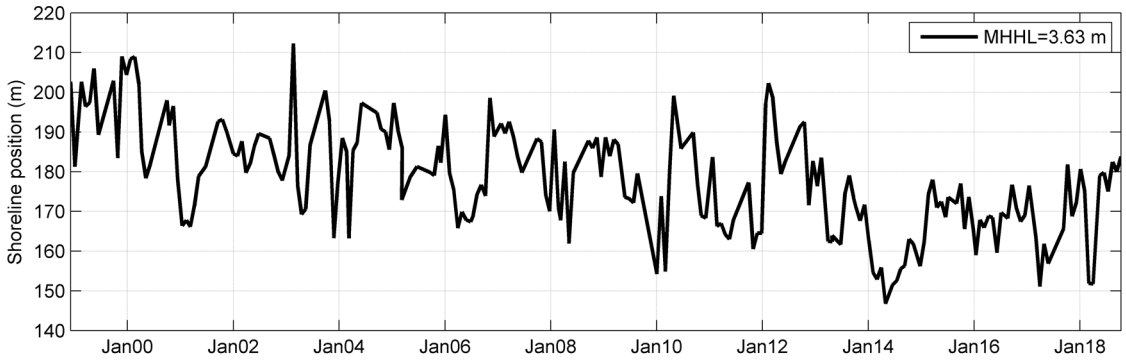

Fig. 4-6. Time-series of shoreline positions at the Campo Poseidón beach profile considering the MHHL contour as the reference level.

4.4 Results

This section presents the performance of the proposed equilibrium cross-shore shoreline evolution model applied to the two selected study sites. In both cases, the time series of waves at the DOW points were propagated to the breaking point using linear wave theory and the Thornton and Guza (1983) linear breaking criterion. The wave breaking conditions have been used to obtain the incident wave energy, which is the main model driver.

The calibration procedure consists of finding the best model fit using an error minimizing technique to solve the calibration parameters. To do this, an iteration algorithm was used to find the proportionality constants of accretion, C^{+}, and erosion, C^{-}, that produced the lowest RMSE between the modeled and measured shoreline positions.

Section 4.4.1 presents the results from Nova Icaria Beach, and Section 4.4.2 presents the results from Campo Poseidón.

4.4.1 Model results from Nova Icaria Beach

Jara et al. (2015) analyzed the shoreline evolution of Nova Icaria Beach during a natural beach oscillation time period that spanned from January 2005 to January 2007 using two equilibrium cross-shore shoreline evolution models. They successfully calibrated and validated their proposed model (named the JA15 model) and the YA09 model. From that research, the present study inherits the YA09 model calibration parameters obtained from the six-month period between January and June 2005 (a=-0.068106 m^2/m, b=6.13 m^2, C^{+}=-2.4·10^{-4} $m^{-2}s^{-1}$, C^{-}=-1.1·10^{-4} $m^{-2}s^{-1}$). It should be noted that the optimal erosion and accretion change rate coefficients, $C^{\pm}$, are of the same order of magnitude.

The proposed model has been validated for a time period of one and a half years (see Fig. 4-7d). The first and last five months correspond to the natural oscillations of Nova Icaria Beach before and after the sediment bypass period (approximately from October 2002 to June 2003), respectively (Ojeda and Guillén, 2006).

During the sediment bypass period (gray shaded area in Fig. 4-7d), the shoreline position of Nova Icaria Beach advanced at a rate of 11.55 m/yr (see Fig. 4-7a). Fig. 4-7b shows the EEF that defines the equilibrium shoreline position based on the incident wave energy. It is important to highlight that the beginning of the EEF (to the left in this case) is applicable to Nova Icaria Beach's situation before the sediment bypass, while the end of the function governs the beach variability after the sediment bypass.

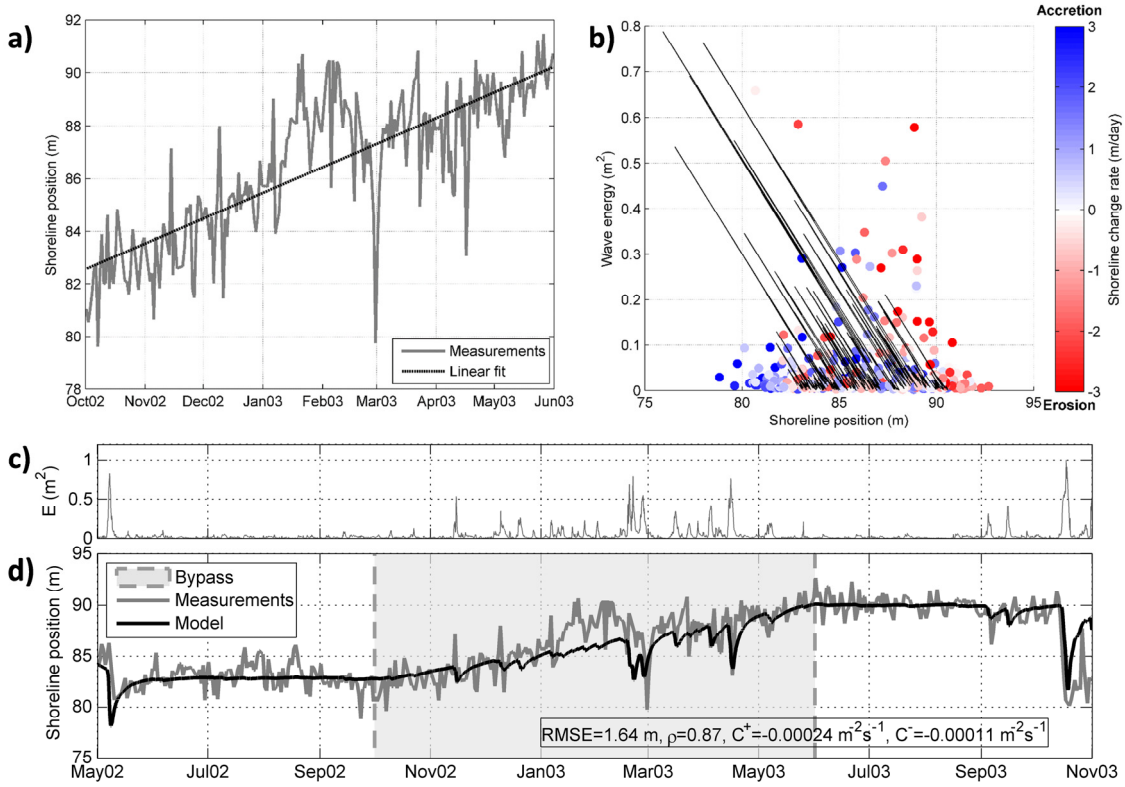

Fig. 4-7. Results for Nova Icaria Beach. a) Linear fit to the shoreline evolution during the bypass period. b) EEF (black line) considering the complete study period. c) Time series of incident wave energy at the breaking point. d) Validation of the proposed shoreline evolution model.

According to the results presented in Fig. 4-7d, the proposed cross-shore shoreline equilibrium model including the trend term allows the simulation of the progressive shoreline advance in accordance with the sediment supply contributed during the bypass period from Bogatell Beach to Nova Icaria Beach. In addition, the model exhibits robust behavior when simulating the general shoreline advances and retreats.

Both observed and modeled shoreline positions show fast erosion after major storms and slower accretion in the post-storm recovery period. For example, given the time series of incident wave energy at the breaking point (see Fig. 4-7c), a storm of greater intensity occurred in mid-October 2003; this storm is reflected by a strong shoreline retreat (Fig. 4-7d).

The resulting RMSE between the observed and modeled shoreline positions is 1.62 m, which is similar to the expected error due to the image rectification (1 m at the northern tip of the pocket beach) and to the results obtained by Jara et al. (2015) for the study period of 2005-2007. The correlation coefficient, ρ, between the observed and modeled shoreline positions is 0.87, which is a clear result indicating a strong correlation.

4.4.2 Model results from Campo Poseidón

In the case of the Campo Poseidón beach profile, the first 3 years (December 1998-December 2001) of shoreline measurements were considered for calibration purposes (see the gray shaded area in Fig. 4-8d). Because the beach experiences a continuous retreat at a rate of 1.5 m/yr according to Fernández et al. (1990), the calibration period must filter this trend to obtain the model calibration parameters (a, b and $C^{\pm}$). An iteration technique was used to find the best set of free parameters that minimize the RMSE between the modeled and observed shorelines. The resulting calibration parameters are a=-0.0027 m^2/m, b=0.5595 m^2, C^{+}=-5.7·10^{-4} $m^{-2}s^{-1}$ and C^{-}=-9.7·10^{-5} $m^{-2}s^{-1}$.

Then, the proposed model was validated for more than thirteen years of shoreline measurements (from January 2002 until July 2015), as shown in Fig. 4-8d. Although the shoreline position record obtained from the beach profile surveys is approximately 20 years (see Section 4.3.2.3), the simulation was run until mid-2015 based on the wave data availability (see Section 4.3.2.2).

During the study period, the shoreline position at the Campo Poseidón beach profile retreated at a rate of -1.55 m/yr (see Fig. 4-8a). In this case, the beginning of the EEF (to the right in Fig. 4-8b) is related to the linear relationship (E-S) defined for the calibration procedure, and then, the EEF evolves based on the sediment loss rate.

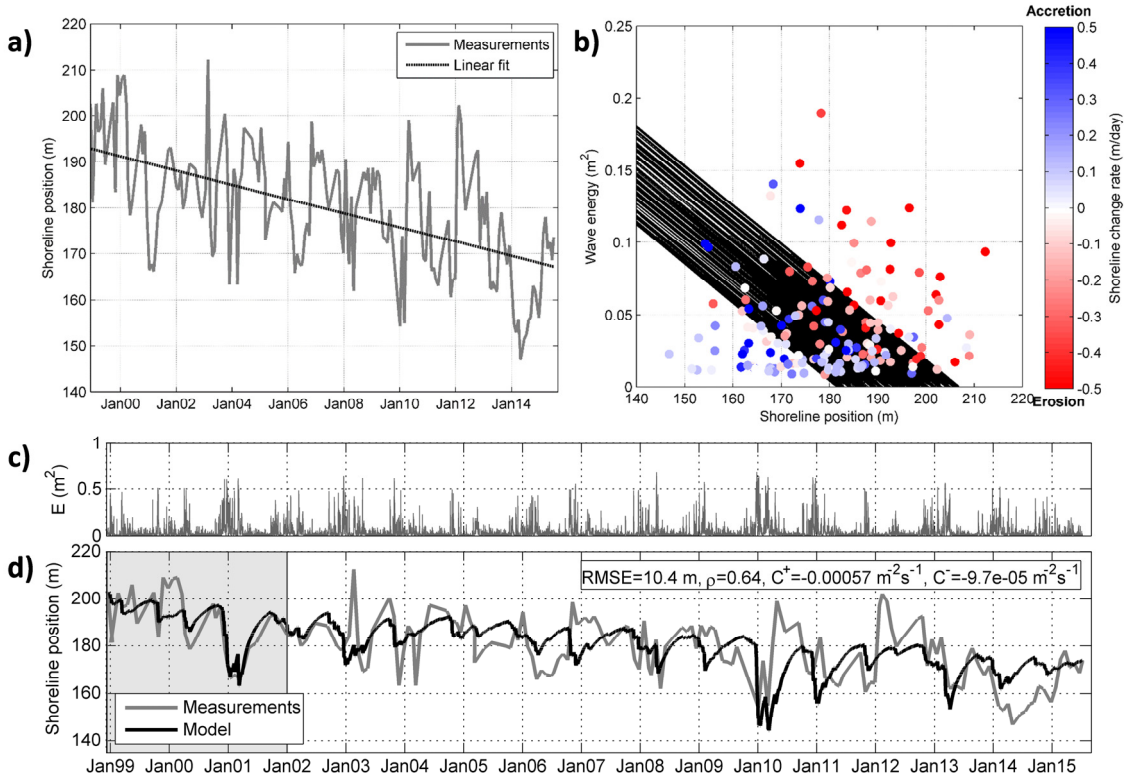

Fig. 4-8. Results at Campo Poseidón. a) Linear fit to the shoreline evolution. b) EEF (black line) considering the complete study period. c) Time series of incident wave energy at the breaking point. d) Calibration (gray shaded period) and validation of the proposed shoreline evolution model.

Fig. 4-8c shows a strong seasonal variation of the incident wave energy, with strong storms during winter periods and low energy waves during the summers. The results presented in Fig. 4-8b reveal that the model, again, has achieved good performance, successfully reproducing the general advance/retreat shoreline trend. The resulting RMSE is 10.4 m, and the correlation coefficient, ρ, between the observed and modeled shoreline positions is 0.64, which is a satisfactory correlation.

4.5 Discussion

According to the results presented in Section 4.4, the proposed model showed significant skill in reproducing the shoreline evolution at two study sites with different characteristics: 1. Nova Icaria Beach was subjected to sediment supply in a microtidal environment, and 2. Campo Poseidón was subjected to sediment loss in a mesotidal environment. In addition, the data sources used to obtain the time series of the shoreline positions were different in both cases; in the first, data came from video-camera images, and in the second, data came from beach profile surveys.

The study site of Nova Icaria Beach has been used for direct model validation because the sediment bypass period from Bogatell Beach was defined a priori, and the calibration parameters

were inherited from Jara et al. (2015). During the first five months, the model uses a linear EEF with v_{lt}=0 m/yr; then, the EEF evolves during the bypass period at the rate of sediment increase, and it finally continues with the last linear EFF and v_{lt}=0 m/yr for the next five months. On the other hand, the study site of Campo Poseidón has been completely predictive, and the model has achieved an overall good performance, simulating nearly 16 years of shoreline evolution. In this case, the value of the loss rate recorded with historical data (v_{lt}=1.5 m/yr) by Fernández et al. (1990) has been considered, and it has been applied to the long-term in a continuous erosion trend, which results in a recessive EEF.

To assess the advantages of the proposed model, Fig. 4-9 shows a comparative model simulation for the two study sites considering two scenarios: 1. Model includes trend term (same results of Section 4.4), and 2. Model establishes v_{lt}=0 m/yr during the entire study period. Table 4-1 summarizes the values of the mean squared error and correlation coefficient found in this comparative analysis.

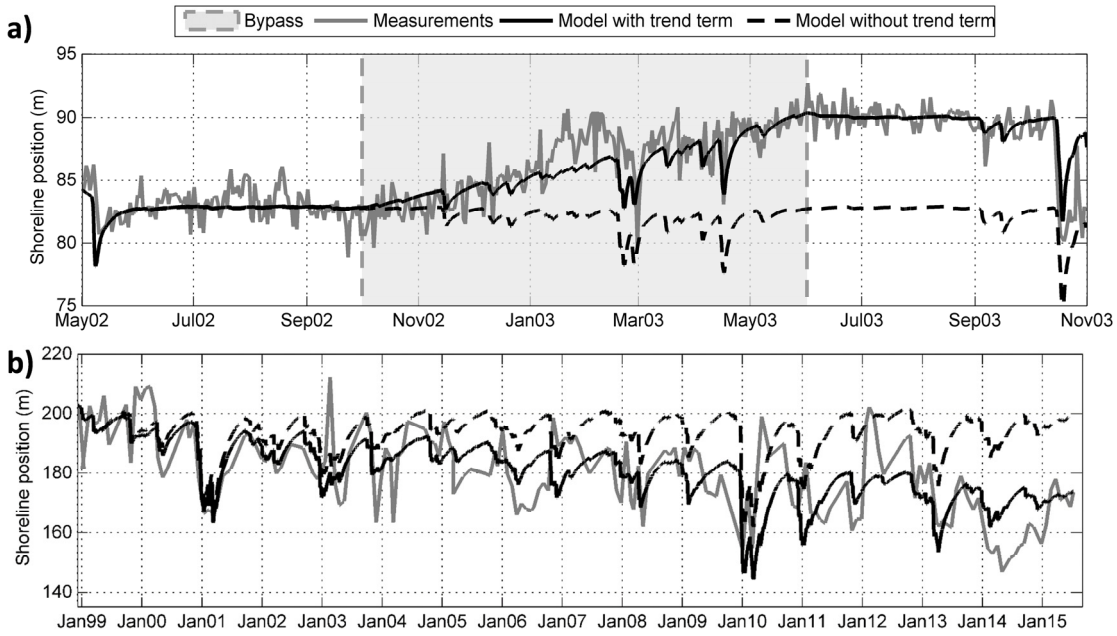

Fig. 4-9. Comparison of results using the proposed model including the trend term versus the model without the trend term at a) Nova Icaria Beach and b) Campo Poseidón.

Table 4-1. Root mean square error and correlation coefficient between the observed and modeled shoreline positions at Nova Icaria Beach and Campo Poseidón considering two scenarios.

Model	**Nova Icaria Beach**			**Campo Poseidón**		
	RMSE (m)	**ρ**	**v_{lt} (m/yr)**	**RMSE (m)**	**ρ**	**v_{lt} (m/yr)**
Without trend term	5.18	0.08	n/a	18.7	0.31	n/a
With trend term	1.64	0.87	11.55	10.4	0.64	-1.5

According to Fig. 4-9, as expected, when the equilibrium shoreline evolution model does not consider the trend term, it tries to reproduce the shoreline advancing and retreating oscillations around an average position over time; however, the model does not consider net volume changes on the beach. The values presented in Table 4-1 reflect the weak correlation between the observed and modeled shoreline positions when the model does not include the trend term.

Another test that should be highlighted is what would happen if the linear trend term were added after the YA09 model results (similar to the LP12 model), but considering that the EEF is constant over time (not including the rate parameter). This assumption is represented in Fig. 4-10, for the case of Nova Icaria Beach. As it is observed, it would be feasible to find a good result by adding the linear change rate during the bypass period; however, if the model assumes a constant EEF, the simulation will tend to the established equilibrium condition, from which, the model is not able to assimilate that the beach has changed its sediment volume over time.

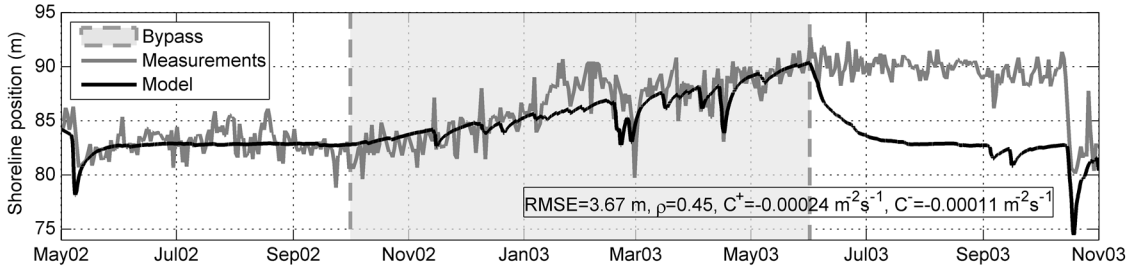

Fig. 4-10. Simulation considering the linear trend term added after the YA09 model result (bypass period), but assuming that the EEF is constant over time.

It should be noted that the proposed model assumes that v_{lt} is linearly constant during the forecasting period; nonetheless, as indicated in Section 4.1, in reality, there are multiple sources or sinks of sediments on beaches (e.g., littoral sediment drift alongshore, nourishments, cliff retreat) and they are variable over time. Therefore, assuming a constant rate, the proposed model captures only the general tendency, but the nonlinear changes cannot be precisely resolved. For example, the month of February 2003 in the simulated results of Nova Icaria Beach and the years 2010 and 2012 in the simulated results of Campo Poseidón had more advanced shoreline position records than did the model predictions. Note that in those periods where the model is not able to replicate the shoreline response, it should be also due to the others assumptions described in detail in Section 4.2.1 (not consideration of wave directionality, changes in the wave-driven model component speed or changes of the physical beach parameters).

In order to make the term v_{lt} and the other parameters (a, b, C^+ and C^-) variable over the time, it would be possible to include a data assimilation algorithm, such as the Kalman Filter, previously proposed by Long and Plant, (2012). This algorithm would automatically adjust the rate parameters during the runtime to best fit any available observed data at the concurrent time step.

However, after the last available observation is assimilated, the parameters will remain constant for the entire forecasting period.

The limitations inherited by assuming a linear trend constant suggest that the proposed model could even improve its prediction by including a better prediction of the source or sink variability, e.g., a littoral sediment drift alongshore function obtained from historical seasonal analysis or a sediment discharge function associated with streamflow hydrographs of rivers, among others.

Finally, time series of shoreline measurements in different sites with diverse beach characteristics and wave conditions would be useful to widely validate the robustness of the shoreline evolution model, including the analytical form of the EEF proposed in this chapter.

4.6 Conclusions

- This present study proposes an extension of the equilibrium shoreline evolution model originally developed by Yates et al., (2009). The new model adds a trend parameter due to unresolved processes (constant rate of sediment gain or loss), which in turn modifies the EEF as a pathway that advances or retreats over time. The model is capable of reproducing the shoreline response due to cross-shore forcing over a variety of temporal scales. It is a reduced-complexity empirical evolution model that requires few calibration parameters and is computationally efficient.
- The model showed significant skill in reproducing the shoreline evolution during one and a half years at Nova Icaria Beach and more than sixteen years at Campo Poseidón. Both study sites showed strong seasonal variation, with slow accretion for periods of low-energy waves and faster erosion during high-energy wave events.
- The results were statistically significant considering that the correlation coefficient between the observed and modeled shoreline exceeded 0.6 in both study sites. In general, the small-scale erosion-accretion trend and the sediment gain or loss tendency in the medium-long term have been well represented at qualitative and quantitative levels.

5 A SHORELINE EVOLUTION MODEL BASED ON CROSS-SHORE AND PLANFORM EQUILIBRIUM MODELS [§]

5.1 Introduction

To date, the equilibrium shoreline evolution models for cross-shore migration have been used in multiple studies, and they assume the variation in shoreline position occurs in different ways: 1. shoreline position as a point that advances/retreats along a beach profile (e.g., Mole et al., 2012; Davidson et al. 2013, 2013b; Birrien et al., 2018; Lemos et al., 2017; Yates et al., 2011) (see Fig. 5-1a); 2. shoreline position as the average distance along a monitored stretch of the beach (e.g., Phillips et al., 2017; Van de Lageweg et al., 2013; Splinter et al., 2016; Castelle et al., 2014;

[§] This Chapter is based on Jaramillo et al. (2020c): Jaramillo, C., Jara, M.S., González, M., Medina, R., 2019. A shoreline evolution model for embayed beaches based on cross-shore and planform equilibrium models. Submitted to Coast. Eng.

Biausque et al., 2016; Blossier et al., 2016; Davidson et al., 2010; Doria et al., 2016; Stokes et al., 2015; Yates et al., 2009) (see Fig. 5-1b); or 3. shoreline position as the average distance along the entire beach assumed as a linear solid (e.g., Jara et al. 2015) (see Fig. 5-1c). No author has evaluated the shoreline position variation by means of an equilibrium cross-shore evolution model, which considers the entire beach as an embayed planform (see Fig. 5-1d).

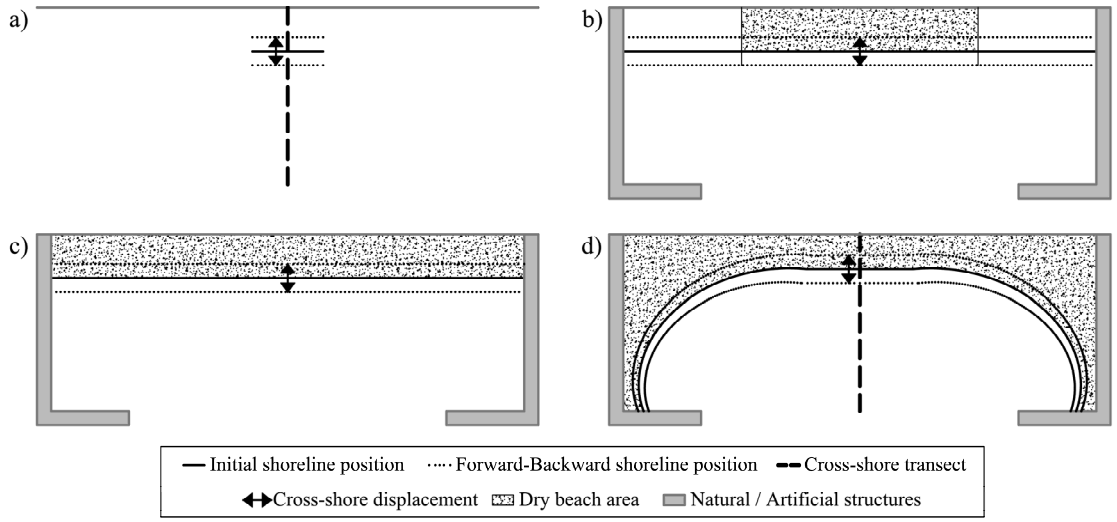

Fig. 5-1. Cross-shore variability scheme, considering a) point along beach transect, b) monitored coastline stretch, c) beach as a linear solid and d) embayed beach.

It is important to highlight that the calculation of the entire embayed shoreline beach evolution by means of existing equilibrium models would require discretizing the beach into transects or stretches, and then, the model would be applied for each one of them, which translates into multiple model calibrations and significant additional computational costs.

Based on the concepts outlined above, the purpose of this Chapter is to present a new shoreline evolution model for embayed beaches, IH-MOOSE (MOdel Of Shoreline Evolution), by the integration of a cross-shore model and an equilibrium beach planform shape expression (see Fig. 5-1d), that is applicable over time-scales that may span days, months or several years.

Collaroy–Narrabeen embayment has been selected as a pilot case to validate the proposed model. This is one of the most studied beaches in the coastal engineering field because of the unique long-term (multi-decadal), high resolution (monthly) survey dataset (five transects) monitoring program (Turner et al., 2016). These data were used by Harley et al., 2011, who concluded that 60 % of the Narrabeen shoreline variability was associated with cross-shore oscillations.

This chapter is organized as follows: the theoretical development, including the hypothesis, governing equations, and methodology of the proposed shoreline evolution model, is presented

in Section 5.2. Section 5.3 describes all the data related to the study site. The model results are shown in Section 5.4. A discussion on the model assumptions, limitations and capabilities is presented in Section 5.5. Finally, the main conclusions are summarized in Section 5.6.

5.2 Model development

In this section, the main hypothesis and assumptions that characterize the proposed shoreline evolution model (IH-MOOSE) are described. Then, the model development and the governing equations are explained. Finally, a summary of the procedure used for the model integration is presented.

5.2.1 Hypotheses and assumptions

The proposed model is based on two main hypotheses: 1) the beach profile and beach planform tend to have an equilibrium shape, and 2) the beach profile and beach planform are linked so that any variation in the shoreline position due to the cross-shore process will affect the planform shape and *vice versa*.

IH-MOOSE is a reduced-complexity model based on previous developments; the model is available in the literature and accounts for simplified cross-shore and longshore processes. The model considers the transect in the most wave-exposed section of the beach as the cross-shore control profile (CCP) (see Fig. 5-2), which governs the forward/backward shoreline displacement in the straight alignment. For its definition, translational movement is based on the model developed by Yates et al., (2009) and is applied wave-by-wave to the CCP. This model primarily captures the shoreline displacement forced by wave-driven cross-shore sediment transport. The resulting shoreline position from the model is then used as a boundary to obtain the initial condition for the down-coast control point, P_0, which is the starting point of the parabolic beach planform; this process follows the expression defined by Hsu and Evans (1989). Therefore, the cross-shore model evolves wave by wave on the CCP, while the entire parabolic coastline is assumed to be instantaneous in response to each step of time.

It is important to note that the IH-MOOSE model is mainly applicable for beaches governed by cross-shore migration and exclusively for embedded beaches with a parabolic planform. Fig. 5-2 shows a global model scheme that considers a complete embayed beach with two headlands that govern the wave diffraction at the extremes. The parabolic contour associated with the closure depth, h*, is indicated only to emphasize that the sediment must be contained in the physiographic

unit. Considering the CCP in the middle of the beach, the y-axis and x-axis of the reference coordinate system lie parallel to the beach and normal to the shoreline, respectively.

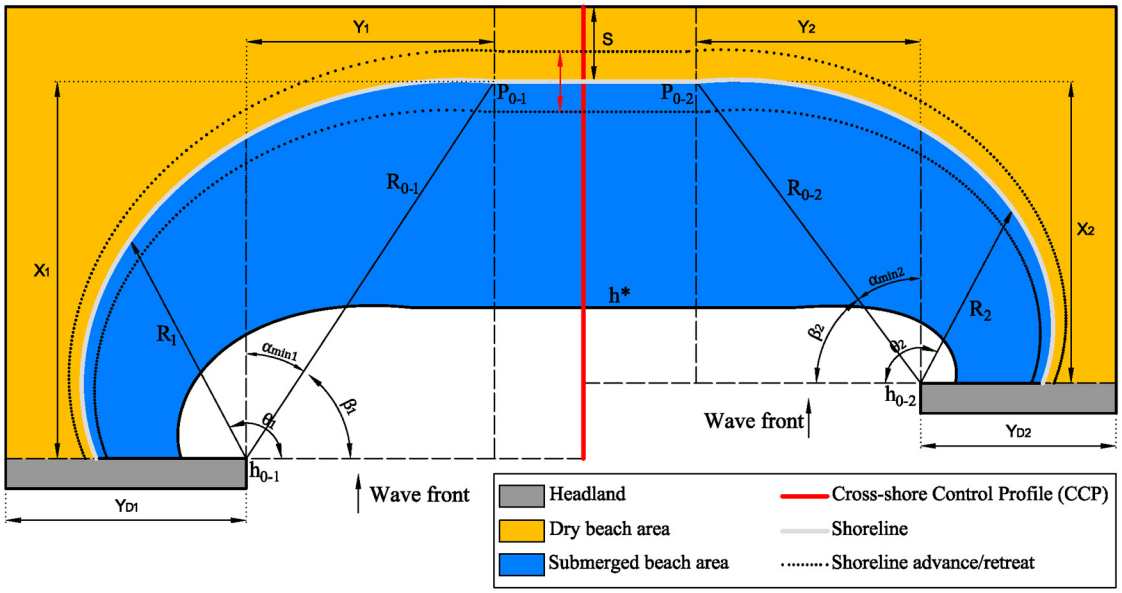

Fig. 5-2. IH-MOOSE model scheme, taking into account a complete embayed beach with two headlands that govern the wave diffraction at the extremes. The red line corresponds to the cross-shore control profile (CCP), while the gray line is the parabolic beach shoreline. The variables with subscript 1 are related to the left parabola, while the subscript 2 refers to the right parabola.

The parabolic planform infers a series of hypotheses, such as those concluded by González and Medina (2001): 1. the longitudinal gradients of wave height on the beach are governed only by the diffraction of the control point (diffraction point) and the refraction over the sandy beach. Local diffraction by islands, shallows, etc., cannot be represented; 2. only longshore currents associated with the wave-induced currents are important; and 3. only one point of diffraction exists. If there is more than one, they should not interact mutually along the beach.

The IH-MOOSE model solely considers shoreline migration, and it neglects the effects of beach rotation or breathing mode. The model assumes that all the beach bathymetric levels follow a parabolic shape, from which the shoreline advance/retreat corresponds to a homothetic movement between parabolas. This hypothesis enables the definition of an idealized beach, where the profiles located in the shadow area behind the headland are effectively more reflective than the profiles located in the exposed area of the beach.

Overall, the IH-MOOSE model shifts from considering the shoreline variability of a unique section to evaluating the entire shoreline evolution.

5.2.2 Governing equations

This section presents the details of the selected cross-shore and planform equilibrium models, which define the bases of the IH-MOOSE governing equations.

5.2.2.1 Equilibrium cross-shore evolution model

Among the several shoreline evolution models related to cross-shore sediment transport that are available in the literature, the model developed by Yates et al. (2009), "YA09 model", has been selected for use in the present study because this model has been one of the most widely used in recent years. In any case, it should be noted that any other equilibrium shoreline evolution model could be used.

YA09 model has been described in detail above in Section 4.2. The reader is referred to Yates et al. (2009) for a full description of the model.

5.2.2.2 Equilibrium planform model

As presented in Section 2.3.2, several empirical equations have been derived to mimic the equilibrium planform. The three major empirical embayed shape models (i.e., logarithmic spiral, parabolic bay shape, and hyperbolic-tangent shape) differ in mathematical functions, coordinate systems, origins, and controlling parameters related to wave direction and bay geometry (Klein *et al.*, 2003; Hsu *et al.*, 2010). The parabolic bay shape equation (PBSE) proposed by Hsu and Evans (1989) is the most widely used model in coastal engineering practices (González et al., 2010) and has received the recognition of the Coastal Engineering Manual (USACE, 2002) for coastal sediment processes and shore protection projects. Due to the above, the IH-MOOSE model has adopted the PBSE to define the shoreline shape (see Fig. 5-2). It is a second-order polynomial equation in a parabolic form:

$$R = R_0 \cdot \left(C_0 + C_1 \frac{\beta}{\theta} + C_2 \left(\frac{\beta}{\theta} \right)^2 \right) \tag{47}$$

where R_0 is the control line length joining the updrift diffraction point, h_0 to the down-coast control point, P_0. β is the wave obliquity, i.e., the angle between the incident wave crest (assumed linear) and the control line. The control line length, R_0, is also angled β to the tangent at the down-coast beach end. C_0, C_1, and C_2 are coefficients that depend on the wave obliquity, β. The radius, R, is measured from the diffraction point to any location on the parabolic shoreline at an angle, θ, measured from the wave crest (Hsu and Evans 1989).

The wave obliquity, β, is given as:

$$\beta = 90° - \alpha_{min} \tag{48}$$

The angle α_{min} (see Fig. 5-2) is a function of the dimensionless distance of the beach to the wavelength X/L at the diffraction point. González and Medina (2001) provided guidance on locating the down-coast control point and proposed an analytical expression for α_{min} estimation:

$$\alpha_{min} = arctan\left[\frac{\left(\frac{\beta_r^4}{16} + \frac{\beta_r^2 \cdot X}{2 \cdot L}\right)^{1/2}}{X/L}\right]; \quad \beta_r = 2.13 \tag{49}$$

The scaling wavelength, L, is calculated using the mean water depth along the wave front close to the control point, hd, and the mean wave period associated with the wave height exceeding 12 h per year, Hs_{12}, known as Ts_{12} (González and Medina, 2001):

$$L = \frac{gTs_{12}{}^2}{2\pi} tanh\left(\frac{2\pi h_d}{L}\right) \tag{50}$$

The three C constants in Eq. (47) are related to the reference angle β (see Fig. 5-3). Numerically, these coefficients may be expressed by fourth-order polynomials as follows:

$$C_0 = 0.0707 - 0.0047\beta + 0.000349\beta^2 - 0.00000875\beta^3 + 0.00000004765\beta^4 \tag{51}$$

$$C_1 = 0.9536 + 0.0078\beta - 0.0004879\beta^2 + 0.0000182\beta^3 - 0.0000001281\beta^4 \tag{52}$$

$$C_2 = 1 - C_0 - C_1 \tag{53}$$

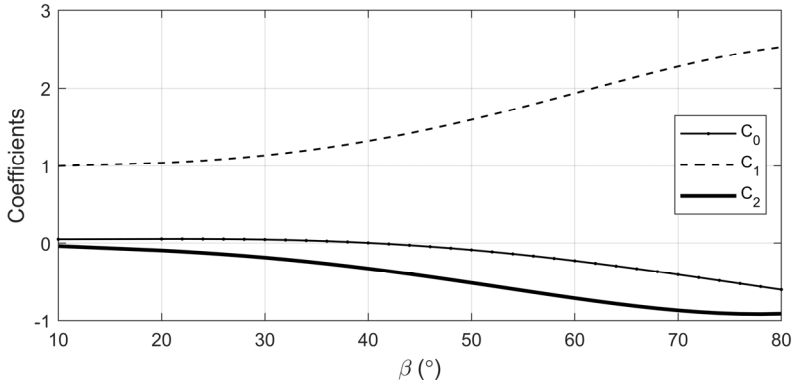

Fig. 5-3. The C coefficients of the parabolic SEP as a function of the wave obliquity, β.

It should be noted that the wave-front orientation at the diffraction point corresponds with the front of the mean energy flux direction of the waves, Θ_{FE}, at the control point (CP) area (González and Medina, 2001).

5.2.2.2.1 Sensitivity analysis of parabolic planform

According to Section 5.2.2.2, the PBSE proposed by Hsu and Evans (1989) is a function of four variables (X, Θ_{FE}, Ts_{12}, and h_d). Fig. 5-4 shows a sensitivity analysis of this parabolic expression, considering three different values for each variable. As noted, the parabolic shoreline is especially sensitive to changes in X and Θ_{FE}, while changes in Ts_{12} and h_d have less of an effect.

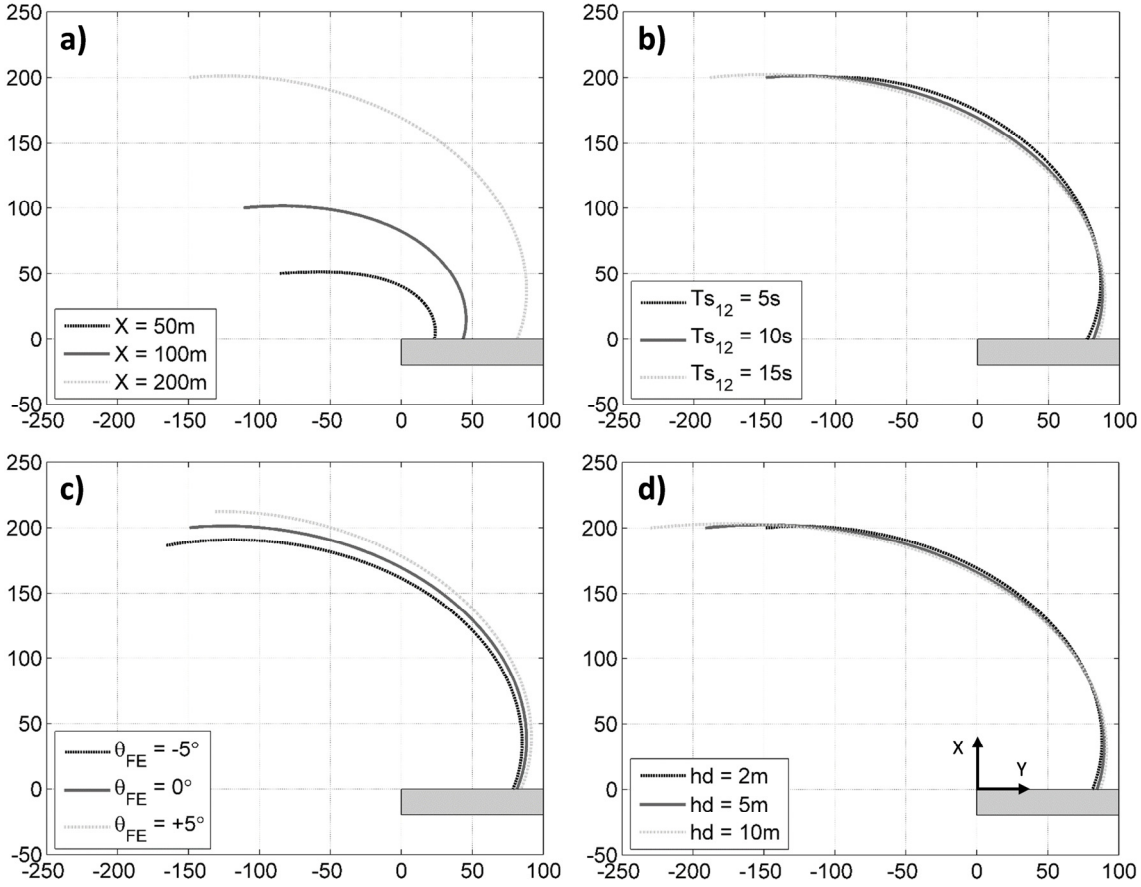

Fig. 5-4. Parabolic beach planform Eq. (47), considering a) Variation of X. Θ_{FE} =0°, Ts_{12}=10s, hd=2 m; b) Variation of Ts_{12}. Θ_{FE} =0°, X=200 m, hd=2 m; c) Variation of Θ_{FE}. X=200 m, Ts_{12}=10 s, hd=2 m; and d) Variation of hd. X=200 m, Θ_{FE}=0°, Ts_{12}=10 s. X (cross-shore), Y (longshore/axis of the abscissas) in meters.

The X displacement is translated into a homothetic advance/retreat of the parabolic shoreline such that the distance between two parabolas at the down-coast control points, P_0, is greater than the distance between both parabolas at the most sheltered zone.

5.2.3 Model implementation

The structure suggested for the IH-MOOSE model (see Fig. 5-5) can be summarized in the following steps:

- INPUT DATA:
    - DATA COLLECTION: Offshore wave climate data, shoreline position measurements, and bathymetric data are required to apply the IH-MOOSE model. A detailed high-resolution beach bathymetry is essential for accurately simulating hydrodynamic processes.
    - CLUSTERING WAVE DATA: The clustering of the offshore wave climate has been obtained by means of the maximum dissimilarity algorithm (MDA). The aim of this algorithm is to select a set of sea states that covers the entire domain and boundaries of the data space of the wave parameters (e.g., Hs, Tp, θ_w) (Camus et al., 2011).
    - WAVE PROPAGATION: A wave transformation model is required to downscale the wave climate from offshore to the coast. In this case, the well-known Coastal Modeling System (SMC) developed by the University of Cantabria (UC) for the Dirección General de Costas (State Coastal Office) of the Spanish Environmental Ministry (González et al., 2007) was used. This user-friendly system was specifically designed to understand the processes that affect the coastal zone and establish a methodology to evaluate coastal projects and their effects on the coastal zone. The SMC encompasses numerical models grouped into different temporal and spatial scales. The wave transformation module (OLUCA) is part of a morphological evolution model for coastal areas, known as the MOPLA module. OLUCA is a parabolic weakly nonlinear combined refraction and diffraction model that simulates the behavior of monochromatic waves (OLUCA-RD) and a random sea (OLUCA-SP) over irregular bottom bathymetry (González et al., 2007). This model includes the effect of shoaling, refraction, energy dissipation (bottom friction and wave breaking), diffraction and wave–current interaction.
    - WAVE TIME SERIES RECONSTRUCTION: An interpolation technique based on radial basis functions (RBFs) (Franke, 1982) was carried out for wave time series reconstruction. This interpolation method has been successfully applied in many fields and is convenient and efficient for scattered and multivariate data. For more information on RBFs, see Camus et al., (2011).

- CROSS-SHORE CALCULATION: This step consists of the application of the equilibrium cross-shore evolution model (see Section 5.2.2.1) on the CCP. This calculation encompasses the wave time series reconstruction nearshore (on the CCP), the incident wave energy (E) calculation, the equilibrium energy function (EEF) definition and the calibration/validation of the cross-shore model. At the end of this step, the modeled shoreline positions are obtained for the entire study period.
- EQUILIBRIUM PLANFORM GOVERNING VARIABLES DETERMINATION: This step encompasses the calculation of the variables required for the parabolic beach planforms definition (see Section 5.2.2.2). First, it is necessary to identify the CP that governs the wave diffraction on the study beach. This point is located on an invariable location during the entire model simulation. Then, the interpolation technique described previously is used to reconstruct the wave time series on the selected diffraction point. The resultant wave series is used to determine the mean energy flux direction. The last sub-step consists of defining a reference parabola from which the measurements of shoreline position, S, or dry beach area, A, are taken.
- PARABOLIC PLANFORM ESTIMATION: The shoreline positions obtained from the cross-shore model along the CCP are then used to obtain the corresponding beach planform parabolas series fitted to the Hsu and Evans 1989 equation (see Section 5.2.2.2).

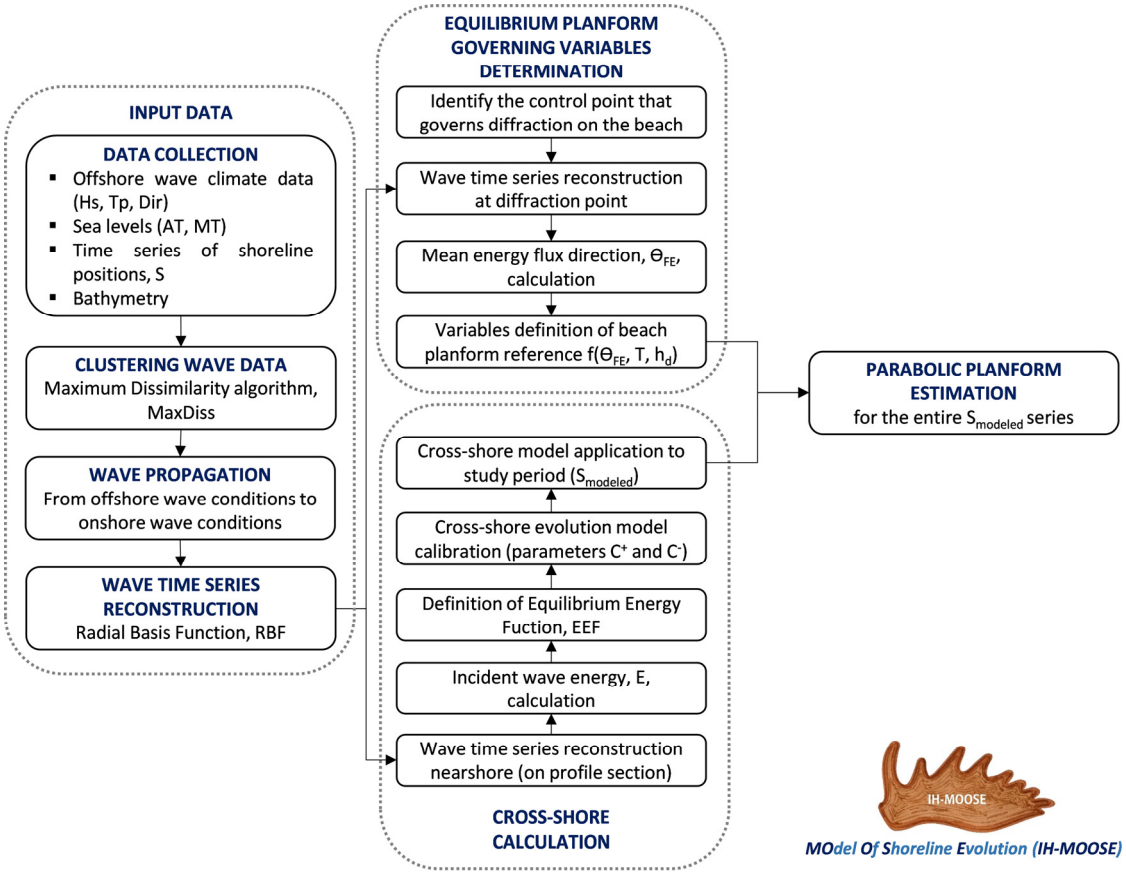

Fig. 5-5. Flow chart of the IH-MOOSE model.

5.3 Study site

The selected study site corresponds to the Collaroy–Narrabeen embayment, which is located on the southeast coastline of Australia, approximately 20 km north of the Sydney Harbour (see Fig. 5-6). This east-facing embayment is the longest sandy system in the Sydney region (Wainwright et al., 2015). It is composed of two beaches that make up 3.6 km coastal stretch: Collaroy Beach is located to the south, and Narrabeen Beach is located to the north.

The embayment (hereafter simply referred to as Narrabeen Beach) is bounded at the northern end by Narrabeen Headland and at the southern end by the 1.5 km-long prominent headland known as Long Reef Point. This latter provides significant sheltering from the predominantly SSE offshore wave climate (Harley and Turner, 2008). Additionally, it is worth highlighting the presence of a small, intermittently opened and closed lagoon located at the northern end of the beach, named Narrabeen Lagoon (Morris and Turner, 2010).

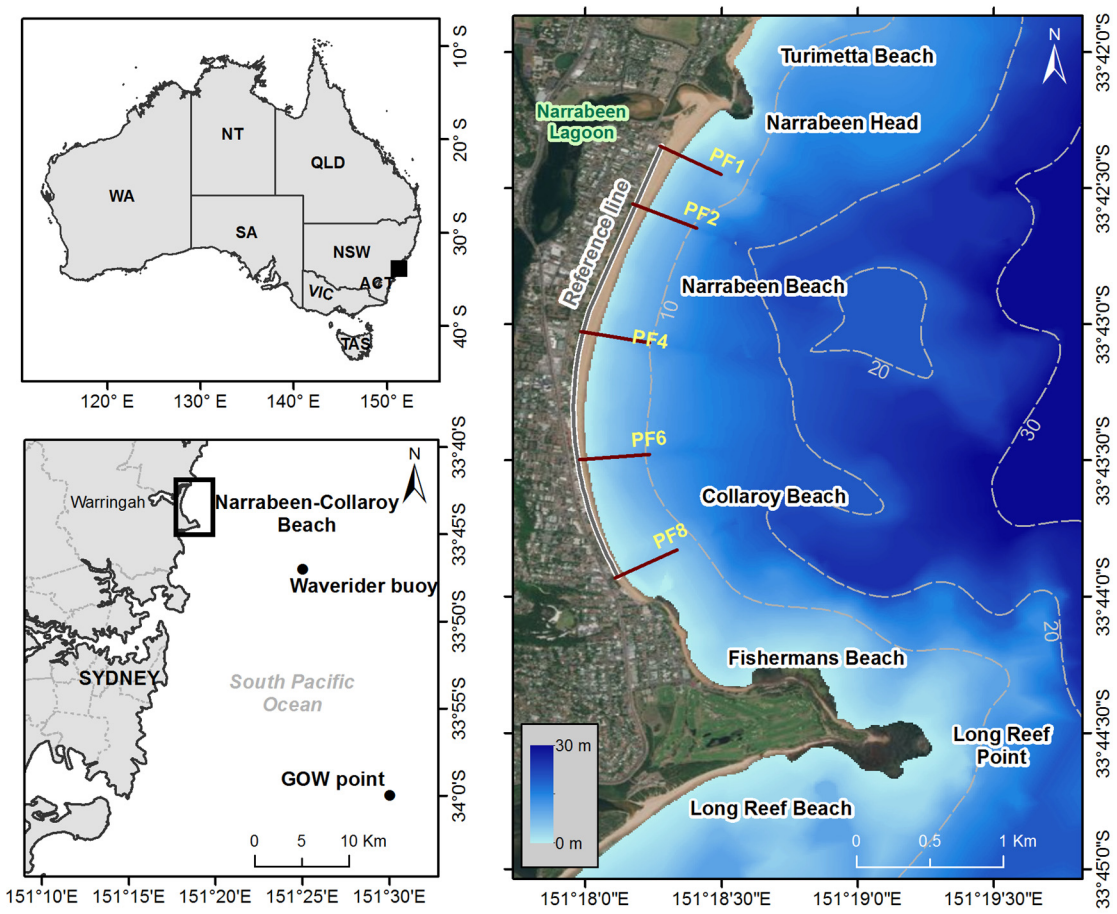

Fig. 5-6. Narrabeen Beach location in southeastern Australia, including the "Global Ocean Waves" (GOW) position at latitude 34S and longitude 151.5E, waverider buoy, beach bathymetry, locations of the five monthly survey transects (PF1, PF2, PF4, PF6, and PF8) and parabolic reference line to estimate shoreline position and dry beach area.

The Narrabeen Beach morphology changes frequently between all states; however, it predominantly exhibits an intermediate state, tending to be more dissipative and reflective under higher and lower conditions, respectively (Wright et al., 1985). The median sediment grain size is roughly uniform alongshore ($D_{50} \approx 0.3$ mm) and is composed of fine to medium quartz sand with 30% carbonate fragments. There are minimal sediment interactions between Narrabeen Beach, the lagoon and the adjacent beaches, such that the sediment contained within the embayment can be considered a closed system (Harley *et al.*, 2011).

The cross-shore variability of Narrabeen Beach has been evaluated using several equilibrium cross-shore evolution models (e.g., Mole et al. 2012; Splinter et al. 2014; Davidson et al. 2017), resulting in good performance.

5.3.1 Marine conditions

The waverider buoy and the wave reanalysis database Global Ocean Waves (GOW) point (Reguero et al., 2012) (see Fig. 5-6) were the data references used to define the marine conditions of the study area.

Based on water level variability, the coastline of southeastern Australia experiences a semidiurnal and microtidal tidal regime; the average spring tide range is 1.6 m, and the average neap tide range is 1.2 m (Wright et al., 1985). The effect of tides on the morphology of Narrabeen Beach is significantly less than that of waves (Short and Trembanis, 2004).

Regarding wave conditions, this study considered available data in deep waters and near the coast. On the one hand, the public available Narrabeen-Collaroy coastal monitoring program (http://narrabeen.wrl.unsw.edu.au/) provides continuous (hourly) wave time-series at 10 m water depths for each of the five cross-shore profile lines; these data are obtained by wave propagation from the directional waverider buoy (80 m depth) (Turner et al., 2016). These data have been used to force the cross-shore model (see Section 5.2.2.1). On the other hand, a GOW point developed by IHCantabria has been used to access long-time series in deep water and then to determine the mean energy flux direction at the CP (see Section 5.2.2.2).

In general, the deepwater wave climate of the Sydney region is of moderate to high wave-energy, characterized by a mean deep water significant wave height (Hs) of approximately 1.6 m and a corresponding peak wave period (Tp) of nearly 9.8 s, with waves predominantly from the SSE direction. The two headlands that border Narrabeen Beach redistribute the wave energy in the nearshore such that the northern end of the embayment is characteristically more exposed to the predominant southerly swell direction (Harley et al., 2011). On the opposite side, sheltering effects from Long Reef Point create a general gradient of decreasing wave heights from north to south under typical SSE waves (Turner et al., 2016). For further details of the Sydney region wave climate, see Harley et al., 2010 and Mortlock and Goodwin, 2015.

5.3.2 Shoreline data

The publicly available Narrabeen-Collaroy monitoring program is now one of the longest records of coastline variability. It provides data series of beach profile surveys at five cross-shore locations along the Narrabeen Beach (see Fig. 5-6, north to south, hereafter identified as PF1, PF2, PF4, PF6, and PF8). These profiles were regularly measured by Professor Andrew Short and members of the Coastal Studies Unit, University of Sydney, in two distinct periods. During the first three decades, a simple and traditional survey technique was employed (Emery, 1961); from 2004 onwards, the monitoring program has used new and emerging survey technologies, such as

high-accuracy RTK-GPS technology (Turner et al., 2016). Surveys were undertaken at low tide, and profiles were recorded at 10-m cross-shore intervals from a fixed benchmark at the landward limit.

The shoreline positions were referred to the mean sea level, MSL. Fig. 5-7 shows the shoreline evolution of the five beach profiles in a normalized way, i.e., by means of an index defined as the shoreline position index (SPI) following Harley et al. (2015). This is a simple measure used to determine the erosion/accretion state of a beach in relation to its average during the evaluation period. A positive SPI value indicates that the shoreline position is more advanced with respect to the period average, while a negative SPI indicates an eroded shoreline position with respect to the average position.

$$SPI(t) = 10\frac{\left(S(t) - \overline{S(t)}\right)}{std\left(S(t)\right)} \tag{54}$$

where S(t) is the shoreline position at time "t", $\overline{S(t)}$ is the arithmetic mean shoreline position for the analysis period, and $std\left(S(t)\right)$ is the standard deviation.

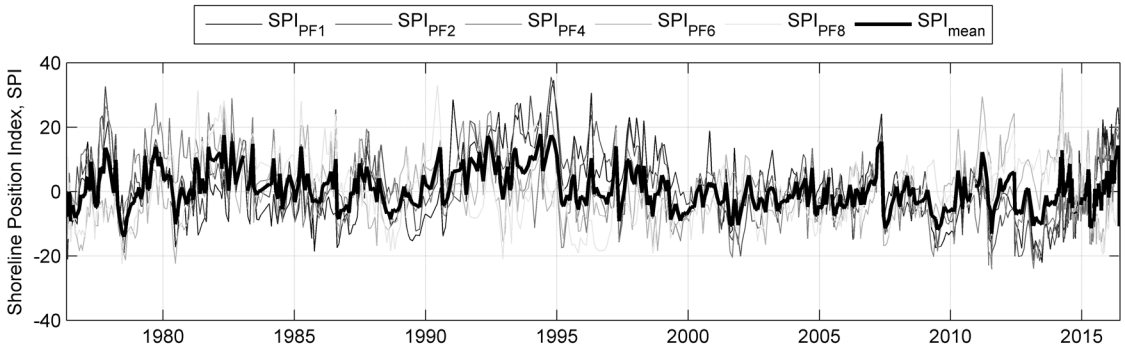

Fig. 5-7. Shoreline position index for each beach profile highlighting the mean SPI.

To obtain the monthly series of the complete coastline, the measurements of the five beach profiles were adjusted to 4th-degree polynomials between PF1 and PF8.

5.4 Results

Following the sequence of the model flow chart (see Fig. 5-5), this section separately presents the first instance of the cross-shore and longshore approximations. Next, the final model result is achieved through the integration of both approximations for Narrabeen Beach.

5.4.1 Cross-shore calculation

Following the Narrabeen shoreline variability analysis developed by Short and Trembanis (2004) and Harley et al., (2011), the study period spanned from January 1993 to the end of December 1998 was chosen. This period was selected because it was mainly controlled by cross-shore shoreline migration. In this case, the beach profile PF2 located on the straight section of the coast was designated as the control transect (CCP) for cross-shore displacement.

The upper panel of Fig. 5-8 shows the incoming wave energy represented by the squared significant wave height (H_s^2) at 10-m water depths of PF2. The bottom panel represents the YA09 model simulation along the CCP over monthly surveyed shoreline data over 6 years.

An iteration algorithm has been used to find the proportionality constants of accretion, C^+, and erosion, C^-, that produce the lowest RMSE between the modeled and measured shoreline positions. The best fit for the calibration parameters is presented in the lower panel text box of Fig. 5-8.

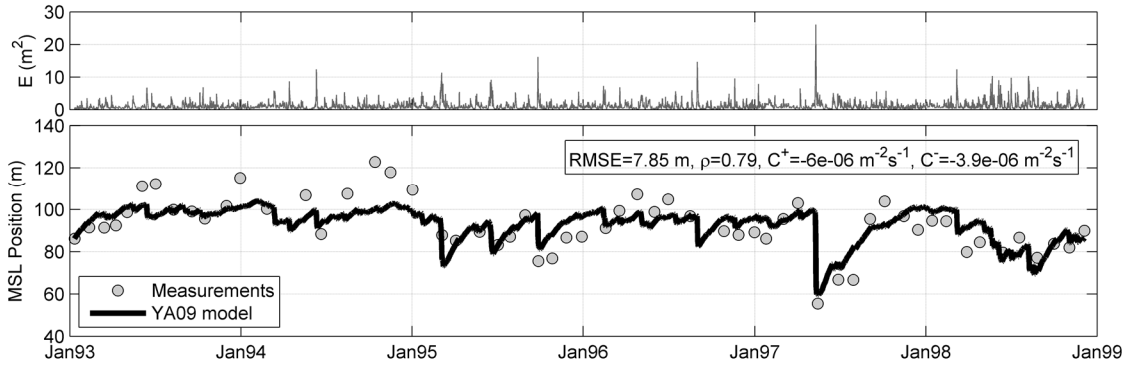

Fig. 5-8. YA09 model application to 6 years of monthly surveyed shoreline data at PF2 at Narrabeen Beach. The model is driven with the wave time-series at 10-m water depth and calibrated to the entire record.

The resulting RMSE is 7.85 m in a beach profile that experiences cross-shore displacements greater than 60 m (flanked by the maximum advance/retreat). The correlation coefficient, ρ, between the observed and modeled shoreline positions is 0.79, which is a result of a strong correlation.

According to the results, the general accretion-retreat trend along PF2 is well represented with the YA09 model at both qualitative and quantitative levels. Both observed and modeled shoreline positions show fast erosion after major storms and slower accretion in the post-storm recovery period. For instance, a storm with greater intensity occurred on 11/05/1997; during this storm, the beach profile retreated more than 40 m and subsequently recovered in less than 6 months.

5.4.2 Longshore calculation

To assess the longshore approximation, it is necessary to identify the CP that governs the wave diffraction on the study beach. Narrabeen Beach attributes its curved shape to the presence of the prominent headland Long Reef Point at the southern end of the embayment. It has been recognized that the CP is located in the vicinity of the headland on a rocky seabed at a depth h_d=20 m.

The GOW reanalysis data point located at latitude 34°S and longitude 151.5°E has been used to access long-time series in deep water (see Fig. 5-6). The maximum dissimilarity algorithm, MDA, was applied to the hourly 39-year-long time series (1979-2017) to select a representative subset. The number of selected cases to be propagated determines the accuracy of the methodology used to reconstruct sea state time series in shallow water. Camus et al., (2011) demonstrated that in the selection of 100 cases, the errors in the estimation of wave parameters are stabilized.

From the above, 100 sea states were selected from the GOW time series to be propagated from the offshore area to the coast using the OLUCA-SP model, which solves the parabolic approximation of the mild-slope equation for spectral waves. After propagating the selected sea states, the OLUCA-SP model output provides the wave field in the whole grid. From these results, the wave time series on the CP were reconstructed using the RBF interpolation technique (Franke, 1982).

In this study, the mean energy flux direction (θ_{EF}) was considered a directional descriptor of the parabolic planform orientation. The mean energy flux direction was calculated for the completely reconstructed waves series on the CP, obtaining a value of θ_{EF}= 109.3°N. On the other hand, the mean wave period associated with the wave height exceeding 12 h per year, Ts_{12}, resulted in nearly 11 s.

Once the variables that define the PBSE proposed by Hsu and Evans (1989) are obtained (θ_{EF}, Ts_{12} and h_d), it is possible to reproduce the complete parabolic coastline as a function of the cross-shore X distance. Fig. 5-9 shows a preliminary analysis, where the good fit of the parabolic planform is supported by the available orthophotos from the New South Wales (NSW) Government Spatial Services at Narrabeen Beach. The north end, above PF1, is excluded from the analysis due to the influence of the intermittently open–closed Narrabeen Lagoon system (see Fig. 5-6).

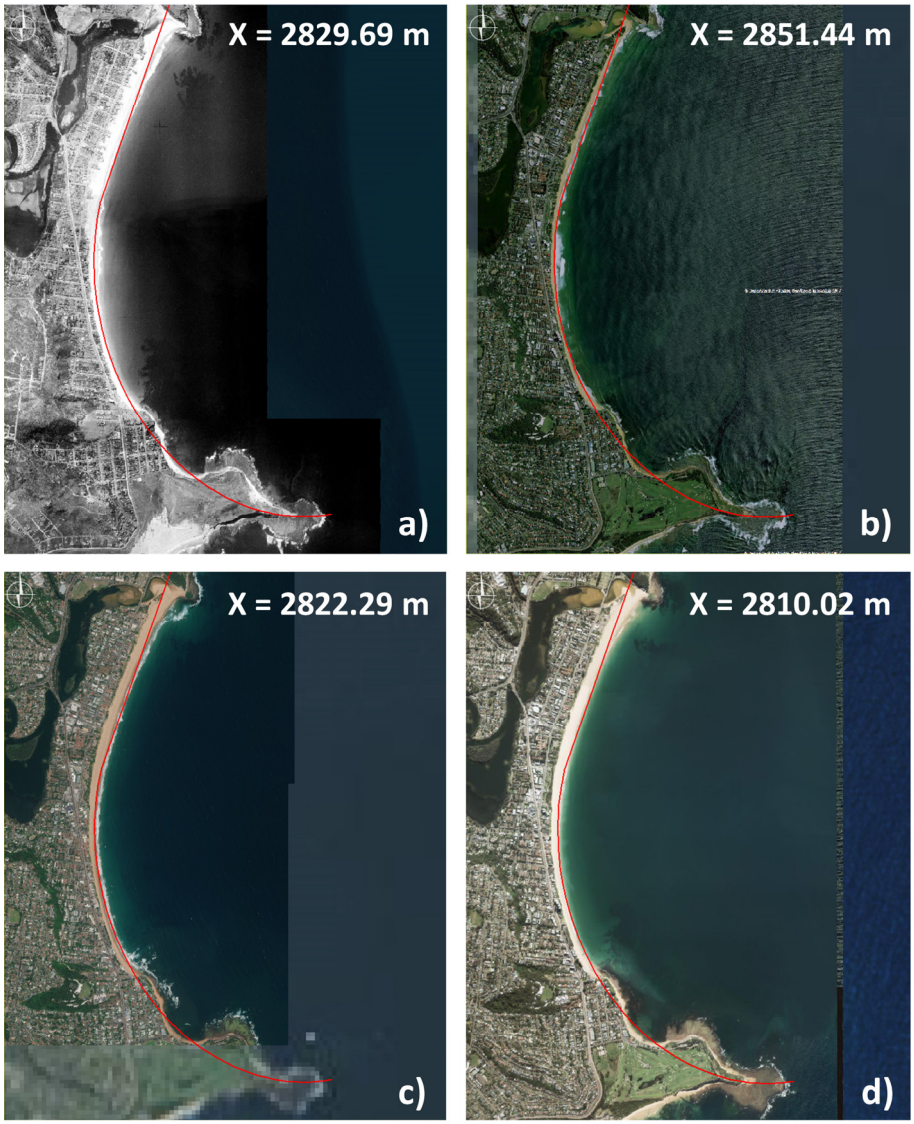

Fig. 5-9. Hsu and Evans (1989) parabolic planform adjustment on NWS-Orthophotos at Narrabeen Beach. a) 1943, b) 30/05/2011, c) 20/12/2015 and d) 06/04/2016.

5.4.3 Model integration

The shoreline positions obtained in Section 5.4.1 have been used to acquire the corresponding beach planform parabola series of the entire study period, which have been fitted to the Hsu and Evans (1989) equation, with the parameters (Θ_{FE}, Ts_{12}, and h_d) found in Section 5.4.2. From this, shoreline positions can be obtained at any transect or coastline stretch along the beach.

As a sample of the model's predictive capacity to determine the shoreline position, Fig. 5-10 shows the evolution of the measured *versus* modeled shoreline positions of the five beach profiles along Narrabeen Beach, as well as the error metric, RMSE. In general, the results are very satisfactory from PF2 to PF8; this last site is located in the most sheltered zone of the beach.

Nonetheless, it should be noted that the results for PF1 are worse; this result is mainly due to its proximity to the mouth of Narrabeen Lagoon, whose morphodynamic escapes from the equilibrium model applicability.

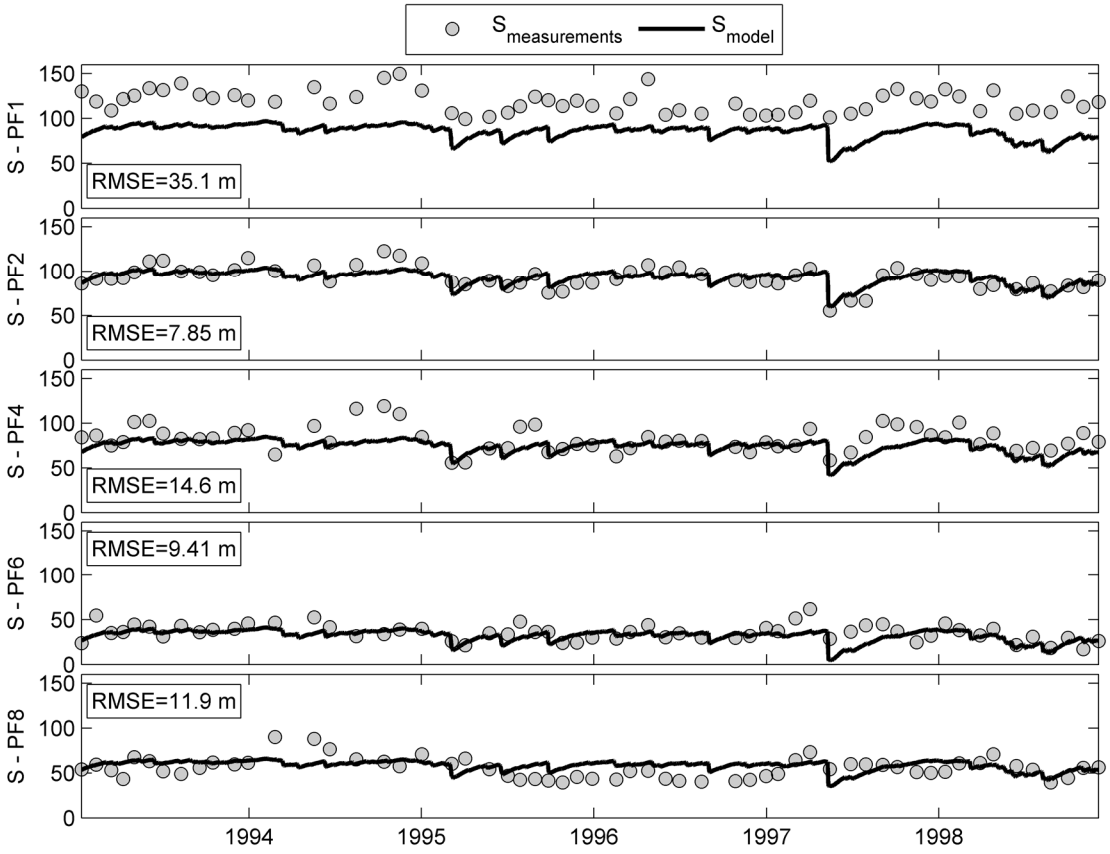

Fig. 5-10. Evolution of measured versus modeled shoreline positions for the five beach profiles.

Comparatively, Fig. 5-11 presents the results of the five beach profiles if only the YA09 model was used, taking into account the calibration conditions found for the CCP (PF2). This means that the same EEF and calibration parameters obtained in Section 5.4.1 are considered for the model simulations. In this case, the YA09 model has been forced with the incident wave energy at 10-m water depths in each one of the five cross-shore profiles available in the public Narrabeen-Collaroy monitoring program.

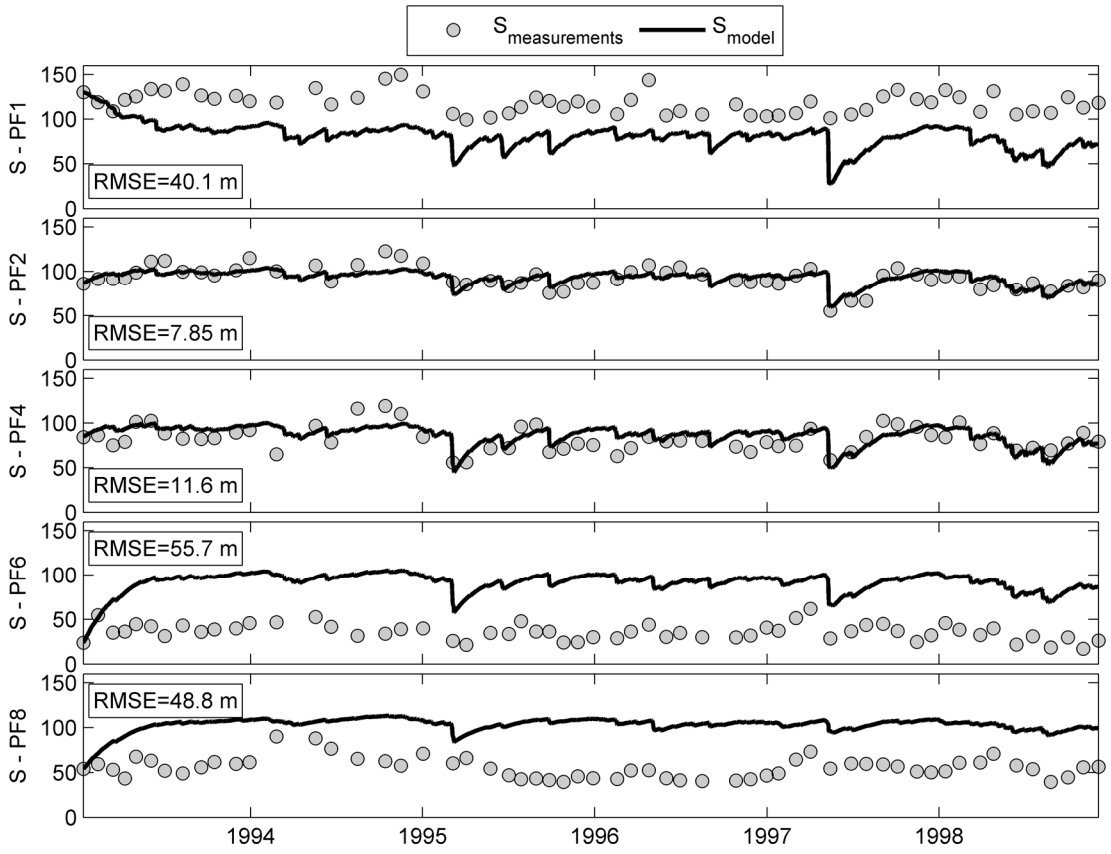

Fig. 5-11. YA09 model application to the five beach profiles considering PF2 calibration conditions. The model has been forced with the incident wave energy at 10-m water depths of each beach profile.

According to Fig. 5-10 and Fig. 5-11, clearly, a better result is obtained with the proposed model, and the PF4 simulation of Fig. 5-11 is only slightly better, considering that it has been forced with its respective incoming wave energy. From the above, the proposed model successfully reaches the general forward/backward displacement of the Narrabeen Beach shoreline evolution.

5.5 Discussion

Beach morphological prediction is of considerable importance for coastal modelers. Traditional process-based morphodynamic modeling systems are valuable tools to simulate storm effects on beaches; however, their computational cost prevents their application to multi-annual morphological changes. In contrast, equilibrium shoreline evolution models are computationally efficient and can capture long-term morphological changes; therefore, these models have aroused the interest of multiple coastal researchers.

Following the recent upsurge of interest for the equilibrium models, the present study proposes a new reduced-complexity model for cross-shore evolution based on previous developments

available in the literature. IH-MOOSE is a versatile model that comprises the integration of the beach profile and beach planform. In this case, the YA09 model was chosen for shoreline migration, while the beach planform was considered as the parabolic expression defined by Hsu and Evans (1989); even so, it is worth highlighting that the model could preserve its integration bases and be adapted to other combinations between cross-shore and planform equilibrium models.

The proposed model allows the acquisition of the entire shoreline evolution of embayed beaches that are governed by unidirectional incoming waves or, more specifically, embayed beaches subjected mainly to cross-shore variability. From the resultant parabolic beach shoreline series, it is possible to know the shoreline position at any transect or coastline stretch along the beach, as presented in Section 5.4.3. Otherwise, the equilibrium shoreline evolution models for cross-shore migration available in the literature need to be calibrated differentially for each transect or coastal stretch using local wave time-series for each profile to reproduce the evolution of the entire beach shoreline.

In summary, the proposed model acquires the entire beach shoreline, starting from the evolution of a single beach profile that is linked to the beach planform. It is important to note that the obtained shoreline evolution allows the estimation of the derived results, such as the dry beach width or emerged area.

The dry beach area is a parameter of great interest to coastal engineers and managers because it provides an initial estimation of the beach trends during the study period, as well as an initial view of its response to natural processes and human actions (Ojeda and Guillén, 2008). In addition, this parameter is fundamental for tourism because it determines the amount of space available for beach users. For example, Harley et al., (2014) valued Italian tourist beaches through the dry beach area, considering that the beach space for umbrellas and deck chairs is often rented out to beach users on a daily to a seasonal basis.

To calculate the dry beach area of a parabolic shoreline, the procedure described in Appendix 4 could be used. Fig. 5-12 shows the dry beach area evolution at Narrabeen Beach obtained by the new model in comparison with the dry beach area measurements. These latter measurements were calculated as the area enclosed by the polygon formed between the shorelines adjusted to 4^{th}-degree polynomials using the five beach profile surveys, the lateral contours (PF1 and PF8) and the parabolic reference line that fits with the seaward dune vegetation (see Fig. 5-6).

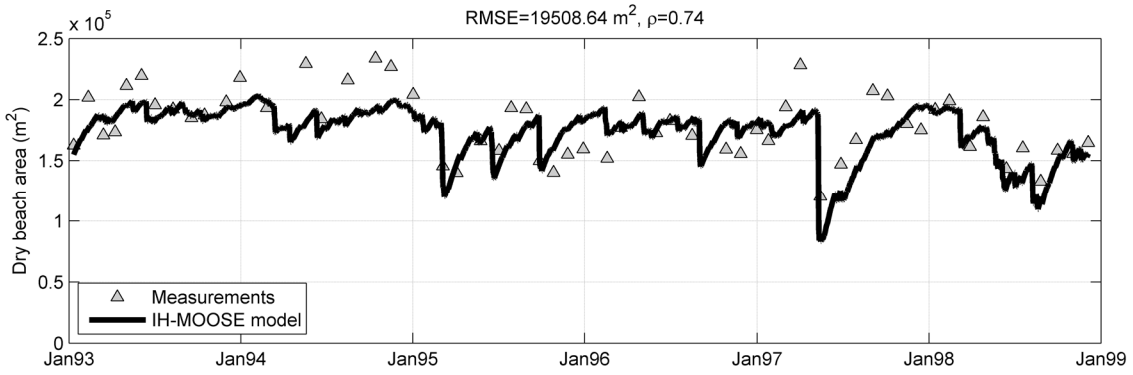

Fig. 5-12. IH-MOOSE model performance over 6 years at Narrabeen Beach.

According to the results, the IH-MOOSE model reaches the general trend of the dry beach area evolution; however, during 1994, the model remains slightly below the measurements. It should be noted that this limitation is related to the cross-shore model adjustment (see Fig. 5-8) but not to the beach profile and planform integration.

The resulting RMSE is close to 11% compared to the average dry beach area ($\bar{A}$ = 179080.62 m^2) during the study period. Considering the monitored beach length, the average error is approximately 6.5 m along the coast. The correlation coefficient between the observed and modeled dry beach areas reflects a strong correlation.

Further developments of IH-MOOSE will be required to improve its application for a greater range of beaches. More specifically, it would be significant to integrate shoreline movements, such as beach rotation or beach breathing, to accomplish the principal's three shoreline variability modes (Ratliff and Murray, 2014). In addition, the very long term could be assessed by considering the influence of sea-level rise on shoreline change.

5.6 Conclusions

- This chapter presented a new proposal of an equilibrium shoreline evolution model, named IH-MOOSE. It consists of a heuristic cross-shore evolution model governed by the homothetic forward/backward shoreline movement, assumes the entire coastline is a parabolic planform, and is applicable over time scales spanning days, months or several years. The model is mainly applicable to beaches influenced by onshore-offshore migration and exclusively for embayed beaches, as these beaches are one of the most prominent physiographic features on the oceanic margin of many countries in the world.
- In conclusion, IH-MOOSE is a reduced-complexity numerical shoreline cross-shore evolution model that requires a few calibration parameters and is computationally

efficient and versatile. From a single monitoring beach profile, the model is able to obtain the evolution of the entire beach coastline.

- Nearly 3 km of the Narrabeen Beach coastline (bounded between PF1 and PF8) have been evaluated. The model showed significant skills in terms of reproducing the shoreline position and dry beach area evolution over six years, demonstrating that it is able to adequately reproduce the storm response and subsequent recovery, which are mostly induced by cross-shore processes.

6 AN EQUILIBRIUM-BASED SHORELINE ROTATION MODEL**

6.1 Introduction

In addition to assessing and quantifying shoreline rotation, the scientific community has also attempted to predict the variability of this phenomenon on medium- to long-term time scales; nevertheless, few shoreline rotation evolution models are available in the literature. To date, only

** This Chapter is based on Jaramillo et al. (2020a): Jaramillo, C., Gonzalez, M.E., Medina, R., Turki, I., 2020. An equilibrium-based shoreline rotation model. Submitted to Coast. Eng.

the models proposed by Turki et al., (2013a) and Blossier et al., (2015); (2017) have been identified (see more details in Section I).

The models cited above are founded on the core ideas build upon earlier disequilibrium concepts introduced by Wright and Short (1984) and Wright et al. (1985). Their main hypothesis states that the instantaneous beach state response depends on the instantaneous "disequilibrium" state, which is the difference between the instantaneous and equilibrium forcing conditions. It should be noted that this hypothesis has also been employed as the cornerstone of multiple other evolution models to predict the natural variability of cross-shore displacement of the shoreline (e.g., Kriebel and Dean, 1993; Yates et al., 2009; Davidson et al., 2010; 2013; Jara et al., 2015; Jaramillo et al., 2020) and other morphological beach parameters, such as sediment grain size (e.g., Prodger et al., 2016), beach slope (e.g., Madsen and Plant, 2001), beach profile state (e.g., Ludka et al., 2015), and barline migration (e.g., Plant et al., 1999; Blossier et al., 2017).

The present study proposes a new equilibrium-based shoreline rotation model based on the kinetic equation defined by Yates et al. (2009) that was inspired by Wright and Short, (1984), Wright et al. (1985) and Miller and Dean, (2004). To demonstrate the model performance, the evolutionary processes of shoreline rotation at Narrabeen Beach and Tairua Beach are evaluated. Both beaches are well-known study sites in the coastal engineering field owing to their long-term (multiyear), high-resolution survey datasets developed through their corresponding monitoring programs.

It is worth mentioning that rotation has been previously identified along Narrabeen Beach (e.g., Ranasinghe et al., 2004; Short and Trembanis, 2004; Harley et al., 2011; Short et al., 2014) and Tairua Beach (e.g., Bryan et al., 2013; Van de Lageweg et al., 2013; Biausque et al., 2016; Blossier et al., 2017). In both cases, the rotation has been recognized as a secondary movement that explains the shoreline variability. For example, Harley et al. (2011) found through empirical orthogonal function (EOF) method at Narrabeen Beach, that the dominant mode of shoreline variability (60% of variability) is an onshore-offshore sediment exchange, while the rotational signal was a secondary mode accounting for approximately 25% of the overall shoreline variability. On the other hand, Blossier et al. (2017) found through a principal component analysis (PCA) that more than 60% of the variability of Tairua Beach is dominated by the shoreline moving through combinations of migration and rotation. Secondary behaviors represented by subsequently modes account mainly for rotation.

This chapter is organized as follows: first, the theoretical development of the proposed model is explained in Section 6.2. Section 6.3 describes all the data related to the selected study sites. The model results are shown in Section 6.4. A discussion on the model assumptions, limitations and

capabilities are presented in Section 6.5. Finally, the main conclusions are summarized in Section 6.6.

6.2 Model development

6.2.1 Model hypotheses and assumptions

As previously mentioned in the introduction, the natural variability of many beach parameters can be inferred in some way by using simple equilibrium beach evolution models. These models aim to evaluate the variability of a beach in response to storms, seasonal and interannual changes.

The model proposed in this study describes changes in shoreline orientation; in other words, the proposed model captures the evolution of the rotation of a beach. This approach implies a series of assumptions and hypotheses that are summarized in this subsection.

Essentially, following the orthogonality hypothesis of the morphodynamic processes (longitudinal and transversal movements of a beach) (de Vriend et al., 1993; González et al., 2010), this study has adopted the methodology presented by Turki et al. (2013b). This methodology states that the total shoreline movement could be separated into two components, one associated with translation in cross-shore direction and the other representing the rotation movement due to the alongshore variation in beach planform. Therefore, the rotation of a beach is assumed to be isolated from other beach movements; that is, beach rotation is independent of cross-shore beach migration and beach breathing. To obtain its definition, beach rotation has been considered to depend mainly on the power and the directionality of the incident waves.

Similar to Turki et al., (2013b) and Harley et al., (2013), the shoreline orientation, α_s, is defined in this study by employing the following process: 1) the time-averaged dry beach width is subtracted from all measured data; 2) a linear-regression fit of these demeaned values is applied; and 3) the shoreline orientation is considered the angle between the line perpendicular to the linear-regression fit and geographic north (as presented in Fig. 6-1a). The left panel of Fig. 6-1 shows a general scheme of the main variables used in the model: the shoreline orientation and the corresponding power and direction of the incoming waves. The right panel of Fig. 6-1 shows an example of how the shoreline rotation is calculated.

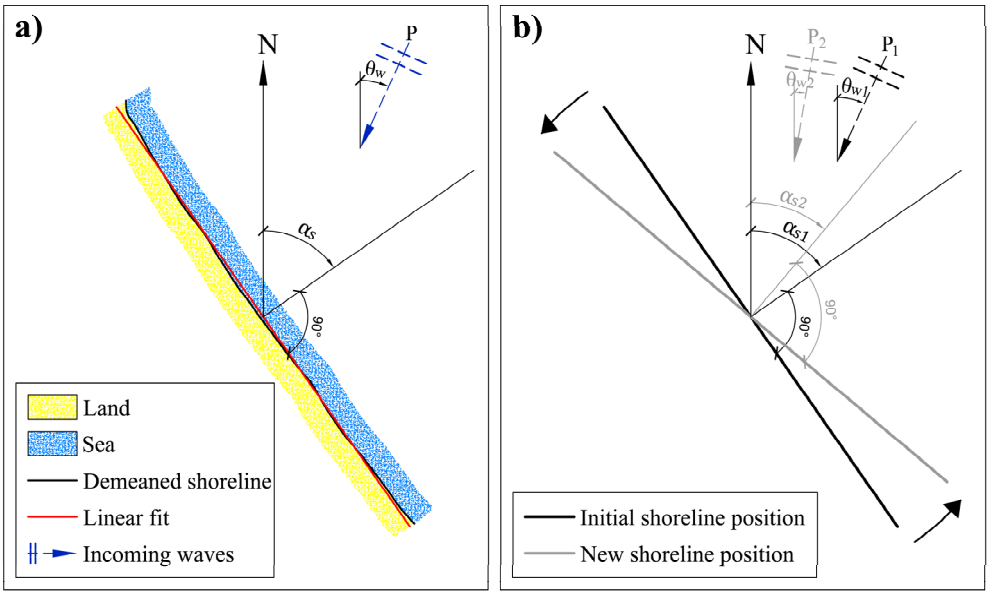

Fig. 6-1. a) General scheme with the main model variables; shoreline orientation, α_s, as the angle between the line perpendicular to the linear-regression fit of the demeaned shoreline and the geographic north, the incoming wave power, P, and the incident wave direction, θ_w. b) Beach rotation scheme; in this case, the initial shoreline position (solid black line) is associated with the incident wave power, P_1, and the incident wave direction,θ_{w_1}; which rotates counterclockwise based on wave power, P_2 and wave direction, θ_{w_2}. As a result, the beach rotates from an initial shoreline orientation, α_{s1} to a new shoreline orientation, α_{s2}.

Another of the most relevant simplifying hypotheses of the proposed model is that a single wave point is assumed as a model forcing. This wave point is used to characterize the power and direction of the incoming waves governing the entire beach. Therefore, the proposed model assumes the following hypotheses regarding wave forcing: 1) the waves are homogeneous along the beach, and 2) to assign a single wave value to the whole beach, a representative point outside the active beach profile, that is, outside the closure depth, must be selected (Hallermeier, 1977). For this reason, it would not be valid to select a nearshore wave forcing within the active beach profile.

The proposed model does not account for short-scale processes such as beach cusp formation, alongshore variable bar welding, or rip current embayments (Splinter et al., 2014). In addition, apart from the shoreline orientation, this model does not explicitly consider any physical beach characteristics such as the mean grain size or the length of the active beach profile. Nonetheless, the model parameters (a, b, L^+ and L^-, see Section 6.2.2) that define the equilibrium condition and the model velocity are intrinsically related to the morphological beach parameters. From the above, variations in the calibration parameter values between sites are implicitly associated with the beach's physical characteristics.

Additionally, the proposed model does not explicitly include any additional parameter related to the tidal range; nonetheless, as suggested by Castelle et al. (2014), equilibrium shoreline evolution models can be applied to a range of elevation contours in the intertidal zone with satisfactory efficiency.

6.2.2 Equation development

Based on the concepts discussed in previous works and the observations utilized by this study, the authors propose the following model for the temporal evolution of the shoreline orientation:

$$\frac{d\alpha_s(t)}{dt} = L^{\pm}\mathrm{P}\Delta\alpha_s(\theta_w) \tag{55}$$

where $\alpha_s(t)$ is the shoreline orientation (°) at the time "t", P is the incident wave power, which is considered a weighting factor of the model that results from the product between the squared significant wave height, Hs^2, and the wave peak period, Tp, $P = Hs^2 \cdot Tp$, (m^2s). $L^{\pm}$ represents the proportionality constants ($m^{-2}s^{-2}$); L^+ corresponds to clockwise shoreline rotation, and L^- corresponds to counterclockwise rotation. $\Delta\alpha_s(\theta_w)$ (see Eq. (56)) is the shoreline orientation disequilibrium:

$$\Delta\alpha_s(\theta_w) = \alpha_s - \alpha_{s_{eq}} \tag{56}$$

where $\alpha_{s_{eq}}$ is the asymptotical equilibrium shoreline orientation. It is important to highlight that if a theoretical beach case is being evaluated, assuming that the shoreline is absolutely straight and the incident waves direction, θ_w, is completely uniform over the entire beach length, it could be expected that $\alpha_{s_{eq}} \cong \theta_w$; nonetheless, by assuming the wave conditions outside the active beach profile as the model forcing, there is a proportional relationship between $\alpha_{s_{eq}}$ and θ_w. For simplicity, a linear relationship between the equilibrium shoreline orientation and the incident wave direction is assumed:

$$\alpha_{s_{eq}} = \frac{\theta_w - b}{a} \tag{57}$$

where a (-) and b (°) are empirical parameters.

The equilibrium shoreline orientation for a given wave direction (Eq. (57)) is defined in this study as the equilibrium wave direction function (EWDF). This function corresponds to the best adjustment between the measurements, separating the positions that will undergo a clockwise rotation from the measurements that will rotate in the opposite direction (counterclockwise).

Fig. 6-2 shows an EWDF example for the proposed model based on the study site of Tairua Beach (see Section 6.3.1). The black line is the corresponding empirical approximation of the EWDF, and the points are consecutive measurements that are colored according to the shoreline orientation change rate.

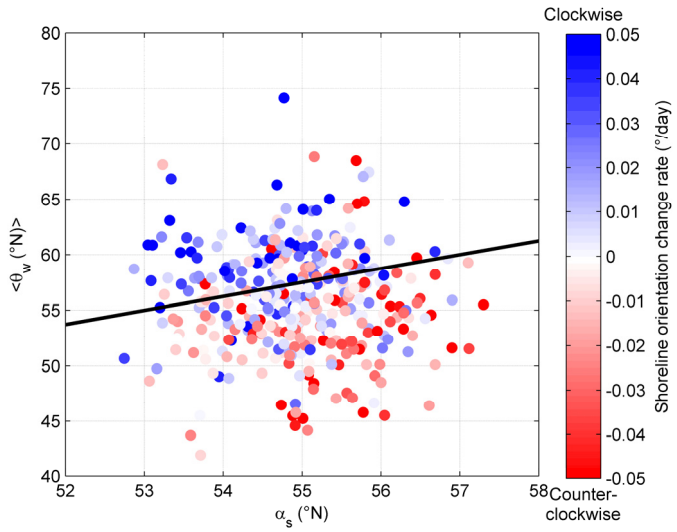

Fig. 6-2. Shoreline orientation change rate, $\frac{d\alpha_s}{dt}$ (see color scale), versus the average wave direction between observations, <θ_w (°N)>, and the initial shoreline orientation, α_s(°N). The solid black line is the most accurate equilibrium relationship, namely, the EWDF.

In this case, the approach to equilibrium is exponential, and the solution to Eqs. (55)-(57) takes the following form:

$$\alpha_s(t) = \left(\alpha_{s_0} - \alpha_{s_{eq}}\right) e^{-L^{\pm}Pt} + \alpha_{s_{eq}} \tag{58}$$

where α_{s_0} is the initial shoreline orientation.

In summary, the model formulation presented above has four calibration parameters (a, b, L^+ and L^-). The parameters a and b define the equilibrium condition (EWDF) and are determined from the available surveys considered for calibration purposes, and $L^{+/-}$ control the shoreline rotation rate, either clockwise or counterclockwise.

6.3 Study sites

This section presents the selected study sites, the wave characterization of the studies areas as the main driving force of the proposed equilibrium shoreline evolution model and the corresponding derived shoreline position datasets.

The selected study sites are two beaches in the South Pacific Ocean of the insular region known as Oceania. The right panel of Fig. 6-3 corresponds to Tairua Beach in New Zealand, while the left panel corresponds to Narrabeen Beach in Australia.

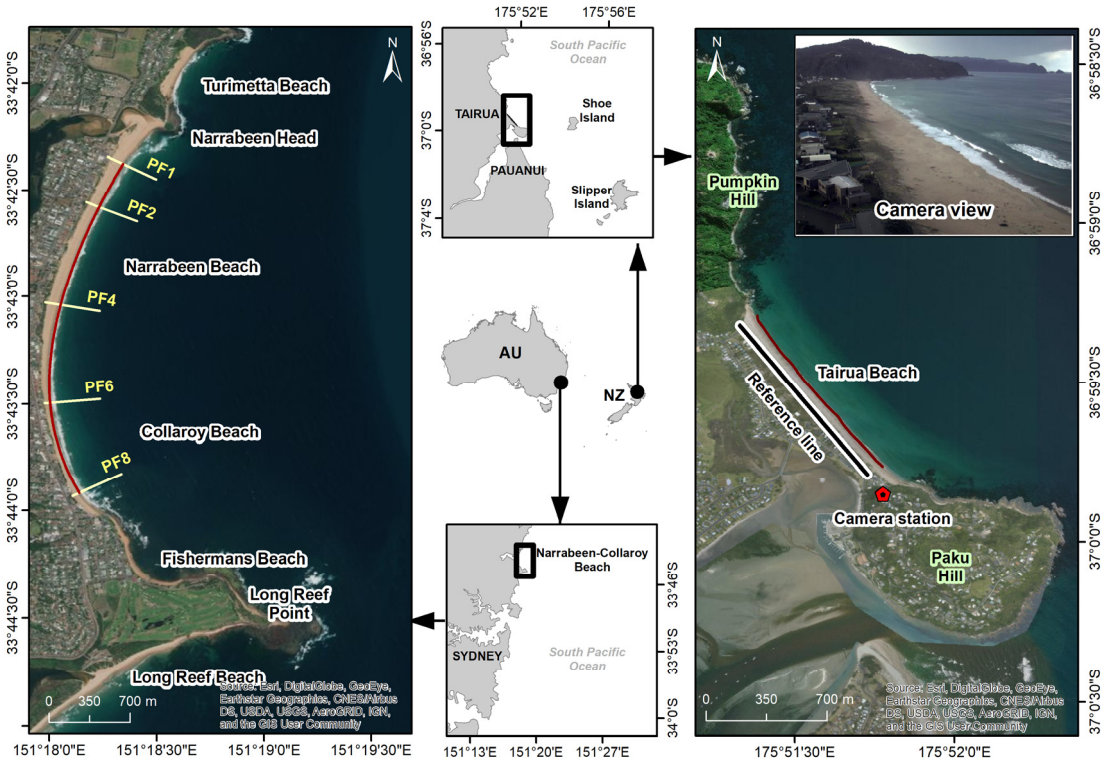

Fig. 6-3. Locations of the selected study sites. Narrabeen Beach (lower and left panels), including the locations of the five monthly survey transects (PF1, PF2, PF4, PF6, and PF8) and an example of the shoreline as a polynomial of degree 4 (red line). Tairua Beach (upper and right panels), including the reference line to estimate the shoreline position, the camera station with its corresponding view and an example of the video-derived shoreline (red line).

6.3.1 Tairua Beach

6.3.1.1 Study site

Tairua beach is an embayed 1.2 km long sandy beach located on the eastern coast of the Coromandel Peninsula, North Island, New Zealand (see Fig. 6-3). The embayed beach is bounded by the promontory Pumpkin Hill at the north end and by the extinct volcano Paku Hill at the south end. The average direction normal to the beach is close to 53° with respect to north; the beach

mainly faces easterly and north-easterly long-traveling swell and storm waves coming from the Pacific Ocean. The beach is partly sheltered from waves by Shoe Island, located 3 km east of Paku Hill (Blossier et al., 2017).

The beach sediment is characterized by coarse sand with a median grain size between 0.3 and 0.6 mm (Blossier et al., 2017). According to the classification of Wright and Short, (1984), the beach is an intermediate beach that is characterized by the presence of crescentic sandbar patterns and well-developed rip channels (Coco et al., 2005).

6.3.1.2 Marine conditions

The study zone is located in a microtidal environment, where the tidal level range is between 1.2 m (neap) and 2 m (spring) (Bogle et al., 2001).

The wave climate acting in the vicinity of Tairua Beach was acquired from Shoreshop Data provided by the University of Auckland (Montaño et al., 2019). The wave climate corresponds to a wave hindcast from 1979 to 2016 developed by MetOcean. The selected wave point is located at -36.988° latitude and 175.864° longitude (approximately 600 m offshore from the beach with a water depth of approximately 8 m).

A statistical analysis of the wave conditions is presented in Fig. 6-4, which shows a scatter diagram that correlates the significant wave height, Hs, with the peak period, Tp, and the directional roses of Hs for all months, austral winter months (June, July, and August) and austral summer months (December, January, and February). Considering all the data series, the most frequent waves come from the NE (48.2% of the time), followed by waves from the ENE (47.5%). Hs and Tp have ranges of 0.1–4.4 m and 2.2–22.1 s, respectively. The annual mean significant wave height, Hs, is 0.7 m and the significant wave height exceeded 12 hours per year (Hs_{12}) is approximately 3.4 m. During summer months, the wave distribution shows that waves coming from the northeast are dominant, while during the winter, waves coming from the east-northeast are dominant.

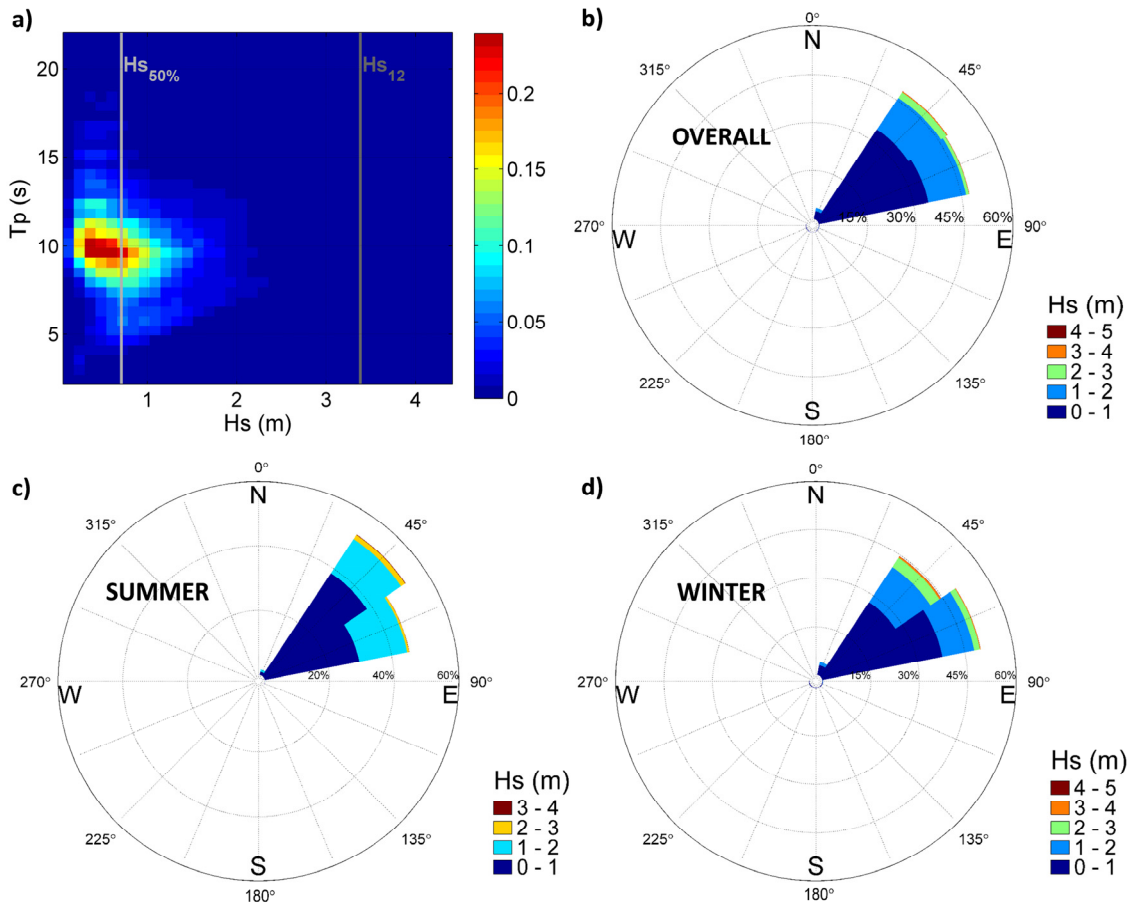

Fig. 6-4. Wave characteristics of a wave point at Tairua Beach: scatter diagram Hs-Tp (a), directional roses of Hs for all months (b), summer months (c) and winter months (d).

6.3.1.3 Shoreline orientation data

In this study, shoreline records of Tairua Beach were also obtained from Shoreshop data processed by the University of Auckland (Montaño et al., 2019). These publicly available data correspond to video-derived shorelines over 15 years spanning from January 1999 to December 2013.

Approximately daily shoreline records were obtained by a video-camera system funded by the Waikato Regional Council and the National Institute of Water and Atmospheric Research (NIWA). The video-monitoring station is part of the NIWA-based 'Cam-Era' network, installed during September 1997 on Paku Hill, and overlooks Tairua Beach from the southern end at an elevation of approximately 70 m (Almar et al., 2008) (see camera view in Fig. 6-3).

The system automatically collects 600 individual oblique images over a period of 15 min every hour (but only during the day). The shoreline records were obtained from time-exposures images (snapshot series averaged over 15 min), which were rectified, geo-referenced and rotated using intrinsic and extrinsic camera parameters (Van de Lageweg et al., 2013).

Each shoreline from the Shoreshop Data was processed to obtain its corresponding average beach orientation (as presented in Fig. 6-1). Fig. 6-5 shows the evolution of the beach orientation in a normalized way by means of an index defined by Harley et al. (2015) namely, the beach orientation index (BOI). The BOI is a simple measure to assess whether the beach orientation is more clockwise or counterclockwise with respect to the long-term average. A positive BOI value indicates a clockwise beach position with respect to the period average, while a negative BOI indicates a counterclockwise beach position with respect to the average position.

$$BOI(t) = 10\frac{\left(\alpha_s(t) - \overline{\alpha_s(t)}\right)}{std\left(\alpha_s(t)\right)} \tag{59}$$

where α_s(t) is the shoreline orientation at time "t", $\overline{\alpha_s(t)}$ is the arithmetic mean shoreline orientation for the analysis period and $std\left(\alpha_s(t)\right)$ is the standard deviation.

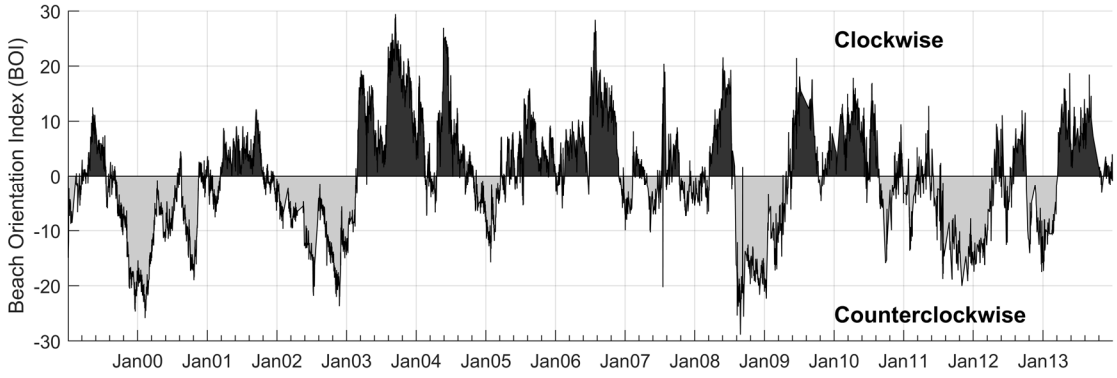

Fig. 6-5. Evolution of the beach orientation index (BOI) at Tairua Beach.

As shown in Fig. 6-5, throughout the 14 years of data, clear rotation events are observed at Tairua Beach, for example, the clockwise rotation recorded from the end of 2002 to the beginning of 2003 and the counterclockwise rotation that occurred during mid-2008. The most clockwise position with respect to the long-term average resulted in September 2003, while the most counterclockwise position was recorded in August 2008.

6.3.2 Narrabeen Beach

6.3.2.1 Study site

The general characterisation of Narrabeen Beach has been previously described in detail in Section 5.3.

6.3.2.2 Marine conditions

The wave climate close to Narrabeen Beach was acquired from a point within the wave reanalysis database Global Ocean Waves (GOW), developed by IHCantabria (Perez et al. 2017). The GOW database uses a global mesh (0.5° longitude by 0.5° latitude) and an hourly resolution. The GOW model has been calibrated and validated globally using instrumental measurements of buoys and satellite altimetry data extracted from satellite images (Reguero et al., 2012). Detailed descriptions of the GOW database can be found in Reguero et al. (2012) and Perez et al. (2017).

This study uses the results given by the GOW model of an offshore point located at -34° latitude and 151.5° longitude using data within the period between 1979 and 2015. This point provides hourly sea states with different wave parameters (e.g., significant wave height Hs, peak period Tp, mean wave direction θm, etc.).

Fig. 6-6 shows the scatter diagram Hs-Tp, and the directional roses of Hs for all months, winter months and summer months. Taking into account all the data series, the most frequent waves come from the SSE (21% of the time), followed by waves from the S (20%), which are the most energetic waves, and SE (14%). Hs and Tp have ranges of 0.4–9.0 m and 3.0–23.6 s, respectively. The wave climate exhibits strong seasonal modulation with an annual mean significant wave height, Hs, of 1.5 m and the Hs_{12} is approximately 5.9 m. During summer months, wave distribution shows a dominance of waves coming from directions around the east while during the winter the dominance is of the waves coming from the south.

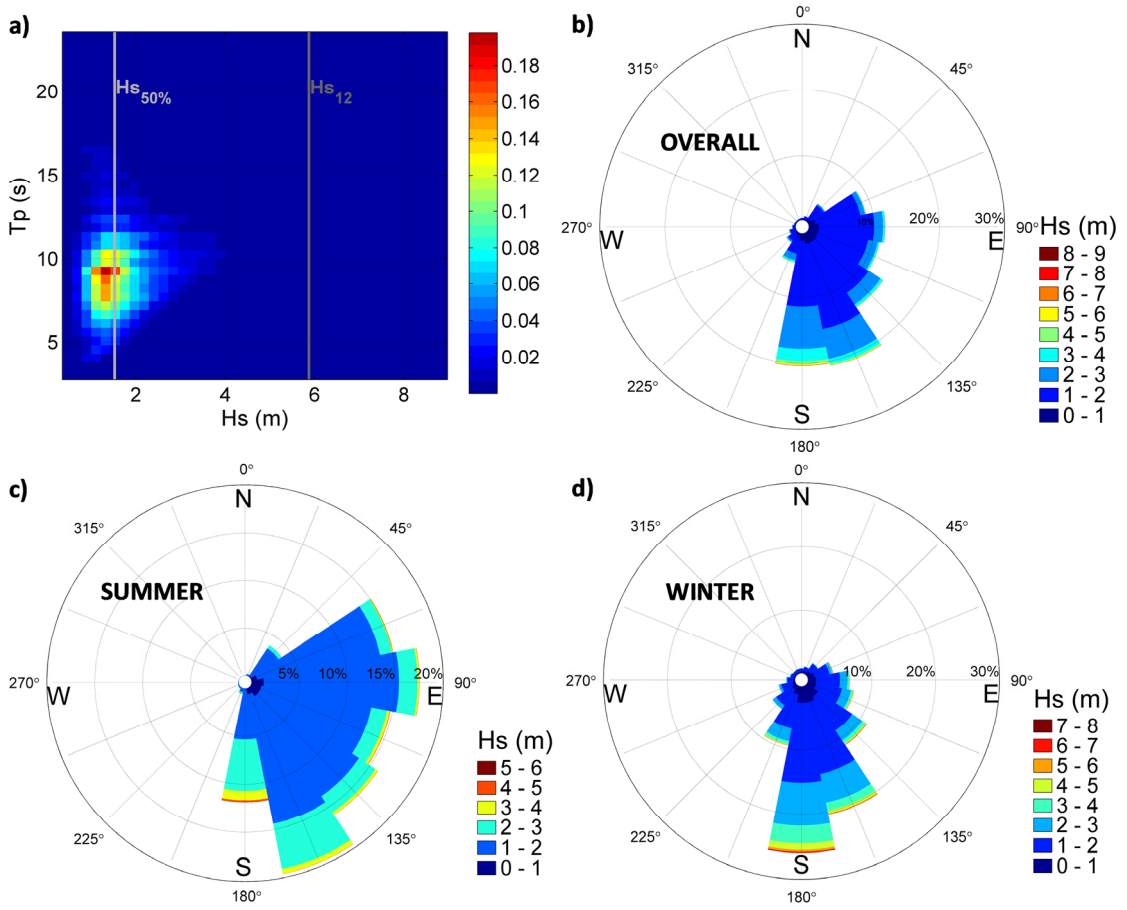

Fig. 6-6. Wave characteristics of the selected GOW point near Narrabeen Beach: scatter diagram Hs-Tp (a), directional roses of Hs for all months (b), summer months (c) and winter months (d).

Regarding the variability of the water level, the coastline of southeastern Australia experiences a semidiurnal and microtidal tidal regime, where the average spring tide range is 1.6 m and the average neap tide range is 1.2 m (Wright et al., 1985).

6.3.2.3 Shoreline orientation data

This study employs time series of the coastline variability at Narrabeen Beach obtained from the publicly available Narrabeen-Collaroy monitoring program, which provides data series of beach profile surveys at five cross-shore locations (see Fig. 6-3, north to south, hereafter identified as PF1, PF2, PF4, PF6, and PF8). These profiles have been measured on a monthly basis by the University of Sydney since 1976. Surveys were undertaken at low tide, and the profiles were recorded at 10-m cross-shore intervals from a fixed benchmark at the landward limit.

From each field campaign, measurements of the five beach profiles were used to define the complete coastline. On this basis, a corresponding linear adjustment to the demeaned shoreline was obtained (as presented in Fig. 6-1) to finally obtain the average beach orientation. Fig. 6-7 shows the beach orientation index for the period spanning four decades from 1976 to 2016.

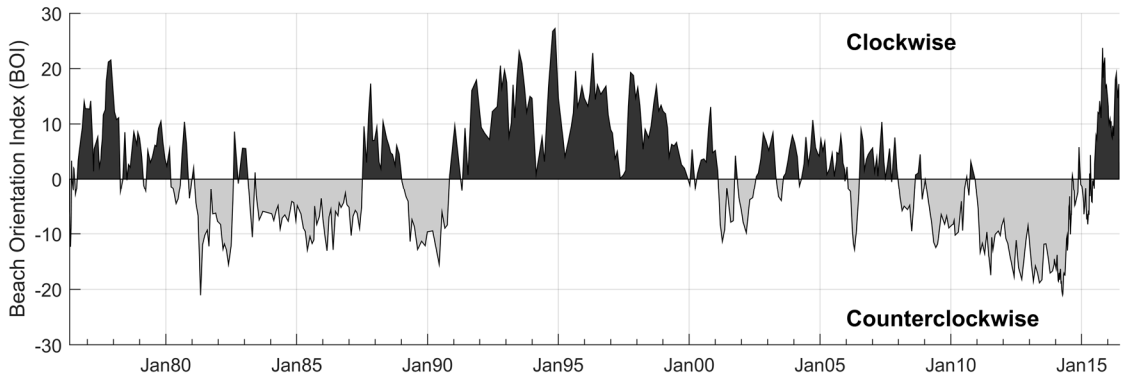

Fig. 6-7. Evolution of the beach orientation index (BOI) at Narrabeen Beach.

During the 40 years of the evolution of the BOI presented in Fig. 6-7, the most clockwise position with respect to the long-term average occurred in October 1994, while the most counterclockwise position was recorded in March 2014. Multiple rotation events are evident, however, such as the prolonged counterclockwise rotation recorded from mid-2006 to mid-2014 and the subsequent accentuated clockwise rotation that was maintained until the end of 2015.

6.4 Results

This section presents the performance of the proposed equilibrium-based empirical shoreline rotation model applied to the two selected study sites. In both cases, the rotation model was executed to hindcast the full dataset of observations during the selected study periods; the model predictive capacity with different calibration periods is presented later in Section 6.5.4.

To execute the model, it is necessary to find the best-fitting model parameters. In this study, the calibration parameters a and b of the EWDF have been determined from the observations using the wave direction averaged over the period between successive surveys (biweekly data in Tairua Beach and monthly data at Narrabeen Beach). Then, an iteration algorithm was used to find the proportionality constants that define the clockwise shoreline rotation rate, L^+, and counterclockwise shoreline rotation rate, L^-, which produced the lowest RMSE between the modeled and measured shoreline positions.

The model performance is investigated using the root-mean-square error, the correlation coefficient, ρ, the Brier Skill Score (see Eq. (40)), BSS (Murphy and Epstein, 1989) and the Skill index, s, or index of agreement (Willmott, 1981). The BSS (see Eq. (60)) measures the ratio of improvement in accuracy of the forecast over a benchmark model, compared to the total possible improvement in accuracy (Sutherland et al., 2004).

$$BSS = 1 - \frac{\sum[|x - x_m| - \Delta x]^2}{\sum(x - x_b)^2} \tag{60}$$

where Δx is the estimated measurement error in the data, assumed to be in the order of 0.05º and x_b is the baseline condition given by a linear trend (in time) of the data as done in similar analysis (e.g. Davidson et al., 2013; Splinter et al., 2018). According to van Rijn et al. (2003), the BSS coefficient can be classified as "bad" (<0.0), "poor" (0.0-0.3), "reasonable/fair" (0.3-0.6), "good" (0.6-0.8) and "excellent" (0.8-1.0).

Section 6.4.1 presents the results from Tairua Beach, and Section 6.4.2 presents the results from Narrabeen Beach.

6.4.1 Model results from Tairua Beach

In the case of Tairua Beach, from the approximately daily video-derived shoreline records, biweekly shoreline orientations were chosen to define the EWDF. Then, the shoreline orientation variability due to beach rotation was simulated during the period encompassing all available shoreline data (14 years, from 1999 to 2013).

The upper and middle panels of Fig. 6-8 show the temporal evolution of the incident wave power and wave direction, respectively. The complete simulation of the proposed shoreline orientation evolution model (solid black line) is presented in the lower panel.

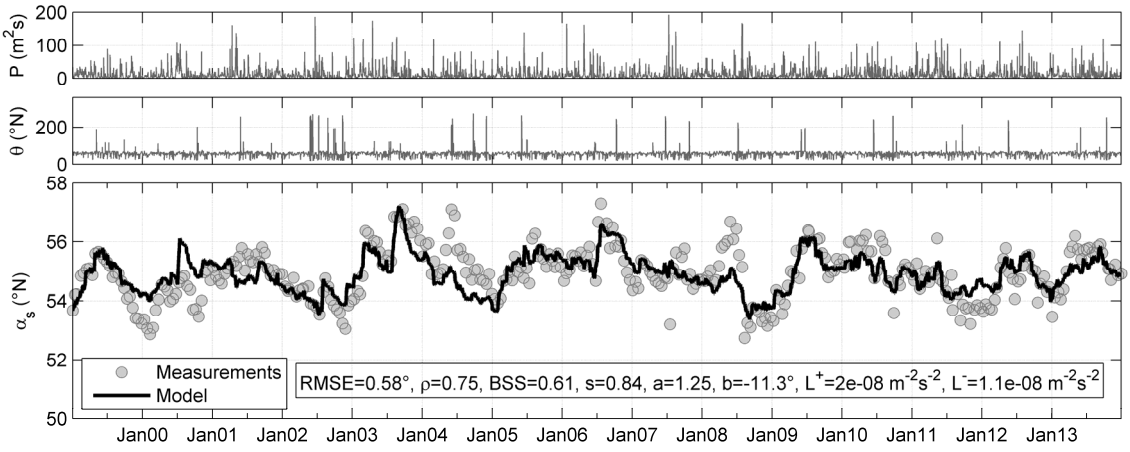

Fig. 6-8. Results for Tairua Beach. Time series of incident wave power (upper panel), wave direction (middle panel) and validation of the proposed shoreline orientation evolution model (lower panel).

According to the results, in some specific short periods, for example, the summers of 2000 and 2012 and the winter of 2004, the model did not accurately resolve the shoreline response, as these seasons were periods in which the beach rotation exceeded the average model speed. Nonetheless, it should be highlighted that the general variability of the beach orientation is effectively

represented by the model. The resulting RMSE between the observed and modeled shoreline positions is 0.58°, the correlation coefficient, ρ, is 0.75, the Brier Skill Score, BSS is 0.61 and the Skill index, s is 0.84; all of them are considered as satisfactory quantitative statistic values.

In accordance with the seasonal variability of the wave direction (see Section 6.3.1.2), the shoreline orientation at Tairua Beach tends to rotate clockwise from summer to winter and counterclockwise from winter to summer. As reported by Van de Lageweg et al., (2013), the shoreline at Tairua Beach rotates relatively quickly (less than a month) during the winter storm events when the storms are accompanied by strong alongshore components, and the beach gradually returns to its original shape during the summer months.

6.4.2 Model results from Narrabeen Beach

Although the monthly shoreline position records obtained from the beach profile surveys at Narrabeen Beach start in April 1976, the beach orientation analysis in this study begins in January 1979 due to the availability of wave data. Therefore, the shoreline orientation variability is evaluated below for all of the available data period (37 years, from January 1979 to December 2015).

Fig. 6-9 shows the results from Narrabeen Beach. The upper and middle panels show the temporal evolution of the incident wave power and wave direction, respectively, at the selected wave point. The lower panel shows the complete simulation of the proposed shoreline orientation evolution model.

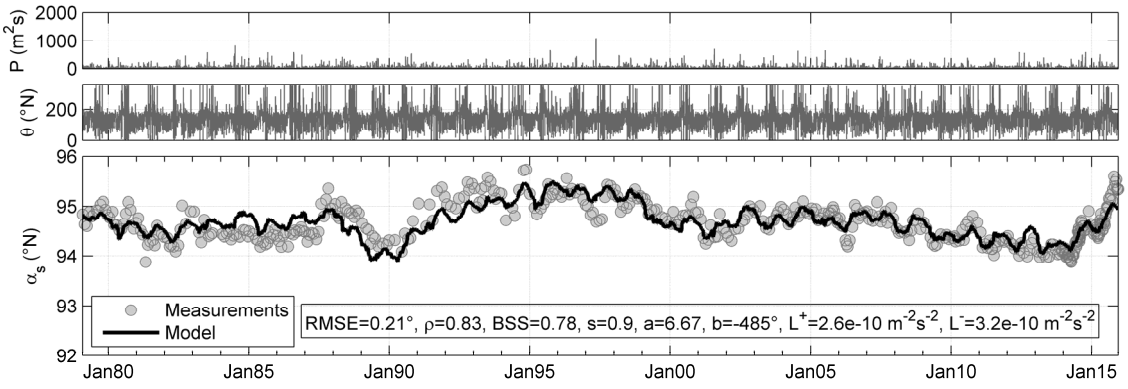

Fig. 6-9. Results for Narrabeen Beach. Time series of incident wave power (upper panel), wave direction (middle panel) and validation of the proposed shoreline orientation evolution model (lower panel).

The upper panel of Fig. 6-9 reflects the strong seasonal variation of the incident wave power, with strong storms during the winter periods and low-energy waves during the summers. The results presented in the lower panel of Fig. 6-9 reveal again that the model achieved a good performance, successfully reproducing the general variability of the shoreline orientation. It should be noted

that from 1995 onwards, the model performance is quite robust, adjusting very well to the measurements; the model predictions fall slightly below the measurements only during the period between 1990 and 1995, but it maintains the multiyear rotation trend. The resulting quantitative statistic values are satisfactory: RMSE=0.21°, ρ=0.83, BSS=0.78 and s=0.90.

In general terms, the behavior of Narrabeen Beach is similar to that of Tairua Beach; both beaches tend to rotate clockwise from summer to winter and counterclockwise from winter to summer, which is directly correlated with the directional wave variation between seasons (see Section The embayment rotation cycles at Narrabeen have been observed at seasonal time scales (M. D. Harley et al., 2011) and interannually due to influences by El Niño-Southern Oscillation (Ranasinghe et al., 2004; Short and Trembanis, 2004).6.3.2.2).

6.5 Discussion

According to the results presented in Section 6.4, the proposed model can effectively reproduce the evolution of the shoreline orientation at the two selected study sites. It is worth noting that both study sites exhibit intermediate beach states and similar sediment grain sizes, and both beaches are subject to microtidal environments; still, Narrabeen Beach is three times longer than Tairua Beach. Additionally, the data sources used to obtain the time series of the shoreline positions were different in both cases; at Tairua Beach, the data came from video-camera images, whilst at Narrabeen Beach, the data came from beach profile surveys.

Table 6-1 shows a summary of the quantitative statistics obtained in Section 5.4. Additionally, others statistics for model evaluation are included, such as Nash-Sutcliffe efficiency (NSE), which is a normalized indicator that determines the relative magnitude of the residual variance compared to the measured data variance (Nash and Sutcliffe, 1970), and the root mean square error to the standard deviation of measured data (RSR).

Table 6-1. The correlation coefficient, root mean square error, Nash-Sutcliffe efficiency and the ratio of the root mean square error to the standard deviation of measured data between the observed and modeled shoreline orientations at Tairua Beach and Narrabeen Beach.

	ρ	RMSE (°)	BSS	s	NSE	RSR
Tairua Beach	0.75	0.58	0.61	0.84	0.56	0.66
Narrabeen Beach	0.83	0.21	0.78	0.90	0.69	0.56

Regarding the magnitude of the RMSE between the modeled and measured shoreline orientations, the RMSE was greater in Tairua Beach (RMSE=0.58°) than in Narrabeen Beach (RMSE=0.21°);

nonetheless, the maximum variability of the shoreline orientation recorded at Tairua Beach reached up to 5°, while it did not reach 2° in Narrabeen Beach. According to Moriasi et al. (2007), the model simulation can be judged as satisfactory if NSE > 0.50 and RSR <= 0.70, ranges in which the values of Table 6-1 are found. The convincing results are confirmed by relatively high values of BSS and s.

Turki et al., (2013b) concluded that the greater the length of the beach and its sediment grain size, the slower its rotation response. In this case, considering that both selected study sites have similar sediment grain size, the beach length seems to be directly related to the differences between beach rotation rates. In accordance to the parameters L^+ and L^-, Tairua Beach has rotation speeds (both clockwise and counterclockwise) which are much faster than those of Narrabeen Beach (see Fig. 8 and Fig. 9). From the above, in the case of Tairua Beach, changes in the shoreline orientation are more readily evident on times scales of days to weeks (even months) related to storm events and seasonal changes, while in the case of Narrabeen Beach, the rotation movement takes place on longer time scales (with variations occurring between the seasonal and interannual time scales). Both the observational data and the model simulations suggest clockwise rotation from austral summer to winter and counterclockwise rotation in the opposite order.

In general terms, the proposed model reached good agreement with the measurements; nevertheless, it should be recognized that the model is subjected to a number of hypotheses (see Section 6.2.1) that might limit its applicability. For example, considering that the parabolic shoreline configuration of an embayed beach is simplified into a linear shape, the proposed model is unable to capture small-scale plan-form movements. On the other hand, the proposed model neglects the existence of sinks or sources acting on the overall sediment balance of the beach. However, to take into account sediment variations derived from diverse sources (e.g., alongshore littoral sediment drift, sediment discharge by rivers, nourishments, dune erosion, cliff retreat or aeolian sediment transport), the model could be adapted following the model of Jaramillo et al., (2020), in which the equilibrium condition evolves over time depending on the net sediment gains or losses.

Additionally, considering that the model parameters (a, b, L^+, L^-) remain constant throughout the execution, the model is not able to accurately reproduce the variability of the shoreline orientation due to possible changes in storm intensity, the rate of sea-level rise, or human interventions. To vary the model parameters over time, it is possible to include a data assimilation algorithm, such as the Kalman filter, previously proposed by Long and Plant, (2012) for cross-shore migration. This algorithm would automatically adjust the rate parameters during the runtime to best fit any available observed data at the concurrent time step. However, after the last available observation

is assimilated, the parameters will remain constant for the entire forecasting period (Vitousek et al., 2017). It should be noted that the data assimilation of historical records improves estimates of model parameters and therefore improve confidence in long-term predictions; nonetheless, there needs to be a justification for this time-varying response.

Despite the possible limitations inferred by the simplifying model's hypotheses, the model, which is computationally efficient and easy to apply, is able to reproduce the general variability of the shoreline orientation. A series of analyses are presented below: first a comparison of the proposed model to the semi-empirical model proposed by Turki et al. (2013a) (hereafter TU13 model), second the model performance is evaluated considering the Principal Component Analysis (PCA) method, third the BOI evolution instead of the shoreline orientation evolution, then, four model sensitivity analyses considering different calibration periods, weighting factors, fewer calibration parameters and initial shoreline orientation values.

6.5.1 Comparison with the TU13 model

This subsection presents a comparison of the proposed model with the semi-empirical TU13 model, which, as mentioned above, was pioneer in modeling the shoreline rotation. TU13 model relates the shoreline rotation rate to the amount of wave energy available for alongshore sediment transport, taking into account that the longshore transport depends on the angle between the breaking waves and the shoreline, and reaches zero when waves are normal to the beach. This model was able to reproduce the shoreline rotation of three embayed beaches in Barcelona (Spain) for a period of one year (Turki et al., 2013a).

TU13 model was initially defined in terms of shoreline response, R, i.e. the distance of advance or retreat due to the shoreline rotation. To be equivalent to the model proposed in this study, the TU13 model has been expressed in terms of shoreline orientation as follows:

$$\frac{\partial \alpha}{\partial t} = \frac{2K}{l^2 \cdot h^*} \cdot \rho_w \cdot g \cdot (H_b - H_{cr})^2 \cdot C_{gb} \cdot sin(\gamma_b) cos(\gamma_b) \tag{61}$$

where K is a coefficient accounting for the sediment properties ($m^2s^2kg^{-1}$), h* is the closure depth (m), l is the shoreline length (m), ρ_w is the water density (kg m^{-3}), g is the gravity acceleration (ms^{-2}), H_b is the breaking wave height (m), c_{gb} is the wave group celerity at breaking (ms^{-1}) and γ_b represents the instantaneous angle between the wave crest at breaking and the long-term equilibrium shoreline. Further details of the model can be found in Turki et al. (2013a). The comparison of the proposed model (black line) with the TU13 model (red line) to the case of Narrabeen beach is presented in Fig. 6-10.

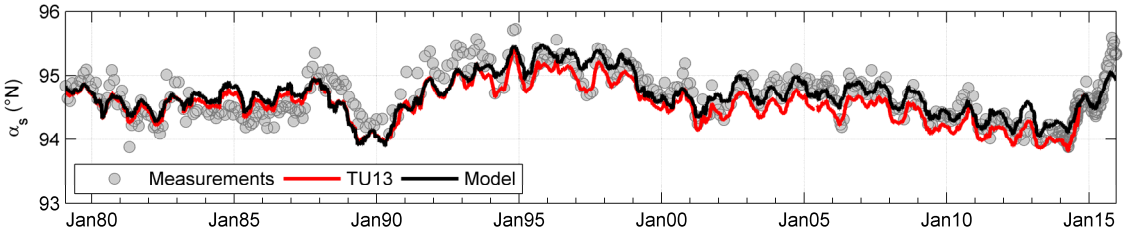

Fig. 6-10. Comparison of the proposed model with the TU13 model at Narrabeen beach.

The results show that the shoreline orientation observations are in agreement with both models. As a qualitative analysis, it could be concluded that the performance of both models is quite similar from the beginning of the simulation until mid-1993, from then on, the TU13 model is slightly below the model proposal until the end of 2014 when both tend to follow the same trajectory. Generally, the proposed model seems to be more correlated during the full period. Table 6-2 presents some quantitative statistics to assess the goodness of fit of both models. The estimated values are similar, being slightly better using the proposed model in this study.

Table 6-2. Models comparison considering the correlation coefficient, root mean square error, Brier Skill Score, Skill index, Nash-Sutcliffe efficiency and the ratio of the root mean square error to the standard deviation of measured at Narrabeen Beach.

Model	ρ	RMSE (°)	BSS	s	NSE	RSR
Proposed model	0.83	0.21	0.78	0.90	0.69	0.56
TU13	0.82	0.22	0.77	0.89	0.67	0.57

Finally, it should be underlined that the TU13 model was initially defined for shoreline rotation analysis in the medium term for pocket beaches with small lengths. This study has shown that this model has also achieved a good performance in the long term, considering the 37 years of shoreline orientation evolution at Narrabeen beach. On the other hand, the proposed model has been defined to reproduce the variability at a full timescale, from short to long term, also for long beaches.

6.5.2 Model considering Principal Component Analysis

This subsection shows the performance of the proposed model considering the shoreline orientation variability obtained from the use of the Principal Component Analysis (PCA) method at Tairua Beach. The PCA method is a commonly used technique to separate the temporal and spatial variability of shoreline data. This method, also known as the empirical orthogonal function (EOF) method has been widely applied in coastal morphology (Medina et al., 1994) and more specifically, used by several authors to decompose the shoreline variability at Narrabeen Beach

(e.g. Short and Trembanis, 2004; Harley et al., 2011; Short et al., 2014) and Tairua Beach (e.g. Blossier et al., 2015; 2017).

The purpose of the PCA method is to describe shoreline changes by using the least number of functions, called eigenfunctions. The first eigenfunction represents the dominant mode, which accounts for the greatest variance, while successive eigenfunctions represent the greatest amount of the remaining variance (Medellín et al., 2008). Considering x the cross-shore axis and y the alongshore axis, x_{yt} can be explained by the summation of eigenfunctions multiplied by coefficients as follows:

$$x(y,t) = \sum_{n=1}^{N} \lambda_n C_n(t) e_n(y) \tag{62}$$

where λ_n are weighing factors, $C_n(t)$ are eigenfunctions which depend only on t, and $e_n(y)$ represents eigenfunctions which depend only on y. A detailed description of the PCA method can be found in statistics books (e.g. Daultrey, 1976; Jackson, 1991).

Fig. 6-11 presents the first three shoreline PCA modes at Tairua Beach. The first mode accounts for 52.6% of the observed shoreline variability; the second contains 25.4% and the third 6.09 %. These first three modes represent a total of 84% of the shoreline variability.

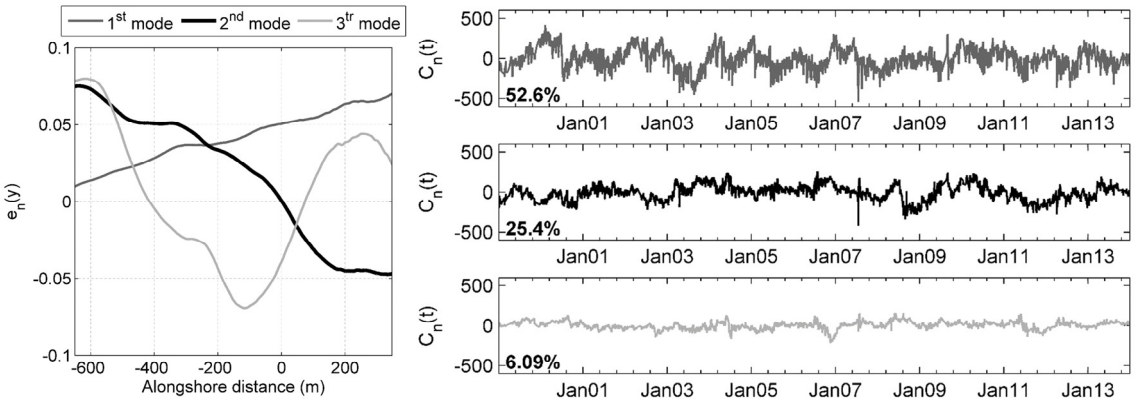

Fig. 6-11. PCA for shoreline variability at Tairua Beach. Spatial eigenfunctions (left panel) and temporal eigenfunctions (right panel).

As previously concluded by Blossier et al. (2015); (2017) using the PCA method through seven years of shoreline variability at Tairua Beach, they identified that the two primary orthogonal modes of shoreline behavior largely describe the shoreline migration and rotation movements. The first mode mainly represents the shoreline migration, while the second tends to represent rotation movement; however, the temporal evolution of these first two modes suggests a combined behavior, so each shoreline movement is not explained or accounted by a single mode.

In spite of this, Fig. 6-12 shows the proposed model performance considering the shoreline orientation variation obtained from the reconstruction of the component or mode 2.

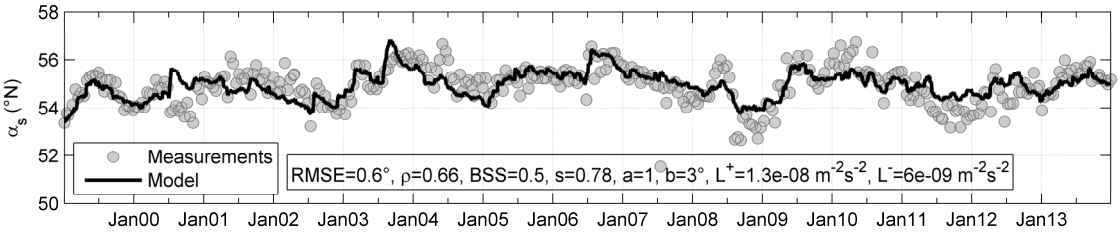

Fig. 6-12. Model simulation considering the shoreline orientation from PCA "rotation" component 2 at Tairua Beach. The shoreline orientation is considered the angle between the line perpendicular to the linear-regression fit of the data and geographic north.

The results show that the proposed model achieves reasonable performance in reproducing the general shoreline orientation variability obtained from the second mode of the PCA method; however, the results have not been as accurate as in Fig. 6-8. In this case, the rate parameter L^- is an order of magnitude lower, so the model response is slower to reproduce counterclockwise rotations.

For all the above reasons, highlighting that the rotation movement is inferred by more than one PCA mode, it is suggested to evaluate the proposed model assuming the shoreline orientation variability following the method described in Section 6.2.1, which better captures the rotation movement.

6.5.3 Model in terms of BOI

Another way to evaluate the shoreline rotation would be through the beach orientation index, BOI. This subsection presents the model performance considering the BOI evolution instead of the shoreline orientation evolution. To do this, the variable α_s is replaced by BOI in equations (55), (56), (57) and (58). The model results considering the BOI evolution are presented in Fig. 6-12 to both selected beaches, Tairua Beach (upper panel) and Narrabeen Beach (lower panel).

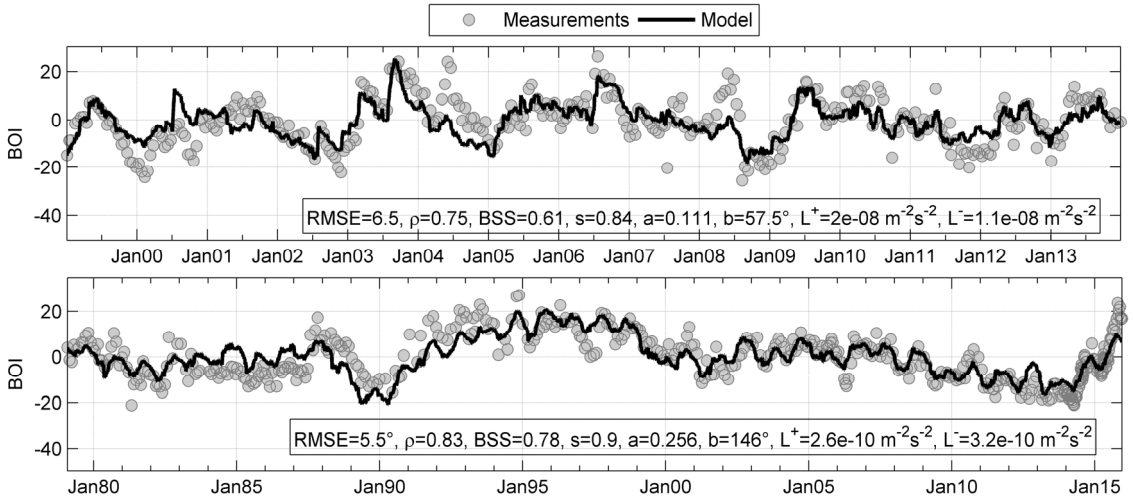

Fig. 6-13. BOI evolution at Tairua Beach (upper panel) and Narrabeen Beach (lower panel).

As expected, since the BOI is a normalized metric derived from the shoreline orientation, the results of the proposed model are basically the same. It should be underlined that in both cases, the qualitative statistics ρ, BSS and s, and the proportionality constants $L^{\pm}$ are equal to the results presented in Fig. 6-8 and Fig. 6-9. Only the values of RMSE and the coefficients a and b, which define the EWDF, change.

6.5.4 Model sensitivity to the calibration period

This subsection presents the ability of the proposed model to forecast the variability of the shoreline orientation considering different calibration time periods. Fig. 6-14 shows three forecasting tests by means of 4-years training periods using the 14-year dataset at Tairua Beach.

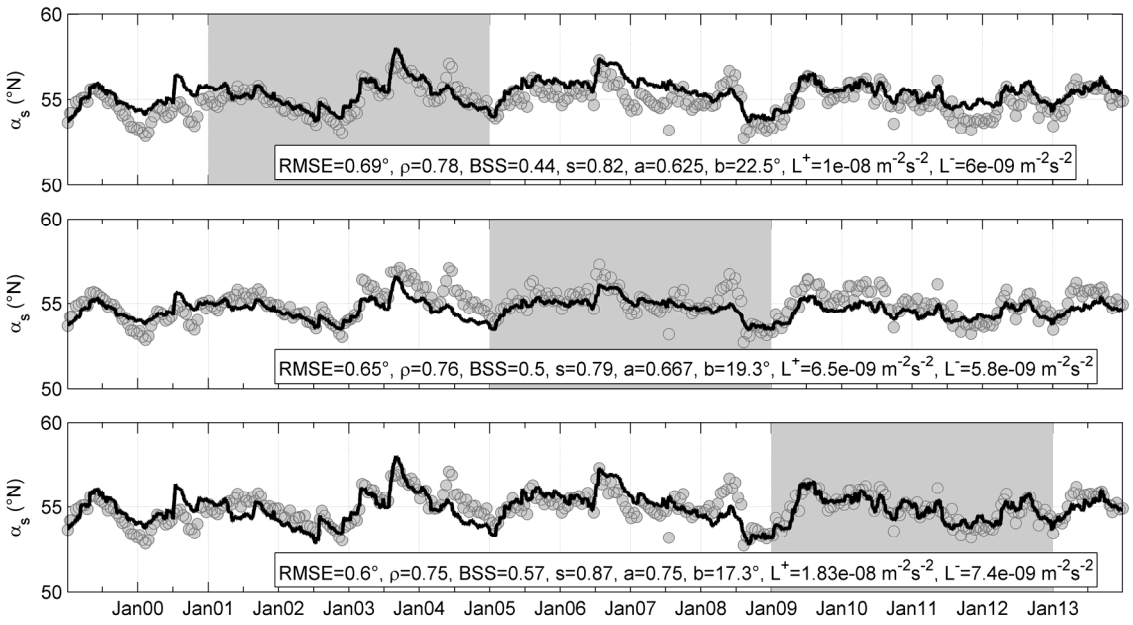

Fig. 6-14. Model validation (black line) over measurements (circles) at Tairua Beach considering different calibration time periods (shadow zone): 2001-2005 (upper panel), 2005-2009 (middle panel) and 2009-2013 (lower panel).

The results confirm that the proposed model shows good performance in reproducing the variability of the beach orientation considering different calibration periods. In all three cases, the correlation coefficients between the observations and modeled results were greater than 0.75. The simulation with the 2001-2005 calibration period showed the highest RMSE; however, this simulation also resulted in the best correlation. The simulation with the 2005-2009 calibration period resulted in slower proportionality constants $L^{\pm}$, which smoothed the model's behavior.

The parameters L^{+} and L^{-}, which define the rotation speed, tended to exhibit a similar order of magnitude; however, to achieve greater stabilization of the calibration parameters, a longer calibration period is required.

6.5.5 Model sensitivity to different weighting factors

This subsection presents a model sensitivity analysis according to different weighting factors. The selected model forcings, such as the square root of the incident wave energy, $E^{1/2}$ (e.g., Yates et al., 2009; Jaramillo et al., 2020), the wave energy, E (e.g., Blossier et al., 2017), the wave power, P (e.g., Lemos et al., 2018) and the dimensionless fall velocity, Ω (e.g., Wright and Short, 1984; Davidson and Turner, 2009), are commonly used in equilibrium-based shoreline evolution models

Fig. 6-15 presents the model simulation results considering the abovementioned weighting factors for both Tairua Beach (upper panel) and Narrabeen Beach (bottom panel). It should be noted that the EWDF was fixed in both cases, so the constants a and b correspond to the values found in Sections 6.4.1 and 6.4.2. Next, Table 6-3 compiles the calibration parameters $L^{\pm}$ together with the RMSE and correlation coefficient corresponding to each simulation. As presented in the table, the constants $L^{\pm}$ change units according to the selected forcing.

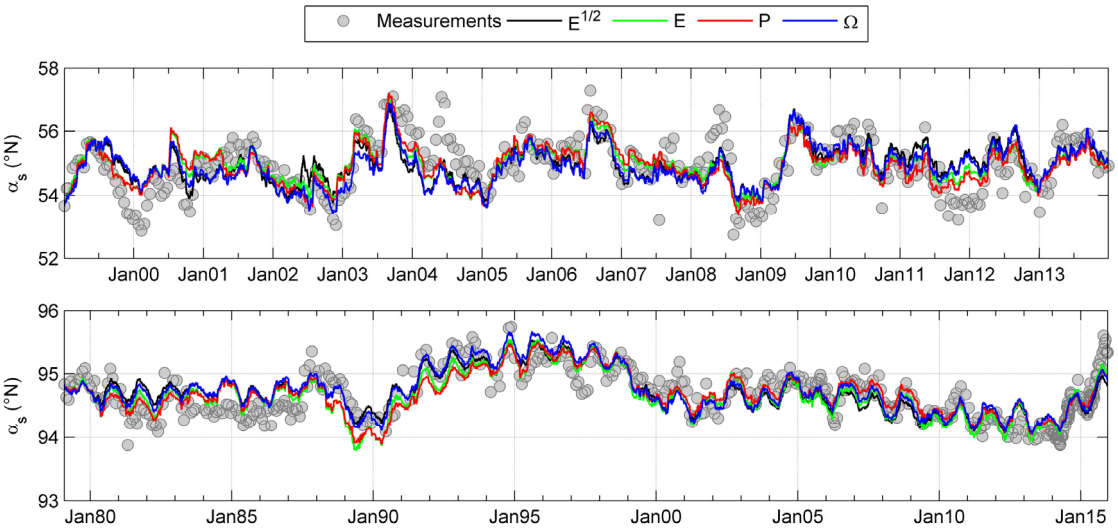

Fig. 6-15. Model sensitivity to different weighting factors applied on Tairua Beach (upper panel) and Narrabeen Beach (lower panel).

Table 6-3. Proportionality constants $L^{\pm}$, correlation coefficient, root mean square error, Brier Skill Score and Skill index between the observed and modeled shoreline orientations at Tairua Beach and Narrabeen Beach considering different weighting factors.

	Weighting factor	L^-	L^+	ρ	RMSE (°)	BSS	s
Tairua Beach	$E^{1/2}$	2.64E-07 $m^{-1}s^{-1}$	1.41E-07 $m^{-1}s^{-1}$	0.66	0.65	0.49	0.76
	E	2.17E-07 $m^{-2}s^{-1}$	9.10E-08 $m^{-2}s^{-1}$	0.76	0.57	0.62	0.82
	P	2.00E-08 $m^{-2}s^{-2}$	1.10E-08 $m^{-2}s^{-2}$	0.75	0.58	0.61	0.84
	Ω	9.00E-10 s^{-1}	6.00E-10 s^{-1}	0.67	0.65	0.50	0.78
Narrabeen Beach	$E^{1/2}$	5.97E-09 $m^{-1}s^{-1}$	5.19E-09 $m^{-1}s^{-1}$	0.8	0.23	0.74	0.88
	E	3.20E-09 $m^{-2}s^{-1}$	3.70E-09 $m^{-2}s^{-1}$	0.83	0.22	0.77	0.90
	P	2.60E-10 $m^{-2}s^{-2}$	3.2E-10 $m^{-2}s^{-2}$	0.83	0.21	0.78	0.90
	Ω	2.50E-11 s^{-1}	2.30E-11 s^{-1}	0.82	0.22	0.75	0.90

As shown in Fig. 6-15 and Table 6-3, the different model results exhibit similar behavior. In all cases, the model was able to reproduce the general shoreline rotation trend, obtaining strong correlations between the observed and modeled shoreline orientations. It should be highlighted that the results with a relatively poor adjustment were obtained using $E^{1/2}$, while the best results were obtained using the wave energy or wave power as the model forcing. This study recommends using the proposed model (Eq. (55)) taking into account the wave power as the weighting factor, which includes the wave energy and the effect of the wave period.

6.5.6 Model sensitivity to fewer calibration parameters

As presented above in Section 6.2.2, the proposed model assumes four calibration parameters (a, b, L^+ and L^-), where a and b define the slope and position of the EWDF and $L^{+/-}$ the rotation rate (either clockwise or counterclockwise). This subsection presents the model performance considering three, two, and one calibration parameters following the expressions presented in Table 6-4.

Table 6-4. Alternative shoreline rotation models considering three, two, and one calibration parameters.

Model	Calibration parameters
$\frac{d\alpha_s(t)}{dt} = LP\left(\alpha_s - \alpha_{s_{eq}}\right); \alpha_{s_{eq}} = \frac{\theta - b}{a}$ (63)	a, b and L
$\frac{d\alpha_s(t)}{dt} = L^{\pm}P(\alpha_s - \theta); \alpha_{s_{eq}} \cong \theta$ (64)	L^+ and L^-
$\frac{d\alpha_s(t)}{dt} = LP(\alpha_s - \theta); \alpha_{s_{eq}} \cong \theta$ (65)	L

Fig. 6-16 shows the simulation results considering the abovementioned alternative shoreline rotation models (see Table 6-4) for both Tairua Beach (upper panel) and Narrabeen Beach (bottom panel). Table 6-5 compiles the calibration parameters together with the quantitative statistics corresponding to each simulation.

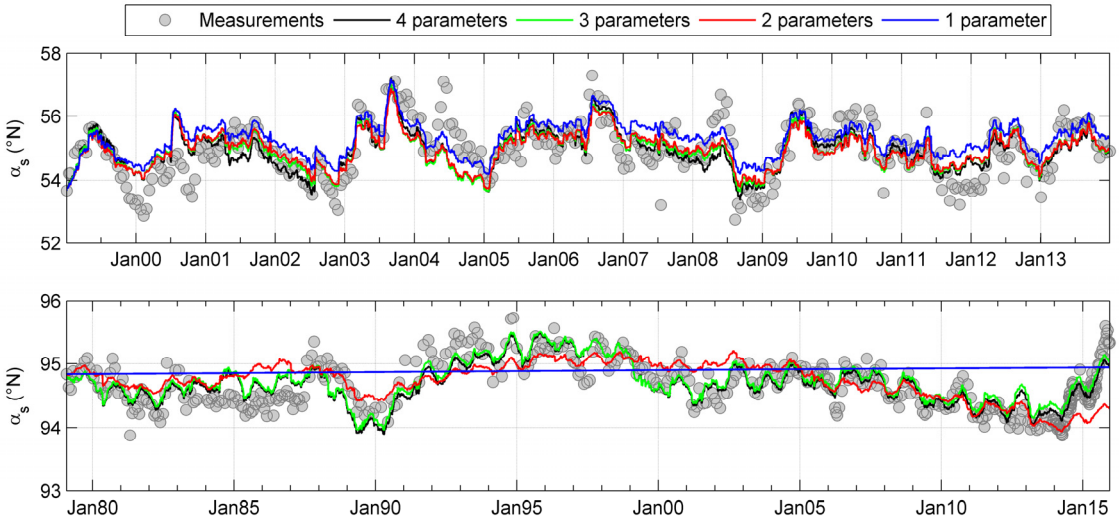

Fig. 6-16. Model sensitivity to fewer calibration parameters applied to Tairua Beach (upper panel) and Narrabeen Beach (lower panel).

Table 6-5. Calibration parameters (a, b, L^+ and L^-) and quantitative statistics (ρ, RMSE, BSS and s) obtained at Tairua Beach and Narrabeen Beach considering alternative shoreline rotation models.

	Model	a	b (°)	L^+ ($m^{-2}s^{-2}$)	L^- ($m^{-2}s^{-2}$)	ρ	RMSE (°)	BSS	s
Tairua Beach	4 parameters	1.25	-11.25	2.00E-08	1.10E-08	0.75	0.58	0.61	0.84
	3 parameters	1.15	-7.85	1.20E-08	1.20E-08	0.74	0.59	0.59	0.81
	2 parameters	1.00	0.00	9.00E-09	1.00E-08	0.74	0.59	0.59	0.81
	1 parameter	1.00	0.00	9.00E-09	9.00E-09	0.74	0.68	0.44	0.77
Narrabeen Beach	4 parameters	6.67	-485.00	2.60E-10	3.20E-10	0.83	0.21	0.78	0.90
	3 parameters	7.33	-545.00	3.20E-10	3.20E-10	0.83	0.22	0.75	0.88
	2 parameters	1.00	0.00	7.00E-12	1.50E-10	0.58	0.34	0.36	0.77
	1 parameter	1.00	0.00	5.00E-14	5.00E-14	-0.18	0.46	-0.28	0.42

According to the results presented in Fig. 6-16 and Table 6-5, the proposed model showed nearly the same skills using four or three calibration parameters (considering $L^+=L^-$). This can be explained because the shoreline rotation movement tends to be symmetric to an EWDF adjusted to the measurements of the selected study sites.

When the model has been run with two calibration parameters, the RMSE increased by 3 % and the correlation decreased by 1 % at Tairua Beach; while the RMSE increased by 59 % and the correlation decreased by 30 % at Narrabeen Beach. These results reflect a satisfactory model prediction in the case of Tairua Beach and a clear reduction in the model's ability to predict the shoreline orientation evolution at Narrabeen Beach. Unlike Tairua Beach, which is practically straight and the incident wave direction tends to be uniform over its entire length, Narrabeen Beach is longer with a significant planform curvature derived from the wave diffraction and the consequent wave height gradient alongshore. As a result, the incident waves undergo a marked transformation to shore, indicating that in this case, the parameters a and b are required to adjust the EWDF.

Regarding the last alternative, when the model has been run with only one calibration parameter (L), the result has been satisfactory again at Tairua Beach, obtaining the same correlation as with two or three parameters, but an increase of the RMSE in 19 % concerning the reference model (four parameters). Contrary, the model with a single calibration parameter has not been able to reproduce the shoreline orientation variability at Narrabeen Beach. This is because, as shown in the previous results, when $\alpha_{s_{eq}} \cong \theta$, L^+ must be significantly lower than L^- and on the other hand, if these rates were equal ($L^+=L^-$), the EWDF must be adjusted to the measurements. Thus, when

the model is run in these conditions at Narrabeen Beach, L tends to 0 and therefore the result tends to α_0.

6.5.7 Model sensitivity to initial shoreline orientation value

In the model executions presented in the previous sections, the simulation started at the shoreline orientation, α_{s_0}, defined by the first measurement of the data record; however, it should be noted that this value can affect the model performance.

Fig. 6-17 shows the effects of the initial condition on the model simulation results of Tairua Beach (upper panel) and Narrabeen Beach (lower panel); the model calibration parameters (a, b, L^+ and L^-) correspond to the values found in Section 6.4.1 and Section 6.4.2. The variation limits of the initial condition were defined as the maximum and minimum values from the data records of each beach. To compare the results for the two beaches, the simulations were limited to the first 10 years and 6° on the y-axis.

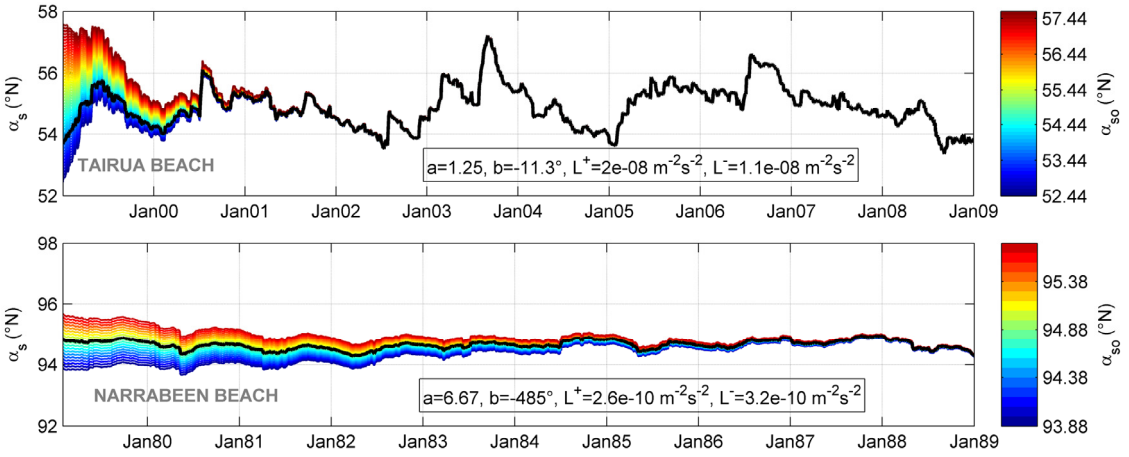

Fig. 6-17. Model sensitivity to initial shoreline orientation value, α_{s_0}, for Tairua Beach (upper panel) and Narrabeen Beach (lower panel). The black line corresponds to the best-fit simulation considering the initial shoreline orientation as the first measurement.

As presented in Fig. 6-17, the simulation converges in approximately 2 years in the case of Tairua Beach, while in the case of Narrabeen Beach convergence takes place over 6 years. This temporal difference between the two study sites is related to the time needed for each beach to find its unique balance. On Narrabeen Beach, convergence takes much longer than on Tairua Beach due to the speed of this process, which is intrinsically related to the beach's morphodynamic characteristics. It is worth noting that the convergence time has been studied in different kinds of shoreline evolution models and has been distinguished as beach memory (e.g., Turki et al., 2013a, Jara et al., 2018). According to Jara et al., (2018), beach memory is defined as the time during

which the antecedent wave conditions have a significant influence on the current shoreline position.

6.6 Conclusions

- This study proposes a new equilibrium-based empirical shoreline rotation model derived from a shoreline migration formulation, which assumes that the rotation movement is induced by the incoming wave power and direction. The proposed evolution model boasts a reduced complexity because it requires relatively few calibration parameters and is computationally efficient. The shoreline orientation evolves towards an equilibrium angle by means of a linear relationship between the equilibrium wave direction and the shoreline orientation, defined as the equilibrium wave direction function (EWDF).
- The proposed model showed satisfactory skill at reproducing the variability of the shoreline orientation during fifteen years at Tairua Beach and thirty-seven years at Narrabeen Beach; the rotation evolution model was capable of reproducing the shoreline orientation over a variety of temporal scales (short, medium and large scales). At both study sites, the observations and model simulations suggested clockwise rotation from austral summer to winter and counterclockwise rotation in the opposite order; however, it should be pointed out that in the case of Tairua Beach, changes in the shoreline orientation were more evident on scales of days to weeks (even months), while in the case of Narrabeen Beach, the rotation movement took place on longer time scales.
- Overall the results between the observed and modeled shoreline orientations have been satisfactory considering the evaluated quantitative statistics in both study sites; in Narrabeen Beach (RMSE=0.21º, ρ=0.83, BSS=0.78, s=0.90, NSE=0.69 and RSR=0.56) and Tairua Beach (RMSE=0.58º, ρ=0.75, BSS=0.61, s=0.84, NSE=0.56 and RSR=0.66). In general, the clockwise and counterclockwise shoreline rotations were well represented both qualitatively and quantitatively.
- Finally, time series of shoreline measurements at different sites with diverse beach characteristics and wave conditions would be useful for broadly validating the robustness of the proposed shoreline rotation model.

7 CONCLUSIONS AND FUTURE RESEARCH

The overall aim of this thesis was to develop a new equilibrium-based shoreline evolution model integrating planform and profile in the medium to long-term scales. In order to achieve this goal, a number of improvements and new models were developed; undoubtedly a step forward in our ability to model and evaluate the shoreline variability of embayed beaches for engineering applications as well as for research purposes.

This chapter presents the conclusions, main contributions of the work and some suggestions for future research.

7.1 Conclusions

In Chapters 3, 4, 5 and 6 where each specific objective was addressed, the results, discussions and conclusions obtained for each one of the defined objectives were included.

From a global point of view, the conclusions of this thesis are presented below, in response to the

research questions posted in Chapter 1:

- **RQ1:** Is it possible to calibrate and validate equilibrium shoreline evolution models using mid-resolution satellite images datasets?

This question was addressed in Chapter 3. It was concluded that mid-resolution satellite-derived shorelines obtained with accurate sub-pixel acquisition techniques (e.g. SHOREX algorithm) are valid and extremely useful data for calibration and validation of equilibrium shoreline evolution models. It should be highlighted that satellite images have the great advantage of providing information anywhere in the world and at any time of the year, regardless of the season; nonetheless, satellite images have certain limitations, such as the temporal frequency of satellite observations, and that the image visualization can be compromised by the presence of clouds or other agents (distortion, failures, etc.).

This work explored the applicability of satellite-derived shorelines by means of a comparative analysis using shoreline datasets derived from a video-camera system and satellite imagery on model calibration and validation for Nova Icaria Beach and Cala Millor Beach. In both cases, the general erosion-accretion trend was adequately represented by equilibrium shoreline evolution models compared to shoreline measurements at a qualitative and quantitative level.

- **RQ2:** How could the variability of the beach profile volume be included in the equilibrium-based shoreline evolution models?

This question was addressed in Chapter 4. It was concluded that equilibrium-based shoreline evolution models have to add a rate of change component, which in turn modifies the relationship between the equilibrium shoreline position and the incident wave energy, as a function that advances or retreats over time. Chapter 4 presented a new model, which showed significant skill in reproducing the shoreline evolution during one and a half years at Nova Icaria Beach, where a period of sediment contribution were reported, and more than sixteen years at Campo Poseidón, where there is a continuous sediment loss due to sediment drift alongshore.

- **RQ3:** Is it possible to model the cross-shore variability of embayed beaches in the medium-long term?

This question was addressed in Chapter 5. It was concluded that the cross-shore variability of embayed beaches can be modeled by means of the integration between beach profile and beach planform processes. The new proposed model, named IH-MOOSE, is a reduced-complexity model based on the integration of cross-shore and planform equilibrium models. This new approach obtains the entire beach coastline evolution over time scales spanning months, several years or decades. In contrast, previous similar models needed to discretize the beach into transects

or stretches to evaluate the entire embayed shoreline beach evolution, and this process represents a significant computational cost. The proposed model has been applied to the Collaroy–Narrabeen embayment, Australia and showed overall good performance. The results demonstrated that the model successfully achieves the general erosion–accretion trend of the entire shoreline and the dry beach area evolution.

- **RQ4:** How to model the shoreline rotation in the medium to long term?

This question was addressed in Chapter 6. It was concluded that in order to simulate in a simple and efficient way the variability of the shoreline orientation is appropriated an equilibrium-based shoreline rotation model. This chapter presented a new heuristic model based on the assumption that beach rotation movement is induced by the incoming wave power and direction. This model was applied in two embayed beaches located in the South Pacific Ocean. Almost fifteen years of shoreline positions extracted from hourly time-averaged images captured at Tairua Beach, New Zealand, and thirty-seven years of shoreline position data acquired from beach profile surveys at Narrabeen Beach, Australia, were used to evaluate the model performance. Results demonstrated that the model successfully represents the general shoreline orientation variability.

7.2 Future research

The results of this thesis contribute to coastal researchers and engineers to cover some of the existing gaps related to equilibrium-based shoreline modeling; however, there are some topics that are still open for further investigation in the future. In this sense, the main issues to be addressed in future research works are listed as follows:

- Explore the sea level variation processes in the equilibrium-based shoreline evolution models. From this, it is expected that these models will be able to capture shoreline recession resulting from passive flooding due to sea-level rise and extend their applicability to the very long term.
- Explore the applicability of the equilibrium-based shoreline evolution models proposed in this thesis for gravel or pebble beaches.
- Explore the concepts that define the equilibrium-based evolution models for other beach profile contours; not only shoreline but also barline, closing depth, dune foot, among others.
- The existing equilibrium-based shoreline evolution models successfully reproduce the dominant timescale of the series under study; however, they fail to capture multiple timescales in detail (e.g. Pianca et al., 2015; Almar et al., 2017). Therefore, it would be

attractive to improve the model proposals presented in this thesis by allowing for the implementation of multiple morphological timescales using multiple forcing timescales; for example, investigating the methodology proposed by Schepper et al., (2019).

In addition to the above-mentioned future lines of research, a series of additional developments are presented below, which without becoming lines of research due to their lesser entity, constitute tasks to complement or improve the work carried out in the present thesis:

- Integrate the cross-shore displacement (adding the trend term), beach planform and beach rotation concepts into a single equilibrium-based shoreline evolution model.
- In relation to Chapter 4, the limitations inherited by assuming a linear trend constant suggested that the proposed model could even improve its prediction by including a better prediction of the source or sink variability, e.g., a littoral sediment drift alongshore function obtained from historical seasonal analysis or a sediment discharge function associated with streamflow hydrographs of rivers, among others.
- Analyze the IH-MOOSE model performance by considering other combinations between cross-shore (e.g. Davidson et al., 2013; Castelle et al., 2014; Splinter et al., 2014; Jara et al., 2015) and planform equilibrium models (e.g. Yasso 1965; Tan and Chiew 1994; Moreno and Kraus 1999). In order to make the IH-MOOSE applicable to study cases with irregular beach planforms (presence of near-shore islands and/or rocky bottoms, as well as the effect of several diffraction points), it would be necessary to resort to a process-based model such as the one proposed by Gainza et al., (2018).

7.3 Financial Support

This work could not be possible without the funding from:

- The Spanish Ministry of Economy, Industry, and Competitiveness under Grant BIA2017-89491-R (Beach-Art Project).
- The Society for the Regional Development of Cantabria, SODERCAN group under Grant ID16-IN-045 (SMC2020 Project).
- The Environmental Hydraulics Institute of the University of Cantabria.

The author acknowledges their support.

8 REFERENCES

Almar, R., Coco, G., Bryan, K.R., Huntley, D.A., Short, A.D., Senechal, N., 2008. Video observations of beach cusp morphodynamics. Mar. Geol. 254, 216–223. https://doi.org/10.1016/j.margeo.2008.05.008

Almar, R., Marchesiello, P., Almeida, L.P., Thuan, D.H., Tanaka, H., Viet, N.T., 2017. Shoreline response to a sequence of typhoon and monsoon events. Water 9. https://doi.org/10.3390/w9060364

Almonacid-Caballer, J., Sánchez-garcía, E., Pardo-pascual, J.E., Balaguer-beser, A.A., Palomar-vázquez, J., 2016. Evaluation of annual mean shoreline position deduced from Landsat imagery as a mid-term coastal evolution indicator. Mar. Geol. 372, 79–88. https://doi.org/10.1016/j.margeo.2015.12.015

Anders, F.J., Byrnes, M.R., 1991. Accuracy of shoreline change rates as determined from maps and aerial photographs. Shore and Beach January, 17–26.

Anderson, D., Ruggiero, P., Antolinez, J.A.A., Mendez, F.J., Allen, J., 2018. A climate index optimized for longshore sediment transport reveals interannual and multi-decadal littoral cell rotations. J. Geophys. Res. Earth Surf. https://doi.org/10.1029/2018JF004689

Angnuureng, D.B., Almar, R., Senechal, N., Castelle, B., Addo, K.A., Marieu, V., 2015. Shoreline Evolution Under Sequences of Storms From 6-Year Video Observation At a Meso-Macrotidal Beach. Coast. Sediments 2015 1–13.

Antolínez, J.A.A., Méndez, F.J., Anderson, D., Ruggiero, P., Kaminsky, G.M., 2019. Predicting climate driven coastlines with a simple and efficient multi-scale model. J. Geophys. Res. Earth Surf. 2018JF004790. https://doi.org/10.1029/2018JF004790

Baban, S.M.J., 1995. The use of Landsat imagery to map fluvial sediment discharge into coastal waters. Mar. Geol. 123, 263–270. https://doi.org/10.1016/0025-3227(95)00003-H

Bakker, W.T., 1970. The Dynamics of a Coast With a Groyne System. 12th Conf. Coast. Eng. 6th, 115–120. https://doi.org/http://dx.doi.org/10.9753/icce.v12.%25p

Bayram, B., Acar, U., Seker, D., Ari, A., 2008. A Novel Algorithm for Coastline Fitting through a Case Study over the Bosphorus. J. Coast. Res. 244, 983–991. https://doi.org/10.2112/07-0825.1

Berenguer, J.M., Enríquez, J., 1989. Design of Pocket Beaches. The Spanish Case, in: Coastal Engineering 1988. pp. 1411–1425. https://doi.org/10.1061/9780872626874.106

Bernabeu, a. M., Medina, R., Vidal, C., 2003. A morphological model of the beach profile integrating wave and tidal influences. Mar. Geol. 197, 95–116. https://doi.org/10.1016/S0025-3227(03)00087-2

Bernabeu, A.M., 1999. Desarrollo, validación y aplicaciones de un modelo general de perfil de equilibrio en playas. Universidad de Cantabria.

Biausque, M., Senechal, N., Blossier, B., Bryan, K.R., 2016. Seasonal Variations in Recovery Timescales of Shorelines on an Embayed Beach. J. Coast. Res. 75, 353–357. https://doi.org/10.2112/SI75-071.1

Birrien, F., Atkinson, A., Shimamoto, T., Baldock, T.E., 2018. Hysteresis in the evolution of beach profile parameters under sequences of wave climates - Part 2; Modelling. Coast. Eng. 133, 13–25. https://doi.org/10.1016/j.coastaleng.2017.12.001

Blossier, B., Bryan, K.R., Daly, C.J., Winter, C., 2017. Shore and bar cross-shore migration, rotation and breathing processes at an embayed beach. J. Geophys. Res. Earth Surf. https://doi.org/10.1002/2017JF004227

Blossier, B., Bryan, K.R., Daly, C.J., Winter, C., 2016. Nearshore sandbar rotation at single-barred embayed beaches. J. Geophys. Res. Ocean. 121, 2286–2313. https://doi.org/10.1002/2015JC011031

Blossier, Brice, Bryan, K.R., Daly, C.J., Winter, C., 2016. Spatial and temporal scales of shoreline morphodynamics derived from video camera observations for the island of Sylt, German Wadden Sea. Geo-Marine Lett. https://doi.org/10.1007/s00367-016-0461-7

Blossier, B., Bryan, K.R., Winter, C., 2015. Simple Pocket Beach Rotation Model Derived From Linear Analysis. Coast. sediments 2015 1–13.

Boak, E.H., Turner, I.L., 2005. Shoreline Definition and Detection: A Review. J. Coast. Res. 21, 688–703. https://doi.org/10.2112/03-0071.1

Boateng, I., Bray, M., Hooke, J., 2012. Estimating the fluvial sediment input to the coastal sediment budget: A case study of Ghana. Geomorphology 138, 100–110. https://doi.org/10.1016/j.geomorph.2011.08.028

Bodge, K., 1992. Representing equilibrium beach profiles with an exponential expression. J. Coast. Res. 47–55.

Bogle, J.A., Bryan, K.R., Black, K.P., Hume, T.M., Healy, T.R., 2001. Video observations of rip formation and evolution. J. Coast. Res. 117–127. https://doi.org/10.2307/25736280

Boon, J., Green, M., 1988. Caribbean Beach-face slopes and beach equilibrium profiles. Coast. Eng. 1618–1630. https://doi.org/doi:10.9753/icce.v21.

Bouguet, J.-Y., 2015. Camera calibration toolbox for Matlab [WWW Document]. URL http://www.vision.caltech.edu/bouguetj/calib_doc/

Bowen, A.J., 1980. Simple models of nearshore sedimentation, beach profiles and longshore bars, in: The Coastline of Canada. pp. 1–11.

Bowman, D., Guillén, J., López, L., Pellegrino, V., 2009. Planview Geometry and morphological characteristics of pocket beaches on the Catalan coast (Spain). Geomorphology 108, 191–199. https://doi.org/10.1016/j.geomorph.2009.01.005

Brignone, M., Schiaffino, C.F., Isla, F.I., Ferrari, M., 2012. A system for beach video-monitoring: Beachkeeper plus. Comput. Geosci. 49, 53–61. https://doi.org/10.1016/j.cageo.2012.06.008

Bruun, P., 1954. Coast erosion and the development of beach profiles. Tech. Memo. No. 44 82.

Bryan, K.R., Foster, R., MacDonald, I., 2013. Beach rotation at two adjacent headland-enclosed beaches. J. Coast. Res. 2095–2100. https://doi.org/10.2112/SI65-354

Burvingt, O., Masselink, G., Scott, T., Davidson, M., Russell, P., 2018. Climate forcing of regionally-coherent extreme storm impact and recovery on embayed beaches. Mar. Geol. 401, 112–128. https://doi.org/10.1016/j.margeo.2018.04.004

Camfield, F.E., Morang, A., 1996. Defining and interpreting shoreline change. Ocean Coast. Manag. 32, 129–151. https://doi.org/10.1016/S0964-5691(96)00059-2

Camus, P., Mendez, F.J., Medina, R., 2011. A hybrid efficient method to downscale wave climate

to coastal areas. Coast. Eng. 58, 851–862. https://doi.org/10.1016/j.coastaleng.2011.05.007

Camus, P., Mendez, F.J., Medina, R., Tomas, A., Izaguirre, C., 2013. High resolution downscaled ocean waves (DOW) reanalysis in coastal areas. Coast. Eng. 72, 56–68. https://doi.org/10.1016/j.coastaleng.2012.09.002

Castelle, B., Bujan, S., Ferreira, S., Dodet, G., 2017. Foredune morphological changes and beach recovery from the extreme 2013/2014 winter at a high-energy sandy coast. Mar. Geol. 385, 41–55. https://doi.org/10.1016/j.margeo.2016.12.006

Castelle, B., Marieu, V., Bujan, S., Ferreira, S., Parisot, J.P., Capo, S., Sénéchal, N., Chouzenoux, T., 2014. Equilibrium shoreline modelling of a high-energy meso-macrotidal multiple-barred beach. Mar. Geol. 347, 85–94. https://doi.org/10.1016/j.margeo.2013.11.003

Coco, G., Payne, G., Bryan, K.R., Rickard, D., Ramsay, D., Dolphin, T., 2005. The use of imaging systems to monitor shoreline dynamics Giovanni, in: ArabianCoast 2005.

Cohn, N., Ruggiero, P., Vries, S. De, Kaminsky, G.M., 2018. New insights on coastal foredune growth : the relative contributions of marine and aeolian processes. Geophys. Res. Lett. https://doi.org/10.1029/2018GL077836

Crowell, M., Leatherman, S.P., Buckley, M.K., 1991. Historical Shoreline Change: Error Analysis and Mapping Accuracy. J. Coast. Res. 7, 839–852. https://doi.org/10.1017/CBO9781107415324.004

Dabees, M., Kamphuis, W.J., 1998. Oneline, a Numerical Model for Shoreline Change. 26th Coast. Eng. Conf. 2668–2681. https://doi.org/http://dx.doi.org/10.1061/9780784404119.202

Dai, Z.-J., Liu, J.T., Lei, Y.-P., Zhang, X.-L., 2010. Patterns of Sediment Transport Pathways on a Headland Bay Beach—Nanwan Beach, South China: A Case Study. J. Coast. Res. 26, 1096–1103. https://doi.org/10.2112/JCOASTRES-D-09-00097.1

Daly, C.J., Bryan, K.R., Roelvink, J. a., Klein, H.F., Hebbeln, D., Winter, C., 2011. Morphodynamics of Embayed Beaches: The Effect of Wave Conditions. J. Coast. Res. 1003–1007.

Daly, C.J., Bryan, K.R., Winter, C., 2014. Wave energy distribution and morphological development in and around the shadow zone of an embayed beach. Coast. Eng. 93, 40–54. https://doi.org/10.1016/j.coastaleng.2014.08.003

Daly, C.J., Winter, C., Bryan, K.R., 2015. On the morphological development of embayed beaches. Geomorphology 248, 252–263. https://doi.org/10.1016/j.geomorph.2015.07.040

Davidson-Arnott, R.G.D., Bauer, B.O., 2009. Aeolian sediment transport on a beach: Thresholds, intermittency, and high frequency variability. Geomorphology 105, 117–126. https://doi.org/10.1016/j.geomorph.2008.02.018

Davidson, M. a., Lewis, R.P., Turner, I.L., 2010. Forecasting seasonal to multi-year shoreline change. Coast. Eng. 57, 620–629. https://doi.org/10.1016/j.coastaleng.2010.02.001

Davidson, M. a., Turner, I.L., 2009. A behavioral template beach profile model for predicting seasonal to interannual shoreline evolution. J. Geophys. Res. 114, F01020. https://doi.org/10.1029/2007JF000888

Davidson, M. A., Splinter, K.D., Turner, I.L., 2013. A simple equilibrium model for predicting shoreline change. Coast. Eng. 73, 191–202. https://doi.org/10.1016/j.coastaleng.2012.11.002

Davidson, Mark A., Turner, I.L., Splinter, K.D., 2013. Predicting Shoreline Response To Cross-Shore Processes in a Changing Wave Climate. Coast. Dyn. 431–442.

Davidson, M.A., Turner, I.L., Splinter, K.D., Harley, M.D., 2017. Annual prediction of shoreline erosion and subsequent recovery. Coast. Eng. 130, 14–25. https://doi.org/10.1016/j.coastaleng.2017.09.008

Dean, R., 1991. Equilibrium beach profiles: characteristics and applications. J. Coast. Res. 7, 53–84.

Dean, R., 1977. Equilibrium beach profiles : U.S. Atlantic and Gulf coasts. Dept. of Civil Engineering and College of Marine Studies University of Delaware, Newark Del.

Dean, R.G., 1987. Coastal Sediment Processes: Toward Engineering Solutions, in: Proceedings of Coastal Sedirnents'87. ASCE, pp. 1–24.

Dean, R.G., Healy, T.R., Dommerholt, A.P., 1993. A "blind-folded" test of equilibrium beach profile concepts with New Zealand data. Mar. Geol. 109, 253–266. https://doi.org/10.1016/0025-3227(93)90064-3

Dolphin, T.J., Vincent, C.E., Wihsgott, J., Belhache, M., Bryan, K.R., 2011. Seasonal rotation of a mixed sand-gravel beach. J. Coast. Res. 65–69.

Doria, A., Guza, R.T., O'Reilly, W.C., Yates, M.L., 2016. Observations and modeling of San Diego beaches during El Niño. Cont. Shelf Res. 124, 153–164. https://doi.org/10.1016/j.csr.2016.05.008

Douglas, B.C., Crowell, M., Leatherman, S.P., 1998. Considerations for shoreline position

prediction. J. Coast. Res. 14, 1025–1033.

Ekercin, S., 2007. Coastline Change Assessment at the Aegean Sea Coasts in Turkey Using Multitemporal Landsat Imagery. J. Coast. Res. 233, 691–698. https://doi.org/10.2112/04-0398.1

Elshinnawy, A.I., Medina, R., González, M., 2018a. On the influence of wave directional spreading on the equilibrium planform of embayed beaches. Coast. Eng. 133, 59–75. https://doi.org/10.1016/j.coastaleng.2017.12.009

Elshinnawy, A.I., Medina, R., González, M., 2018b. Dynamic equilibrium planform of embayed beaches: Part 1. A new model and its verification. Coast. Eng. 133, 59–75. https://doi.org/10.1016/j.coastaleng.2018.01.010

Elshinnawy, A.I., Medina, R., González, M., 2018c. Dynamic equilibrium planform of embayed beaches: Part 2. Design procedure and engineering applications. Coast. Eng. 135, 123–137. https://doi.org/10.1016/j.coastaleng.2018.01.001

Elshinnawy, A.I., Medina, R., González, M., 2017. On the relation between the direction of the wave energy flux and the orientation of equilibrium beaches. Coast. Eng. 127, 20–36. https://doi.org/10.1016/j.coastaleng.2017.06.009

Emery, K.O., 1961. A simple method of measuring beach profiles. Limnology and Oceanography.

Espinosa, V., Rodríguez, I., 2009. Evolución costera del tramo comprendido entre San Juan de los Terrenos y playas de Vera (Almería). Rev. la Soc. geológica España. 22, 3–12.

Farris, A.S., List, J.H., 2007. Shoreline Change as a Proxy for Subaerial Beach Volume Change. J. Coast. Res. 233, 740–748. https://doi.org/10.2112/05-0442.1

Fenster, M.S., Dolant, R., Elder, J.F., 1993. A New Method for Predicting Shoreline Positions from Historical Data. J. Coast. Res. 9, 147–171.

Fernández, A.J., Pina, G.G., Cuena, G., Ramirez, J.L., 1992. A Field Experiment on a Nourished Beach. Coast. Eng. Proc. 2043–2056.

Fernández, A.J., Pina, G.G., Muñoz, Á., 1990. Sand Bypassing to" Playa De Castilla"(Huelva Spain). Coast. Eng. 3183–3193. https://doi.org/10.9753/icce.v22.%p

Foody, G., Muslim, A.M., Atkinson, P.M., 2005. Super-resolution mapping of the waterline from remotely sensed data. Int. J. Remote Sens. 26, 5381–5392. https://doi.org/10.1080/01431160500213292

Franke, R., 1982. Scattered data interpolation: tests of some methods. Math. Comput. 38, 181–

181. https://doi.org/10.1090/S0025-5718-1982-0637296-4

Gainza, J., González, E.M., Medina, R., 2018. A process based shape equation for a static equilibrium beach planform. Coast. Eng. 136, 119–129. https://doi.org/10.1016/j.coastaleng.2018.02.006

Gómez-Pujol, L., Orfila, A., Alvarez-Ellacuria, A., Terrados, J., Tintoré, J., 2013. Posidonia oceanica beach-cast litter in Mediterranean beaches: a coastal videomonitoring study. J. Coast. Res. 1768–1773. https://doi.org/10.2112/SI65-299

González, M., Medina, R., 2001. On the application of static equilibrium bay formulations to natural and man-made beaches. Coast. Eng. 43, 209–225. https://doi.org/10.1016/S0378-3839(01)00014-X

González, M., Medina, R., Gonzalez-Ondina, J., Osorio, a., Méndez, F.J., García, E., 2007. An integrated coastal modeling system for analyzing beach processes and beach restoration projects, SMC. Comput. Geosci. 33, 916–931. https://doi.org/10.1016/j.cageo.2006.12.005

González, M., Medina, R., Losada, M., 2010. On the design of beach nourishment projects using static equilibrium concepts: Application to the Spanish coast. Coast. Eng. 57, 227–240. https://doi.org/10.1016/j.coastaleng.2009.10.009

Gorman, L., Morang, A., Larson, R., 1998. Monitoring the coastal environment; Part IV: Mapping, shoreline changes, and bathymetric analysis. J. Coast. Res. 14, 61–92.

Guariglia, A., Buonamassa, A., Losurdo, A., Saladino, R., Trivigno, M.L., Zaccagnino, A., Colangelo, A., 2006. A multisource approach for coastline mapping and identification of shoreline changes. Ann. Geophys. 49, 295–304.

Guillén, J., García-Olivares, A., Ojeda, E., Osorio, A., Chic, O., González, R., 2008. Long-Term Quantification of Beach Users Using Video Monitoring. J. Coast. Res. 246, 1612–1619. https://doi.org/10.2112/07-0886.1

Hagenaars, G., de Vries, S., Luijendijk, A.P., de Boer, W.P., Reniers, A.J.H.M., 2018. On the accuracy of automated shoreline detection derived from satellite imagery: A case study of the sand motor mega-scale nourishment. Coast. Eng. 133, 113–125. https://doi.org/10.1016/j.coastaleng.2017.12.011

Hallermeier, R., 1977. Calculating a yearly limit depth to the active beach profile. Coast. Eng. Res. Cent. FORT BELVOIR VA.

Hallermeier, R.J., 1981. Critical wave conditions for sand motion initiation. Coast. Eng. Res. Cent. FORT BELVOIR VA. https://doi.org/http://dx.doi.org/10.5962/bhl.title.47737

Hannv, Z., Qigang, J., Jiang, X., 2013. Coastline extraction using support vector machine from remote sensing image. J. Multimed. 8, 175–182. https://doi.org/10.4304/jmm.8.2.175-182

Hanson, H., Aarninkhof, S., Capobianco, M., Beach, W.P., 2003. Modelling of Coastal Evolution on Yearly to Decadal Time Scales Modelling of Coastal Evolution on Yearly to Decadal. J. Coast. Res.

Hanson, H., Brampton, A., Capobianco, M., Dette, H.., Hamm, L., Laustrup, C., Lechuga, A., Spanhoff, R., 2002. Beach nourishment projects, practices, and objectives—a European overview H. Coast. Eng. 47, 81–111.

Hanson, H., Kraus, N., 1991. GENESIS: Generalized Model for Simulating Shoreline Change. Report 1.

Hanson, H., Larson, M., 2000. Simulating coastal evolution using a new type of N-line model. Coast. Eng. 2000 2808–2821.

Harley, M.D., Andriolo, U., Armaroli, C., Ciavola, P., 2013. Shoreline rotation and response to nourishment of a gravel embayed beach using a low-cost video monitoring technique: San Michele-Sassi Neri, Central Italy. J. Coast. Conserv. 18, 551–565. https://doi.org/10.1007/s11852-013-0292-x

Harley, M.D., Turner, I.L., 2008. A simple data transformation technique for pre-processing survey data at embayed beaches. Coast. Eng. 55, 63–68. https://doi.org/10.1016/j.coastaleng.2007.07.001

Harley, M.D., Turner, I.L., Kinsela, M.A., Middleton, J.H., Mumford, J., Splinter, K.D., Phillips, M.S., Simmons, J.A., David, J., Short, A.D., 2017. Extreme coastal erosion enhanced by anomalous extratropical storm wave direction. Sci. Rep. 1–9. https://doi.org/10.1038/s41598-017-05792-1

Harley, M. D., Turner, I.L., Short, a. D., Ranasinghe, R., 2011. A reevaluation of coastal embayment rotation: The dominance of cross-shore versus alongshore sediment transport processes, Collaroy-Narrabeen Beach, southeast Australia. J. Geophys. Res. Earth Surf. 116, 1–16. https://doi.org/10.1029/2011JF001989

Harley, Mitchell D., Turner, I.L., Short, A.D., Ranasinghe, R., 2011. Assessment and integration of conventional, RTK-GPS and image-derived beach survey methods for daily to decadal coastal monitoring. Coast. Eng. 58, 194–205. https://doi.org/10.1016/j.coastaleng.2010.09.006

Harley, M.D., Turner, I.L., Short, A.D., Ranasinghe, R., 2010. Interannual variability and controls

of the Sydney wave climate. Int. J. Climatol. 30, 1322–1335. https://doi.org/10.1002/joc.1962

Harley, M.D., Turner, I.L., Simmons, J. a, Splinter, K.D., 2015. 40 Years and Still Going Strong : the Past , Present and Future of Coastal Monitoring At Narrabeen-Collaroy Beach. Coast. Conf. Proc. 1–10.

Hayden, B.P., Felder, W.N., Fisher, J.S., Resio, D.T., Vincent, L.C., Dolant, R., 1975. Systematic variations in inshore bathymetry.

Hoeke, R.K., Zarillo, G.A., Synder, M., 2001. A GIS-Based Tool for Extracting Shoreline Postions from Aerial Imagery (BeachTools) 1–12.

Holman, R. a., Stanley, J., 2007. The history and technical capabilities of Argus. Coast. Eng. 54, 477–491. https://doi.org/10.1016/j.coastaleng.2007.01.003

Hsu, J.R.-C., Silvester, R., Xia, Y.M., 1987. New characteristics of equilibrium shaped bays, in: Eighth Australasian Conference on Coastal and Ocean Engineering. pp. 140–144.

Hsu, J.R.-C., Yu, M.-J., Lee, F.-C., Benedet, L., 2010. Static bay beach concept for scientists and engineers: A review. Coast. Eng. 57, 76–91. https://doi.org/10.1016/j.coastaleng.2009.09.004

Hsu, J.R.C., Evans, C., 1989. Parabolic Bay Shapes and Applications. Proc. Inst. Civ. Eng. 87, 557–570. https://doi.org/10.1680/iicep.1989.3778

Infantes, E., Terrados, J., Orfila, A., Cañellas, B., Álvarez-Ellacuria, A., 2009. Wave energy and the upper depth limit distribution of Posidonia oceanica. Bot. Mar. 52, 419–427. https://doi.org/10.1515/BOT.2009.050

Inman, D.L., Elwany, M.H., Jenkins, S.A., 1993. Shorerise and Bar-berm profiles on Ocean Beaches. J. Geophys. Res. 98, 18,181-18,199. https://doi.org/10.5811/westjem.2011.5.6700

Inman, D.L., Nordstrom, C.E., 1971. On the Tectonic and Morphologic Classification of Coasts. J. Geol. 79, 1–21. https://doi.org/10.1086/627583

Jara, M.S., González, M., Medina, R., 2015. Shoreline evolution model from a dynamic equilibrium beach profile. Coast. Eng. 99, 1–14. https://doi.org/10.1016/j.coastaleng.2015.02.006

Jara, M.S., González, M., Medina, R., Jaramillo, C., 2018. Time-Varying Beach Memory Applied to Cross-Shore Shoreline Evolution Modelling. J. Coast. Res. 345, 1256–1269. https://doi.org/10.2112/jcoastres-d-17-00041.1

Jaramillo, C., Gonzalez, M.E., Medina, R., Turki, I., 2020a. An equilibrium-based shoreline rotation model. Submitt. to Coast. Eng.

Jaramillo, C., Jara, M.S., González, M., Medina, R., 2020b. A shoreline evolution model considering the temporal variability of the beach profile sediment volume (sediment gain / loss). Coast. Eng. 156, 103612. https://doi.org/10.1016/j.coastaleng.2019.103612

Jaramillo, C., Jara, M.S., González, M., Medina, R., 2020c. A shoreline evolution model for embayed beaches based on cross-shore and planform equilibrium models. Submitt. to Coast. Eng.

Jaramillo, C., Sánchez-García, E., Jara, M.S., González, M., Medina, R., Palomar-Vázquez, J.M., 2020d. Sub-pixel satellite derived shorelines as valuable data for equilibrium shoreline evolution models. Submitt. to Cont. Shelf Res.

Jiménez, J.A., Osorio, A., Marino-Tapia, I., Davidson, M., Medina, R., Kroon, A., Archetti, R., Ciavola, P., Aarnikhof, S.G.J., 2007. Beach recreation planning using video-derived coastal state indicators. Coast. Eng. 54, 507–521. https://doi.org/10.1016/j.coastaleng.2007.01.012

Kalnay, E., Kanamitsu, M., Kistler, R., Collins, W., Deaven, D., Gandin, L., Iredell, M., Saha, S., White, G., Woollen, J., Zhu, Y., Chelliah, M., Ebisuzaki, W., Higgins, W., Janowiak, J., Mo, K.C., Ropelewski, C., Wang, J., Leetmaa, A., Reynolds, R., Jenne, R., Joseph, D., 1996. The NCEP/NCAR 40-year reanalysis project. Bull. Am. Meteorol. Soc. https://doi.org/10.1175/1520-0477(1996)077<0437:TNYRP>2.0.CO;2

Klein, A.H., Vargas, A., Raabe, A.L.A., Hsu, J.R.C., 2003. Visual assessment of bayed beach stability with computer software. Comput. Geosci. 29, 1249–1257. https://doi.org/10.1016/j.cageo.2003.08.002

Klein, A.H.D.F., Filho, L.B., Schumacher, D.H., 2002. Short-Term Beach Rotation Processes in Distinct Headland Bay Beach Systems. J. Coast. Res. 18, 442–458. https://doi.org/10.2307/4299093

Komar, P., Inman, D., 1970. Longshore sand transport on beaches. J. Geophys. Res. 75, 5914–5927. https://doi.org/10.1029/JC075i030p05914

Komar, P.D., Mcdougal, W.G., 1994. The Analysis of Exponential Beach Profiles. J. Coast. Res. 10, 59–69.

Kriebel, B.D.L., Dean, R.G., 1993. Convultion method for time-dependent beach-profile response 119, 204–226.

Kriebel, D.L., Kraus, N.C., Larson, M., 1991. Engineering Methods for Predicting Beach Profile

Response, in: Coastal Sediments. ASCE, pp. 557–571.

Krumbein, W.C., 1944. Shore processes and beach characteristics, in: Technical Memorandum Nº 3, Beach Erosion Board. p. 33.

Kuleli, T., Guneroglu, A., Karsli, F., Dihkan, M., 2011. Automatic detection of shoreline change on coastal Ramsar wetlands of Turkey. Ocean Eng. 38, 1141–1149. https://doi.org/10.1016/j.oceaneng.2011.05.006

Kuriyama, Y., 2002. Medium-term bar behavior and associated sediment transport at Hasaki, Japan. J. Geophys. Res. 107, 3132. https://doi.org/10.1029/2001JC000899

Lacey, E.M., Peck, J. a, 1998. Long-term beach profile variations along the south shore of Rhode Island, U.S.A. J. Coast. Res. 14, 1255–1264.

Lane, C., Short, A.D., Strauss, D., Tomlinson, R., Tan, C., Blumenstein, M., 2009. Technologies for the Assessment and Prediction of Coastal Hazards. Proc. 5th West. Aust. State Coast. Conf. WA, Aust.

Larson, M., Kraus, N.C., Wise, R. a., 1999. Equilibrium beach profiles under breaking and non-breaking waves. Coast. Eng. 36, 59–85. https://doi.org/10.1016/S0378-3839(98)00049-0

Lazarus, E.D., Harley, M.D., Blenkinsopp, C.E., Turner, I.L., 2019. Environmental signal shredding on sandy coastlines. Earth Surf. Dyn. Discuss. 1–15.

Leblond, P.H., 1972. On the formation of spiral beaches. Coast. Eng. 1331–1345.

LeBlond, P.H., 1979. An Explanation of the Logarithmic Spiral Plan Shape of Headland-Bay Beaches. J. Sediment. Res. Vol. 49, 1093–1100. https://doi.org/10.1306/212F78BA-2B24-11D7-8648000102C1865D

Lemos, C., Floc'h, F., Yates, M., Le Dantec, N., Marieu, V., Hamon, K., Cuq, V., Suanez, S., Delacourt, C., 2018. Equilibrium modeling of the beach profile on a macrotidal embayed low tide terrace beach. Ocean Dyn. 68, 1207–1220. https://doi.org/10.1007/s10236-018-1185-1

Lemos, C., Floc, F., Yates, M., Dantec, N. Le, Marieu, V., Hamon, K., Cuq, V., Suanez, S., Delacourt, C., 2017. Equilibrium modeling of the Beach Profile on a Macrotidal Embayed Beach, in: Coastal Dynamics. pp. 760–771.

Li, J., Roy, D.P., 2017. A global analysis of Sentinel-2a, Sentinel-2b and Landsat-8 data revisit intervals and implications for terrestrial monitoring. Remote Sens. 9. https://doi.org/10.3390/rs9090902

Limber, P.W., Barnard, P.L., Vitousek, S., Erikson, L.H., 2018. A Model Ensemble for Projecting Multidecadal Coastal Cliff Retreat During the 21st Century. J. Geophys. Res. Earth Surf. https://doi.org/10.1029/2017JF004401

Lippmann, T.C., Holman, R.A., 1990. The spatial and temporal variability of sandbar morphology. J. Geophys. Res. 95, 11590–11590.

Liu, H., Jezek, K.C., 2004. Automated extraction of coastline from satellite imagery by integrating Canny edge detection and locally adaptive thresholding methods. Int. J. Remote Sens. 25, 937–958. https://doi.org/10.1080/0143116031000139890

Long, J.W., Plant, N.G., 2012. Extended Kalman Filter framework for forecasting shoreline evolution. Geophys. Res. Lett. 39, 1–6. https://doi.org/10.1029/2012GL052180

Ludka, B.C., Guza, R.T., O'Reilly, W.C., 2018. Nourishment evolution and impacts at four southern California beaches: A sand volume analysis. Coast. Eng. 136, 96–105. https://doi.org/10.1016/j.coastaleng.2018.02.003

Ludka, B.C., Guza, R.T., O'Reilly, W.C., Yates, M.L., 2015. Field evidence of beach profile evolution toward equilibrium. J. Geophys. Res. Ocean. 120, 7574–7597. https://doi.org/10.1002/2015JC010893

Luijendijk, A., Hagenaars, G., Ranasinghe, R., Baart, F., Donchyts, G., Aarninkhof, S., 2018. The State of the World's Beaches. Sci. Rep. 1–11. https://doi.org/10.1038/s41598-018-24630-6

Madsen, a. J., Plant, N.G., 2001. Intertidal beach slope predictions compared to field data. Mar. Geol. 173, 121–139. https://doi.org/10.1016/S0025-3227(00)00168-7

Maiti, S., Bhattacharya, A.K., 2009. Shoreline change analysis and its application to prediction: A remote sensing and statistics based approach. Mar. Geol. 257, 11–23. https://doi.org/10.1016/j.margeo.2008.10.006

Mason, D.C., Gurney, C., Kennett, M., 2000. Beach Topography Mapping: A Comparison of Techniques. J. Coast. Conserv. 6, 113–124. https://doi.org/10.1007/bf02730475

McGranahan, G., Balk, D., Anderson, B., 2007. The rising tide: Assessing the risks of climate change and human settlements in low elevation coastal zones. Environ. Urban. 19, 17–37. https://doi.org/10.1177/0956247807076960

McLean, R., Shen, J.-S., 2006. From Foreshore to Foredune: Foredune Development Over the Last 30 Years at Moruya Beach, New South Wales, Australia. J. Coast. Res. 221, 28–36. https://doi.org/10.2112/05A-0003.1

Medina, R., Marino-Tapia, I., Osorio, A., Davidson, M., Martin, F.L., 2007. Management of dynamic navigational channels using video techniques. Coast. Eng. 54, 523–537. https://doi.org/10.1016/j.coastaleng.2007.01.008

Medina, R., Vidal, C., Losada, M.A., Roldan, A.J., 1992. Three-Mode Principal Component Analysis of Bathymetric Data, applied to “Playa de Castilla” (Huelva, Spain). Coast. Eng. Proc. 1, 2265–2278.

Mentaschi, L., Vousdoukas, M.I., Pekel, J.-F., Voukouvalas, E., Feyen, L., 2018. Global long-term observations of coastal erosion and accretion. Sci. Rep. 8, 12876. https://doi.org/10.1038/s41598-018-30904-w

Miller, H.C., 1999. Field measurements of longshore sediment transport during storms. Coast. Eng. 36, 301–321. https://doi.org/10.1016/S0378-3839(99)00010-1

Miller, J.K., Dean, R.G., 2007. Shoreline variability via empirical orthogonal function analysis: Part I temporal and spatial characteristics. Coast. Eng. 54, 111–131. https://doi.org/10.1016/j.coastaleng.2006.08.013

Miller, J.K., Dean, R.G., 2004. A simple new shoreline change model. Coast. Eng. 51, 531–556. https://doi.org/10.1016/j.coastaleng.2004.05.006

Mínguez, R., Espejo, a., Tomás, a., Méndez, F.J., Losada, I.J., 2011. Directional calibration of wave reanalysis databases using instrumental data. J. Atmos. Ocean. Technol. 28, 1466–1485. https://doi.org/10.1175/JTECH-D-11-00008.1

Mole, M.A., Davidson, M.A., Turner, I.L., Splinter, K.D., Goodwin, I.D., Short, A.D., 2012. Modelling multi-decadal shoreline variability and evolution. Int. Conf. Coast. Eng. 2009. https://doi.org/10.9753/icce.v33.sediment.98

Montaño, J., Coco, G., Antolinez, J.A.A., Beuzen, T.O.M., Bryan, K., Cagigal, L., Castelle, B., Davidson, M., Goldstein, E., Vega, R.A.I.I., Murray, B., Plant, N., Robinet, A., Rueda, A., Senechal, N., Simmons, J., Splinter, K., Stephens, S., Townend, I., Vitousek, S., Vos, K., 2019. SHORECASTS : a blind-test of shoreline models, in: Coastal Sediments 2019. pp. 627–631.

Moore, B.., 1982. Beach Profile EvolutioninRespon se to Changes in Water Level and Wave Height. University of Delaware.

Moore, L.J., 2000. Shoreline mapping techniques. J. Coast. Res. (ISSN 0749-0208) 16, 111–124. https://doi.org/10.2112/03-0071.1

Moreno, L.J., Kraus, N.C., 1999. Equilibrium Shape of Headland-Bay Beaches for Engineering

Design. Proc. Coast. Sediments ’99 1, 860–875.

Morris, B.D., Turner, I.L., 2010. Morphodynamics of intermittently open-closed coastal lagoon entrances: New insights and a conceptual model. Mar. Geol. 271, 55–66. https://doi.org/10.1016/j.margeo.2010.01.009

Mortlock, T.R., Goodwin, I.D., 2015. Directional wave climate and power variability along the Southeast Australian shelf. Cont. Shelf Res. 98, 36–53. https://doi.org/10.1016/j.csr.2015.02.007

Muñoz-Perez, J.J., Lopez De San Roman-Blanco, B., Gutierrez-Mas, J.M., Moreno, L., Cuena, G.J., 2001. Cost of beach maintenance in the Gulf of Cadiz (SW Spain). Coast. Eng. 42, 143–153. https://doi.org/10.1016/S0378-3839(00)00054-5

Muslim, A.M., Foody, G.M., Atkinson, P.M., 2007. Shoreline Mapping from Coarse–Spatial Resolution Remote Sensing Imagery of Seberang Takir, Malaysia. J. Coast. Res. 236, 1399–1408. https://doi.org/10.2112/04-0421.1

Neumann, B., Vafeidis, A.T., Zimmermann, J., Nicholls, R.J., 2015. Future coastal population growth and exposure to sea-level rise and coastal flooding - A global assessment. PLoS One 10. https://doi.org/10.1371/journal.pone.0118571

Nieto, M.A., Garau, B., Balle, S., Simarro, G., Zarruk, G.A., Ortiz, A., Tintoré, J., Álvarez-Ellacuría, Gómez-Pujol, L., Orfila, A., 2010. An open source, low cost video-based coastal monitoring system. Earth Surf. Process. Landforms 35, 1712–1719. https://doi.org/10.1002/esp.2025

Ojeda, E., Guillén, J., 2008. Shoreline dynamics and beach rotation of artificial embayed beaches. Mar. Geol. 253, 51–62. https://doi.org/10.1016/j.margeo.2008.03.010

Ojeda, E., Guillén, J., 2006. Shoreline variability of barcelona city beaches in response to storms and artificial nourishment (2001-2003). Coast. Dyn. 2005 - Proc. Fifth Coast. Dyn. Int. Conf. 1–11. https://doi.org/10.1061/40855(214)67

Ojeda, E., Guillén, J., Ribas, F., 2011. Dynamics of single-barred embayed beaches. Mar. Geol. 280, 76–90. https://doi.org/10.1016/j.margeo.2010.12.002

Osorio, A.F., Pérez Muñoz, J.C., Ortiz Alarcón, C. a., Medina, R., 2007. Técnicas basadas en imágenes de video para cuantificar variables ambientales en zonas costeras, in: Avances En Recursos Hidráulicos. pp. 51–64.

Palalane, J., Fredriksson, C., Marinho, B., Larson, M., Hanson, H., Coelho, C., 2016. Simulating cross-shore material exchange at decadal scale. Model application. Coast. Eng. 116, 57–66.

https://doi.org/http://dx.doi.org/10.1016/j.coastaleng.2016.05.007

Palomar-Vázquez, J., Almonacid-Caballer, J., Pardo-Pascual, J.E., Sánchez-García, E., 2018. SHOREX : a new tool for automatic and massive extraction of shorelines from LANDSAT AND SENTInel 2 imagery, in: Proceedings of the 7 Th International Conference on the Application of Physical Modelling in Coastal and Port (Coastlab18). Santander, pp. 1–8.

Pardo-Pascual, J., Sánchez-García, E., Almonacid-Caballer, J., Palomar-Vázquez, J., Santos, E.P. de los, Fernández-Sarría, A., Balaguer-Beser, Á., 2018. Assessing the Accuracy of Automatically Extracted Shorelines on Microtidal Beaches from Landsat 7, Landsat 8 and Sentinel-2 Imagery. Remote Sens. 2018, Vol. 10, Page 326 10, 326. https://doi.org/10.3390/RS10020326

Pardo-Pascual, J.E., Almonacid-Caballer, J., Ruiz, L.A., Palomar-Vázquez, J., 2012. Automatic extraction of shorelines from Landsat TM and ETM+ multi-temporal images with subpixel precision. Remote Sens. Environ. 123, 1–11. https://doi.org/10.1016/j.rse.2012.02.024

Pelnard-Considere, R., 1956. Essai de theorie de l'evolution des formes de rivage en plages de sable et de galets. Les Energies la Mer Compte Rendu Des Quatr. Journees L'hydraulique, Paris 13, 14 15 Juin 1956; Quest. III, Rapp. 1, 74-1-10.

Peña, C., Covarsl, M.F., 1994. Project, works and monitoring at Barcelona olympic beaches, in: Coastal Engineering. pp. 3564–3578.

Perez, J., Menendez, M., Losada, I.J., 2017. GOW2: A global wave hindcast for coastal applications. Coast. Eng. 124, 1–11. https://doi.org/10.1016/j.coastaleng.2017.03.005

Perlin, M., Dean, R.G., 1983. A numerical model to simulate sediment transport in the vicinity of coastal structures. Tech. Rep. CERC 83-10. US Army Corps Eng. 119 pp.

Perlin, M., Dean, R.G., 1979. Prediction of beach planforms with littoral controls. Proc. 16th Coast. Eng. Conf. ASCE 1818–1838.

Phillips, M.S., Harley, M.D., Turner, I.L., Splinter, K.D., Cox, R.J., 2017. Shoreline recovery on wave-dominated sandy coastlines: The role of sandbar morphodynamics and nearshore wave parameters. Mar. Geol. 385, 146–159. https://doi.org/10.1016/j.margeo.2017.01.005

Pianca, C., Holman, R., Siegle, E., 2015. Shoreline variability from days to decades: Results of long-term video imaging. J. Geophys. Res. C Ocean. 120, 2159–2178. https://doi.org/10.1002/2014JC010329

Plant, N.G., Holman, R. a., Freilich, M.H., 1999. A simple model for interannual sandbar behavior. J. Geophys. Res. 104.

Prodger, S., Russell, P., Davidson, M., Miles, J., Scott, T., 2016. Understanding and predicting the temporal variability of sediment grain size characteristics on high-energy beaches. Mar. Geol. 376, 109–117. https://doi.org/10.1016/j.margeo.2016.04.003

Ranasinghe, R., McLoughlin, R., Short, A., Symonds, G., 2004. The Southern Oscillation Index, wave climate, and beach rotation. Mar. Geol. 204, 273–287. https://doi.org/10.1016/S0025-3227(04)00002-7

Ratliff, K.M., Murray, a. B., 2014. Modes and emergent time scales of embayed beach dynamics. Geophys. Res. Lett. 41, 7270–7275. https://doi.org/10.1002/2014GL061680

Rea, C.C., Komar, P.D., 1975. Computer Simulation Models of a Hooked Beach Shoreline Configuration. SEPM J. Sediment. Res. Vol. 45. https://doi.org/10.1306/212f6e6a-2b24-11d7-8648000102c1865d

Reguero, B.G., Losada, I.J., Méndez, F.J., 2019. A recent increase in global wave power as a consequence of oceanic warming. Nat. Commun. 1–14. https://doi.org/10.1038/s41467-018-08066-0

Reguero, B.G., Menéndez, M., Méndez, F.J., Mínguez, R., Losada, I.J., 2012. A Global Ocean Wave (GOW) calibrated reanalysis from 1948 onwards. Coast. Eng. 65, 38–55. https://doi.org/10.1016/j.coastaleng.2012.03.003

Requejo, S., Medina, R., González, M., 2008. Development of a medium–long term beach evolution model. Coast. Eng. 55, 1074–1088. https://doi.org/10.1016/j.coastaleng.2008.04.005

Ribas, F., Ojeda, E., Price, T.D., Guillén, J., 2010. Assessing the Suitability of Video Imaging for Studying the Dynamics of Nearshore Sandbars in Tideless Beaches. IEEE Trans. Geosci. Remote Sens. 48, 2482–2497. https://doi.org/10.1109/TGRS.2009.2039576

Robinet, A., Castelle, B., Idier, D., Marieu, V., Splinter, K.D., Harley, M.D., 2017. On a Reduced-Complexity Shoreline Model Combining Cross-Shore and Alongshore Processes. Coast. Dyn. 1853–1862.

Robinet, A., Idier, D., Castelle, B., Marieu, V., 2018. A reduced-complexity shoreline change model combining longshore and cross-shore processes: the LX-Shore model. Environ. Model. Softw. 109, 1–16. https://doi.org/10.1016/j.envsoft.2018.08.010

Rózyński, G., Larson, M., Pruszak, Z., 2001. Forced and self-organized shoreline response for a beach in the southern Baltic Sea determined through singular spectrum analysis. Coast. Eng. 43, 41–58. https://doi.org/10.1016/S0378-3839(01)00005-9

Sánchez-García, E., Balaguer-beser, A., Pardo-pascual, J.E., 2017. C-Pro : A coastal projector monitoring system using terrestrial photogrammetry with a geometric horizon constraint. ISPRS J. Photogramm. Remote Sens. 128, 255–273. https://doi.org/10.1016/j.isprsjprs.2017.03.023

Sánchez-García, E., Pardo-Pascual, J.E., Balaguer-Beser, A., Almonacid-Caballer, J., 2015. Analysis of the shoreline position extracted from landsat TM and ETM+ imagery. Int. Arch. Photogramm. Remote Sens. Spat. Inf. Sci. - ISPRS Arch. 40, 991–998. https://doi.org/10.5194/isprsarchives-XL-7-W3-991-2015

Schepper, R., De Vries, S., Reniers, A., Katsman, C., Almar, R., Bergsma, E., Davidson, M., 2019. Multi-Timescale Shoreline Modelling, in: Coastal Sediments 2019. pp. 2200–2210. https://doi.org/10.1142/9789811204487_0188

Sedrati, M., Anthony, E.J., 2007. A brief overview of plan-shape disequilibrium in embayed beaches: Tangier bay (Morocco). Méditerranée 108, 125–130. https://doi.org/10.4000/mediterranee.190

Short, A.D., Bracs, M. a, Turner, I.L., 2014. Beach oscillation and rotation: local and regional response at three beaches in southeast Australia. J. Coast. Res. SI70, 712–717. https://doi.org/10.2112/SI-120.1

Short, A.D., Trembanis, A.C., 2004. Decadal Scale Patterns in Beach Oscillation and Rotation Narrabeen Beach, Australia: Time Series, PCA and Wavelet Analysis. J. Coast. Res. 202, 523–532. https://doi.org/10.2112/1551-5036(2004)020[0523:DSPIBO]2.0.CO;2

Short, A.D., Trembanis, A.C., Turner, I.L., 2000. Beach oscillation, rotation and the Southern Oscillation, Narrabeen Beach, Australia. Coast. Eng. Proc. 2439–2452. https://doi.org/doi:10.1061/40549(276)191

Silvester, R., 1970. Growth of Crenulate Shaped Bays to Equilibrium. J. Waterw. Harb. Coast. Eng. Div. 96, 275–287.

Silvester, R., 1960. Stabilization of sedimentary coastlines. Nature 188, 467–469. https://doi.org/10.1038/188467a0

Silvester, R., Ho, S.K., 1972. Use of crenulate shaped bays to stabilize coasts, in: Coastal Engineering. ASCE, pp. 1347–1365.

Silvester, R., Tsuchiya, Y., Shibano, T., 1980. Zeta Bays, pocket beaches and headland control., in: Proceedings of the 17th International Conference on Coastal Engineering. pp. 1306–1319. https://doi.org/10.1061/9780872622647.079

Smith, R.K., Bryan, K.R., 2007. Monitoring Beach Face Volume with a Combination of Intermittent Profiling and Video Imagery. J. Coast. Res. 234, 892–898. https://doi.org/10.2112/04-0287.1

Splinter, K.D., Davidson, M.A., Turner, I.L., Beuzen, T., 2014a. Estimating shoreline response in a changing wave climate. Coast. Eng. Proc. 1, 37. https://doi.org/http://dx.doi.org/10.9753/icce.v34.sediment.37

Splinter, K.D., Kearney, E.T., Turner, I.L., 2018. Drivers of alongshore variable dune erosion during a storm event: Observations and modelling. Coast. Eng. 131, 31–41. https://doi.org/10.1016/j.coastaleng.2017.10.011

Splinter, K.D., Turner, I.L., Davidson, M. a., 2013. How much data is enough? The importance of morphological sampling interval and duration for calibration of empirical shoreline models. Coast. Eng. 77, 14–27. https://doi.org/10.1016/j.coastaleng.2013.02.009

Splinter, K.D., Turner, I.L., Davidson, M. a., Barnard, P., Castelle, B., Oltman-Shay, J., 2014b. A generalized equilibrium model for predicting daily to interannual shoreline response. J. Geophys. Res. F Earth Surf. 119, 1–23. https://doi.org/10.1002/2014JF003106

Splinter, K.D., Turner, I.L., Reinhardt, M., Ruessink, G., 2017. Rapid adjustment of shoreline behavior to changing seasonality of storms: observations and modelling at an open-coast beach. Earth Surf. Process. Landforms 42, 1186–1194. https://doi.org/10.1002/esp.4088

Stokes, C., Davidson, M., Russell, P., 2015. Observation and prediction of three-dimensional morphology at a high-energy macrotidal beach. Geomorphology 243, 1–13. https://doi.org/10.1016/j.geomorph.2015.04.024

Swart, D.H., 1974. A schematization of Onshore-Offshore Transport. Coast. Eng. Proc. 1. https://doi.org/10.9753/icce.v14.%p

Taborda, R., Silva, A., 2012. COSMOS: A lightweight coastal video monitoring system. Comput. Geosci. 49, 248–255. https://doi.org/10.1016/j.cageo.2012.07.013

Tan, S.-K., Chiew, Y.-M., 1994. Analysis of bayed beaches in static equilibrium. J. Waterw. Port, Coast. Ocean Eng. - ASCE 120, 145–153. https://doi.org/10.1061/(ASCE)0733-950X(1994)120:2(145)

Thomas, T., Phillips, M.R., Williams, a. T., 2010. Mesoscale evolution of a headland bay: Beach rotation processes. Geomorphology 123, 129–141. https://doi.org/10.1016/j.geomorph.2010.06.018

Thomas, T., Phillips, M.R., Williams, A.T., Jenkins, R.E., 2011. Medium timescale beach

rotation; gale climate and offshore island influences. Geomorphology 135, 97–107. https://doi.org/10.1016/j.geomorph.2011.08.002

Thomas, T., Rangel-Buitrago, N., Phillips, M., Anfuso, G., Williams, A., 2015. Mesoscale Morphological Change, Beach Rotation and Storm Climate Influences along a Macrotidal Embayed Beach. J. Mar. Sci. Eng. 3, 1006–1026. https://doi.org/10.3390/jmse3031006

Thomas, T., Rangel-Buitrago, N., Phillips, M.R., Anfuso, G., Williams, A.T., Oakley, J.A., 2016. Subaerial Rotation on an Open Coast Beach: Pendine West Wales, UK. J. Coast. Res. 75, 482–486. https://doi.org/10.2112/SI75-097.1

Thornton, E.B., Guza, R.T., 1983. Transformation of wave height distribution. J. Geophys. Res. 88, 5925. https://doi.org/10.1029/JC088iC10p05925

Tintoré, J., Medina, R., Gómez-Pujol, L., Orfila, A., Vizoso, G., 2009. Integrated and interdisciplinary scientific approach to coastal management. Ocean Coast. Manag. 52, 493–505. https://doi.org/10.1016/j.ocecoaman.2009.08.002

Tolman, H.L., 1992. Effects of Numerics on the Physics in a Third-Generation Wind-Wave Model. J. Phys. Oceanogr. https://doi.org/10.1175/1520-0485(1992)022<1095:EONOTP>2.0.CO;2

Tonnon, P.K., Huisman, B.J.A., Stam, G.N., van Rijn, L.C., 2018. Numerical modelling of erosion rates, life span and maintenance volumes of mega nourishments. Coast. Eng. 131, 51–69. https://doi.org/10.1016/j.coastaleng.2017.10.001

Toure, S., Diop, O., Kpalma, K., Maiga, A., 2019. Shoreline Detection using Optical Remote Sensing: A Review. ISPRS Int. J. Geo-Information 8, 75. https://doi.org/10.3390/ijgi8020075

Turki, I., Medina, R., Coco, G., Gonzalez, M., 2013a. An equilibrium model to predict shoreline rotation of pocket beaches. Mar. Geol. 346, 220–232. https://doi.org/10.1016/j.margeo.2013.08.002

Turki, I., Medina, R., González, M., 2012. Beach memory. Coast. Eng. 1–7.

Turki, I., Medina, R., Gonzalez, M., Coco, G., 2013b. Natural variability of shoreline position: Observations at three pocket beaches. Mar. Geol. 338, 76–89. https://doi.org/10.1016/j.margeo.2012.10.007

Turki, I., Medina, R., Kakeh, N., González, M., 2015. Shoreline relaxation at pocket beaches. Ocean Dyn. 65, 1221–1234. https://doi.org/10.1007/s10236-015-0869-z

Turner, I.L., Harley, M.D., Short, A.D., Simmons, J. a, Bracs, M. a, Phillips, M.S., Splinter, K.D., 2016. A multi-decade dataset of monthly beach profile surveys and inshore wave forcing at Narrabeen, Australia. Sci. Data 3, 1–13. https://doi.org/10.1038/sdata.2016.24

USACE, 2002. Coastal Engineering Manual. U.S. Army Corps of Engineers, Washington, DC.

Van de Lageweg, W.I., Bryan, K.R., Coco, G., Ruessink, B.G., 2013. Observations of shoreline-sandbar coupling on an embayed beach. Mar. Geol. 344, 101–114. https://doi.org/10.1016/j.margeo.2013.07.018

van Rijn, L.., Walstra, D.J.., Grasmeijer, B., Sutherland, J., Pan, S., Sierra, J.., 2003. The predictability of cross-shore bed evolution of sandy beaches at the time scale of storms and seasons using process-based Profile models. Coast. Eng. 47, 295–327. https://doi.org/10.1016/S0378-3839(02)00120-5

Velegrakis, F., Schimmels, S., 2013. Predicting Beach Face rotation on a Meso Tidal, Steeply Sloping Beach. Coast. Dyn. 1835–1846.

Vellinga, P., 1983. Predictive computational model for beach and dune erosion druing storm surges. DELFT, NETHERLANDS, DELFT Hydraul. LAB., FEB. 1983.

Vitousek, S., Barnard, P.L., Limber, P., Erikson, L., Cole, B., 2017. A model integrating longshore and cross-shore processes for predicting long-term shoreline response to climate change. J. Geophys. Res. Earth Surf. 782–806. https://doi.org/10.1002/2016JF004065

Vos, Kilian, Splinter, K.D., Harley, M.D., Simmons, J.A., Turner, I.L., 2019. CoastSat: a Python toolkit to extract shorelines from publicly available satellite imagery. Environ. Model. Softw. 122, 104528. https://doi.org/10.1016/j.envsoft.2019.104528

Vos, K., Splinter, K.D., Harley, M.D., Simmons, J.A., Turner, I.L., 2019. Capturing intra-annual to multi-decadal shoreline variability from publicly available satellite imagery. Coast. Eng. https://doi.org/10.1016/j.coastaleng.2019.04.004

Vousdoukas, M., 2013. ORASIS- a coastal video monitoring platform, in: EGU General Assembly. p. 3036.

Wainwright, D.J., Ranasinghe, R., Callaghan, D.P., Woodroffe, C.D., Jongejan, R., Dougherty, A.J., Rogers, K., Cowell, P.J., 2015. Moving from deterministic towards probabilistic coastal hazard and risk assessment: Development of a modelling framework and application to Narrabeen Beach, New South Wales, Australia. Coast. Eng. 96, 92–99. https://doi.org/10.1016/j.coastaleng.2014.11.009

White, K., El Asmar, H.M., 1999. Monitoring changing position of coastlines using Thematic

Mapper imagery, an example from the Nile Delta. Geomorphology 29, 93–105. https://doi.org/10.1016/S0169-555X(99)00008-2

Widyantara, I.M.O., Putra, I.M.D.A., Adnyana, I.B.P., 2017. COVIMOS: A Coastal Video Monitoring System. J. Electr. Electron. Informatics 1, 1. https://doi.org/10.24843/JEEI.2017.v01.i01.p01

Wiggins, M., Scott, T., Masselink, G., Russell, P., McCarroll, R.J., 2019. Coastal embayment rotation: Response to extreme events and climate control, using full embayment surveys. Geomorphology 327, 385–403. https://doi.org/10.1016/j.geomorph.2018.11.014

Wijnberg, K.M., Terwindt, J.H.J., 1995. Extracting decadal morphological behaviour from high-resolution, long-term bathymetric surveys along the Holland coast using eigenfunction analysis. Mar. Geol. 126, 301–330. https://doi.org/10.1016/0025-3227(95)00084-C

Wind, H.G., 1994. An analytical model of crenulate shaped beaches. Coast. Eng. 23, 243–253. https://doi.org/10.1016/0378-3839(94)90004-3

Work, P.A., Dean, R.G., 1991. Effect of varying sediment size on equilibrium beach profiles, in: Coastal Sediments ’91. pp. 890–904.

Wright, L.., Short, a. ., Green, M.., 1985. Short-term changes in the morphodynamic states of beaches and surf zones: An empirical predictive model. Mar. Geol. 62, 339–364. https://doi.org/10.1016/0025-3227(85)90123-9

Wright, L.D., Nielsen, P., Short, A.D., Coffey, F.C., Green, M.O., 1982. Nearshore and surfzone morphodynamics of a storm wave environment : eastern Bass Strait, Australia (No. CSU-TR-82/3).

Wright, L.D., Short, A.D., 1984. Morphodynamic variability of surf zones and beaches: a synthesis. Mar. Geol. Elsevier Sci. Publ. B.V 56, 93–118.

Yasso, W., 1965. Plan Geometry of Headland Bay Beaches. J. Geol. 73, 702–714.

Yates, M.L., Guza, R.T., O’Reilly, W.C., 2009. Equilibrium shoreline response: Observations and modeling. J. Geophys. Res. Ocean. 114, 1–16. https://doi.org/10.1029/2009JC005359

Yates, M.L., Guza, R.T., O’Reilly, W.C., Hansen, J.E., Barnard, P.L., 2011. Equilibrium shoreline response of a high wave energy beach. J. Geophys. Res. Ocean. 116, 1–13. https://doi.org/10.1029/2010JC006681

Young, A.P., 2018. Decadal-scale coastal cliff retreat in southern and central California. Geomorphology 300, 164–175. https://doi.org/10.1016/j.geomorph.2017.10.010

Yousefi, S., Mirzaee, S., Tazeh, M., Pourghasemi, H., Karimi, H., 2015. Comparison of different algorithms for land use mapping in dry climate using satellite images : a case study of the Central regions of Iran. Desert 20, 1–10.

9 APPENDICES

APPENDIX 1: STATIC EQUILIBRIUM BEACH PROFILE MODELS

Various authors have extensively analyzed static equilibrium beach profiles, SEBPs. Some of the most representative SEBPs found in the literature are summarized below, in chronological order.

The first equilibrium profile formulation date back to the middle of the 20th century when great interest was aroused in processes related to sediment transport.

Bruun (1954) analyzed beach profiles on the Danish coast of the North Sea and in Mission Bay (California), finding the following expression:

$$h(x) = Ax^{2/3} \tag{A.1}$$

Where h(x) is the water depth at a distance x from the coastline, and A is a scale parameter, mainly dependent on sediment characteristics.

Swart (1974) carried out a series of tests in a laboratory tank, obtaining empirical relationships between beach profile geometric characteristics and wave and sediment transport conditions. The active beach profile was considered in four zones so that empirical expressions were defined for each of them.

Next, Dean (1977) adjusted by means of least squares 504 profiles taken by Hayden et al., (1975) along the Atlantic coast of the United States from Long Island to Mexico, to the form:

$$h(x) = Ax^{n'} \tag{A.2}$$

Where n'=2/3, as well as Bruun (1954). It should be noted that other authors have obtained different values of n'; such as Wright et al. (1982) who proposed n'=2/5 and Boon and Green (1988) n'=1/2.

Dean (1977) gave a theoretical basis to his model based on the assumption that energy dissipation per unit volume, D*, in the breaking zone is constant. It further defines that the scale parameter, A, can be expressed in terms of D*, as follows:

$$A = \left(\frac{24}{5}\frac{D^*}{\rho g^{3/2}\gamma^2}\right)^{2/3} \tag{A.3}$$

Where g is the acceleration due to gravity, ρ is the seawater density and γ a constant of proportionality between wave height and breaking depth.

Bowen (1980) concluded that when the transverse sediment transport at each point of the profile is null, it is because it has reached its equilibrium state. Similar to the expression proposed previously by Bruun (1954), Bowen (1980) obtained a new approximation of the beach profile, as a function of the sediment fall velocity, w_f, the wave radian frequency, $\sigma = {}^{2\pi}/_{T}$, and the acceleration due to gravity, g:

$$h = \mathrm{g}\left(\frac{5.7 w_f}{\sigma^2}\right)^{2/5} \tag{A.4}$$

Dean (1987) developed an abacus (see Fig. A.1) in which he considered Moore's (1982) ratio of scale parameter A, as a function of sediment size, D, with the sediment fall velocity. From this relationship, he obtained the following expression:

$$A = 0.51 \cdot \left(w_f\right)^{0.44} \tag{A.5}$$

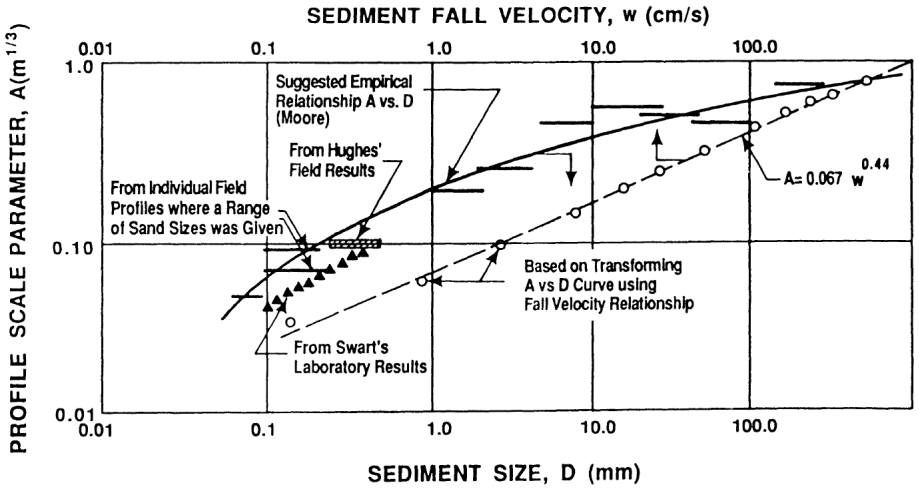

Fig. A.1. Variation of the scale parameter, A, as a function of grain size, D, and the sediment fall velocity, w_f. Taken from Dean, (1991).

Kriebel et al., (1991) also related the scale parameter A to the sediment fall velocity, taking into consideration that a fraction of the wave energy dissipation per unit volume due to wave breaking must be equal to the energy dissipation associated with suspended sediment falling under its own submerged weight. Its equation results in the following form:

$$A = 2.25 \cdot \left(\frac{{w_f}^2}{g}\right)^{1/3} \tag{A.6}$$

From two-dimensional and three-dimensional laboratory tests of dunes erosion with irregular waves, Vellinga (1983) developed an expression for SEBP that includes the effect of significant wave height at deepwater depths, H_{0s}, and the sediment fall velocity:

$$\left(\frac{7.6}{H_{0s}}\right)h = 0.47 \cdot \left[\left(\frac{7.6}{H_{0s}}\right)^{1.28}\left(\frac{w_f}{0.0268}\right)^{0.56}x + 18\right] - 2.0 \tag{A.7}$$

Subsequently, in a new analysis of his test results, he concluded that the erosion profile could be defined by a potential curve, similar to that proposed by Bruun (1954), where the best-fit exponent for his tests was n=0.78:

$$h(x) = Ax^{0.78} \tag{A.8}$$

It should be noted that most of the applications and formulations related to the concept of SEBP have been carried out taking into account a single sediment grain size for the entire beach profile. However, there are some exceptions, such as Work and Dean, (1991) and Dean et al., (1993), who evaluated the SEBP theory taking into account varying grain size across-shore.

Bodge (1992) developed a model of exponential SEBP given by the expression:

$$h = B'\left(1 - e^{-k_1 x}\right) \tag{A.9}$$

where B' and k are empirical coefficients.

Following with the exponential SEBP, Komar and Mcdougal (1994) evaluated beach profiles along the coast of the Nile Delta, in such a way that they modified the expression of Bodge (1992) so that it was linked to the slope of the beachfront, m, and to the damping coefficient, k_1:

$$h = \frac{m'}{k}\left(1 - e^{-k_1 x}\right) \tag{A.10}$$

After the diversity of proposals by numerous authors who consider SEBP of a single stretch, new proposals are developed that contemplate SEBPs in two stretches. In this way, Inman et al. (1993) analyzed 23 historical profiles (1950-1989) of the San Diego region and proposed a profile of two sections with the shape of Bruun (1954) each. The section closest to the coast is governed by broken waves and has been named *Bar-Berm Profile*; while the farthest section or *Shorerise Profile* is where the waves have not broken yet (see Fig. A.2).

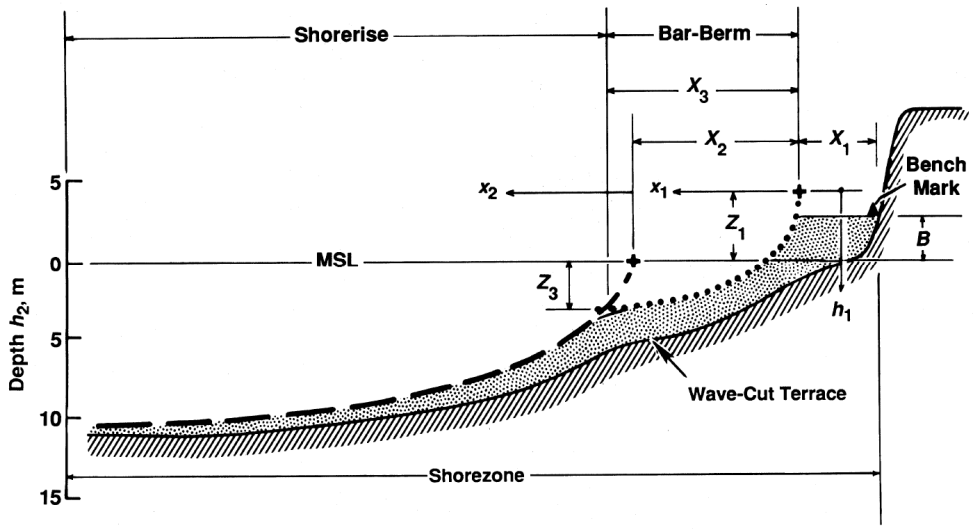

Fig. A.2. SEBP of two sections proposed by Inman et al. (1993).

Bernabeu, (1999) continued with a model similar to that proposed by Inman et al. (1993), considering a biparabolic SEBP, where the inflection point is associated with breaking wave location. The two sections are (see Fig. A.3):

- Surf profile: section from the coastline to the breaking point.
- Shoaling profile: section from the breaking point to deep water.

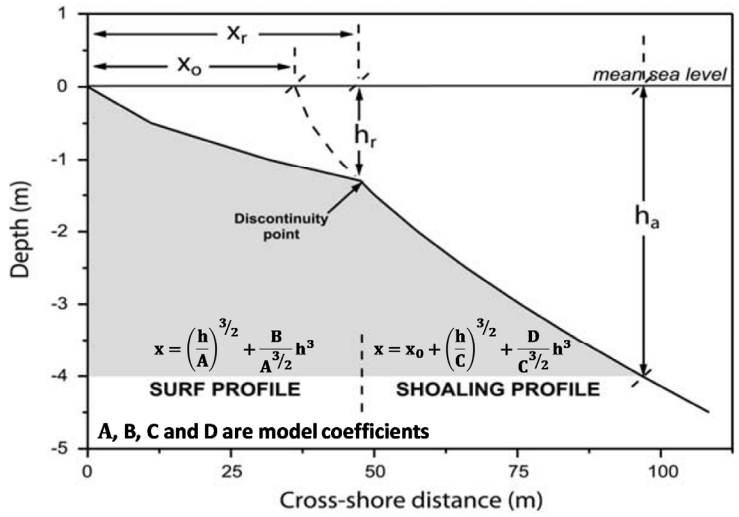

Fig. A.3. Biparabolic SEBP proposed by Bernabeu, (1999). Modified from Bernabeu et al., (2003).

Larson et al. (1999) also proposed a biparabolic SEBP, with sections before and after the wave breaking point. In this case, the surf profile follows the traditional form $h(x) = Ax^{n'}$, where n'=2/3; whereas for the shoaling profile three different models are proposed, where n varies between 0.15 and 0.30; according to theoretical approaches based on energy dissipation processes, small-scale sediment transport or medium sediment transport.

Subsequently, more complex SEBP were developed, such as the three sections SEBP proposed by Requejo et al., (2008). It considers the surf and shoaling profiles, as well as a third profile in which the conditions remain constant between two consecutive instants of time (see Fig. A.4).

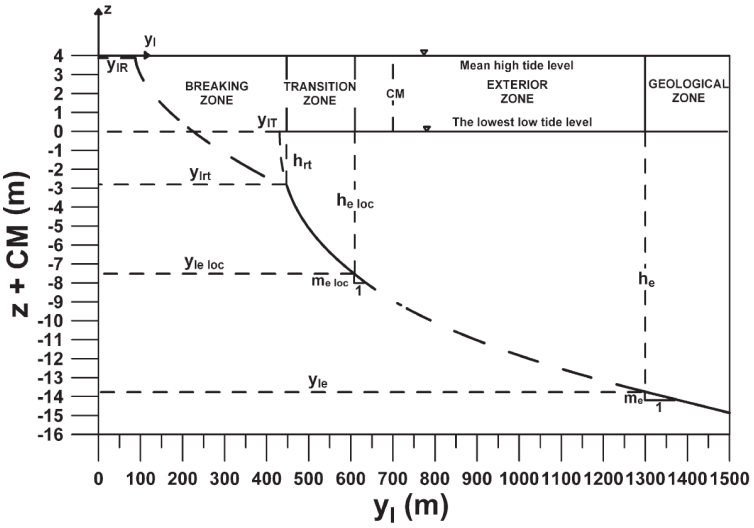

Fig. A.4. Three-section SEBP proposed by Requejo et al., (2008).

APPENDIX 2: STATIC EQUILIBRIUM BEACH PLANFORM MODELS

Numerous researchers have recognized the existence of a pattern in the planform shape of beaches located sheltered from a cape or headland. This section compiles the main empirical equations found in the literature to obtain and fit the Static Equilibrium Planform (SEP) of embayed beaches.

Krumbein (1944) was a pioneer in describing the planform of embayed beaches as a configuration similar to a logarithmic spiral function (*log-spiral*), in which the radius of curvature increases progressively. This function is given by:

$$R_2 = R_1 e^{\theta' cot\alpha} \tag{A.11}$$

Where R_2 is the length of the radius that starts from the spiral center to a point on the curve. R_1 is the length of radius to the arbitrary origin of angle measurement. θ' is the variable angle between R_1 and R_2 and α is a characteristic constant angle between the tangent to the curve and radius at any point along the spiral (see Fig. A.5).

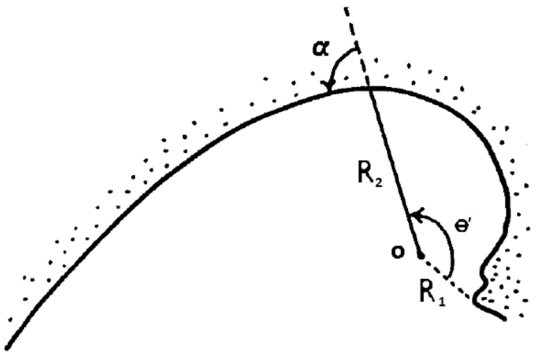

Fig. A.5. Log-spiral beach planform scheme. Modified from Moreno and Kraus (1999).

Silvester (1960) proposed a SEP called "*half-heart*", obtained from tests of physical modeling of a straight beach bounded between two obstacles, under the incidence of an incident wave of 45°, without the additional supply of sediments.

Yasso (1965) stated that the curvature of embayed beaches could be defined by a logarithmic spiral, following a shape known as "*crenulate shaped bay*". He evaluated the SEP of four bays on the East and West coasts of the United States and found a good approximation to the logarithmic spiral shape; however, the choice of the spiral origin remained challenging. Silvester (1970)

supported the expression proposed by Yasso (1965) and suggested that the spiral center does not necessarily have to coincide with the control point.

Silvester and Ho (1972) concluded that the wave diffraction and refraction significantly influence the final shape of the beach. They found a relationship between the angle α, and the incidence wave angle, which they called β, for the stabilization design of embayed beaches in Singapore. Besides, Rea and Komar, (1975) analyzed bays with logarithmic spiral shape through numerical modeling. They concluded that the coastline will always try to reach an equilibrium configuration governed by refraction and diffraction patterns of the outer waves, and by the distribution of the energy flux.

Leblond (1972) showed how waves that strike at an oblique angle to the coastline could initiate erosion that eventually led to the formation of hook-like beaches. Leblond (1979) calculated the arrival time of diffracted waves at the control point, with waves propagating at shallow depths simultaneously breaking along the beach.

Berenguer and Enríquez (1989) evaluated 24 embayed beaches on the Spanish Mediterranean coast in order to evaluate beach planform shape, beach profile shape, and sediment distribution. In their study, they concluded that these embayed beaches were adequately adjusted to logarithmic spiral SEP. They defined an expression to relate the maximum distance from the pole of the spiral to the coast, A_1, with the separation between the headlands that shelter the beach, S^*:

$$A_1 = 25 + 0.85S^* \tag{A.12}$$

Hsu et al., (1987) analyzed experimental data from HHBs, and found that the logarithmic spiral did not adjust from a point where the coastline was straight and parallel to the incident waves. It was then that Hsu and Evans (1989) developed a parabolic SEP (see Fig. A.6) for engineering purposes from fitting the planform of 27 different beaches in static equilibrium.

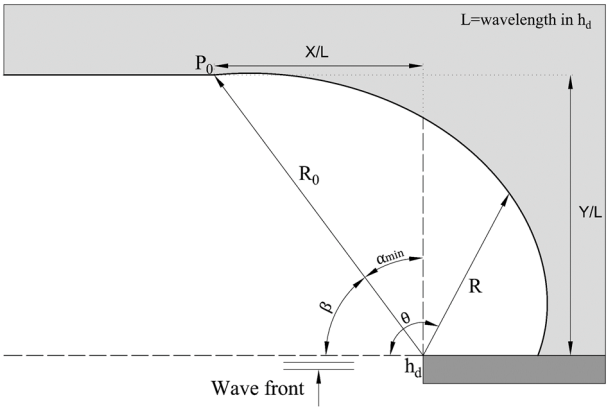

Fig. A.6. Parabolic SEP scheme proposed by Hsu and Evans (1989).

This parabolic function is able to adequately predict areas that the logarithmic spiral is unable to represent. The main parameters are related to the wave front properties and the location of the control point. Hsu and Evans (1989) proposed the following second-order polynomial equation:

$$R = R_0 \cdot \left(C_0 + C_1 \frac{\beta}{\theta} + C_2 \left(\frac{\beta}{\theta} \right)^2 \right) \tag{A.13}$$

where R_0 is the control line length joining the updrift diffraction point, h_0 to the down-coast control point, P_0. β is the wave obliquity, i.e., the angle between the incident wave crest (assumed linear) and the control line. The control line length, R_0, is also angled β to the tangent at the down-coast beach end. C_0, C_1, and C_2 are coefficients that depend on the wave obliquity, β. The radius, R, is measured from the diffraction point to any location on the parabolic shoreline at an angle, θ, measured from the wave crest (Hsu and Evans 1989). González and Medina, (2001) provided guidance on locating the down-coast control point.

Subsequently, Tan and Chiew (1994) proposed a modification of the parable of Hsu and Evans (1989) expressing C_0 and C_1 in terms of α, and $C_2=\alpha_{st}$; obtaining the following expression:

$$\frac{R}{R_0} = [1 - \beta \cot(\beta) + \alpha_{st}] + [\beta \cot(\beta) - 2\alpha_{st}] \left(\frac{\beta}{\theta} \right) + \alpha_{st} \left(\frac{\beta}{\theta} \right)^2 \tag{A.14}$$

where:

$$\alpha_{st} = 0.277 - 10^{\left({}^{\beta\pi}/_{180} - 1.105 \right)} \tag{A.15}$$

Wind (1994) presented an analytical model for beaches sheltered by a single structure in which it is assumed that the coastline displacement is a function of the shape, which in turn varies according to the polar angle and time. This author showed that in the long term the model approximates the SEP presented by Hsu and Evans (1989).

Moreno and Kraus (1999) developed another beach planform approximation called "*hyperbolic-tangent*" through the analysis of 46 beaches of mixed beach stability; not exclusively beaches in static equilibrium. Their proposal is defined by the following expression in Cartesian coordinates:

$$y' = \pm a_1 tanh^{m_1}(b_1 x') \tag{A.16}$$

Where "y'" is the perpendicular distance to the coast, "x'" is the distance along the coast; while a_1, b_1 and m_1 are empirical coefficients.

Hsu et al., (2010) provided an updated overview to date of the latest research and summary of the static bay beach concept.

Finally, more recently, Elshinnawy et al., (2017) estimated the relationship between the direction of the wave energy flux and the orientation of equilibrium beaches. Elshinnawy et al., (2018) identified the influence of wave directional spreading on the equilibrium planform of embayed beaches and Elshinnawy et al., (2018b); (2018c) proposed a new model and design procedure, respectively, for dynamic equilibrium planform.

APPENDIX 3: EQUILIBRIUM-BASED SHORELINE EVOLUTION MODELS

The equilibrium-based shoreline evolution models can be further separated in agreement with the sediment transport direction; longshore transport, which is performed along the coastline and transverse or cross-shore transport, which takes place perpendicular to it. In the following, the equilibrium-based models according to the sediment transport direction are detailed. Special mention is made to the model proposed by Yates et al., (2009), which has been one of the main references in this thesis.

- **Equilibrium-based shoreline evolution models for cross-shore movement**

The first model of equilibrium cross-shore evolution models dates back to the proposal of Wright and Short, (1984), who highlighted the relationship among morphodynamic equilibrium, relative energy and relative rates of erosion or accretion. They defined the following expression:

$$\frac{dR'(t)}{dt} = k \cdot \Omega^2\left(\Omega - \Omega_{eq}\right) \tag{A.17}$$

where R'(t) is the shoreline response at time "t", k is a proportionality constant that represents the relaxation speed of the system and Ω and Ω_{eq} are the dimensionless fall velocity corresponding to the incident and equilibrium conditions, respectively.

Kriebel and Dean (1993) defined that the response rate of a beach profile should be proportional to the difference between the instantaneous beach profile shape and its final or equilibrium shape. Thus, they proposed the following first-order kinetic equation:

$$\frac{dR'(t)}{dt} = \frac{1}{Ts} \cdot \left(R'_{eq} - R'(t)\right) \tag{A.18}$$

where R'(t) is the shoreline response at time "t", R'_{eq} is the maximum potential advance or retreat produced in equilibrium and Ts is the characteristic response time or relaxation time of the model.

To solve the differential equation, Kriebel and Dean (1993) developed a convolution method, in which the beach response to steady-state forcing conditions is approximately exponential in time. Through laboratory tests they evaluated an initially flat beach, which was subjected to a fixed

water level and constant wave conditions, finding that the response at any contour depth as a function of time, R'(t), can be calculated as follows:

$$R'(t) = R'_{eq}\left(1 - e^{-t/T_s}\right) \tag{A.19}$$

Subsequently, Miller and Dean (2004) numerically resolved the integral form of the model proposed by Kriebel and Dean (1993), evaluating the beach profile response to variations in sea level due to the combination of astronomical tide, meteorological tide, and wave set-up. The differential expression proposed by Miller and Dean (2004) is:

$$\frac{dS(t)}{dt} = k\big(S_{eq}(t) - S(t)\big) \tag{A.20}$$

where S(t) is the shoreline position and $S_{eq}(t)$ is the equilibrium shoreline position determined by the forcing at the time "t". k is a constant governing the rate at which the shoreline approaches equilibrium. Through finite differences, they obtained the following solution to the differential equation:

$$S^{n+1} = \frac{S^n + A\left[\left(S_{eq}^{n+1} + S_{eq}^{n}\right) - S^n\right]}{1 + \frac{k\Delta t}{2}} \tag{A.21}$$

Using equilibrium beach profile theory, and Bruun-type conservation of volume argument, the equilibrium shoreline change, $\Delta S_{eq}(t)$ due to a combination of wave-induced setup, and storm surge can be shown to be approximately:

$$\Delta S_{eq}(t) = -W^*(t)\left(\frac{0.068H_b(t) + S}{B + 1.28H_b(t)}\right) \tag{A.22}$$

where $H_b(t)$ is the breaking wave height, B is the berm height, and W*(t) is the width of the active surf zone defined out to the breakpoint. It should be noted that Miller and Dean (2004) unsuccessfully attempted to establish empirical relationships between the model calibration parameter, and the considered forcing.

Yates et al., (2009) proposed a model referred as "YA09", in which the equilibrium shoreline position is linearly related to the incident wave energy:

$$\frac{\partial S(t)}{\partial t} = C^{\pm} \cdot E^{1/2}\big(E - E_{eq}\big) \tag{A.23}$$

where S(t) and E are the shoreline position and the local incident energy, respectively, at time "t", E_{eq} is the equilibrium energy, $E^{1/2}$ is an energy weighting factor that avoids non-physical changes, $C^{\pm}$ are proportionality constants of accretion, C^{+}, when $\Delta E < 0$, or erosion, C^{-}, when $\Delta E > 0$; being $\Delta E = (E - E_{eq})$.

Yates et al., (2009) defined a linear biunivocal relationship between equilibrium wave energy and shoreline position (see Fig. A.7). This relationship is known as the equilibrium energy function (EEF):

$$E_{eq}(S) = aS + b \tag{A.24}$$

where a and b are model calibration parameters.

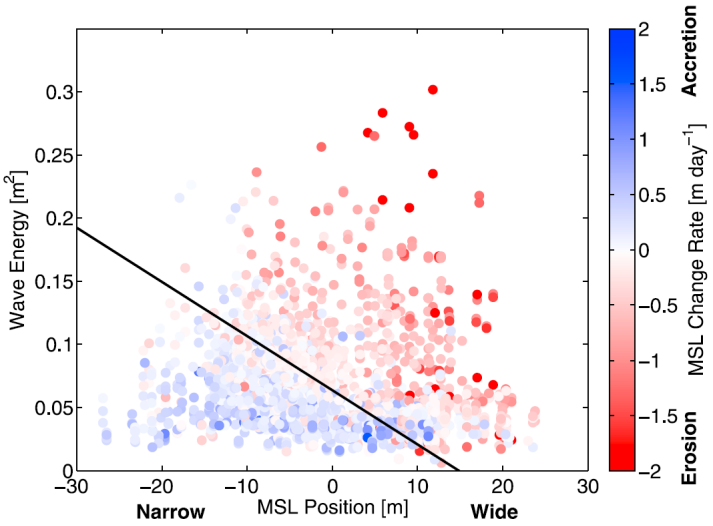

Fig. A.7. Relationship between the incident wave energy and the shoreline position. Taken from Yates et al., (2009).

Assuming that energy is constant in a sea state and integrated into the initial equation (A.23), Yates et al., (2009) obtained the following expression, in which the shoreline position approaches equilibrium exponentially:

$$S(t) = (S_0 - S_{eq})e^{-aC^{\pm}E^{1/2}t} + S_{eq} \tag{A.25}$$

where S_0 is the initial shoreline position at instant $t=t_0$, from which the shoreline position is obtained at the beginning of the next sea state, S_1, at instant $t_i=t_0+\Delta t$. To determine the evolution in the next sea state, the initial position to consider will be the end of the previous one, and so on, making the model applicable to the medium term. Thus, the model is defined as a succession of N sea states characterized by their corresponding wave heights, assuming the hypothesis of stationary waves during each sea state of the series, Δt.

The YA09 model has been applied in various beaches, originally in Torrey Pines, USA (Yates et al., 2009); then, the model was applied in Ocean Beach, USA (Yates et al., 2011), Truc Vert, France (Castelle et al., 2014), Porsmilin, France (Lemos et al., 2017), and others, and it resulted in good performance. The reader is referred to Yates et al. (2009) for a full description of the model.

It should be noted that Yates et al., (2011) concluded that the calibration coefficients of the YA09 model appeared to depend partly (implicitly) on morphological characteristics of each beach, such as the sediment grain size.

Long and Plant, (2012) included a linear trend term, ν_{lt}, for the longshore approximation in the YA09 model, adding also the Kalman filter, as a data assimilation framework that uses sparse observations to generate an updated forecast of shoreline position and to estimate unobserved geophysical variables and model parameters:

$$\frac{dS(t)}{dt} = \nu_{lt} + C^{\pm}E^{1/2} \cdot \Delta E(S) \tag{A.26}$$

Following the bases of the YA09 model, Doria et al., (2016) analyzed sixteen years of shoreline and wave observations at five southern California beaches. They proposed extending the scope of the YA09 model by considering the influence of large-scale phenomena such as El Niño and La Niña; in such a way that, to reduce the overestimation predicted by the original YA09 model during winters of El Niño years, they proposed: 1) including a non-erodible back beach cross-shore location, S_{bb}, obtained from aerial photographic and lidar surveys, and 2) using non-linear alternative forms of equilibrium energy (e.g. cubic forms) that gradually diminish the mobility of highly eroded coasts. The expression of YA09 model modified by Doria et al., (2016) results:

$$\frac{dS(t)}{dt} = \begin{cases} C^{\pm}E^{1/2} \cdot \Delta E(S) & \text{for } S > S_{bb} \\ 0 \text{ for } S \leq S_{bb} \end{cases} \tag{A.27}$$

Davidson and Turner (2009) were based on the imbalance concept of Wright et al., (1985) and presented a two-dimensional profile model, known as DT09. This model was calibrated and tested against a 6-year time series of shoreline position, derived from a coastal imaging system at the Gold Coast, Australia. The model is of the form:

$$\frac{dz'(x,t)}{dt} = R^{*}\left|\Omega_{eq} - \Omega(t)\right|\Omega^{n}(t)\emptyset'(\mathrm{x,t}) \tag{A.28}$$

where $\emptyset'$ is a dimensionless shape function describing the form and direction (erosion/accretion) of the profile change, x is the cross-shore distance and z' is the vertical displacement of the beach.

R^* is a response rate parameter (m/s). Ω_{eq} represents the equilibrium dimensionless fall velocity, and n is a calibration parameter difficult to define, due to the complexity of the model. Davidson and Turner (2009) proposed n=2 as the best fit.

Next, Davidson et al. (2010) simplified the 2-D behavioral-template DT09 model into a one-dimensional (1-D) model. This new model, known as DLT10 was calibrated and tested using five-years of weekly video-derived shoreline data from the Gold Coast, Australia. The kinetic equation takes the form:

$$\frac{dS(t)}{dt} = \mathrm{b}' + \mathrm{c}\big(\Omega_{eq} - \Omega(t)\big)\Omega^{\mathrm{k}}(t) \tag{A.29}$$

where c and k are model calibration parameters and b' is a linear rate of net shoreline progradation or retreat.

Davidson et al. (2013) made a series of modifications on the previous model, which resulted in the model DST13 or ShoreFor model, which takes the following form:

$$\frac{dS(t)}{dt} = \mathrm{b}' + C^{\pm}P^{1/2}\big(\Omega_{eq}(t) - \Omega(t)\big) \tag{A.30}$$

where P is the incident deepwater wave power ($P=Ho^2Tp$), where Ho is the deepwater wave height and Tp the peak wave period. Following Yates et al., (2009), $C^{\pm}$ is separated into erosion ($C^{-}$when $\Omega > \Omega_{eq}$) and accretion (C^{+},when $\Omega < \Omega_{eq}$) components.

In this case, the disequilibrium term $\Delta\Omega = \Omega_{eq}(t) - \Omega(t)$ now incorporates a time-varying equilibrium condition, $\Omega_{eq}(t)$. Based on the premise that both shoreline and morphological change are inter-related, they defined $\Omega_{eq}(t)$ as the weighted average of the antecedent dimensionless fall velocity:

$$\Omega_{eq}(t) = \frac{\sum_{j=0}^{\frac{D'}{\Delta t}} \Omega_j 10^{-j\Delta t/\emptyset}}{\sum_{j=0}^{\frac{D'}{\Delta t}} 10^{-j\Delta t/\emptyset}} \tag{A.31}$$

Where D' represents the total window width of the weighted average and ∅ is the memory decay rate. Values from ∅ were tested between 5 and 380 days and the optimal value D'=2∅ was adopted. Thus, the two new parameters D' and ∅ were reduced to one. The ShoreFor model was initially calibrated and validated at Gold Coast and Narrabeen Beach, Australia. Subsequently, authors such as Stokes et al. (2015) applied the model in Perranporth Beach on the northwest coast of Cornwall, United Kingdom finding satisfactory results.

Castelle et al. (2014) analyzed 8-year time series of incident wave energy data with monthly measured data at Truc Vert Beach in France, which is a mesotidal beach, highly energetic and with multiple bars. They used the YA09 and DST13 models defining the shoreline position at different levels (z=0 m, 0.4 m, 1.5 m, 3 m and 6 m). In order to use the DST13 model in energy terms and to be compatible with the YA09 model, they defined the following assumption by modifying the equilibrium dimensionless fall velocity, for equilibrium wave energy:

$$E_{eq}(t) = \frac{\sum_{j=0}^{2\emptyset/\Delta t} E_j 10^{-j\Delta t/\emptyset}}{\sum_{j=0}^{2\emptyset/\Delta t} \mathrm{j} = 0} \tag{A.32}$$

Castelle et al. (2014) concluded that the equilibrium shoreline evolution models work both on beaches without bars and/or microtidal, as well as on mesotidal beaches with the presence of bars. The best shoreline proxy at Truc Vert beach was the mean high water level (MHWL), where the inner-bar and berm dynamics have little influence on the shoreline cross-shore displacement. The results of both models showed very similar skills.

Based on DST13 model, Splinter et al. (2014) proposed a new equilibrium model which included time-varying terms describing both the magnitude and direction of shoreline response as a result of onshore/offshore sediment transport between the surf zone and the beach face:

$$\frac{dS(t)}{dt} = \mathrm{c}(F^{+} + rF^{-}) + \mathrm{b}' \tag{A.33}$$

where c is referred to as the rate parameter; b' is a linear term to acknowledge longer-term processes and F is the forcing term, which in turn is split into two separate accretion (F^{+}) and erosion (F^{-}) components. The erosion component is multiplied by an erosion ratio (r), which accounts for the different physical processes associated with accretion and erosion. The erosion ratio is numerically evaluated in the model as:

$$r = \left| \frac{\sum_{i=0}^{n} \langle F_i^{+} \rangle}{\sum_{i=0}^{n} \langle F_i^{-} \rangle} \right| \tag{A.34}$$

where | | indicates the absolute value, ⟨⟩ indicates a numerical operation that removes the linear trend but preserves the record mean, and n is the total record length. Regarding the forcing term:

$$F = P^{0.5} \frac{\Delta\Omega}{\sigma_{\Delta\Omega}} \tag{A.35}$$

where P is the breaking wave energy flux, $\Delta\Omega$ is the dimensionless fall velocity disequilibrium and $\sigma_{\Delta\Omega}$ is the standard deviation of $\Delta\Omega$.

Jara et al. (2015) developed a model hereafter referred to as "JA15". This model was based on YA09 model, excluding the term $E^{1/2}$ for energy weighting:

$$\frac{\partial S(t)}{\partial t} = C^{\pm} \cdot \left(E - E_{eq}\right) \tag{A.36}$$

In this case, the new model defined a relationship between the shoreline position and the equilibrium energy (EEF) by means of several measurable morphological characteristics of the beach, which remain unchanged during the study period (D_{50}, B, Vs, γ, x_t and h_t; see Fig. A.8): the sediment grain size, D_{50} (Dean 1991); berm height of the beach, B; sediment volume in the active beach profile, Vs; Thornton and Guza's (1983) linear breaking criterion, γ; and the horizontal position, xt, and depth, ht, of a steady toe in the theoretical equilibrium beach profile model (Jara et al., 2015) at the closure depth of the active beach profile.

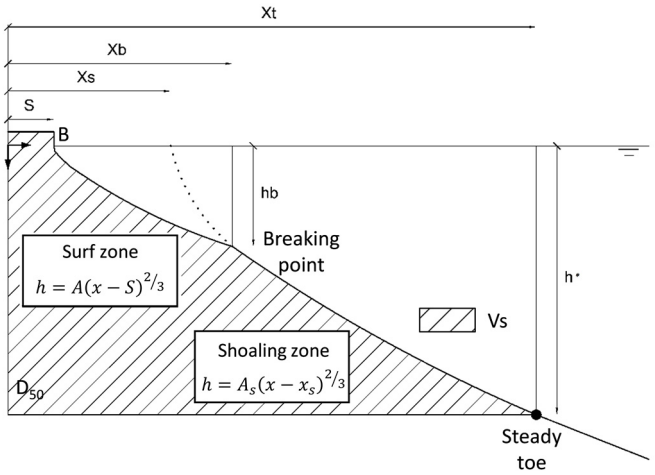

Fig. A.8. Bi-parabolic equilibrium profile, including invariants. Modified from Jara et al., (2015).

JA15 model was successfully calibrated and validated by means of two years of daily video-camera shoreline monitoring at Nova Icaria Beach, Spain.

- **Equilibrium-based shoreline evolution models for longshore movement**

One of the pioneering equilibrium-based shoreline evolution models for longshore movement was developed by Turki et al., (2013a), who suggested a semi-empirical formulation based on the hypothesis that the shoreline rotation rate can be related to the alongshore component of the wave energy flux. The model is expressed in terms of the following kinetic equation to define the beach response variation (see Fig. A.9):

$$\frac{\partial R'(t)}{\partial t} = \omega \cdot \left(R'_{\text{eq}} - R'(t)\right) \tag{A.37}$$

where R'(t) is the shoreline response, and R'$_{eq}$ is the long-term equilibrium one. ω is the beach change rate which is inversely proportional to the characteristic time scale, Ts, of the shoreline response $\omega = {}^{1}/_{Ts}$. Ts governs the time required for the shoreline to respond to new forcing conditions and to reach a new equilibrium position.

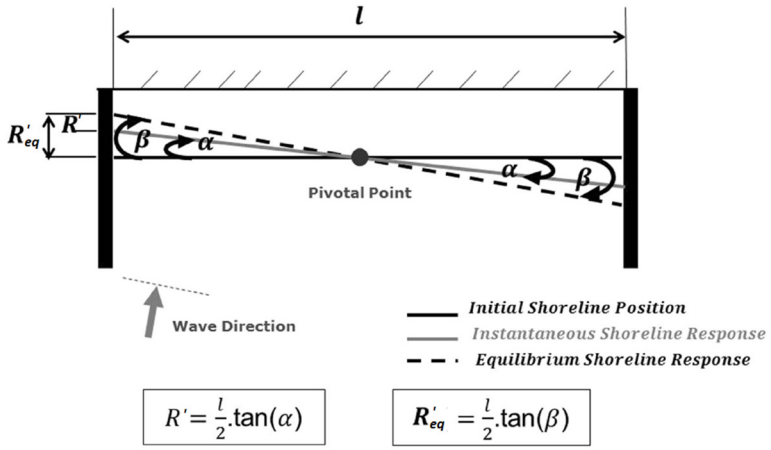

Fig. A.9. Scheme of shoreline rotation model proposed by Turki et al., (2013a). Modified from Turki et al., (2015).

This model, exclusively applicable for embayed beaches, was successfully applied over one year of video-derived shoreline data in three beaches located at Barcelona city, subjected to microtidal regime.

Then, Blossier et al. (2015) related the shoreline rotation rate to the amount of wave energy available for alongshore sediment transport, defining the equilibrium orientation of the shoreline as the normal to the incidence wave direction, θ_w. The proposed model resulted as follows:

$$\frac{\partial \alpha_s}{\partial t} = K \cdot \left(m \cdot E_y + n_1\right) \tag{A.38}$$

where α_s is the shoreline orientation, K is a constant (Eq. (A.37)), m and n_1 are free dimensionless parameters of the model and E_y is the alongshore component of the wave energy, assimilated to the square of the significant wave height and the incident wave angle θ_w:

$$E_y = E \cdot \cos(\theta_w) \cdot sen(\theta_w) \tag{A.39}$$

$$K = \frac{1}{T_d \cdot L' \cdot \sigma_y} \tag{A.40}$$

where L' is the half-length of the shoreline, σ_y is the standard deviation of the shoreline and T_d=1 day.

Subsequently, using Canonical Correlation Analysis, CCA, Blossier et al., (2017) proposed a modified shoreline rotation model, which is also based on the formulation proposed by Turki et al., (2013a):

$$\frac{d\alpha_s(t)}{dt} = C_{\alpha_s}\mathrm{E}[sen(\theta_w)\cdot\cos(\theta_w) - \alpha_s\cos(2\theta_w)] \tag{A.41}$$

where $\alpha_s(t)$ and E are the shoreline orientation and the incident wave energy, respectively and C_{α_s} is a free coefficient of the model. This model was successfully applied over 7-years of video-derived shoreline data at Tairua Beach, New Zealand subjected to microtidal regime.

APPENDIX 4: DRY BEACH AREA CALCULATION

The calculation of dry beach area for a PBSE consists of a mathematical development among polar and Cartesian coordinates. Fig. A.10 shows a scheme indicating the coordinate axes and the areas subject to be calculated: submerged area, A_1 and dry beach area, A_2. The dotted lines delimit an arbitrary section of submerged beach area (bounded by α_1 and α_2 angles), which can be obtained by the following expression:

$$A_1 = \frac{1}{2}\int_{\alpha_1}^{\alpha_2}\left(R_0\left(C_0 + C_1\frac{\beta}{\theta} + C_2\left(\frac{\beta}{\theta}\right)^2\right)\right)^2 d\theta \tag{A.42}$$

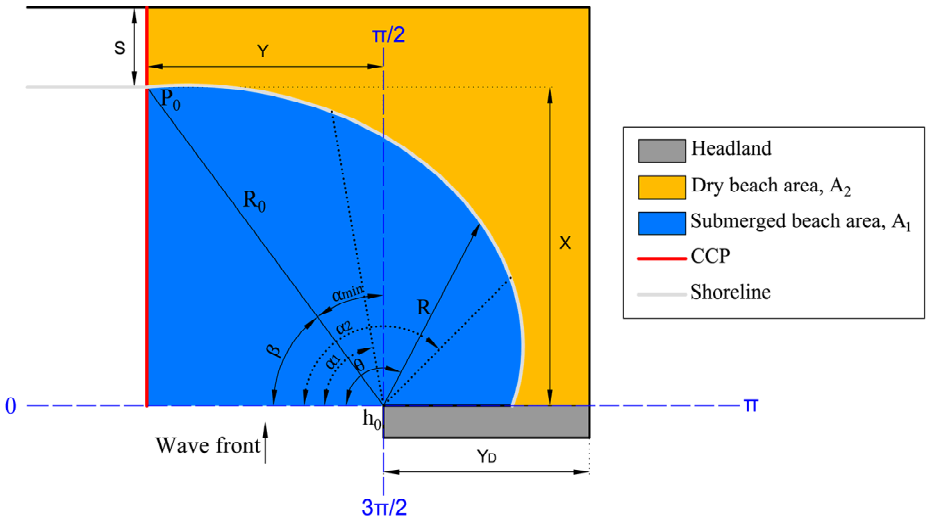

Fig. A.10. Scheme indicating the original polar coordinate system and beach areas: submerged beach area, A1 and dry beach area, A2.

According to Fig. A.10 and Eq.(A.42), considering $\alpha_1 = \beta$ and $\alpha_2 = \pi$, the areas can be written:

$$A_1 = {R_0}^2 \cdot \left[\left(\frac{1}{2}{C_0}^2 \cdot (\pi - \beta) - \left(\frac{1}{\pi} - \frac{1}{\beta}\right) \cdot \left(\frac{1}{2}{C_1}^2\beta^2 + C_0C_2\beta^2\right) - \frac{1}{6}{C_2}^2\beta^4 \cdot \left(\frac{1}{\pi^3} - \frac{1}{\beta^3}\right) + C_0C_1\beta \cdot (ln(\pi) - ln(\beta)) - \frac{1}{2}C_1C_2\beta^3 \cdot \left(\frac{1}{\pi^2} - \frac{1}{\beta^2}\right)\right) + \frac{sen(\beta) \cdot cos(\beta)}{2}\right] \tag{A.43}$$

$$A_2 = (Y + Y_D) \cdot (X + S) - A_1 \tag{A.44}$$

where S is the shoreline position given by the cross-shore model, and Y_D corresponds to the dike length. Fig. A.11 presents a list of three generic cases that determine the dry beach area calculation according to the limits that border the PBSE.

CASE	SCHEME	AREAS
1	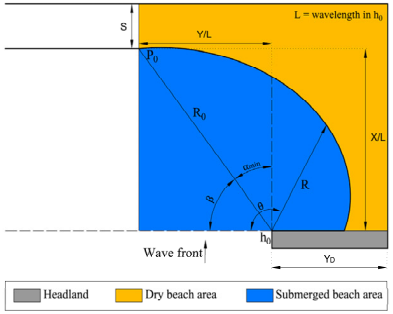	$\alpha_1 = \beta$ and $\alpha_2 = \pi$ $A_1 = {R_0}^2 \cdot \left[\left(\frac{1}{2}{C_0}^2 \cdot (\pi - \beta) - \left(\frac{1}{\pi} - \frac{1}{\beta}\right) \cdot \left(\frac{1}{2}{C_1}^2\beta^2 + C_0C_2\beta^2\right) - \frac{1}{6}{C_2}^2\beta^4 \cdot \left(\frac{1}{\pi^3} - \frac{1}{\beta^3}\right) + C_0C_1\beta \cdot (ln(\pi) - ln(\beta)) - \frac{1}{2}C_1C_2\beta^3 \cdot \left(\frac{1}{\pi^2} - \frac{1}{\beta^2}\right)\right) + \frac{sen(\beta) \cdot cos(\beta)}{2}\right]$ $A_2 = [(R_0 cos(\beta) + Y_D) \cdot (R_0 sen(\beta) + S)] - A_1$
2	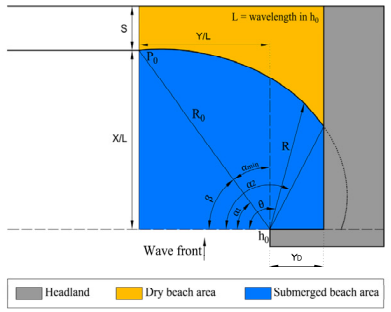	$\alpha_1 = \beta$ and α_2 delimited by the border $A_1 = {R_0}^2 \cdot \left[\left(\frac{1}{2}{C_0}^2 \cdot (\alpha_2 - \beta) - \left(\frac{1}{\alpha_2} - \frac{1}{\beta}\right) \cdot \left(\frac{1}{2}{C_1}^2\beta^2 + C_0C_2\beta^2\right) - \frac{1}{6}{C_2}^2\beta^4 \cdot \left(\frac{1}{{\alpha_2}^3} - \frac{1}{\beta^3}\right) + C_0C_1\beta \cdot (ln(\alpha_2) - ln(\beta)) - \frac{1}{2}C_1C_2\beta^3 \cdot \left(\frac{1}{{\alpha_2}^2} - \frac{1}{\beta^2}\right)\right) + \frac{sen(\beta) \cdot cos(\beta)}{2}\right] + \frac{{Y_D}^2 \cdot tan(\pi - \alpha_2)}{2}$ $A_2 = [(R_0 cos(\beta) + Y_D) \cdot (R_0 sen(\beta) + S)] - A_1$
3	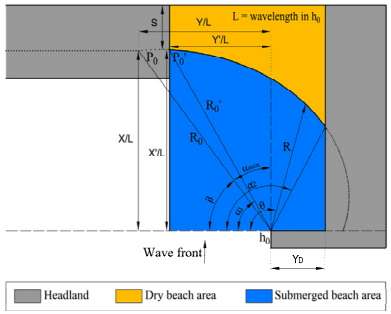	α_1 and α_2 delimited by the border $A_1 = {R_0}^2 \cdot \left[\left(\frac{1}{2}{C_0}^2 \cdot (\alpha_2 - \alpha_1) - \left(\frac{1}{\alpha_2} - \frac{1}{\alpha_1}\right) \cdot \left(\frac{1}{2}{C_1}^2\beta^2 + C_0C_2\beta^2\right) - \frac{1}{6}{C_2}^2\beta^4 \cdot \left(\frac{1}{{\alpha_2}^3} - \frac{1}{{\alpha_1}^3}\right) + C_0C_1\beta \cdot (ln(\alpha_2) - ln(\alpha_1)) - \frac{1}{2}C_1C_2\beta^3 \cdot \left(\frac{1}{{\alpha_2}^2} - \frac{1}{{\alpha_1}^2}\right)\right)\right] + \frac{{R_0}'^2 \cdot sen(\alpha_1) \cdot cos(\alpha_1)}{2} + \frac{{Y_D}^2 \cdot tan(\pi - \alpha_2)}{2}$ $A_2 = ({R_0}' cos(\alpha_1) + Y_D) \cdot ({R_0}' sen(\alpha_1) + S) - A_1$

Fig. A.11. Different cases for submerged beach area, A1 and dry beach area, A2.